

THE UNIVERSITY OF HULL

**Relationship between Surface Mechanical Properties and
Foam Stability**

being a Thesis submitted for the Degree of

Doctor of Philosophy

in the University of Hull

by

Yuan Pang
(B. Eng., M. Eng.)

May 2019

Acknowledgements

I would like to express sincere thanks to my supervisor Dr Paul Stevenson for not only providing excellent guidance through my PhD education but also encouraging me to experience diverse culture while studying abroad. I am grateful to my co-supervisor Dr Jay Wadhawan, who has been always giving great advice during my studying. A very special gratitude to Prof. Bernie Binks for enlightening discussions we had about particle-stabilised foams. The staff in mechanic workshop are appreciated for building the device of foam stability measurement, especially Mr Stuart Butterick. I am also grateful to the Lab technician Mr Mark Jeffries for his continuous support. The financial support from the China Scholarship Council (CSC) of the Chinese government and the University of Hull is gratefully acknowledged. At last but not least, I would like to thank my wife Ms Rui Zhang and my parents for their support in life and work during the last four years.

Abstract

This thesis is concerned with foam stability and surface mechanical properties (including surface tension and surface rheological properties) of liquid-air interfaces of foams. In particular, the question as to which surface mechanical property (or properties) primarily governs (or govern) foam stability, the optimal hydrophobicity range of particle to stabilise foam, and the reason why the particle with that hydrophobicity are capable of stabilising foam in terms of the modification of surface mechanical properties of liquid-air interfaces of particle-stabilised foams are investigated systematically in this thesis. In respect of relating foam stability to surface mechanical properties, the oscillating pendant droplet method of obtaining surface rheological properties, the repeatability of dynamic surface tension measurements of ionic surfactant solution using the static pendant droplet method, and the measurement of foam stability using a modified Bikerman test of Li *et al.* (2010) that controls the relative humidity at the top of column have been studied as a matter of priority. The dependency of surface rheological properties on oscillation frequency and amplitude has been described and this dependency indicates that the measurement of surface rheological properties of different surfactant solutions should be performed at a fixed oscillation frequency and amplitude in order to obtain convincing observations of the relationship between surface mechanical properties and foam stability. Furthermore, it has been demonstrated that the observable differences of dynamic surface tension results between different trials are due to the presence of trace amounts of highly surface-active impurities and it is necessary to perform large numbers of independent trials of dynamic surface tension measurement and then calculate the arithmetic mean of all dynamic surface tension results to obtain the dynamic surface tension value of ionic surfactant solutions with highly surface-active impurity. Moreover, the observation of the dependency of foam stability upon environmental relative humidity has been confirmed and extended. It is precisely to facilitate the investigation of the relationship between foam stability and surface mechanical properties that the environmental relative humidity has to be controlled at a constant value. Foam stability is correlated to surface rheological properties including surface elasticity, surface dilatational viscosity and Gibbs elasticity under the condition that the effect of surface tension on foam stability is kept approximately constant and therefore eliminated. It has been shown that both surface tension and surface rheological properties affect the stability of surfactant-stabilised foams, however, surface tension appears to play more important role, with respect to the stability of surfactant-stabilised foams. The stability of foams stabilised by the mixtures of particles and surfactants, as well as the relationship between surface mechanical properties and stability of particle-stabilised foams, is also studied in this thesis. It has been experimentally demonstrated that only intermediately hydrophobic particles can enhance foam stability by the addition of particles to surfactant solutions, since these particles affect the surface mechanical properties by increasing surface elasticity and Gibbs elasticity whereas decreasing equilibrium surface tension and surface dilatational viscosity, which has a synergistically positive effect on the stability of particle-stabilised foams.

Table of Contents

Acknowledgements.....	i
Abstract.....	ii
Table of Contents.....	iii
List of Figures.....	vii
List of Tables.....	xvi
Nomenclature.....	xxiii
Chapter 1 Introduction and Literature Review.....	1
1.1 Introduction.....	2
1.1.1 Motivation and Novelty.....	2
1.1.2 Aim and Objectives.....	4
1.2 Foam Stability.....	5
1.2.1 Measurement of Foam Stability.....	6
1.2.2 General Concept of Foam Structure.....	9
1.2.3 Mechanisms Causing Foam Instability.....	12
1.3 Basic Principles of Surfactants.....	17
1.3.1 Introduction to Surfactants.....	18
1.3.2 Behaviour in Bulk Solutions.....	20
1.3.3 Surfactant Adsorption at Gas-liquid Interface.....	24
1.3.4 Surfactant Adsorption at Solid-liquid Interfaces.....	26
1.4 Surface Mechanical Properties of Air-liquid Interfaces in Foams.....	32
1.4.1 Surface Tension.....	32
1.4.2 Surface Rheological Properties.....	41
1.5 Particle-stabilised Foams.....	49
1.5.1 Fundamental of Particles.....	49

1.5.2 Stability of Particle-stabilised Foams	54
1.6 Thesis Structure	58
Chapter 2 Measurement of Surface Rheological Properties	62
2.1 Introduction.....	63
2.2 Theoretical Derivation of Surface Rheological Properties	63
2.3 Experimental Details.....	73
2.4 Dependency of Surface Rheological Properties upon Oscillation Frequency and Amplitude.....	77
2.5 Summary	84
Chapter 3 Repeatability of Dynamic Surface Tension Measurement.....	85
3.1 Introduction.....	86
3.2 Initial Measurement of Dynamic Surface Tension	87
3.2.1 Experimental Details.....	87
3.2.2 Unexpected Systematic Change of Dynamic Surface Tension Results.....	89
3.3 Confirmation of the Unexpected Observation	93
3.4 Cause of the Unexpected Observation.....	100
3.4.1 Effect of Highly Surface-active Impurity on Dynamic Surface Tension Measurement.....	100
3.4.2 Verification of the Effect of Highly Surface-active Impurity on Dynamic Surface Tension Results.....	103
3.5 Statistical Analysis of Dynamic Surface Tension Results.....	107
3.5.1 Proposal of a Hypothesis	107
3.5.2 Method of Statistical Hypothesis Testing.....	110
3.5.3 Results of Statistical Hypothesis Testing.....	114
3.6 Summary	116
Chapter 4 Effect of Environmental Relative Humidity on Foam Stability....	118
4.1 Introduction.....	119

4.2 Experimental Details.....	119
4.3 Effect of Environmental Relative Humidity on Foam Stability	124
4.4 Summary	129
Chapter 5 Dependency of Foam Stability upon Surface Tension and Surface Dilatational Properties	130
5.1 Introduction.....	131
5.2 Different Surfactant Solutions with Approximately the Same Equilibrium Surface Tension	131
5.3 Relationship between Surface Rheological Properties and Foam Stability.....	137
5.4 Summary	147
Chapter 6 Particle-stabilised Foams.....	149
6.1 Introduction.....	150
6.2 Effect of Silica Particles (at Fixed Particle Concentration) on the Stability of Foams Stabilised by Cationic Surfactant at Different Concentrations	150
6.2.1 Hydrophobicity of Silica Particles	150
6.2.2 Foam Stability Measurement	156
6.3 Effect of Particle Concentration on the Stability of Foams Stabilised by Mixtures of Cationic Surfactant and Silica Particles	165
6.3.1 Foam Stability Measurement	165
6.3.2 Hydrophobicity of Silica Particles	167
6.4 Relationship between the Stability of Particle-stabilised Foams and Surface Mechanical Properties	171
6.4.1 Surface Mechanical Properties of DTAB Solutions with and without Colloidal Silica Dispersions (3 wt%) at Different Surfactant Concentrations	171

6.4.2 Surface Mechanical Properties of Mixtures of DTAB Solutions (0.1 × CMC) and Colloidal Silica Dispersions at Different Particle Concentrations	178
6.5 Summary	183
Chapter 7 Conclusions and Recommendations for Future Work	185
7.1 Conclusions.....	186
7.2 Recommendations for Future Work.....	189
References.....	192
Appendices.....	214
Appendix A Influence of Noise upon Results Obtained by Droplet Shape Analyser	214
Appendix B Original Results and Inferred Parameters of Surface Rheological Properties Measurements in Chapter 2.....	218
Appendix C Detailed Results of Dynamic Surface Tension Measurement in Chapter 3.....	222
Appendix D Effectiveness of Drying Agent to Dry Compressed Air	237
Appendix E Detailed Results of Foam Stability Measurement in Chapter 4	241
Appendix F Detailed Results of Equilibrium Surface Tension, Foam Stability and Surface Rheological Properties Measurements in Chapter 5	247
Appendix G Detailed Results of Foam Stability and Surface Rheological Properties Measurements in Chapter 6	258

List of Figures

Figure 1-1. The representative photos of wet foam and dry foam which are taken from the bottom and the top of a foam column respectively	11
Figure 1-2. A schematic diagram of Kelvin bubble, film, Plateau border and node.....	12
Figure 1-3. The foam drainage equation and drainage velocity of mobile channel-dominated model, rigid channel dominated model, node-dominated model and network-dominated model	14
Figure 1-4. Generalised structure of a surfactant.....	18
Figure 1-5. Schematic representation of surface tension of a surfactant solution as a function of surfactant concentration	22
Figure 1-6. Schematic representation of monomers and micelles in bulk solutions	23
Figure 1-7. Schematic representation of adsorption mechanisms of ionic surfactant at hydrophilic (oppositely charged) solid surface to interpret the four-region model and the two-step model of adsorption isotherm.....	29
Figure 1-8. A schematic representation of adsorption mechanism of non-ionic surfactant at solid surface.....	30
Figure 1-9. Schematic representation of the attractive forces between water molecules at the air-water interface and in the bulk	33
Figure 1-10. Dynamic surface tension of SDS solution (1.788 g/L) at different stages of purification as a function of time	39
Figure 1-11. Variation of modulus of surface dilatational visco-elasticity as a function of oscillation frequency for aqueous sodium caseinate system at different concentrations	46

Figure 1-12. Schematic representation of a solid particle at the air-water interface.....	51
Figure 1-13. The overall approach that applied in this thesis	59
Figure 2-1. Typical experimental results of surface tension variation and surface area disturbance obtained by the oscillating pendent droplet method.	72
Figure 2-2. The flow chart of the oscillating pendant droplet method to obtain surface elasticity, surface dilatational viscosity and Gibbs elasticity	73
Figure 2-3. Schematic diagram of the droplet shape analyser (Krüss, DSA100R). 1. The dosing unit 2. Light source 3. Stage 4. Camera 5. Computer.....	75
Figure 2-4. Surface elasticity, surface dilatational viscosity and Gibbs elasticity of SDS solution at the concentration of 0.087 g/L in 8.766 g/L NaCl aqueous solution as a function of oscillation frequency	79
Figure 2-5. Surface elasticity, surface dilatational viscosity and Gibbs elasticity of SDS solution at the concentration of 0.087 g/L in 8.766 g/L NaCl aqueous solution as a function of oscillation amplitude	80
Figure 2-6. Relative amplitude of surface area disturbance and amplitude of surface tension variation of SDS solution at the concentration of 0.087 g/L in 8.766 g/L NaCl aqueous solution as a function of oscillation frequency and amplitude.....	81
Figure 3-1. Dynamic surface tension results of sodium tridecyl sulfate solution at the concentration of 1.301 g/L (i.e. 2.68 % above the CMC).....	90
Figure 3-2. Dynamic surface tension results of SDS solution at the concentration of 0.288 g/L in 0.584 g/L NaCl aqueous solutions (i.e. approximately 25% of the CMC).....	91

Figure 3-3. Comparison between different runs of average arithmetic mean and average range of dynamic surface tension between different trials of sodium tridecyl sulfate solution (1.301 g/L).....	98
Figure 3-4. Comparison between different runs of average arithmetic mean and average range of dynamic surface tension between different trials of SDS solution (0.288 g/L in 0.584 g/L NaCl)	98
Figure 3-5. The arithmetic mean and the dispersion of dynamic surface tension between 100 trials of three surfactant solutions.....	106
Figure 3-6. The flowchart for the statistical hypothesis testing.....	111
Figure 4-1. The representative photograph of the experimental system for measuring foam stability under conditions of controlled-humidity.....	121
Figure 4-2. The schematic diagram of the experimental system for measuring foam stability under conditions of controlled-humidity	122
Figure 4-3. Representative photograph of produced foams with a square of 100 mm ² area	124
Figure 4-4. The foam height of SDS solution with different environmental relative humidities at the top of the column.....	126
Figure 4-5. The equilibrium foam height as a function of environmental relative humidity	127
Figure 5-1. Dynamic surface tension results of TX-100 solution (0.066 g/L), sodium tridecyl sulfate solution (1.301 g/L) and DTAB solution (4.954 g/L)	134
Figure 5-2. Dynamic surface tension results of TX-100 solution (0.066 g/L), sodium tridecyl sulfate solution (1.301 g/L) and DTAB solution (4.954 g/L) against $t^{-1/2}$	135

Figure 5-3. The representative photo of foams produced from TX-100 solution (0.066 g/L), DTAB solution (4.954 g/L) and sodium tridecyl sulfate solution (1.301 g/L)	139
Figure 5-4. The evolution of foam height of TX-100 solution (0.066 g/L), DTAB solution (4.954 g/L) and sodium tridecyl sulfate solution (1.301 g/L) with environmental humidity at 70%	140
Figure 6-1. Photos of mixtures of colloidal silica particles (3 wt%) and DTAB solutions at different concentrations after 24 hours	153
Figure 6-2. A schematic diagram of variation of particle hydrophobicity with increasing surfactant concentration caused by the surfactant adsorption at the particle surface	155
Figure 6-3. The bubble size (i.e. arithmetic mean bubble diameter) of DTAB surfactant solutions with and without 3 wt% colloidal silica dispersions at different surfactant concentrations.....	158
Figure 6-4. The foam height comparison of foams produced by DTAB solutions with and without 3 wt% colloidal silica dispersions at different surfactant concentrations	161
Figure 6-5. The bubble size (i.e. arithmetic mean bubble diameter) and equilibrium foam height of foams produced from mixtures of DTAB solutions at the concentration of $0.1 \times \text{CMC}$ and colloidal silica dispersions at different particle concentrations	167
Figure 6-6. Photographs of mixtures of DTAB solutions ($0.1 \times \text{CMC}$) and colloidal silica particles at different concentrations after 24 hours	168
Figure 6-7. A schematic diagram of variation of particle hydrophobicity with increasing particle concentration caused by the surfactant adsorption at particle surface	170

Figure 6-8. The surface mechanical properties of DTAB solutions both with and without 3 wt% colloidal silica dispersions at different surfactant concentrations	175
Figure 6-9. The surface mechanical properties of mixtures of DTAB solutions at the concentration of $0.1 \times \text{CMC}$ and colloidal silica dispersions at different concentrations	182
Figure A-1. The dynamic surface tension results obtained from the oscillating pendant droplet method with and without the polyfoam	215
Figure A-2. Fourier analyses of dynamic surface tension results obtained with and without the polyfoam	216
Figure C-1. Dynamic surface tension results of sodium tridecyl sulfate solution (1.301 g/L) of run 2.....	222
Figure C-2. Dynamic surface tension results of sodium tridecyl sulfate solution (1.301 g/L) of run 3.....	223
Figure C-3. Dynamic surface tension results of sodium tridecyl sulfate solution (1.301 g/L) of run 4.....	223
Figure C-4. Dynamic surface tension results of sodium tridecyl sulfate solution (1.301 g/L) of run 5.....	224
Figure C-5. Dynamic surface tension results of sodium tridecyl sulfate solution (1.301 g/L) of run 6.....	224
Figure C-6. Dynamic surface tension results of sodium tridecyl sulfate solution (1.301 g/L) of run 7.....	225
Figure C-7. Dynamic surface tension results of sodium tridecyl sulfate solution (1.301 g/L) of run 8.....	225
Figure C-8. Dynamic surface tension results of sodium tridecyl sulfate solution (1.301 g/L) of run 9.....	226

Figure C-9. Dynamic surface tension results of sodium tridecyl sulfate solution (1.301 g/L) of run 10.....	226
Figure C-10. Dynamic surface tension results of SDS solution (0.288 g/L in 0.584 g/L NaCl) of run 2.....	227
Figure C-11. Dynamic surface tension results of SDS solution (0.288 g/L in 0.584 g/L NaCl) of run 3.....	228
Figure C-12. Dynamic surface tension results of SDS solution (0.288 g/L in 0.584 g/L NaCl) of run 4.....	228
Figure C-13. Dynamic surface tension results of SDS solution (0.288 g/L in 0.584 g/L NaCl) of run 5.....	229
Figure C-14. Dynamic surface tension results of SDS solution (0.288 g/L in 0.584 g/L NaCl) of run 6.....	229
Figure C-15. Dynamic surface tension results of SDS solution (0.288 g/L in 0.584 g/L NaCl) of run 7.....	230
Figure C-16. Dynamic surface tension results of SDS solution (0.288 g/L in 0.584 g/L NaCl) of run 8.....	230
Figure C-17. Dynamic surface tension results of SDS solution (0.288 g/L in 0.584 g/L NaCl) of run 9.....	231
Figure C-18. Dynamic surface tension results of SDS solution (0.288 g/L in 0.584 g/L NaCl) of run 10.....	231
Figure C-19. Dynamic surface tension results of DTAB solution (4.954 g/L) of run 1	232
Figure C-20. Dynamic surface tension results of DTAB solution (4.954 g/L) of run 2	232
Figure C-21. Dynamic surface tension results of DTAB solution (4.954 g/L) of run 3	233

Figure C-22. Dynamic surface tension results of DTAB solution (4.954 g/L) of run 4	233
Figure C-23. Dynamic surface tension results of DTAB solution (4.954 g/L) of run 5	234
Figure C-24. Dynamic surface tension results of DTAB solution (4.954 g/L) of run 6	234
Figure C-25. Dynamic surface tension results of DTAB solution (4.954 g/L) of run 7	235
Figure C-26. Dynamic surface tension results of DTAB solution (4.954 g/L) of run 8	235
Figure C-27. Dynamic surface tension results of DTAB solution (4.954 g/L) of run 9	236
Figure C-28. Dynamic surface tension results of DTAB solution (4.954 g/L) of run 10	236
Figure D-1. Schematic diagram of the compressed air humidity measuring system	238
Figure D-2. The evolution of relative humidity in the column.....	238
Figure F-1. Partial enlarged view of dynamic surface tension results of TX-100 solution at the concentration of 0.175 g/L (i.e. at the CMC of TX-100) against $t^{-1/2}$	247
Figure F-2. Partial enlarged view of dynamic surface tension results of TX-100 solution at the concentration of 0.088 g/L (i.e. 50% of the CMC of TX-100) against $t^{-1/2}$	248
Figure F-3. Partial enlarged view of dynamic surface tension results of TX-100 solution at the concentration of 0.070 g/L (i.e. 40% of the CMC of TX-100) against $t^{-1/2}$	249

Figure F-4. Partial enlarged view of dynamic surface tension results of TX-100 solution at the concentration of 0.044 g/L (i.e. 25% of the CMC of TX-100) against $t^{-1/2}$	250
Figure G-1. The evolutions of foam height of mixtures of DTAB solution ($0.1 \times \text{CMC}$) and colloidal silica dispersions at different particle concentrations with the environmental relative humidity of $70.4 \pm 0.5\%$	267
Figure G-2. Partial enlarged view of dynamic surface tension results of DTAB solution ($0.1 \times \text{CMC}$) against $t^{-1/2}$	285
Figure G-3. Partial enlarged view of dynamic surface tension results of mixture of DTAB solution ($0.1 \times \text{CMC}$) and colloidal silica dispersions (3 wt%) against $t^{-1/2}$	286
Figure G-4. Partial enlarged view of dynamic surface tension results of DTAB solution ($0.25 \times \text{CMC}$) against $t^{-1/2}$	287
Figure G-5. Partial enlarged view of dynamic surface tension results of mixture of DTAB solution ($0.25 \times \text{CMC}$) and colloidal silica dispersions (3 wt%) against $t^{-1/2}$	288
Figure G-6. Partial enlarged view of dynamic surface tension results of DTAB solution ($0.5 \times \text{CMC}$) against $t^{-1/2}$	289
Figure G-7. Partial enlarged view of dynamic surface tension results of mixture of DTAB solution ($0.5 \times \text{CMC}$) and colloidal silica dispersions (3 wt%) against $t^{-1/2}$	290
Figure G-8. Partial enlarged view of dynamic surface tension results of mixture of DTAB solution ($1.05 \times \text{CMC}$) and colloidal silica dispersions (3 wt%) against $t^{-1/2}$	291
Figure G-9. Partial enlarged view of dynamic surface tension results of DTAB solution ($2.5 \times \text{CMC}$) against $t^{-1/2}$	292

Figure G-10. Partial enlarged view of dynamic surface tension results of mixture of DTAB solution ($2.5 \times \text{CMC}$) and colloidal silica dispersions (3 wt%) against $t^{-1/2}$	293
Figure G-11. Partial enlarged view of dynamic surface tension results of mixture of DTAB solution ($0.1 \times \text{CMC}$) and colloidal silica dispersions (0.1 wt%) against $t^{-1/2}$	294
Figure G-12. Partial enlarged view of dynamic surface tension results of mixture of DTAB solution ($0.1 \times \text{CMC}$) and colloidal silica dispersions (0.3 wt%) against $t^{-1/2}$	295
Figure G-13. Partial enlarged view of dynamic surface tension results of mixture of DTAB solution ($0.1 \times \text{CMC}$) and colloidal silica dispersions (1 wt%) against $t^{-1/2}$	296
Figure G-14. Partial enlarged view of dynamic surface tension results of mixture of DTAB solution ($0.1 \times \text{CMC}$) and colloidal silica dispersions (9 wt%) against $t^{-1/2}$	297

List of Tables

Table 1-1. Common examples of each type of surfactant	19
Table 1-2. The typical results of surface mechanical properties including equilibrium surface tension, surface elasticity, surface dilatational viscosity and Gibbs elasticity of some common surfactants and surfactant-particle systems in literature	46
Table 2-1. Surface rheological properties of SDS solution at the concentration of 0.087 g/L in 8.766 g/L NaCl aqueous solution as a function of oscillation frequency.....	77
Table 2-2. Surface rheological properties of SDS solution at the concentration of 0.087 g/L in 8.766 g/L NaCl aqueous solution as a function of oscillation amplitude.....	78
Table 3-1. The average arithmetic mean, the average range and the changing trend of dynamic surface tension between different trials in each run of sodium tridecyl sulfate solution (1.301 g/L) and SDS solution (0.288 g/L in 0.584 g/L NaCl).....	96
Table 3-2. The average dynamic surface tension results of trial 1 and trial 10 of 10 runs of sodium tridecyl sulfate solution (1.301 g/L) and SDS solution (0.288 g/L in 0.584 g/L NaCl)	109
Table 3-3. Results of the normality test showing that whether the data sets are drawn from normally distributed populations.....	115
Table 3-4. Results of statistical hypothesis testing	115
Table 4-1. The equilibrium foam height with different environmental relative humidities at the top of the column.....	126
Table 5-1. Results of equilibrium surface tension, surface rheological properties and equilibrium foam height of TX-100 solution (0.066 g/L),	

DTAB solution (4.954 g/L) and sodium tridecyl sulfate solution (1.301 g/L)	136
Table 5-2 Results of equilibrium surface tension, surface rheological properties and equilibrium foam height of SDS solution at different concentrations	143
Table 6-1. The comparison of surface rheological properties, equilibrium surface tension and equilibrium foam height of DTAB solutions with and without 3 wt% colloidal silica dispersions at different surfactant concentration	173
Table 6-2. The comparison of surface rheological properties, equilibrium surface tension and equilibrium foam height of mixtures of DTAB solutions at the concentration of $0.1 \times \text{CMC}$ and colloidal silica dispersions at different particle concentrations	179
Table B-1. Original results of surface rheological properties in each trial at different oscillation frequencies.....	218
Table B-2. Parameters inferred from results given in Table B-1 to obtain Gibbs elasticity in each trial at different oscillation frequencies.....	219
Table B-3. Original results of relative amplitude of surface area disturbance and amplitude of surface tension variation in each trial at different oscillation frequencies	219
Table B-4. Original results of surface rheological properties in each trial at different oscillation amplitudes.....	220
Table B-5. Parameters inferred from results given in Table B-4 to obtain Gibbs elasticity in each trial at different oscillation amplitudes.....	220
Table B-6. Original results of relative amplitude of surface area disturbance and amplitude of surface tension variation in each trial at different oscillation amplitudes	221

Table D-1. The detailed results of relative humidity in the column	239
Table D-2. The relative humidity of environmental air, undried compressed air and dried compressed air	240
Table E-1. The detailed results of evolution of foam height of SDS solution in each independent measurement with relative humidity of 93.4 % at the top of the column.....	242
Table E-2. The detailed results of evolution of foam height of SDS solution in each independent measurement with relative humidity of 71.1 % at the top of the column.....	243
Table E-3. The detailed results of evolution of foam height of SDS solution in each independent measurement with relative humidity of 51.3 % at the top of the column.....	244
Table E-4. The detailed results of evolution of foam height of SDS solution in each independent measurement with relative humidity of 30.5 % at the top of the column.....	245
Table E-5. The detailed results of evolution of foam height of SDS solution in each independent measurement with relative humidity of 10.0 % at the top of the column.....	246
Table F-1. Results of equilibrium surface tension of TX-100 solution at different concentrations	251
Table F-2. The detailed results of evolution of foam height of TX-100 solution (0.066 g/L) in each independent measurement at environmental relative humidity of $70.0 \pm 0.3\%$	252
Table F-3. The detailed results of evolution of foam height of DTAB solution (4.954 g/L) in each independent measurement at environmental relative humidity of $70.0 \pm 0.3\%$	253

Table F-4. The detailed results of evolution of foam height of sodium tridecyl sulfate solution (1.301 g/L) in each independent measurement at environmental relative humidity of $70.0 \pm 0.3\%$ 254

Table F-5. The detailed results of surface rheological properties in each independent measurement of TX-100 solution (0.066 g/L) at oscillation amplitude of 0.25 and oscillation frequency of 0.5 Hz.....255

Table F-6. The detailed results of surface rheological properties in each independent measurement of DTAB solution (4.954 g/L) at oscillation amplitude of 0.25 and oscillation frequency of 0.5 Hz.....256

Table F-7. The detailed results of surface rheological properties in each independent measurement of sodium tridecyl sulfate solution (1.301 g/L) at oscillation amplitude of 0.25 and oscillation frequency of 0.5 Hz257

Table G-1. The detailed results of evolution of foam height of DTAB solution at the concentration of $0.1 \times \text{CMC}$ in each independent measurement at environmental relative humidity of $70.4 \pm 0.5\%$ 258

Table G-2. The detailed results of evolution of foam height of mixture of DTAB solution ($0.1 \times \text{CMC}$) and colloidal silica dispersions (3 wt%) in each independent measurement at environmental relative humidity of $70.4 \pm 0.5\%$ 259

Table G-3. The detailed results of evolution of foam height of DTAB solution at the concentration of $0.25 \times \text{CMC}$ in each independent measurement at environmental relative humidity of $70.4 \pm 0.5\%$ 260

Table G-4. The detailed results of evolution of foam height of mixture of DTAB solution ($0.25 \times \text{CMC}$) and colloidal silica dispersions (3 wt%) in each independent measurement at environmental relative humidity of $70.4 \pm 0.5\%$ 261

Table G-5. The detailed results of evolution of foam height of DTAB solution at the concentration of $0.5 \times \text{CMC}$ in each independent measurement at environmental relative humidity of $70.4 \pm 0.5\%$ 262

Table G-6. The detailed results of evolution of foam height of mixture of DTAB solution ($0.5 \times \text{CMC}$) and colloidal silica dispersions (3 wt%) in each independent measurement at environmental relative humidity of $70.4 \pm 0.5\%$ 263

Table G-7. The detailed results of evolution of foam height of mixture of DTAB solution ($1.05 \times \text{CMC}$) and colloidal silica dispersions (3 wt%) in each independent measurement at environmental relative humidity of $70.4 \pm 0.5\%$ 264

Table G-8. The detailed results of evolution of foam height of DTAB solution at the concentration of $2.5 \times \text{CMC}$ in each independent measurement at environmental relative humidity of $70.4 \pm 0.5\%$ 265

Table G-9. The detailed results of evolution of foam height of mixture of DTAB solution ($2.5 \times \text{CMC}$) and colloidal silica dispersions (3 wt%) in each independent measurement at environmental relative humidity of $70.4 \pm 0.5\%$ 266

Table G-10. The detailed results of evolution of foam height of mixture of DTAB solution ($0.1 \times \text{CMC}$) and colloidal silica dispersions (0.1 wt%) in each independent measurement at environmental relative humidity of $70.4 \pm 0.5\%$ 268

Table G-11. The detailed results of evolution of foam height of mixture of DTAB solution ($0.1 \times \text{CMC}$) and colloidal silica dispersions (0.3 wt%) in each independent measurement at environmental relative humidity of $70.4 \pm 0.5\%$ 269

Table G-12. The detailed results of evolution of foam height of mixture of DTAB solution ($0.1 \times \text{CMC}$) and colloidal silica dispersions (1 wt%) in each

independent measurement at environmental relative humidity of $70.4 \pm 0.5\%$	270
Table G-13. The detailed results of evolution of foam height of mixture of DTAB solution ($0.1 \times \text{CMC}$) and colloidal silica dispersions (9 wt%) in each independent measurement at environmental relative humidity of $70.4 \pm 0.5\%$	271
Table G-14. The detailed results of surface rheological properties in each independent measurement of DTAB solution ($0.1 \times \text{CMC}$) at oscillation amplitude of 0.25 and oscillation frequency of 0.5 Hz.....	272
Table G-15. The detailed results of surface rheological properties in each independent measurement of mixture of DTAB solution ($0.1 \times \text{CMC}$) and colloidal silica dispersions (3 wt%) at oscillation amplitude of 0.25 and oscillation frequency of 0.5 Hz.....	273
Table G-16. The detailed results of surface rheological properties in each independent measurement of DTAB solution ($0.25 \times \text{CMC}$) at oscillation amplitude of 0.25 and oscillation frequency of 0.5 Hz.....	274
Table G-17. The detailed results of surface rheological properties in each independent measurement of mixture of DTAB solution ($0.25 \times \text{CMC}$) and colloidal silica dispersions (3 wt%) at oscillation amplitude of 0.25 and oscillation frequency of 0.5 Hz.....	275
Table G-18. The detailed results of surface rheological properties in each independent measurement of DTAB solution ($0.5 \times \text{CMC}$) at oscillation amplitude of 0.25 and oscillation frequency of 0.5 Hz.....	276
Table G-19. The detailed results of surface rheological properties in each independent measurement of mixture of DTAB solution ($0.5 \times \text{CMC}$) and colloidal silica dispersions (3 wt%) at oscillation amplitude of 0.25 and oscillation frequency of 0.5 Hz.....	277

Table G-20. The detailed results of surface rheological properties in each independent measurement of mixture of DTAB solution ($1.05 \times \text{CMC}$) and colloidal silica dispersions (3 wt%) at oscillation amplitude of 0.25 and oscillation frequency of 0.5 Hz.....	278
Table G-21. The detailed results of surface rheological properties in each independent measurement of DTAB solution ($2.5 \times \text{CMC}$) at oscillation amplitude of 0.25 and oscillation frequency of 0.5 Hz.....	279
Table G-22. The detailed results of surface rheological properties in each independent measurement of mixture of DTAB solution ($2.5 \times \text{CMC}$) and colloidal silica dispersions (3 wt%) at oscillation amplitude of 0.25 and oscillation frequency of 0.5 Hz.....	280
Table G-23. The detailed results of surface rheological properties in each independent measurement of mixture of DTAB solution ($0.1 \times \text{CMC}$) and colloidal silica dispersions (0.1 wt%) at oscillation amplitude of 0.25 and oscillation frequency of 0.5 Hz.....	281
Table G-24. The detailed results of surface rheological properties in each independent measurement of mixture of DTAB solution ($0.1 \times \text{CMC}$) and colloidal silica dispersions (0.3 wt%) at oscillation amplitude of 0.25 and oscillation frequency of 0.5 Hz.....	282
Table G-25. The detailed results of surface rheological properties in each independent measurement of mixture of DTAB solution ($0.1 \times \text{CMC}$) and colloidal silica dispersions (1 wt%) at oscillation amplitude of 0.25 and oscillation frequency of 0.5 Hz.....	283
Table G-26. The detailed results of surface rheological properties in each independent measurement of mixture of DTAB solution ($0.1 \times \text{CMC}$) and colloidal silica dispersions (9 wt%) at oscillation amplitude of 0.25 and oscillation frequency of 0.5 Hz.....	284

Nomenclature

Roman

a_j	A constant relate to the standard normal distribution in eq. 3-5	[-]
A	Surface area	[m ²]
A_c	Cross-sectional area of a channel	[m ²]
A_0	Initial surface area	[m ²]
A^*	Amplitude of surface area disturbance	[m ²]
A'	Relative amplitude of surface area disturbance	[-]
c	Surfactant concentration in the bulk solution	[mol·m ⁻³]
c_0	Equilibrium bulk concentration	[mol·m ⁻³]
c_b	Surfactant concentration in the bulk solution in eq. 1-3	[mol·m ⁻³]
$c(\tau)$	Surfactant concentration at the subsurface in eq. 1-3	[mol·m ⁻²]
c_s	Subsurface concentration in eq. 2-14	[mol·m ⁻²]
D	Diffusion coefficient	[m ² ·s ⁻¹]
D_A	Arithmetic mean bubble diameter	[m]
E	Free energy of particle detachment from gas-liquid interface	[J]
E_i	Overall interaction energy	[J]
E_a	Attractive energy	[J]
E_r	Repulsive energy between colloidal particles	[J]
F	The test statistic of the two-sample F-test of equality of variances	[-]
g	Gravitational acceleration	[m·s ⁻²]
G	Surface shear elastic modulus	[N·m ⁻¹]
H	A constant of integration in eq. 2-8	[-]
H_e	Equilibrium foam height	[m]
i	The sequential image number in chapter 3	[-]
i	The unit imaginary number in chapter 2	[-]
j	The sequential data number	[-]

j_a	Superficial air velocity	$[\text{m}\cdot\text{s}^{-1}]$
k	The sequential data set number	$[-]$
K	Permeability of porous medium	$[\text{m}^2]$
K_H	Surface Henry's law constant	$[\text{m}]$
L	Edge length	$[\text{m}]$
L_0	Edge length of a completely dry foam	$[\text{m}]$
n_k	The size of data set k	$[-]$
n	A variable in eq. 2-8 that satisfies $n^2 = \frac{i\omega}{D}$	$[-]$
n	The number of bubbles covered in a square in eq. 4-2	$[-]$
P	Driving pressure	$[\text{Pa}]$
ΔP	Pressure difference across the gas-fluid interface	$[\text{Pa}]$
ΔP_0	Reference pressure difference at the apex of the droplet	$[\text{Pa}]$
r	Radius of curvature in Figure 1-3	$[\text{m}]$
r	Particle radius in eq. 1-9	$[\text{m}]$
r_k	The sum of the ranks in data set k	$[-]$
R	Universal gas constant	$[\text{J}\cdot\text{K}^{-1}\cdot\text{mol}^{-1}]$
R_A	The average range of dynamic surface tension of 300 images	$[\text{N}\cdot\text{m}^{-1}]$
R_i	The range of dynamic surface tension between 10 trials of i^{th} image	$[\text{N}\cdot\text{m}^{-1}]$
R_1	The first principal radius of curvature	$[\text{m}]$
R_2	The second principal radius of curvature	$[\text{m}]$
SD_A	The average standard deviation of dynamic surface tension of 300 images	$[\text{N}\cdot\text{m}^{-1}]$
SD_i	The standard deviation of dynamic surface tension between independent trials of i^{th} image	$[\text{N}\cdot\text{m}^{-1}]$
S_k^2	The variance of data set k	$[-]$
t	The test statistic of the two-sample Student's T-test and the Welch's test in chapter 3	$[-]$
t	Time	$[\text{s}]$
T	Absolute temperature	$[\text{K}]$

u_{xy}	Shear deformation in the xy -plain	[-]
V	Drainage velocity	[m·s ⁻¹]
V_l	Liquid volume	[m ³]
V_f	Foam volume	[m ³]
W	The test statistic of the Shapiro-Wilk test	[-]
$x_{(j)}$	The j^{th} smallest number in the data set	[-]
x_j	The j^{th} statistic in the data set	[-]
\bar{x}	The arithmetic mean of the data set	[-]
\bar{X}_k	The arithmetic mean of data set k	[-]
z	Vertical height of the given point on the droplet surface to the apex of the droplet in eq. 1-5	[m]
z	Distance from the interface in eq. 2-8	[m]
z	The direction of gravity	[-]
Z	The test statistic of the Wilcoxon rank sum test	[-]

Greek

α	The significance level	[-]
α_c	Flow resistance for a channel	[-]
α_m	Flow resistance for mobile interfaces	[-]
α_n	Flow resistance for a node	[-]
γ	Surface tension in chapter 1	[N·m ⁻¹]
γ_{pa}	Surface tension at particle-air interface in Figure 1-9	[N·m ⁻¹]
γ_{pw}	Surface tension at particle-water interface in Figure 1-9	[N·m ⁻¹]
γ_{aw}	Surface tension at air-water interface in Figure 1-9	[N·m ⁻¹]
Γ	Surface excess	[mol·m ⁻²]
Γ_e	Equilibrium surface excess	[mol·m ⁻²]
Γ^*	The amplitude of surface excess oscillations	[mol·m ⁻²]
Γ'	A complex quantity that represents the amplitude of surface excess oscillations	[mol·m ⁻²]
δ_c	A constant to calculate the channel cross-sectional area	[-]
δ_n	A constant to calculate the node cross-sectional area	[-]

δ_1	A constant to calculate the relationship between edge length, radius of curvature and liquid volume fraction	[-]
ε	Volumetric liquid fraction in chapter 1	[-]
ε	Surface visco-elasticity	[N·m ⁻¹]
ε_r	Surface elasticity	[N·m ⁻¹]
ε_i	Imaginary part of complex surface visco-elasticity	[N·m ⁻¹]
ε_0	Gibbs elasticity	[N·m ⁻¹]
$ \varepsilon $	Modulus of visco-elasticity	[N·m ⁻¹]
ε^*	The liquid fraction of the wet limit foam	[-]
θ	Three-phase contact angle in eq. 1-9	[°]
θ	Surface dilatation in eq. 2-9	[m ² ·s ⁻¹]
θ_{aw}	Three-phase contact angle in Figure 1-9	[°]
μ	Bulk viscosity	[Pa·s]
μ_k	The mean of the population which the data set k is drawn from	[-]
μ_d	Surface dilatational viscosity	[N·s·m ⁻¹]
μ_s	Surface shear viscosity	[Pa·s]
ξ	A notation defined in eq. 2-22	[-]
ξ	A constant to calculate the size of a node	[-]
π	Circular constant	[-]
ρ	Volumetric density	[kg·m ⁻³]
$\Delta\rho$	Density difference between the droplet phase and continuous phase	[kg·m ⁻³]
σ	Surface tension	[N·m ⁻¹]
σ_A	The average of arithmetic mean results of dynamic surface tension over 2 minutes	[N·m ⁻¹]
σ_i	The arithmetic mean result of dynamic surface tension between 10 trials of i^{th} image	[N·m ⁻¹]
σ_{xy}	Shear stress in the xy -plain	[N·m ⁻¹]
σ_e	Equilibrium surface tension	[N·m ⁻¹]
σ^*	Amplitude of surface tension variations	[N·m ⁻¹]
σ'	A complex quantity that represents the amplitude of	[N·m ⁻¹]

	surface tension variations	
Σ	Quotient of equilibrium foam height and superficial air velocity	[s]
τ	A dummy variable defined in eq. 1-3	[s]
φ	Phase angle	[rad]
ω	Angular frequency	[rad·s ⁻¹]
ω_0	Relaxation frequency	[s ⁻¹]

**Chapter 1 Introduction and
Literature Review**

1.1 Introduction

Aqueous foam is generally defined as a colloidal dispersion of a large number of gas bubbles (dispersed phase) in a continuous liquid phase (Cantat *et al.*, 2013). Due to the physical and mechanical properties of aqueous foams such as low bulk density, large specific surface area and characteristic behaviour of both liquids and solids, aqueous foams are widely applied in various industrial applications including fire-fighting, mineral flotation, oil recovery, detergents, food and cosmetics (Weaire *et al.*, 1999). In order to achieve the best performance of aqueous foam in these numerous industrial applications, obtaining stable foam is always an important issue and thus foam stability is a fundamental parameter. The key to producing stable foam is to modify surface properties, especially the surface mechanical properties, by the utilisation of stabilising agent, such as surfactant (Hill *et al.*, 2017). Therefore, the relationship between foam stability and surface mechanical properties is worthy of detailed exploration. Furthermore, surfactant is not the only kind of stabilising agent to obtain stable foam; the use of solid particles to enhance foam stability has drawn much attention recent years (Hunter *et al.*, 2008). However, solid particles can also destabilise foam (Garrett, 2015). Therefore, it is pertinent to investigate the effect of solid particles on foam stability and surface mechanical properties in this current work.

1.1.1 Motivation and Novelty

In the industrial process of enhanced oil recovery (EOR), one of the most commonly used techniques is gas injection, which introduces gases including

natural gas, nitrogen and carbon dioxide into the reservoir to promote oil displacement. This technique accounts for approximately 60% of EOR production in the USA (U.S. Department of Energy, 2019). However, due to the low viscosity and low density associated with any injected gas, many challenges are encountered by this approach, such as poor sweep efficiency, gravity segregation and reservoir heterogeneity (Heller, 1994). In order to alleviate these issues, foams are alternatively injected for mobility control and for blocking and diverting to improve oil recovery efficiency (Schramm *et al.*, 2012). Applications of foams in EOR require an understanding of the basic principles involved in foam generation, propagation, and especially, stability. These fundamentals provide an important base for developing foam applications in EOR. Therefore, it is significant to study foam stabilisation by surfactants and/or particles, and the underlying physicochemical properties in governing foam stability in order to improve the foam applications in EOR.

With regard to the exploration of foam stabilisation and its determinant physicochemical properties, it is still not clear which surface mechanical property (or properties) primarily governs (or govern) foam stability. In this thesis, this issue will be discussed in details. Furthermore, the most commonly used approach at present for stability measurement of particle-stabilised foams (i.e. the hand-shaking method) is less reproducible which could compromise the investigation of foam stabilisation by particles. In this thesis, a more reproducible method to quantify the stability of particle-stabilised foams will be applied and the effect of particles on foam stability and surface mechanical properties will be thoroughly investigated.

1.1.2 Aim and Objectives

The aim of this research is to explore foam stabilisation by surfactants and particles and its relationship to surface mechanical properties of air-liquid interfaces. In particular, two main objectives are achieved in this thesis. The first one is the investigation of the relationship between foam stability and the underlying surface mechanical properties including surface tension and surface rheological properties (such as surface elasticity, surface dilatational viscosity and Gibbs elasticity). The question as to which surface mechanical property (or properties) primarily governs (or govern) foam stability is explored systematically. The second objective is to study the effect of solid particle on foam stability and surface mechanical properties. The optimal hydrophobicity range of particle to stabilise foam is experimentally explored and the reason why the particle with that hydrophobicity are capable of stabilising foam is investigated thoroughly in terms of the modification of surface mechanical properties of liquid-air interfaces of particle-stabilised foams.

In this chapter, the existing literature which are relevant to above-described research objectives are reviewed and then the topics covered in the later chapters of this thesis are introduced. Since foam stability is the major concern in this thesis, the methods to measure foam stability and the general structure of foam which materially influences foam stability, as well as the mechanism that governs foam instability are firstly reviewed in section 1.2. Then, the basic principles of surfactants are described in section 1.3 as surfactants are most commonly used to modify surface properties to increase foam stability.

Furthermore, the literature concerning surface mechanical properties including surface tension and surface rheological properties are reviewed in section 1.4 in order to facilitate to understand their impacts on foam stability. Finally, previous research on particle-stabilised foams in the context of this thesis is considered in section 1.5.

1.2 Foam Stability

From an energetic perspective, foam does not spontaneously form from segregated gas and liquid phases, so energy is required to disperse gas so as to create gas-liquid interfaces. This energy equals to the product of surface tension and surface area created. This requirement illustrates that foam is thermodynamically unstable so that phases tend to separate with time and cause foam collapse (Fameau *et al.*, 2015). A quantity that describes the life time of a foam or the tenacity of a foam is generally termed as foam stability. Although it is a widely used term, there is no accurate physical definition of foam stability and there is no intrinsic measurement of foam stability (Stevenson *et al.*, 2014). In practice, foam stability is normally quantified as the variation of a foam property (for example foam height or foam volume) with time (Malysa *et al.*, 2008). It is also can be quantified as the necessary time needed when a foam property (such as foam height or foam volume) decays to a reference value (such as one-half of foam height or foam volume) (Malysa *et al.*, 2008). It is noted that characterisations of foam stability are always a function of time.

However, besides foam stability, there is another important foam property known as foamability which describes the capacity of foaming agents (such as surfactant solutions) to produce foam (Malysa *et al.*, 2008). Foamability is characterised as the initial amount of foam (for example foam height or foam volume) generated by a foaming agent immediately after the foam generation. It is noted that the quantification of foamability is a time-invariant value, which is different with foam stability. Thus, although foam stability and foamability are closely related, they are two different properties of a foam. However, it has been pointed by Malysa *et al.* (2008) that foam stability and foamability sometimes have been misunderstood and used interchangeably by some researchers. In this current work, only foam stability is considered and foamability is not studied. The terminology as explained above applies to the entire thesis.

In this section, the methods to measure foam stability and the problems inherent will be discussed, before a description of the general structure of foam. Finally, the most important mechanisms that govern foam instability will be reviewed.

1.2.1 Measurement of Foam Stability

Several commonly adopted methods are available to measure foam stability and a frequently used method is Bikerman foam stability test (Bikerman, 1938, 1973) during which a gas is continuously pumped into a surfactant solution to produce foam and simultaneously the foam collapses at its free surface. When the generation rate at the bottom of the foam equals to the collapse rate at the

top of the foam, the foam reaches an equilibrium height. The equilibrium foam height divided by the superficial gas velocity, which was defined by Bikerman as ‘unit of foaminess’, is employed to quantify foam stability and the physical meaning of this value is the residence time of the gas phase in the foam layer (Li, 2012). It is worth pointing out that in the original work of Bikerman (1938, 1973), the so-called ‘unit of foaminess’ was to describe foamability. However, according to the physical meaning of the ‘unit of foaminess’ and the difference between the characterisations of foam stability and foamability (the characterisation of foam stability is a function of time whereas that of foamability is time-invariant), it appears that Bikerman has used foam stability and foamability interchangeably, and the value he defined is actually to describe foam stability rather than foamability. The Bikerman foam stability test is a dynamic foam test (i.e. a gas is kept delivering into the surfactant solution to produce foam continuously) for foam stability (Schramm, 2005) and has been widely applied in different industrial applications including sparkling cider (Blanco-Gomis *et al.*, 2009), protein foam (Pernell *et al.*, 2002), desulphurisation (Hansen *et al.*, 2008) and froth flotation (Barbian *et al.*, 2003, 2005, 2006). In this current work, the Bikerman foam stability test is applied to measure foam stability and the superficial gas velocity is controlled constant during all the measurements. Thus, the equilibrium foam height is utilised to quantify foam stability.

Besides dynamic foam test for foam stability, there are static foam tests (i.e. foam is created beforehand and left statically to record its collapse) for foam stability (Schramm, 2005). One of these static foam tests to characterise foam

stability is Ross and Miles (1941) method which proceeds by pouring a surfactant solution into a reservoir of the same liquid and measuring the height variation of produced foam with time. Furthermore, two static foam tests that are widely used in the brewing industry are the Rudin test and the NIBEM method (Weaire *et al.*, 1999). Both tests are based on quantification of foam collapse to represent foam stability. The Rudin test measures the location of foam-liquid interface as a function of time whereas the NIBEM test records the location of foam-gas interface as a function of time instead. Moreover, there is another static foam test to quantify foam stability by measuring the half-life of foam. The time for one-half of the foam height to collapse is used to represent foam stability (Farrokhpay, 2011).

In fact, the characterisation of foam stability using Bikerman foam stability test can be affected by many external environmental factors. Choung *et al.* (2004) have studied the effect of temperature on foam stability and it was shown that foam became less stable with the increase of solution temperature, which was attributed to the irreversible precipitation of surfactants when the solution temperature was increased. Wang *et al.* (2017) have conducted the similar research and have observed the same phenomenon that foam stability decreased with the increase of solution temperature. It was believed by them that increased temperature reduced bulk viscosity and surface shear viscosity, and this caused increased drainage rate and thus contributed to instability of foam. Besides the effect of temperature on foam stability measurement, the environmental relative humidity also plays vital role on foam stability. Li *et al.* (2010, 2012) have investigated the effect of environmental relative humidity

on static and dynamic foam stability. It has been demonstrated by these authors that foam stability was dependent upon environmental relative humidity, as the evaporation at the top of the foam deteriorated with the decrease of environmental relative humidity, which resulted in higher collapse rate of foam. Champougny *et al.* (2018) have experimentally investigated the influence of environmental humidity on soap film stability. It was found by them that the film length at rupture increased continuously with the relative humidity. However, the effect of environmental relative humidity on foam stability has still been largely overlooked by some researchers and the environmental relative humidity has not been controlled with high precision. For instance, Wang *et al.* (2016) have compared the stability of foams stabilised by different surfactant solutions at the environmental relative humidity of 50-60%, which was considered by them as effectively constant. However, it will be demonstrated in chapter 4 of this thesis that this humidity range still materially influences foam stability.

1.2.2 General Concept of Foam Structure

In subsection 1.2.1, the methods to measure foam stability and the problems inherent with the Bikerman foam stability test have been discussed. Since foam stability is materially affected by the foam geometrical structure (Drenckhan *et al.*, 2015), it is necessary to present a general overview of foam structure in this subsection.

The structure of foam is determined by the minimisation of surface energy for a given liquid volume fraction with considering simple geometric rules at the

scale of bubble (Anazadehsayed *et al.*, 2018). The key parameter that affects the shape of bubble is volumetric liquid fraction (ε), which is defined as the ratio of liquid volume V_l and foam volume V_f , as shown in eq. 1-1

$$\varepsilon = \frac{V_l}{V_f} \quad (1-1)$$

Foams of high liquid fraction are considered to be ‘wet’, whereas those with low liquid fraction are ‘dry’, and the bubbles have a shape that are dependent upon the liquid fraction. Foam with liquid volume fraction higher than 0.15 is considered as wet foam by Drenckhan *et al.* (2015), of which bubble shape approximates to sphere, whereas foam with liquid volume fraction smaller than 0.05 is generally referred as dry foam and the bubble is in the shape of polyhedron (Drenckhan *et al.*, 2015). For a static foam column, wet foam is generally found at the bottom of the column which is close to the foam-liquid interface, whereas dry foam is usually located at the top of the column, which is far away from the foam-liquid interface but close to the gas-foam interface. The representative photos of wet foam and dry foam which are taken from the bottom and the top of a foam column respectively are shown in Figure 1-1.

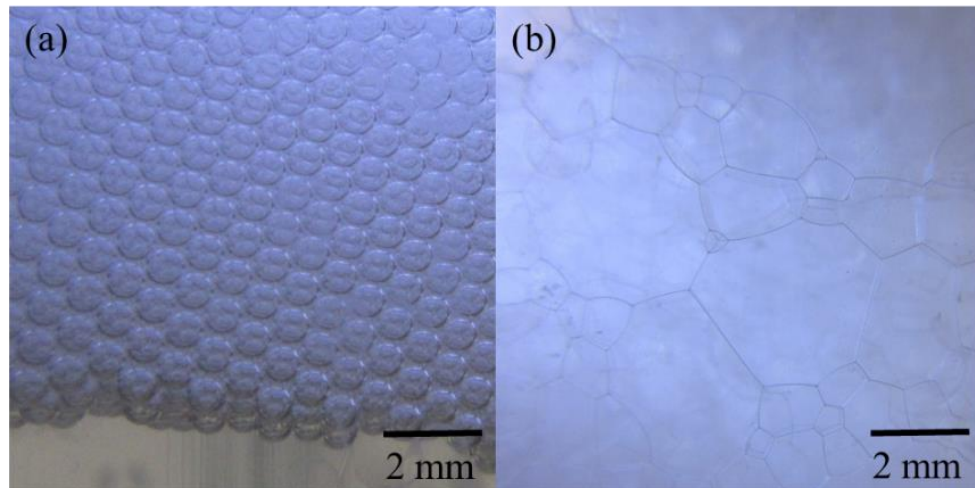


Figure 1-1. The representative photos of wet foam and dry foam which are taken from the bottom and the top of a foam column respectively. (a) Wet foam which is at the bottom of a foam column. (b) Dry foam which is at the top of a foam column.

As can be seen from Figure 1-1, for either wet foam or dry foam, the foam structure consists of three different elements including films (which separates two bubbles), Plateau borders (which are channels between three bubbles and also intersections of three films), and nodes where four Plateau borders meet (Weaire *et al.*, 1999). For wet foam, with an increase of liquid volume fraction, Plateau borders swell and nodes become more rounded and the bubbles tend towards a spherical shape (Weaire *et al.*, 1999). Further increase of liquid volume fraction (approximately larger than 0.35) results in the separation of close-packed bubbles and the loss of foam rigidity, at which condition bubble moves independently and is referred as bubbly liquid instead of wet foam (Langevin, 2017). However, for dry foam, the structure is generally well described by Plateau's law, which rules that three films meet uniformly at 120° angles and four Plateau borders should meet uniformly at the tetrahedral angle of 109.5° (Plateau, 1873). A simple bubble geometry for dry foam which adheres to Plateau's law was proposed by Lord Kelvin considering the minimal surface area (or surface energy) as a tetrakaidecahedral cell (known

as a Kelvin bubble) which contains 14 films, 36 Plateau borders and 12 nodes (Thomson, 1887). A schematic diagram of Kelvin bubble, film, Plateau border and node is shown in Figure 1-2. Furthermore, Weaire *et al.* (1994) have computed a structure of smaller surface area (or surface energy) than Kelvin bubble, which is the optimal structure of dry foam so far in terms of energetic perspective (Drenckhan *et al.*, 2015). However, it is difficult to create experimentally whereas the Kelvin bubble can be easily found or produced in real foam (Weaire *et al.*, 2012).

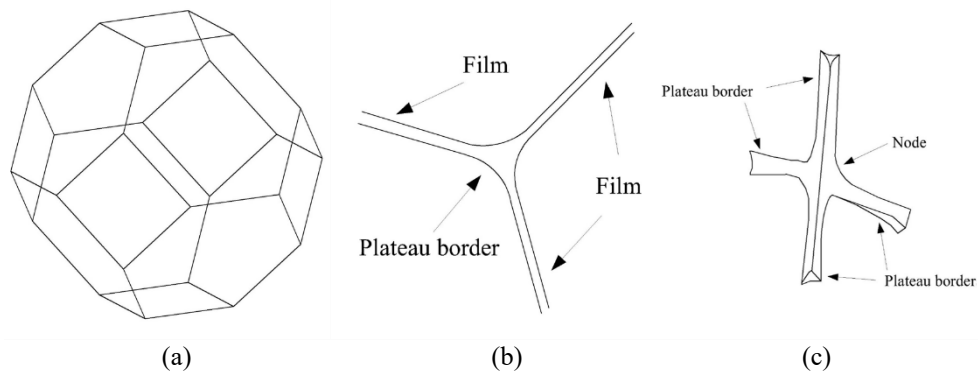


Figure 1-2. A schematic diagram of Kelvin bubble, film, Plateau border and node. (a) The structure of a Kelvin bubble. (b) A cross section of a Plateau border and three films. (c) The shape of a node.

1.2.3 Mechanisms Causing Foam Instability

In subsection 1.2.2, the general overview of foam structure is presented. Due to the distinctive foam geometry, there are three different fundamental mechanisms that cause foam instability, which are foam drainage (flow of liquid out of a foam under the action of gravity), coarsening (diffusion of gas between bubbles due to pressure difference) and coalescence (rupture of liquid films between bubbles or at the surface) (Cantat *et al.*, 2013). These three mechanisms are in fact interdependent (Hilgenfeldt *et al.*, 2001) that foam drainage which leads to dryer foams promotes coarsening and coalescence,

and larger bubbles obtained through coarsening and coalescence are in favour of foam drainage. A brief overview of these three mechanisms will be provided below.

1.2.3.1 Foam Drainage

Foam drainage determines the liquid volume fraction within a foam, which is a key factor for both coarsening and bubble coalescence (Saint-Jalmes *et al.*, 2002). The foam drainage equation describes the drainage process and models the spatio-temporal evolution of liquid volume fraction within the foam (Saint-Jalmes, 2006). Since liquid flowing through foam has viscous dissipation (Kruglyakov *et al.*, 2008), based upon the different assumptions of dominant foam element on viscous dissipation, different foam drainage equations have been proposed. Leonard and Lemlich (1965) have developed a model known as mobile channel-dominated model (Koehler, 2012) that considering the viscous dissipation was only dominated by Plateau borders (or ‘channels’) and the gas-liquid interface was mobile (i.e. considering the surface shear viscosity). Furthermore, Verbist *et al.* (1994) have proposed a model that also assuming the only dominant foam element on viscous dissipation was Plateau border but considering the gas-liquid interface was rigid (i.e. does not flow), which was known as rigid channel-dominated model. Besides above two approaches which ascribe viscous dissipation only to Plateau border, an alternative approach is to neglect the contribution of Plateau border to viscous dissipation and assume that the only dominant foam element on viscous dissipation is node. This approach was proposed by Koehler *et al.* (1999) and was known as the node-dominated model. Moreover, Koehler *et al.* (2000,

2004) have also developed a model combining the contribution of both Plateau border and node to viscous dissipation, which was known as the network-dominated model. The foam drainage equation and drainage velocity of above-mentioned models are shown in Figure 1-3.

Mobile channel-dominated model

Drainage velocity: $V = \frac{A_c}{3\alpha_m\mu} \rho g$ for the forced drainage

Rigid channel-dominated model

Foam drainage equation: $\mu \frac{d\varepsilon}{dt} + \left(\frac{\delta_c}{3\alpha_c\delta_1} \right) \nabla \cdot \left\{ \varepsilon^2 \left[\rho g L^2 + \sqrt{\delta_c} \gamma \nabla \cdot (L \varepsilon^{-1/2}) \right] \right\} = 0$ Drainage velocity: $V = -\frac{\delta_c/\delta_1}{3\alpha_c\mu} L^2 \varepsilon \nabla P$

Node-dominated model

Foam drainage equation: $\mu \frac{d\varepsilon}{dt} + K \rho g \frac{d(L^2 \varepsilon^{3/2})}{dz} - K \sqrt{\delta_c} \gamma \nabla \cdot (L \nabla \varepsilon) = 0$ Drainage velocity: $V \approx \frac{K}{\mu} L_0^2 \varepsilon^{1/2} \nabla P$

Network-dominated model

Drainage velocity: $V = -\frac{\nabla P}{3\mu} A_c \left[\alpha_m \left(1 - \frac{\xi}{L} \frac{r}{L} \right) + \alpha_n \frac{\xi \delta_c^2 r}{2\delta_n^2 L} \right]^{-1} \left[\frac{\xi}{\delta_c} \left(\frac{\delta_n}{\delta_c} - 1 \right) \frac{r}{L} + 1 \right]^{-1}$ for $\varepsilon \leq \varepsilon^*$

Figure 1-3. The foam drainage equation and drainage velocity of mobile channel-dominated model, rigid channel dominated model, node-dominated model and network-dominated model. V is the drainage velocity; A_c is the channel cross-sectional area; α_m is the flow resistance for mobile interfaces; μ is the bulk viscosity; ρ is the volumetric density; g is the gravitational acceleration; ε is the liquid fraction; t is the time; δ_c is a constant to calculate the channel cross-sectional area, which is approximately 0.161 for the Kelvin bubble; α_c is the flow resistance for a channel; δ_1 is a constant to calculate the relationship between edge length, radius of curvature and liquid volume fraction, which is approximately 0.171 for the Kelvin bubble; L is the edge length; γ is the surface tension; P is the driving pressure; K is the permeability of porous medium; z is the direction of gravity; L_0 is the edge length of a completely dry foam; ξ is a constant to calculate the size of the node, which is 1.71 for the Kelvin bubble; r is the radius of curvature; α_n is the flow resistance for a node; δ_n is a constant to calculate the node cross-sectional area, which is approximately 0.543 for the Kelvin bubble; ε^* is the liquid fraction of the wet limit foam that foam with liquid fraction higher than this value is considered as wet foam.

Furthermore, Stevenson (2006) has performed dimensional analysis of foam drainage, and the channel-dominated model and the node-dominated model have been simplified by Stevenson (2006) to simple power-law relationships that correlated the dimensionless drainage rate expressed as a Stokes number with the liquid volume fraction. Stevenson (2007) has applied this power-law approach to describe previous drainage data in a dimensionally constant form so that direct comparison of these data can be achieved. It has been

demonstrated by Stevenson (2007) that the rigid channel-dominated model was not robust as it under-estimated the actual drainage rate. In addition, Stevenson *et al.* (2010) have taken the inertial losses in a foam into consideration besides the viscous dissipation and proposed a viscous-inertial foam drainage equation which has been ascertained to be valid.

1.2.3.2 Coarsening

Coarsening occurs on the same timescale with foam drainage and involves the gas transport between bubbles of different radius, which causes bubbles with radius smaller than the average value to shrink whereas bubbles larger than the average size to grow, thus leading to a growth of the average bubble radius with time (Pitois, 2012). For a suspension of well-separated spherical bubbles, the growth law was analogous to Ostwald ripening proposed by Lifshitz *et al.* (1961) and Wagner (1961) that the average bubble radius increases with the cubic root of time. As for dry foam, the growth law of 2-dimensional foams was proposed by von Neumann (1952) and the generalisation of von Neumann's theory to 3-dimensional foams was performed by MacPherson *et al.* (2007). Whereas for wet foam, the growth law was described by Lemlich (1978), which has been explicitly reviewed by Stevenson (2010) to emphasise its importance in description of coarsening. Furthermore, Lambert *et al.* (2007) have suggested a growth law of bubbles for a moderately wet foam that between the extremes. Glazier *et al.* (1992) have reviewed the bubble scaling behaviour of foams in all cases and they found that generally average bubble radius grew as the square root of time, which was different with the scaling behaviour of well-separated spherical bubbles. This difference is due to the

fact that in foam, gas primarily chooses the smallest path to diffuse, which is through the films between bubbles (Briceño-Ahumada *et al.*, 2017). The characteristic coarsening rate of a foam has been theoretically derived by Hilgenfeldt *et al.* (2001) and was correlated with many physical-chemical and mechanical properties including liquid volume fraction, bubble geometry, film thickness and permeability, gas diffusivity and solubility, and surface tension of the liquid to produce the foam. Moreover, it was shown by Meinders *et al.* (2004) that another surface mechanical property which was surface elasticity also played an important role in coarsening process. It was believed by Rio *et al.* (2014) that the influence of surfactant on coarsening process was potentially mainly due to the increase of surface elasticity, however, as pointed out by Rio *et al.* (2014), this deserved further investigation as the details of this effect remained unclear. In this thesis, the effect of surface elasticity on foam stability will be explored.

1.2.3.3 Coalescence

Since coalescence in foams involves film rupture, the study of single film rupture provides insights to the understanding of coalescence in foams (Langevin, 2015; Bournival *et al.*, 2017). Film drainage is important in the study of film rupture, since it leads films between bubbles extremely thin so that readily to burst. The thin liquid film drains until film rupture occurs and film rupture is caused by the spontaneous growth of thermal fluctuation, which creates a local variation in surface tension (Manev *et al.*, 2005). Since the amplitude of thermal fluctuation is determined by surface elasticity instead of surface tension, thus surface elasticity plays a vital role in film rupture (De

Gennes, 2001). However, the mechanisms account for film rupture cannot fully explain coalescence in foams, as thin liquid films in foams are dynamically deformed and these deformations have not been considered in the study of film rupture (Bournival *et al.*, 2014). It has been shown by Vandewalle *et al.* (2001) that coalescence in foams was an avalanching process that first bubble ruptured due to thermal fluctuations and then caused a cascade of bursting bubbles. Carrier *et al.* (2003) have demonstrated that liquid volume fraction was a key parameter that affected coalescence in foams and coalescence in foams occurred once critical liquid volume fraction has been reached. At the critical liquid volume fraction, thin liquid films in foams are rapidly stretched and dilated, which eventually become unstable and rupture. This mechanism based upon film dilatation indicates the crucial role of surface elasticity and surface dilatational viscosity on bubble coalescence (Colin, 2012). Furthermore, other researchers have reported that coalescence in foams happened at critical bubble size (Georgieva *et al.*, 2009) and critical capillary pressure (Khristov *et al.*, 2002), which were different with the mechanism of critical liquid volume fraction. In fact, it is difficult to distinguish these mechanisms as liquid volume fraction, bubble size and capillary pressure are correlated and vary with time due to foam drainage and coarsening (Rio *et al.*, 2014).

1.3 Basic Principles of Surfactants

Most foams owe their existence to the presence of surfactants that accumulate at gas-liquid interfaces. Surfactants are used to reduce the surface free energy which is the minimum work required to create that surface. Without the

reduction, a tenacious gas-liquid foam could not be produced. Therefore, surfactants play an important role in stabilising foams and thus to understand surfactant behaviours is fundamental in the study of foam stability. In fact, there are two major behaviours of surfactant that require understanding in the context of foam stability, which are the formation of micelles in bulk solutions and the adsorption of surfactant at interfaces including gas-liquid and solid-liquid interfaces. In this section, general structural features and classification of surfactants are introduced, and the behaviour of surfactants in bulk solutions and at interfaces are reviewed.

1.3.1 Introduction to Surfactants

A surfactant is a substance that can adsorb onto the surfaces of the system and significantly reduce surface free energies (Rosen *et al.* 2012). Surfactants have an amphipathic molecular structure consisting of a hydrophobic group that has very little attraction for water and a hydrophilic group that has strong attraction for water. A surfactant molecule is schematically shown in Figure 1-4. The round hydrophilic head is polar or ionic and the hydrophobic tail is non-polar (usually a hydrocarbon chain).

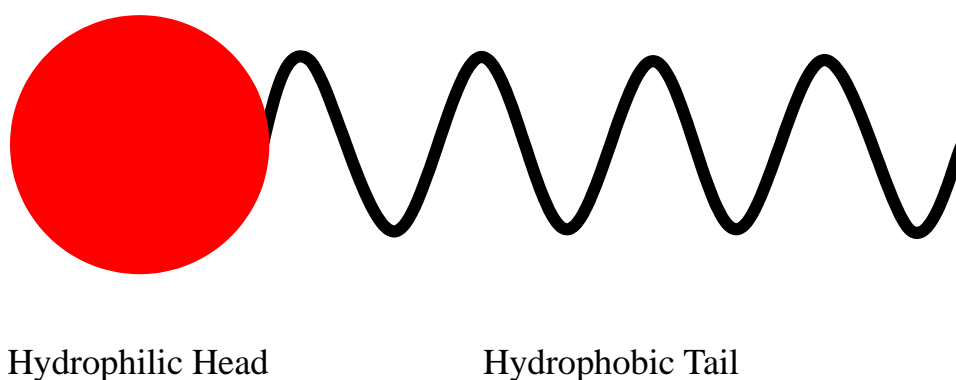


Figure 1-4. Generalised structure of a surfactant

Depending on the nature of the hydrophilic head, surfactants are classified as anionic (negatively charged), cationic (positively charged), zwitterionic (bearing both positive and negative charge) and non-ionic (bearing no apparent ionic charge). Some common examples of each type of surfactant are shown in Table 1-1.

Table 1-1. Common examples of each type of surfactant

Surfactant type	Common examples
Anionic surfactant	RCOO^-Na^+ (soap) $\text{RC}_6\text{H}_4\text{SO}_3\text{Na}^+$ (alkylbenzene sulfonate)
Cationic surfactant	$\text{RNH}_3^+\text{Cl}^-$ (salt of long chain amine) $\text{RN}(\text{CH}_3)_3^+\text{Cl}^-$ (quaternary ammonium chloride)
Zwitterionic surfactant	$\text{RN}^+\text{H}_2\text{CH}_2\text{COO}^-$ (long-chain amino acid) $\text{RN}^+(\text{CH}_3)_2\text{CH}_2\text{CH}_2\text{SO}_3^-$ (sulfobetaine)
Non-ionic surfactant	$\text{RCOOCH}_2\text{CHOHCH}_2\text{OH}$ (monoglyceride of long-chain fatty acid) $\text{R}(\text{OC}_2\text{H}_4)_x\text{OH}$ (polyoxyethylenated alcohol)

These four types of surfactants have all been utilised in industrial applications. Anionic surfactants are the most widely used surfactant type in industrial applications due to the relatively low cost and they are practically applied in most detergents (Lucassen-Reynders, 1981). The primary application of cationic surfactants is to utilise their strong adsorbing tendency onto most solid surfaces (which are usually negatively charged) to modify the characteristics of the solid surfaces (Tadros, 2005). The advantage of non-ionic surfactants is that they are compatible with all the other types of surfactants and thus non-ionic surfactants are usually used with other types of surfactant for better performance (Porter, 1994). Zwitterionic surfactants are

commonly used in cosmetic products because they are typically less irritating to skin and eyes than other types of surfactant (Rosen *et al.*, 2012). In fact, the selection of surfactant for a particular industrial application is informed by their physicochemical properties including surface-activity, chemical stability, solubility, compatibility with ions and other surfactants, biodegradability and toxicity (Porter, 1994; Rosen *et al.*, 2012).

In particular, the surface-active properties of surfactants are the mainly concerned properties in the later subsections (subsections 1.3.2 to 1.3.4) and the behaviour of surfactants in bulk solutions and different interfaces will be reviewed individually. Furthermore, chemical stability of surfactants (especially surfactant hydrolysis in aqueous solution) has an important influence on the determination of surface tension value of surfactant solution (Lunkenheimer *et al.*, 1995), which will be discussed in subsection 1.4.1.

1.3.2 Behaviour in Bulk Solutions

A fundamental characteristic of surfactants is micelle formation in which molecules form colloid-sized clusters in bulk solutions when the surfactant concentration is above a critical concentration. It was shown by Preston (1948) that there was a difference in the changing trend of physicochemical properties of surfactant solutions with increasing surfactant concentration above a critical concentration. For example, the schematic representation of surface tension of a surfactant solution as a function of surfactant concentration is shown in Figure 1-5. It indicates that at first surface tension decreases monotonously with the increase of surfactant concentration until above a critical

concentration that the surface tension remains approximately constant. The similar difference in the changing trend of other properties (such as self-diffusion and equivalent conductivity) with increasing surfactant concentration at this particular concentration has also been observed (Lindman *et al.* 1980). In fact, this difference in the changing trend of physicochemical properties with increasing surfactant concentration at this critical concentration suggests the micelle formation at the same critical concentration, which is known as critical micelle concentration (CMC) (Holmberg *et al.*, 2003). At concentrations lower than the CMC, the dissolved surfactant molecules manifest as monomers. At concentrations above the CMC, the additional surfactants are aggregated as micelles, which are self-assembled structures by monomers and co-exist with monomers at a concentration approximately equal to the CMC. The value of the CMC can be inferred via measurement of any of above-mentioned physicochemical properties with surfactant concentration, although the most commonly used methods are surface tension measurements, fluorescence spectroscopy and electrical conductivity techniques (Rosen *et al.*, 2012). There are many factors affect the values of the CMC in aqueous solutions including the structure of surfactant, electrolyte or organic additives, pH and temperature of the aqueous solutions (Rosen *et al.* 2012).

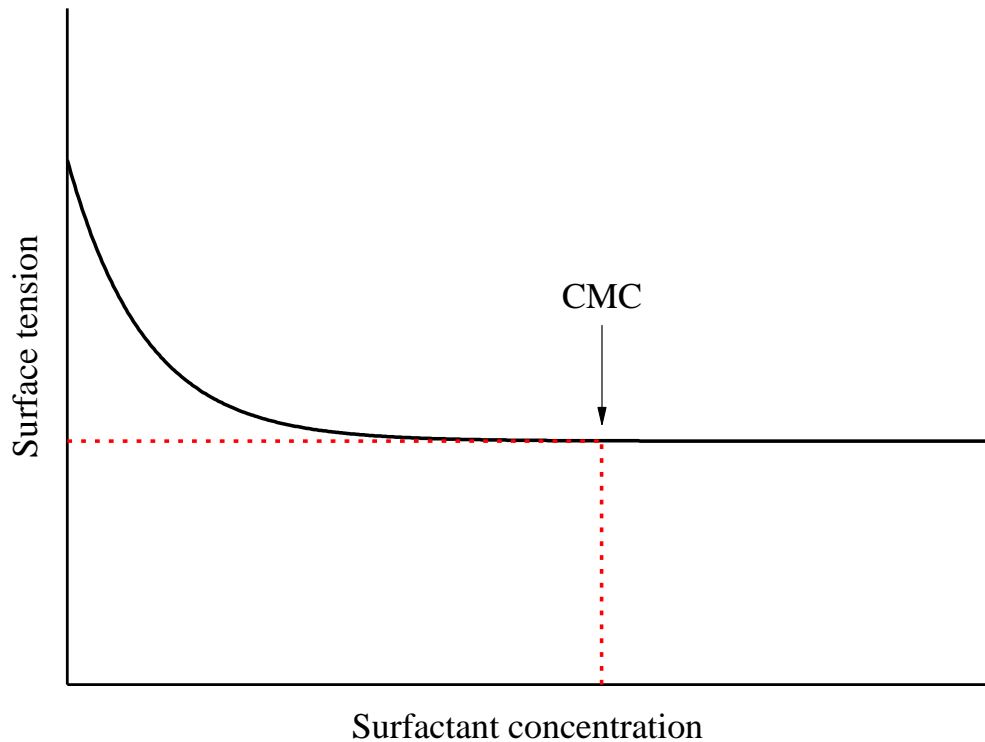
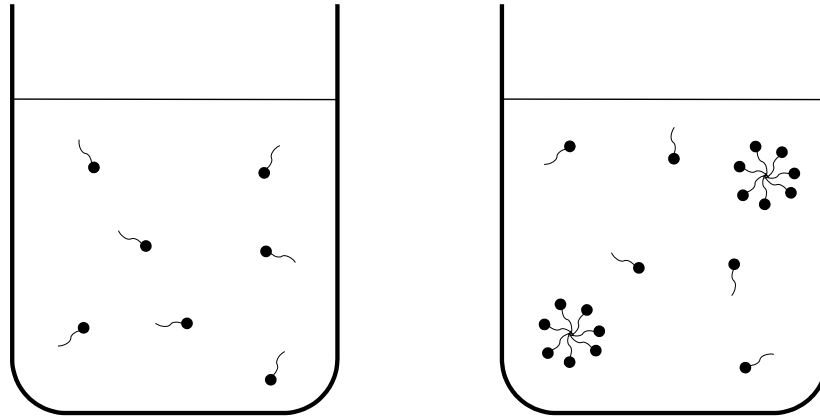


Figure 1-5. Schematic representation of surface tension of a surfactant solution as a function of surfactant concentration

A schematic representation of monomers and micelles in bulk solutions are shown in Figure 1-6. The presence of micelles was originally proposed by McBain (1913) and the structure of micelles was suggested by Hartley (1936) as approximately spherical (with aggregation number of monomers less than 100). However, modern techniques such as light scattering and neutron scattering indicate that micelles are not always spherical. Besides spherical micelles, cylindrical, lamellar and vesicular micelles have all been identified in different systems. It has been demonstrated by Winsor (1968) that variations of temperature, surfactant concentration, surfactant structure, as well as the presence of additives in aqueous solutions, could cause a change of micelle shape.



Solution concentration $<$ CMC Solution concentration $>$ CMC

Figure 1-6. Schematic representation of monomers and micelles in bulk solutions

In fact, the micelle formation is a process of minimising the free energy of the whole system of surfactant solutions. When the solution concentration is lower than the CMC, since micelles are not formed and only monomers exist in surfactant solutions, the hydrophobic group of monomers accumulate at the gas-liquid interface orienting the hydrophobic group away from water to minimise the free energy of the solutions. This process is known as adsorption and the details of this process will be discussed in the next subsection (subsection 1.3.3). However, when surfactants are dissolved in water at a concentration higher than the CMC, originally surfactant molecules adsorb at the gas-liquid interface to minimise the free energy of the solutions and gradually there is no space on the gas-liquid interface for adsorbing additional surfactant molecules to further reduce the free energy of the system. Therefore, as an alternative mechanism to minimise the free energy of the system, the additional surfactant molecules aggregate into micelles with their hydrophobic groups pointing to the interior of the micelles and their hydrophilic groups pointing to the water, which removes the hydrophobic groups from contact

with water and thereby reduces the free energy of the system. Thus, the driving force for micelle formation is the elimination of the contact between hydrophobic groups of surfactant molecules and water, which is known as the hydrophobic effect (Tadros, 2005). However, micelle formation is opposed by the hydrophilic groups of ionic surfactants, as the electrostatic repulsion between hydrophilic groups impedes the micelle formation. This unfavourable effect can be retarded by adding electrolytes to ionic surfactant solutions which screens the electrostatic repulsion between hydrophilic groups and therefore makes micelle formation more favourable.

1.3.3 Surfactant Adsorption at Gas-liquid Interface

In addition to the surfactant characteristic of micelle formation, there is another fundamental characteristic of surfactant that is as important as micelle formation, which is the tendency of surfactant to adsorb at interfaces. In fact, this characteristic is the reason why surfactants are commonly used to modify surface properties to stabilise foams as mentioned in section 1.1. Therefore, it is essential to understand the surfactant adsorption at the gas-liquid interface in terms of the study of stability of surfactant-stabilised foams.

During the process of surfactant adsorption, surfactants spontaneously accumulate at the gas-liquid interface with the hydrophilic groups pointing towards the liquid and the hydrophobic groups pointing towards the gas, which results in the reduction in surface tension. As illustrated above in Figure 1-5, surfactants show a gradual reduction in surface tension with the increase of surfactant concentration until the CMC is reached, above which the

surface tension remains virtually constant. The thermodynamic relationship between surface tension and surface excess (the surfactant concentration at the gas-liquid interface) is described by the Gibbs adsorption isotherm (Gibbs, 1928), which is:

$$\Gamma = -\frac{1}{nRT} \frac{d\gamma}{d \ln c} \quad (1-2)$$

where Γ is the surface excess; n is an integer that takes the value of 1 for non-ionic surfactants and 2 for completely disassociated ionic surfactants; R is the universal gas constant; T is the absolute temperature; γ is the surface tension and c is the surfactant concentration in the bulk solution. According to the Gibbs adsorption isotherm, the surface excess can be obtained from the variation of surface tension with surfactant concentration. The adsorption behaviour of different surfactants at the gas-liquid interface varies with the nature of hydrophilic head group, by which surfactants can be classified as ionic and non-ionic surfactants (which has been discussed in subsection 1.3.1).

For non-ionic surfactants, the surfactant adsorption at the gas-liquid interface is diffusion controlled that firstly the surfactant molecules diffuse from the bulk solution to the subsurface (the subsurface is an imaginary surface in the bulk solution with a thickness of several molecular diameters that directly next to the surface), and then the surfactant molecules adsorb at the gas-liquid interface from the subsurface, which instantaneously establishes a local equilibrium between the gas-liquid interface and the subsurface (Ward *et al.*, 1946). The adsorption process of non-ionic surfactants is described by the equation of Ward and Tordai (1946), which is

$$\Gamma(t) = 2\sqrt{\frac{D}{\pi}} \left[c_b \sqrt{t} - \int_0^{\sqrt{t}} c(\tau) d(\sqrt{t-\tau}) \right] \quad (1-3)$$

where Γ is surface excess; t is the time after the gas-liquid interface is created and τ is a dummy variable with the unit of time; D is the diffusion coefficient; c_b and $c(\tau)$ are the surfactant concentration in the bulk solution and at the subsurface respectively. As for ionic surfactants, the surfactant adsorption process at a gas-liquid interface is much more complicated since the adsorption process is accompanied with the change of surface charge density and surface electrical potential, and thus the electrostatic interaction between the charged surface and the ionic surfactant molecules must be taken into consideration (Borwankar *et al.*, 1988). Therefore, due to the effect of electrostatic interaction, the adsorption of ionic surfactants at the gas-liquid interface is electro-diffusion controlled. An analytical expression of the adsorption of ionic surfactants at the gas-liquid interface has been derived by Vlahovska *et al.* (1997) and it has been demonstrated by them that the effect of electrostatic interaction increased the adsorption time of ionic surfactants at the gas-liquid interface and decelerated the adsorption process.

1.3.4 Surfactant Adsorption at Solid-liquid Interfaces

As mentioned in section 1.1, solid particles have also been shown to engender a stable foam both in combination with surfactants and without surfactants. In the current work, particles are applied in addition to surfactants to increase foam stability. Therefore, in order to understand the effect of particles on surface mechanical properties and thus on foam stability, it is necessary and

important to review the adsorption of surfactants at solid-liquid interface herein.

The adsorption of surfactants at solid-liquid interface can be driven by a number of interactions between surfactant molecules and solid surfaces such as electrostatic interaction (i.e. ion exchange and ion pairing), chemical interaction (usually covalent bonding), hydrophobic bonding (which includes the lateral interaction between surfactant molecules and the interaction between surfactant molecules and hydrophobic sites on the solid surface), hydrogen bonding and dispersion forces (i.e. van der Waals forces) (Zhang *et al.*, 2006). However, the involved interactions for adsorption of ionic and non-ionic surfactants at solid-liquid interfaces are different (Tadros, 2005). Thus, the adsorption of ionic and non-ionic surfactants at solid-liquid interfaces require further discussion. Additionally, the hydrophobicity of solid surface also affects the interaction between surfactant molecules and solid surface (Somasundaran *et al.*, 2000), thus the surfactant adsorption at hydrophobic and hydrophilic solid-liquid interface has to be considered separately.

1.3.4.1 Adsorption of Ionic Surfactants at Solid-liquid Interfaces

The adsorption of ionic surfactants at hydrophobic interfaces is mainly governed by the hydrophobic interaction between the tail groups of surfactant molecules and the solid surface, whereas the electrostatic interaction between surfactant molecules and the surface plays a relatively minor role (Tadros, 2005). When ionic surfactants adsorb at hydrophilic surfaces, the hydrophilic surface normally develops a surface charge as a result of surface equilibrium

which involves potential determining ions (which are generally H^+ and OH^-) and the charge on the hydrophilic surface depends on the nature of the surface, pH of the surfactant solution, ionic strength and other conditions of surfactant solution (Paria *et al.*, 2004). Therefore, the adsorption of ionic surfactants at hydrophilic surfaces can be typically considered as ionic surfactant adsorption at oppositely charged surfaces, of which two adsorption mechanisms have been proposed by Somasundaran *et al.* (1966) and Gao *et al.* (1987), respectively. The associated adsorption isotherm which are interpreted by these two adsorption mechanisms are known as the four-region model (Somasundaran *et al.*, 1966) and two-step model (Gao *et al.*, 1987), individually. Both adsorption mechanisms are moderately for describing adsorption behaviour of certain combinations of surfactant and substrate.

A schematic representation of adsorption mechanisms of ionic surfactants at hydrophilic (oppositely charged) solid surfaces to interpret the four-region model and the two-step model of adsorption isotherm is shown in Figure 1-7. The adsorption mechanism to interpret the four-region model of adsorption isotherm is represented by process (a) in Figure 1-7, whereas process (b) in Figure 1-7 illustrates the adsorption mechanism to interpret the two-step model of adsorption isotherm. From stage I to IV of these two adsorption mechanisms, the surfactant concentration of bulk solution is increased. The major stages of these two adsorption mechanisms are generally the same that firstly surfactant molecules electrostatically adsorb at the solid surface and then the adsorbed surfactant molecules begin to form primary surface aggregates due to the lateral interactions between adsorbed surfactant

molecules and make the solid surface electrically neutralised, and subsequently the surface aggregates grows driven by the hydrophobic interaction between tail groups of surfactant molecules until eventually the saturation level of surface excess has been reached. The major differences between these two adsorption mechanisms are the structure of surfactant aggregates formed during the adsorption process. For process (a), the adsorbed surfactant molecules firstly form a structure of surface aggregates known as hemimicelle during stage II (Somasundaran *et al.*, 1966) and eventually form a bilayer during stage IV, whereas in process (b), the adsorbed surfactant molecules start to form ‘tepee’ structures as described by Atkin *et al.* (2003) and finally form admicelles, which are defined as spherical structures with hydrophilic head groups pointing towards both the solid surface and the solution.

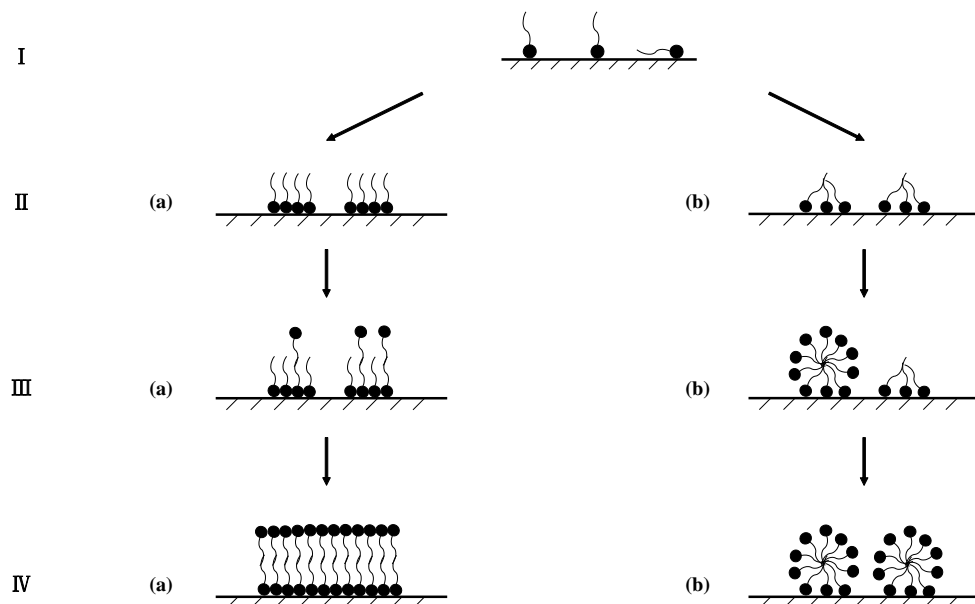


Figure 1-7. Schematic representation of adsorption mechanisms of ionic surfactant at hydrophilic (oppositely charged) solid surface to interpret the four-region model and the two-step model of adsorption isotherm. (a) The adsorption mechanism to interpret the four-region model of adsorption isotherm. (b) The adsorption mechanism to interpret the two-step model of adsorption isotherm. I-IV represent the successive stages of adsorption.

1.3.4.2 Adsorption of Non-ionic Surfactants at Solid-liquid Interfaces

Non-ionic surfactants are physically (rather than electrostatically) adsorbed to surfaces (either hydrophobic or hydrophilic) and thus the adsorption is usually reversible (Paria *et al.*, 2004; Zhang *et al.*, 2006). A schematic representation of adsorption mechanism of non-ionic surfactant at solid surface is shown in Figure 1-8.

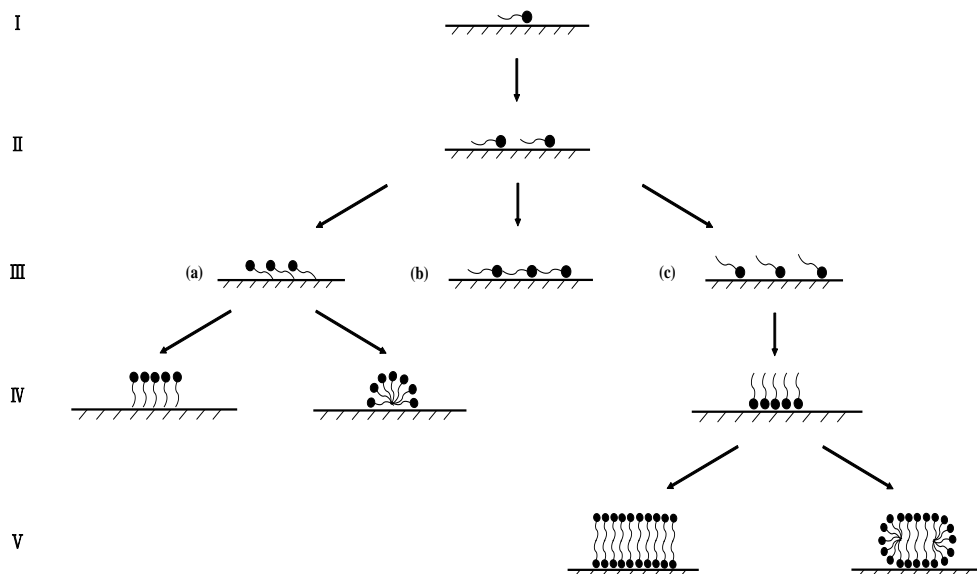


Figure 1-8. A schematic representation of adsorption mechanism of non-ionic surfactant at solid surface. (a) The adsorption of non-ionic surfactant at a hydrophobic surface. (b) The adsorption of non-ionic surfactant at a surface of intermediate hydrophobicity. (c) The adsorption of non-ionic surfactant at a hydrophilic surface. I-V represent the successive stages of adsorption.

The surfactant concentration of bulk solution is increased from stage I to V of the adsorption process. The hydrophobicity of surface determines the orientation of adsorbed surfactant molecules and the structure of surface aggregates (Clunie *et al.*, 1983). However, it is noted that in the beginning stages of the adsorption process (i.e. the stages I and II in Figure 1-8), the adsorptions of non-ionic surfactants at the surfaces of different hydrophobicity are the same that the surfactants lie flat on the surface driven by van der Waals

attraction until achieve the monolayer saturation of adsorbed surfactant molecules. Subsequently, for hydrophobic surfaces, due to the hydrophobic interaction between the tail groups of adsorbed surfactant molecules with the surface, the hydrophilic head groups of adsorbed surfactant molecules are detached from the surface (shown as stage III (a) in Figure 1-8) and because of the further adsorption of surfactant molecules and the hydrophobic interaction between adsorbed surfactants, the adsorbed surfactant molecules form monolayer or hemimicelle with hydrophobic tail groups in contact with the surface and hydrophilic head groups pointing towards the solution (shown as stage IV after stage III (a) in Figure 1-8). The hydrophobic interaction between the adsorbed surfactant molecules and the surface is strong. However, for hydrophilic surfaces, there is an attraction between hydrophilic head groups of adsorbed surfactant molecules and the surface, which leads to the detachment of hydrophobic tail groups of adsorbed surfactant molecules (shown as III (c) in Figure 1-8). Further adsorption of surfactant molecules and the hydrophobic interaction between adsorbed surfactants result in the formation of reversed monolayer with hydrophilic head groups in contact with the surface and hydrophobic tail groups pointing towards the solution (shown as stage IV after stage III (c) in Figure 1-8). In particular, for this reversed structure, more surfactant molecules are further adsorbed and the surface aggregates keep growing to form bilayer or admicelle as shown in stage V of Figure 1-8. In fact, this further growth of surface aggregates is also due to the hydrophobic interactions between surfactant molecules and it has been suggested by Levitz (2002) that the non-ionic surfactant adsorption at hydrophilic surface is due to the strong lateral interaction between surfactant

molecules and the weak interaction between surfactants and the surface. Furthermore, for surfaces of intermediate hydrophobicity, the adsorbed surfactant molecules remain flat on the surface as shown in III (b) of Figure 1-8.

1.4 Surface Mechanical Properties of Air-liquid Interfaces in Foams

As discussed in section 1.1, stabilising agents such as surfactants and particles are applied to modify the surface properties in order to stabilise foams. In particular, it is the surface mechanical properties are explored in this thesis to understand their effects on foam stability. Thus, it is pertinent to review the mechanical properties of gas-liquid interfaces including surface tension and surface rheological properties (such as surface elasticity, surface dilatational viscosity and Gibbs elasticity) herein. Firstly, the principles and measuring methods of surface tension are reviewed. Secondly previous work on surface rheological properties and the problem in terms of relating surface rheological properties (referring specifically to properties of surface dilatational rheology) to foam stability will be reviewed.

1.4.1 Surface Tension

1.4.1.1 Fundamental of Surface Tension

As described in section 1.3, the surface free energy is the minimum amount of work required to create that surface. According to this, the surface free energy per unit area is referred to as the surface tension (Rosen *et al.*, 2012). In order to understand the origin of surface tension, a gas-liquid interface is considered

(see Figure 1-9 in which, for example, an air-water interface is shown). In the bulk, a water molecule is surrounded and attracted by many other molecules through van der Waals forces, which are isotropic. However, for a water molecule in the region of the interface, the attraction forces are no longer isotropic since the contribution of the molecules in the bulk is larger than that of molecules near the surface. Due to the imbalanced forces, the air-water surface is forced to contract and comes under tension, which is known as surface tension (Schramm, 2005).

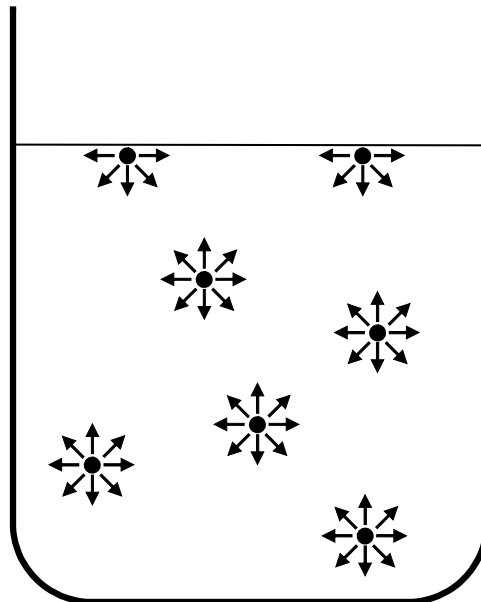


Figure 1-9. Schematic representation of the attractive forces between water molecules at the air-water interface and in the bulk.

Since the surface seeks to minimise its surface area, the bubbles of gas tend to adopt an approximately spherical shape, which reduces the total surface free energy. Across the curved surface, surface tension causes a pressure difference between the inside and outside of the bubble, which can be written as

$$\gamma \left(\frac{1}{R_1} + \frac{1}{R_2} \right) = \Delta P \quad (1-4)$$

where γ is surface tension; R_1 and R_2 are the principal radii of curvature; ΔP is the pressure difference across the gas-liquid interface. This is the Young-Laplace equation, which relates the pressure difference across an interface to the curvature of the interface and the surface tension (Joos, 1999). Furthermore, it is worth stressing that surface tension is a dynamic property that surface tension of a freshly created gas-liquid interface of a surfactant solution will decrease with time until reaching the equilibrium value (Eastoe *et al.*, 2000). The period of this time can vary from milliseconds to days depending on the surfactant type and the concentration of surfactant solution.

There are many methods available for the measurement of surface tension and some commonly used methods rely on the Young-Laplace equation, such as the maximum bubble pressure method, the spinning droplet method and the pendant droplet method (Schramm, 2005). In addition, there are other important methods for measuring surface tension including the Wilhelmy plate, du Noüy ring, and droplet weight and volume method (Eastoe *et al.*, 2000). Among all these methods, the pendant droplet method has been one of the most extensively developed techniques for surface tension measurement (Berry *et al.*, 2015), since this method can measure not only the static value of surface tension (time-invariant value) but also the dynamic surface tension, whereas the most of other methods can only measure the static value of surface tension, such as the Wilhelmy plate and du Noüy ring method (Schramm, 2005). In the current work of this thesis, the pendant droplet method is applied to measure dynamic surface tension of different surfactant solutions and the equilibrium surface tension will be obtained by linear

extrapolation of the dynamic surface tension to infinite time *via* the method of Makievski *et al.* (1997). Thus, in the next subsection, the principle of pendent droplet method for measuring surface tension and the factors that influence the accuracy of surface tension measurement using the pendent droplet method will be discussed.

1.4.1.2 Pendent Droplet Method for Measuring Surface Tension

The central idea of the pendent droplet method is that the droplet shape is related to surface tension and therefore surface tension can be obtained by consideration of the droplet shape (Saad *et al.*, 2016). In fact, the pendant droplet shape is governed only by surface tension and gravity. Surface tension tends to make a droplet spherical whereas gravity tends to elongate a pendant droplet. A pendant droplet can be maintained at the tip of the capillary due to the balance between the force proportional to surface tension and gravitational force. Mathematically, the balance between the force proportional to surface tension and gravitational force conforms to the Young-Laplace equation (eq. 1-4). Because the only external force herein is gravitational force, the pressure difference can be written as

$$\Delta P = \Delta P_0 - \Delta \rho g z \quad (1-5)$$

where ΔP_0 is a reference pressure difference at the apex of the droplet; $\Delta \rho$ is the density difference between the droplet phase and continuous phase; g is the gravitational acceleration; z is the vertical height of the given point on the droplet surface to the apex of the droplet. Thus, the shape of the pendant drop can be determined for known values of surface tension, density difference,

gravitational acceleration and the radius of curvature at the apex of the droplet by integration of the Young-Laplace equation. The converse process that determination of surface tension from the shape of the pendant droplet is how the pendant droplet method works. Typically, this method relies on best fitting theoretical droplet curves obtained from numerical integration of the Young-Laplace equation to the experimental measured shape of the pendant droplet.

Although the theory of the pendant droplet method, as briefly explained above, is straightforward, the process of computation of the surface tension is more protracted and consists of 3 steps. The first step is image analysis in which the experimental profile can be detected from a captured image and subsequently the initial value of the radius of curvature at the apex of the droplet can be obtained. The second step is to generate the theoretical droplet profiles by numerical integration of the Young-Laplace equation for given values of surface tension, density difference, gravitational acceleration and the radius of curvature at the apex of the droplet. Here, density difference and gravitational acceleration are known physical properties; the radius of curvature at the apex of the droplet can be obtained from the image analysis; the surface tension requires an initial estimate. Del Rio *et al.* (1997) have demonstrated that the efficacy of the method was insensitive to the quality of the initial estimate. The third step is an optimisation process to find the best fit of the theoretical curves to the experimental profile to identify the optimal surface tension, which requires an iterative solution. Besides surface tension, other interfacial properties including surface volume, surface area and radius of curvature at the apex can be obtained as well using the pendant droplet method.

According to the process of computation of surface tension in the pendant droplet method, there are four main ‘internal’ factors that influence the accuracy of surface tension measurement using the pendant droplet method, which are: 1. The digital image quality which is determined by the hardware of drop shape analyser including the digital camera and the illumination, 2. The image analysis technique which detects the outline of the droplet, 3. The numerical algorithm of the Young-Laplace equation to obtain theoretical profile, and 4. The optimization technique to find the best fit of the theoretical Laplacian curves to the experimental profile. Much research has been carried out in terms of these ‘internal’ factors to improve the accuracy of surface tension measurement by the pendant droplet method: Hoorfar *et al.* (2004, 2006) have extensively studied the effect of image quality on determination of surface tension. They have demonstrated that problems with hardware performance (including light source, microscope lens and digital camera) could cause errors in the surface tension determination. Different image analysis techniques have been used in the pendant droplet method (Canny, 1986; Cheng *et al.*, 1990; Smith *et al.*, 1997; Zuo *et al.*, 2004; Zholob *et al.*, 2007; Kalantarian *et al.*, 2011, 2013). Saad *et al.* (2011) have compared the surface tension values obtained by using these different image analysis techniques. They have demonstrated that the outline detection technique did not have a significant effect on surface tension results. Several numerical algorithms and various optimisation techniques have been employed in the pendant droplet method (Nelder *et al.*, 1965; Rotenberg *et al.*, 1983; Del Rio *et al.*, 1997; Alvarez *et al.*, 2009). Saad *et al.* (2016) has reviewed these numerical algorithms and optimisation techniques, and it was demonstrated

that the choice of numerical algorithms and optimisation techniques only had a considerable effect on the computation time rather than the accuracy of surface tension determination. It appears that the development of image analysis technique, numerical algorithm and optimisation technique in the pendant droplet method itself cannot significantly further increase the accuracy of the technique.

In addition to these so-called ‘internal factors’ that affect the accuracy of surface tension measurement of the pendant droplet method itself, many ‘external factors’ such as experimental parameters can also affect the repeatability, precision and therefore accuracy of surface tension measurement. The effect of droplet volume on the precision and accuracy of surface tension measurement has been observed and studied by several researchers (Lin *et al.*, 1995, 1996; Morita *et al.*, 2002; Ferrera *et al.*, 2007). It has been found that the accuracy of measured surface tension was dependent upon the droplet volume; the larger the droplet volume, the more accurate the surface tension obtained (Lin *et al.*, 1995, 1996). Generally, it was pointed out by Saad *et al.* (2011) that the droplet volume should be large enough to produce well-formed droplet, which could increase the accuracy of surface tension measurement. Another ‘external factor’ that can influence the accuracy of surface tension measurement is the significant change of surfactant solution concentration in the produced droplet over time. Berry *et al.* (2015) has investigated the effect of evaporation on surfactant solution concentration and therefore the surface tension measurement. It was demonstrated that evaporation caused a local increase in concentration within the droplet over time and therefore a decrease

in surface tension. Furthermore, the effect of trace amounts of highly surface-active impurities on the equilibrium surface tension measurement of main surfactant component has been noticed and explored (Mysels, 1986; Vollhardt *et al.*, 1984, 1990). The presence of highly surface-active impurity in a surfactant solution is normally due to the synthesis or hydrolysis of a surfactant (Lunkenheimer *et al.*, 2004; Fainerman *et al.*, 2010). For sodium alkyl sulfate surfactants, the most common and inevitable impurities are alcohols (for instance, dodecanol as impurity in sodium dodecyl sulfate), which are caused by synthesis or hydrolysis process (Vollhardt *et al.*, 1990, 2000). Mysels (1986) have demonstrated that the presence of dodecanol in sodium dodecyl sulfate (SDS) solutions caused a continuous reduction in the dynamic surface tension curve at long time and ascribed this phenomenon to the relatively rapid adsorption of SDS and the relatively slow adsorption of dodecanol. The dynamic surface tension results of SDS solution (1.788 g/L) at different stages of purification as a function of time obtained by Mysels (1986) are shown in Figure 1-10.

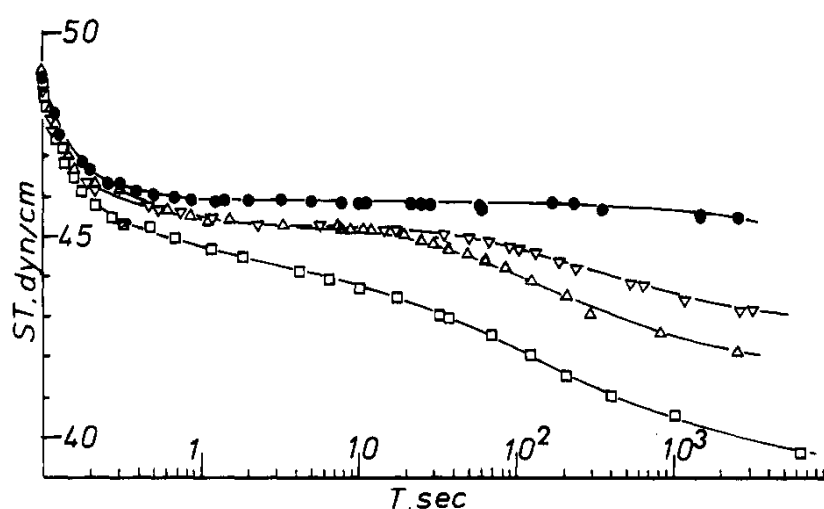


Figure 1-10. Dynamic surface tension of SDS solution (1.788 g/L) at different stages of purification as a function of time. (\square) bulk solution, (\triangle) first-stage purification, (∇) second-stage purification, and (\bullet) third-stage purification. Adapted from Mysels (1986).

Vollhardt *et al.* (1984, 1990) have observed the significant effect of trace amounts of highly surface-active alcohols on the equilibrium surface tension-concentration isotherms of sodium alkyl sulfate solutions and interpreted this observation as a result of the complex adsorption behaviour of the two-component system. In fact, the co-adsorption behaviour of SDS and dodecanol mixtures at the air-water interface (Lu *et al.*, 1995; Vollhardt *et al.*, 2000; Fainerman *et al.*, 2001) and at hydrophobic surfaces (Bain *et al.*, 1994; Ward *et al.*, 1997) has been explored. Lu *et al.* (1995) have demonstrated that the adsorption of SDS at the air-water interface was enhanced by the presence of dodecanol when the SDS concentration was far below the CMC, whereas at the SDS concentration above the CMC, the adsorption of SDS was impaired. Ward *et al.* (1997) have compared the adsorption isotherms of SDS and dodecanol mixtures at solid-water and air-water interfaces, which demonstrated that the adsorption behaviour at different interfaces were similar and the adsorption isotherms at different interfaces shared a number of common features. However, most of the studies focused on the effect of trace amounts of surface-active impurities on equilibrium surface tension and the effect of trace amounts of surface-active impurities on dynamic surface tension has not been fully explored. Fang *et al.* (1992 a & b) have studied the dynamic surface tension of SDS and dodecanol mixtures and only confirmed that SDS and dodecanol adsorbed in different time domains. Therefore, in chapter 3 of this thesis, the effect of trace amounts of highly surface-active impurities on dynamic surface tension measurement using the pendent droplet method will be systematically investigated. It will be demonstrated that trace amounts of surface-active impurities can have an appreciable influence on

dynamic surface tension results and thus affects the accuracy of dynamic surface tension measurements with the pendent droplet method.

1.4.2 Surface Rheological Properties

Besides surface tension, surface rheological properties are another surface mechanical properties that are modified by the adsorption of surfactant, which are also important characteristics that affect foam evolution and foam stability (Kruglyakov *et al.*, 1997). Surface tension is believed to be related to foam stability since the surfactant solutions with smaller surface tension produces more stable foam (Kanokkarn *et al.*, 2017). However, foam stability cannot solely be explained by the reduction of surface tension, as foams comprising of surfaces of equal tension do not necessarily exhibit the same stability (Stubenrauch *et al.*, 2004; Santini *et al.*, 2007). Since surface rheological properties also play an important role in foam stability (Kanner *et al.*, 1969), the previous work about surface rheological properties in the context of relating to foam stability is briefly reviewed in this subsection.

Surface rheology deals with the response of surfaces to external perturbations (Miller *et al.*, 2009), which has been widely studied since its important relevance in many industrial applications including foaming, oil recovery and high-speed coating (Miller *et al.*, 2010). The main types of external perturbation of a surface are shear (i.e. where the shape of an element of surface changes at constant surface area) and dilatation (i.e. where there is a change in area of a surface element but keeps the shape constant), which are induced by shear and dilatational stresses respectively (Ravera *et al.*, 2010).

Thus, the study of surface rheology can be separated into surface shear rheology and surface dilatational rheology (Jaensson *et al.*, 2018).

1.4.2.1 Surface Shear Rheology

Firstly, surface shear rheology is introduced. It is worth stressing that surface shear rheology is different with surface dilatational rheology and the comments about surface shear rheology are not relevant to surface dilatational rheology (which is one of the major concerns in this thesis). For surface shear rheology, in order to characterise the pure viscous (Newtonian) behaviour of ideal liquid-like surfaces, the resistance of an ideal liquid-like surface to shear deformation is interpreted by introducing a surface shear viscosity μ_s , which is characterised by

$$\sigma_{xy} = \mu_s \frac{du_{xy}}{dt} \quad (1-6)$$

where x and y define a plane which can be termed as xy -plain; σ_{xy} is the shear stress in the xy -plain, which is a tensor; u_{xy} is the applied shear deformation in the xy -plain and du_{xy}/dt is the rate of shear deformation. As indicated in eq.1-6, for the pure viscous (Newtonian) behaviour of ideal liquid-like surfaces, shear stress is proportional to the rate of shear deformation and the proportionality factor is the surface shear viscosity (Guzmán *et al.*, 2018). However, it is noted that for some solid-like surfaces, such as surfaces with adsorption of insoluble lipids and polymers, surface shear viscosity is not sufficient to describe the surface response to shear stress, as an elastic behaviour (which can be described by the Hook's law) is observed (Karbaschi

et al., 2014). Thus, a surface shear elastic modulus G is introduced as the proportionality factor between the shear stress and the applied deformation, which is written as

$$\sigma_{xy} = Gu_{xy} \quad (1-7)$$

However, in the case of liquid-like surfaces with soluble adsorption layers formed by low molecular weight surfactants, the surface shear elastic modulus is zero and thus it is not taken into consideration as a characteristic property for surface shear rheology (Langevin, 2014). Therefore, in terms of the gas-liquid interface adsorbed with surfactants, surface shear viscosity is adequate to completely describe surface shear rheology. In order to measure surface shear viscosity, various techniques have been employed which can be classified as indirect and direct methods (Krägel *et al.*, 2010). The indirect techniques analyse surface velocity profiles by using tracer particles, whereas the direct techniques determine the displacement or torque of a measuring probe located in the interface. However, it is noted that values of surface shear viscosity obtained by different methods show inconsistency. It has been pointed out by Stevenson (2005) that there was considerable difference in the values of shear viscosity of surfaces stabilised by soluble surfactants obtained by different methods. This difference was ascribed by Stevenson (2005) to the fact that, for soluble surfactants, only apparent surface shear viscosity could be measured by these methods and the measurement of apparent shear viscosity was experiment-dependent. Much research has been performed to correlate surface shear viscosity to foam stability and it has been found that surface shear viscosity affected foam stability (Edwards *et al.*, 1991). However, it has

also been pointed out by Edwards *et al.* (1991) that foam stability was more dependent upon surface dilatational rheology than surface shear rheology. In fact, for gas-liquid surfaces with soluble adsorption layers formed by low molecular weight surfactants, the response of surface to dilatation dominates over the response of surface to shear, as surface shear viscosity is much smaller than surface dilatational viscosity (Karbarchi *et al.*, 2014; Langevin 2014). Therefore, it is necessary to correlate foam stability to surface dilatational rheology. In this thesis, only surface dilatational rheology will be considered and surface shear rheology is not studied. In particular, the surface rheological properties discussed subsequently in this thesis are only those of dilatational deformation.

1.4.2.2 Surface Dilatational Rheology

Surface dilatational rheology is characterised as a surface dilatational viscoelasticity (Liggieri *et al.*, 2010), which is a complex quantity and consists of real and imaginary parts that represent elastic and viscous responses respectively. The elastic component is known as surface elasticity which describes the elastic energy stored in the surface and the viscous component is known as surface dilatational viscosity which describes the dissipative process within the surface due to the interaction with the adjacent bulk solutions (Mendoza *et al.*, 2014). The mathematical equations to describe surface dilatational rheology will be derived from first principles in chapter 2 as it is one of the main studying objectives of this thesis and needs to be fully understood. The surface rheological properties (including surface elasticity and surface dilatational viscosity) can be obtained by different methods

including Langmuir troughs (Noskov, 2002), surface light scattering (Noskov *et al.*, 2003) and oscillating pendent droplet/bubble (Kovalchuk *et al.*, 2002, 2004, 2005). Revera *et al.* (2010) have reviewed the experimental techniques for surface rheological properties and demonstrated that the oscillating pendent droplet/bubble method was especially effective due to the fast data acquisition and the data interpretation under dynamic conditions, which improved the accuracy of surface rheological property measurement. Shrestha *et al.* (2008) have performed the oscillating bubble method to measure surface dilatational elasticity of mixed surfactant/protein systems. The variation of modulus of surface dilatational visco-elasticity as a function of oscillation frequency for aqueous sodium caseinate system at different concentrations obtained by them is shown in Figure 1-11. They have demonstrated that surface elasticity decreased with increasing surfactant concentration and then remained approximately constant, which has been ascribed by them to the fact that larger surfactant concentration results in larger surface excess and thus surface tension changes less appreciably compared to surface area in response to the surface expansion, which leads to the decrease of surface elasticity.

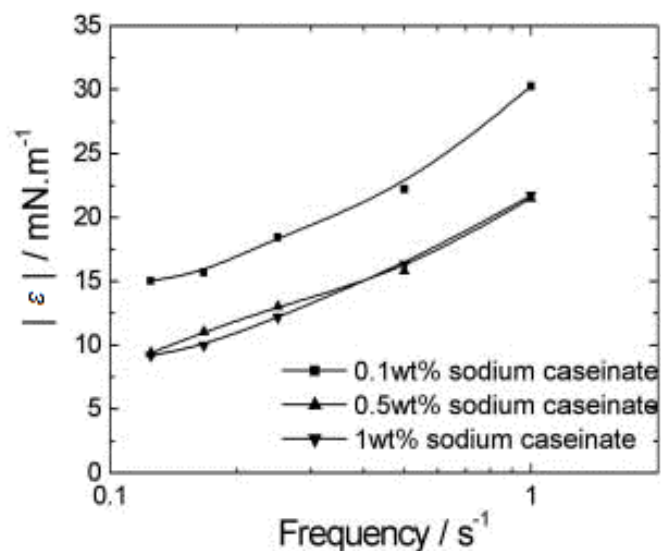


Figure 1-11. Variation of modulus of surface dilatational visco-elasticity as a function of oscillation frequency for aqueous sodium caseinate system at different concentrations. Adapted from Shrestha *et al.* (2008)

The typical results of surface mechanical properties including equilibrium surface tension, surface elasticity, surface dilatational viscosity and Gibbs elasticity of some common surfactants and surfactant-particle systems in literature are shown in Table 1-2.

Table 1-2. The typical results of surface mechanical properties including equilibrium surface tension, surface elasticity, surface dilatational viscosity and Gibbs elasticity of some common surfactants and surfactant-particle systems in literature. These data are obtained from published graphs and therefore should be considered as approximate values.

Samples	Concentration (g/L)	Equilibrium surface tension (mN/m)	Surface elasticity (mN/m)	Surface dilatational viscosity (mN·s/m)	Gibbs elasticity (mN/m)	Investigator
	0.288 (in 0.584 g/L NaCl)	45.00	—	—	—	Fainerman <i>et al.</i> (2010)
	0.288	64.00	—	0.0041 (intrinsic)	25.50	
SDS	0.865	49.00	—	0.0037 (intrinsic)	32.50	Wantke <i>et al.</i> (2003)
	1.730	39.00	—	0.0079 (intrinsic)	20.50	
	2.307	39.50	—	—	—	

	0.317	62.50	—	—	—	
Sodium tridecyl sulfate	0.605	52.00	—	—	—	Varga <i>et al.</i> (2007)
	1.267	38.00	—	—	—	
	0.617	—	2.00 (800 Hz)	0.0131 (800 Hz)	—	Monroy <i>et al.</i> (1998)
	0.925	65.00	4.00 (800 Hz)	0.0194 (800 Hz)	—	
DTAB	2.775	45.00	10.00 (800 Hz)	0.0125 (800 Hz)	—	Espert <i>et al.</i> (1998); Monroy <i>et al.</i> (1998)
	6.167	38.00	3.50 (800 Hz)	0.0044 (800 Hz)	—	
	12.334	38.00	—	—	—	Espert <i>et al.</i> (1998);
	0.001	63.60	—	—	—	
	0.001 (with 1 wt% silica particle)	65.00	—	—	—	
	0.005	60.00	16.00 (0.04 Hz)	—	—	Hunter <i>et al.</i> (2009)
	0.043 (with 0.5 wt% silica particle)	—	19.50 (0.02 Hz)	—	—	
	0.045	46.00	—	—	—	
TX-100	0.065	—	11.00 (0.04 Hz)	0.0002 (intrinsic)	48.50	Hunter <i>et al.</i> (2009); Fruhner <i>et al.</i> (1999)
	0.065 (with 0.5 wt% silica particle)	—	15.60 (0.04 Hz)	—	—	Hunter <i>et al.</i> (2009)
	0.097	—	—	0.0005 (intrinsic)	51.10	
	0.162	—	—	0.0024 (intrinsic)	55.00	Fruhner <i>et al.</i> (1999)
	0.194	33.00	—	—	—	Hunter <i>et al.</i> (2009)

The values and descriptions in brackets of surface elasticity and surface dilatational viscosity indicate the oscillation frequency of the measurement of surface rheological properties.

Many attempts to correlate foam stability to surface dilatational rheology have been reported and reviewed by Langevin (2000), which demonstrated that foam stability was closely related to surface dilatational rheology. However, studies that have attempted to explore the dependency of foam stability upon surface rheological properties have tended to suffer from the deficiency that the latter have not been varied independently of surface tension, so there is a possibility that the surface rheological properties have acted as proxies for surface tension. For instance, Fruhner *et al.* (1999) have measured surface rheological properties and foam stability of several surfactant solutions at different concentrations. They have found that foam stability increased with increasing surface dilatational viscosity. However, this observation could possibly be explained by noting that increased concentration results in a reduction of surface tension, although other factors may also have played a role. Similar problems were also manifest in the research conducted by Wang *et al.* (2016) and Hofmann *et al.* (2017) in that they have changed surface tension and surface rheological properties simultaneously when measuring foam stability of different surfactant solutions. Thus, it is difficult to determine which surface property (or properties) is (or are) truly responsible for the increased foam stability. In this thesis, in order to link surface rheological properties with foam stability, the equilibrium surface tension of different surfactant solutions will be maintained approximately at the same value, thereby enabling the surface rheological properties to be adjusted independently of surface tension.

1.5 Particle-stabilised Foams

As described in section 1.1, foam stability can be promoted by applying appropriate solid particles (Horozov, 2008; Kruglyakov *et al.*, 2011) and particle-stabilised foam with premium stability is useful in many industrial applications such as enhanced oil recovery and froth flotation (Bournival *et al.* 2015; Singh *et al.*, 2015). Since the effect of particles on foam stability and surface mechanical properties is another objective of this thesis (as described in subsection 1.1.2), the fundamental of particles is introduced and the previous work about the stability of particle-stabilised foams is reviewed in this section.

1.5.1 Fundamental of Particles

1.5.1.1 Behaviour of Particles in Bulk Solutions

The system of dispersed particles (the diameter of a particle is approximately between 1 nm and 1 μm) in a bulk solution is considered as a type of colloidal dispersions (Shaw, 1991), which is known as a two-phase system that the dispersed phase is suspended in the continuous phase (emulsion and foam are also two common types of colloidal dispersions). One of the most important characteristics of colloidal dispersions is the substantial amount of interfacial area, which indicates the large interfacial energy of colloidal dispersions. Due to this, most colloidal dispersions are considered as thermodynamically unstable and thus in the case of dispersed particles in bulk solutions, the dispersed particles tend to combine together to form large aggregates to reduce the interfacial energy (Hunter, 1993). In fact, the particle aggregation is due to

the interaction between these particles induced by Brownian motion of colloidal particles (Evertett, 1988), which is the random movement of these particles driven by their thermal energy (Einstein, 1905). The interaction between colloidal particles includes attractive force (i.e. van der Waals force) and repulsive force (i.e. electrostatic repulsive force), and the balance between van der Waals attraction and electrostatic repulsion determines the stability of colloidal dispersion which can be characterised by the aggregation tendency of colloidal particles. Therefore, the overall interaction energy between colloidal particles can be introduced by combining the van der Waals attraction energy and the electrostatic repulsion energy, which is given as

$$E_i = E_a + E_r \quad (1-8)$$

where E_i is the overall interaction energy; E_a is the attractive energy; E_r is the repulsive energy between colloidal particles (Derjaguin *et al.*, 1941; Verwey *et al.*, 1948). It has been demonstrated by Derjaguin *et al.* (1941) and Verwey *et al.* (1948) that the overall interaction energy between colloidal particles was a function of the distance between colloidal particles and an energy barrier that colloidal particles must overcome to aggregate existed. This energy barrier results from the dominant role of repulsive force at intermediate distance between colloidal particles. If colloidal particles have sufficient energy to overcome this energy barrier, they approach to each other and enter into the small distance domain, where attractive force dominates and causes irreversible aggregation. Whereas if colloidal particles only have limited energy and remain at large distance domain, although the repulsive force between

colloidal particles is still smaller than the attractive force between them, this only results in the weak and reversible aggregation between colloidal particles.

1.5.1.2 Particle Adsorption at Gas-liquid Interface

Besides the tendency to aggregate, colloidal particles can be surface active and adsorb at the gas-liquid interface to reduce the area of the gas-liquid interface and thus minimise the free energy of colloidal dispersions. Therefore, this adsorption behaviour of colloidal particles at gas-liquid interface is thermodynamically favourable and spontaneous (Binks *et al.*, 2006). A key parameter that influences the adsorption of colloidal particles at the gas-liquid interface is the hydrophobicity of particles, which determines the three-phase contact angle where solid particles and gas-liquid interface meet. A schematic representation of a solid particle at the air-water interface is shown in Figure 1-12.

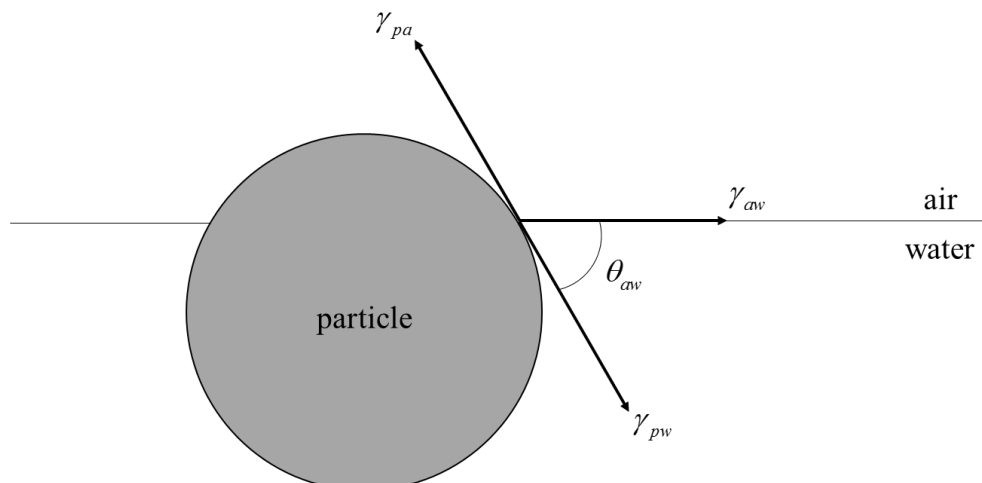


Figure 1-12. Schematic representation of a solid particle at the air-water interface. θ_{aw} represents the three-phase contact angle. γ_{pa} , γ_{pw} and γ_{aw} represent the surface tensions of particle-air, particle-water and air-water interfaces, respectively.

The three-phase contact angle increases with the increase of particle hydrophobicity that more hydrophilic particles demonstrate smaller three-

phase contact angle whereas more hydrophobic particles exhibit larger three-phase contact angle (Binks *et al.*, 2002). In emulsion systems (i.e. considering a particle at an oil-water interface), for a three-phase contact angle above 90°, the particle is considered as hydrophobic, whereas for a three-phase contact angle below 90°, the particle is considered as hydrophilic (Hunter *et al.*, 2008). However, in foam systems (i.e. considering a particle at a gas-liquid interface), the hydrophobic particle (the three-phase contact angle is above 90°) act as anti-foaming agent. In order to stabilise foams, the three-phase contact angle of the particles is kept below 90° (Horozov *et al.*, 2008). Thus, for foam-stabilising particles, particles with the three-phase contact angle close but below 90° are considered as ‘partially hydrophobic’, whereas particles with the three-phase contact angle well below 90° are considered relatively hydrophilic (Bournival *et al.*, 2015). This terminology is used throughout this thesis.

Unlike the reversible adsorption of surfactant molecules at gas-liquid interface, the adsorption of particles at a gas-liquid interface is irreversible as the free energy of particle detachment from gas-liquid interface is significant (Hunter *et al.*, 2008), and is given as

$$E = \pi r^2 \gamma (1 \pm \cos \theta)^2 \quad (1-9)$$

where E is the free energy of particle detachment from gas-liquid interface; r is the particle radius; γ is the surface tension of gas-liquid interface; θ is the three-phase contact angle. The plus sign in the brackets of eq. 1-9 represents removing particles from the interface to the air phase whereas the minus sign

represents removing particles from the interface to liquid phase. Hunter *et al.* (2008) have reviewed this particle detachment energy and pointed out that it was related with the stability of particle-stabilised foams. The stabilisation mechanism of particle-stabilised foams relied on the detachment energy of solid particle from the gas-liquid interface.

Furthermore, colloidal particles not only adsorb at the gas-liquid interface but also interact with each other at the gas-liquid interface as they interact in bulk solutions. The same forces (van der Waals force and electrostatic repulsive force) as described in the last subsection (subsection 1.5.1.1) also play a role on particle interaction at the gas-liquid interface. However, additional particle interaction forces (i.e. dipole repulsive force and capillary attractive force) are introduced due to the presence of gas-liquid interface which makes the interaction between particles at the gas phase are different with that at the liquid phase (Hunter *et al.*, 2008). Since the detachment energy of particles from gas-liquid interface are large, under a perturbation of the gas-liquid interface, the colloidal particles are more likely to move laterally along the gas-liquid interface rather than move into gas phase or liquid phase (Tambe *et al.*, 1994). Therefore, the particle interaction forces at the gas-liquid interface including van der Waals force, electrostatic repulsive force, dipole repulsive force and capillary attractive force are also important in the stability of particle-stabilised foams (Hunter *et al.*, 2008).

1.5.2 Stability of Particle-stabilised Foams

The stability of foams stabilised solely by particles or by mixtures of surfactants and particles are affected by many conditions including particle hydrophobicity, particle concentration and surfactant concentration (Hunter *et al.*, 2008). Among all these conditions, the particle hydrophobicity is of special importance as it determines the position of a particle whether adsorbing on the air-liquid interface or remaining in the liquid (Nguyen *et al.*, 2006). Silica particles are commonly used to stabilise foams and the effectiveness of adding silica particles to stabilise foams is dependent upon the hydrophobicity of the silica particles (Binks, 2002). The hydrophobic particles can attach to the surface of bubble to make the foam more stable. However, silica particles are inherently hydrophilic (Binks *et al.*, 2008) and therefore, silica particles must be hydrophobised before applying to stabilise foams. In fact, there are two methods to hydrophobise silica particles, which are *ex-situ* chemisorption method and *in-situ* physisorption method (Binks *et al.*, 2008). For the *ex-situ* chemisorption method, silica particles are hydrophobised by reacting surface silanol groups with different amounts of dimethyldichlorosilane groups (Binks *et al.*, 2000) or with different types of straight chain alcohols (Hunter *et al.*, 2009). For the *in-situ* physisorption method, silica particles are hydrophobised by adsorption of amphiphilic molecules. Binks *et al.* (2008) has applied cationic surfactants to adsorb on silica particles to modify the particle hydrophobicity. Furthermore, non-ionic surfactant (AlYousef *et al.*, 2018), switchable surfactant (Zhu *et al.*, 2014) and protein (Chen *et al.*, 2018) were also utilised to adsorb on silica particles to

change the particle hydrophobicity. In addition, the interactions between pre-hydrophobised silica particles (obtained with *ex-situ* chemisorption method) and non-ionic surfactants has been investigated by Hunter *et al.* (2009) and it was demonstrated by them that non-ionic surfactants adsorbed at pre-hydrophobised silica particles with head groups pointing towards solutions to render the particles more hydrophilic. Silica particles with modified hydrophobicity (obtained in both methods) have been widely used to stabilise foams by many researchers. However, the observations of optimum hydrophobicity of particle to stabilise foams obtained by various researchers are different. Binks *et al.* (2005) applied hydrophobic silica particles (obtained with *ex-situ* chemisorption method) solely to stabilise foams. It was shown by them that particles with intermediate hydrophobicity were capable of stabilising foams, which had 32% silanol groups remaining on the particle surface. However, Dickinson *et al.* (2004) also applied partially hydrophobic silica particles (obtained with *ex-situ* chemisorption method as well) to stabilise foams and demonstrated that there appeared to be an optimum particle hydrophobicity that gave maximum foam stability, which was approximately 20-33% silanol groups converted on the particle surface. It can be seen that the observed optimum degree of particle hydrophobicity to stabilise foams in these two works are different. Furthermore, Binks *et al.* (2008) have performed the experiments of foams stabilised by mixtures of silica particles and cationic surfactants (the *in-situ* physisorption method to hydrophobise particles) and demonstrated that the most hydrophobic particles obtained in the *in-situ* method yielded completely stable foams, which appears to be different with the observation in Binks *et al.* (2005) that the

intermediately hydrophobic particles (obtained in the *ex-situ* method) resulted in the best foam stability. Note that the method to hydrophobise silica particles applied in Binks *et al.* (2005) and Binks *et al.* (2008) are different, which may contribute to the different observations in these works. Furthermore, Zhu *et al.* (2015) have also performed the similar experiments of foam stabilised by mixtures of silica particles and cationic surfactants, however, their observations appeared to suggest that the most hydrophobic particles have not resulted in the best foam stability, which seems to be different with the observation in Binks *et al.* (2008). In fact, these researchers have performed different methods to produce foams including ‘hand shaking’ method (applied in Binks *et al.* (2005, 2008) and Zhu *et al.* (2015)), aerating method (also applied in Binks *et al.* (2005)) and pressure drop method (applied in Dickinson *et al.* (2004)), whereas foam stability was all quantified by measuring foam collapse over time in their works. However, none of these researchers controlled the relative humidity when producing foams and measuring foam stability, which has been demonstrated by Li *et al.* (2010, 2012) and Champougny *et al.* (2018) to be a determining factor in foam stability measurements. Thus, the results of foam stability obtained by these researchers are likely to be compromised and this could be the reason that the observations of optimum particle hydrophobicity to increase foam stability obtained by them are different. In this thesis, the stability of foams stabilised by mixtures of silica particles and surfactants will be measured by a more reproducible method that a constant environmental relative humidity are maintained during the measurement, and the optimum particle hydrophobicity to increase foam stability will be investigated in chapter 6.

In addition to the issue about the optimal particle hydrophobicity to produce most stable foams, the issue about the underlying reasons for enhanced stability of particle-stabilised foams has also drawn much attentions. It is admitted that the stability of foam produced from surfactants was correlated to surface mechanical properties including surface tension and surface rheological properties (Georgieva *et al.*, 2009). Therefore, the stability of particle-stabilised foams could also be related to the properties of surface with particles adsorbed (Safouane *et al.*, 2007). Some research has been performed to study the mechanical properties of surfaces with particle layers and correlate them to the stability of particle-stabilised foams. Wang *et al.* (2008) have studied the surface rheological properties of silica particle dispersions in the presence of cetyltrimethyl ammonium bromide (CTAB). It was demonstrated by them that the effect of silica particles on surface rheological properties was significant and the interaction between particles and surfactants played an important role in changing the surface mechanical properties. Hunter *et al.* (2009) have investigated the interactions between non-ionic surfactant and hydrophobic nanoparticles and their impact on foam stability. They have observed that surface elasticity of system containing particles was higher than that of system without particles. This observation of increased surface elasticity was ascribed by them to the reduction of available interfacial area for adsorption of free surfactant to the air-liquid interface due to the particle occupation. Safouane *et al.* (2007) have experimentally investigated the effect of particle hydrophobicity on the mechanical properties of surfaces with hydrophobic silica particle layers and it was showed that there was a strong influence of the particle hydrophobicity on the mechanical properties of

surfaces with particle layers. It was also suggested by them that the surface rheological properties were quite small and most likely not related to the stability of particle-stabilised foams. However, Cervantes Martinez *et al.* (2008) have been able to correlate surface mechanical properties with the stability of foams stabilised solely by particles. They argued that particle-stabilised foams became stable against coarsening when surface elasticity was greater than half of equilibrium surface tension. Stocco *et al.* (2009, 2011) have experimentally confirmed this argument and suggested it as a prediction criterion for determining whether particle-stabilised foams were stable or not against coarsening. In the experiments of Stocco *et al.* (2009, 2011), the values of surface elasticity were obtained by using oscillating bubble method which was performed at the oscillating frequency of 1 Hz. However, it was known that surface elasticity were dependent upon oscillating frequency and the smaller oscillating frequency resulted in the smaller surface elasticity (Liggieri *et al.*, 2010). Thus, surface elasticity varies with the measuring oscillation frequency and this may cause above prediction criterion not always valid. In this thesis, it will be demonstrated in chapter 6 that stable particle-stabilised foams can be obtained without satisfying above prediction criterion. In addition, the relationship between stability of particle-stabilised foams and surface mechanical properties will also be described in chapter 6.

1.6 Thesis Structure

After reviewing the previous literature about the subjects of foam stability, surfactants, surface mechanical properties and particle-stabilised foams, the issue of accurate quantification of foam stability, surface tension and surface

rheological properties which compromises the investigation of the relationship between foam stability and surface mechanical properties has been noticed. In addition, with regard to foams stabilised by the mixtures of particles and surfactants, the effect of particles on foam stability and surface mechanical properties, as well as the link between stability of particle-stabilised foams and surface mechanical properties, requires further exploration. Thus, the topics about the measurement of surface rheological properties (chapter 2), the repeatability of dynamic surface tension measurement (chapter 3), the effect of relative humidity on foam stability measurement (chapter 4), the relationship between surface mechanical properties and foam stability (chapter 5) and particle-stabilised foams (chapter 6) are covered in the later chapters of this thesis. The overall approach that applied in this thesis to achieve the aims and objectives as described in subsection 1.1.2 is shown in Figure 1-13.

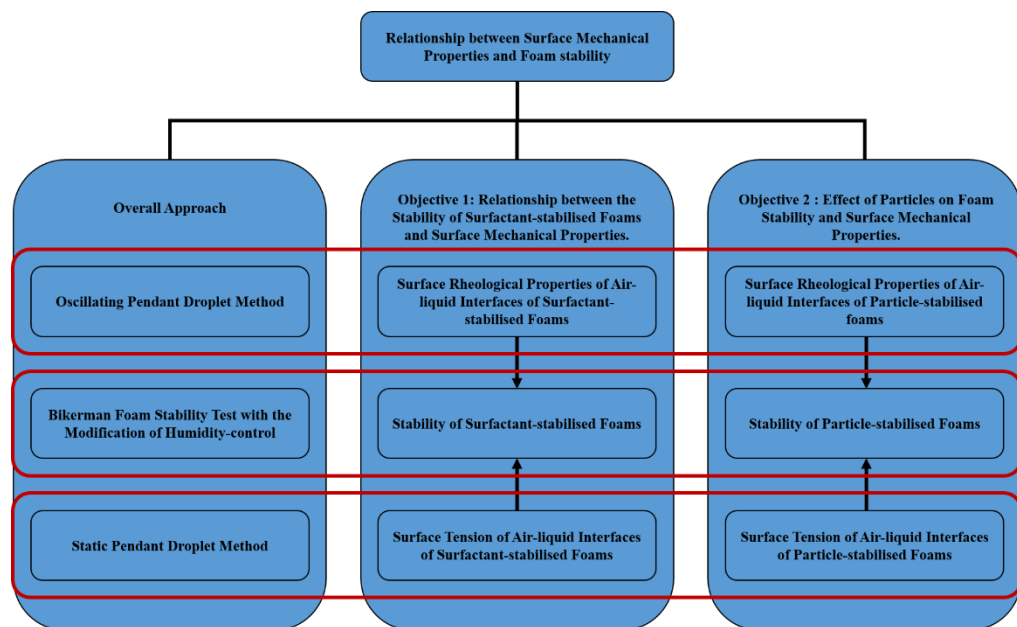


Figure 1-13. The overall approach that applied in this thesis

In chapter 2, the method to obtain surface rheological properties is studied. Firstly, theoretical equations that describe the oscillatory mechanical

properties of a gas-liquid interface are derived from first principles. Subsequently, measurements of surface rheological properties using the oscillating pendent droplet method are described to illuminate the dependency of surface rheological properties on oscillation frequency and amplitude.

In chapter 3, the repeatability of dynamic surface tension measurements of ionic surfactant solution using the static pendant droplet method is investigated. Firstly, an unexpected and repeatable systematic change of dynamic surface tension of sodium alkyl sulfate solutions between different trials is described. Secondly, this unexpected systematic change of dynamic surface tension between different trials is attributed to the presence of trace amounts of highly surface-active impurities and this statement is verified by performing dynamic surface tension measurement of ionic surfactant solution without highly surface-active impurity. Finally, with respect to the pendent droplet method, the way to determine the dynamic surface tension of ionic surfactant solutions with highly surface-active impurity is explored by performing statistical analysis.

In chapter 4, measurements of foam stability at different environmental relative humidities are performed to confirm and extend the observation about the dependency of foam stability upon environmental relative humidity. Furthermore, in chapter 5, foam stability is correlated to surface rheological properties under the condition that the effect of surface tension on foam stability is eliminated. Firstly, different surfactant solutions with approximately the same equilibrium surface tension are obtained. Then, the measurements of foam stability and surface rheological properties of these

surfactant solutions are performed to correlate foam stability with surface rheological properties.

In chapter 6, the stability of foams stabilised by the mixtures of particles and surfactants, as well as the relationship between surface mechanical properties of air-liquid interfaces in particle-stabilised foams and the stability of particle-stabilised foams, is investigated. Firstly, the effect of silica particles (at a fixed particle concentration) on stability of foams stabilised by cationic surfactants at different surfactant concentrations is explored. Secondly, the effect of particle concentration on stability of foams stabilised by mixtures of cationic surfactants and silica particles is studied. Thirdly, the stability of particle-stabilised foams and surface mechanical properties of air-liquid interfaces in particle-stabilised foams are correlated.

Chapter 2 Measurement of Surface Rheological Properties

2.1 Introduction

Surface rheological properties including surface elasticity, surface dilatational viscosity and Gibbs elasticity play a very important role in the dynamic behaviour of surfaces. Since one of the main objectives of this thesis (as described in subsection 1.1.2) is to relate foam stability to surface rheological properties and surface tension to explore which surface property dominates foam stability, the method of obtaining surface rheological properties has to be studied as a matter of priority. In this chapter, firstly, theoretical equations that describe the oscillatory mechanical properties of a gas-liquid interface are derived from first principles. Subsequently, measurements of surface rheological properties using the oscillating pendent droplet method are described to illuminate the dependency of surface rheological properties on oscillation frequency and amplitude.

2.2 Theoretical Derivation of Surface Rheological Properties

During the expansion of a surface with adsorbed surfactant, the presence of the adsorbed layer of surfactant results in a gradient in surface tension that can provide resistance to expansion, which is known as surface elasticity. In addition, the dissipative process of surfactant transport between the surface and the bulk causes a viscous response, which is quantified as surface dilatational viscosity. Therefore, the surface with adsorbed surfactant possesses a surface visco-elastic characteristic and this is defined by Lucassen-Reynders (1981) as

$$\varepsilon = \frac{d\sigma}{d \ln A} \quad (2-1)$$

where σ is the surface tension and A is the surface area. In fact, the surface visco-elasticity is a complex value that the real part ε_r is surface elasticity and the imaginary part ε_i is related to the surface dilatational viscosity μ_d , which is defined as

$$\mu_d = \frac{\varepsilon_i}{\omega} \quad (2-2)$$

where ω is angular frequency of oscillation. Note that the surface with adsorbed surfactant also exhibits resistance to shear. Hence, the surface exhibits surface shear viscosity as well as surface dilatational viscosity. However, the surface shear viscosity is expected to play little role in the behaviour of the surface in the situation that the strong coupling between dilatation and diffusion in the bulk of surfactant solutions (Georgieva *et al.*, 2009), as the surface shear viscosity is several orders of magnitude smaller than the surface dilatational viscosity (Monroy *et al.*, 1998). Note that even though different measurements of surface shear viscosity manifest large uncertainty (Stevenson, 2005), the surface shear viscosity is still much smaller than the surface dilatational viscosity. For instance, the largest value of surface shear viscosity of SDS solution at the concentration of 1.5 g/L that reviewed by Stevenson (2005) is 0.1 $\mu\text{N}\cdot\text{s}/\text{m}$, whilst the surface dilatational viscosity of SDS solution at similar concentration is 8.8 $\mu\text{N}\cdot\text{s}/\text{m}$ (Wantke *et al.*, 2003).

With the expansion of the surface with adsorbed surfactant, mass transfer occurs between the gas-liquid interface and the bulk solution. The surface

elasticity of the surfactant solution at time short enough so that interface-bulk exchange has not happened yet is called Gibbs elasticity and it is defined by Joos (1999) as

$$\varepsilon_0 = -\frac{d\sigma}{d\Gamma} \Gamma_e \quad (2-3)$$

where Γ is surface excess (also known as surface concentration) which is the surfactant concentration at the gas-liquid interface and Γ_e is equilibrium surface excess.

In fact, surface visco-elasticity and Gibbs elasticity can be related and surface visco-elasticity can be introduced as a function of the angular frequency of oscillation. An interface with adsorbed surfactant which is subjected to small area compressions and expansions of a given angular frequency ω and amplitude A^* is considered herein. The resulting surface tension, oscillating with the same angular frequency ω , is measured. If the initial area is A_0 , the area as a function of time can be expressed in exponential form as

$$A = A_0 + A^* e^{i\omega t} \quad (2-4)$$

where A^* is the amplitude of surface area disturbance; t is the oscillation time; i is the unit imaginary number which satisfies $i^2 = -1$. As relative area disturbance are more important than the absolute area disturbance and the amplitude of area disturbance is very small, eq. 2-4 can be written as

$$\ln A = \ln A_0 + A' e^{i\omega t} \quad (2-5)$$

where $A' = \frac{A^*}{A_0}$. The periodic changes in area with an angular frequency ω

creates associated variation in the surface excess

$$\Gamma = \Gamma_e + \Gamma^* e^{i(\omega t + \varphi)} \quad (2-6)$$

where Γ^* is the amplitude of the surface excess oscillations. Note that there is a phase angle φ between the area disturbances and the surface excess oscillations. In order to simplify mathematics, eq. 2-6 can be written as

$$\Gamma = \Gamma_e + \Gamma' e^{i\omega t} \quad (2-7)$$

where $\Gamma' = \Gamma^* e^{i\varphi}$, which is a complex quantity that represents the amplitude of the surface excess oscillations in the unit of $\text{mol}\cdot\text{m}^{-2}$. However, in the book of Dynamic Surface Phenomena of Joos (1999) (which is an important work in the research field of dynamic processes at interfaces), Γ' was defined as the amplitude of the surface tension oscillations, which is in the unit of mN/m . Since the units of Γ and Γ_e are both $\text{mol}\cdot\text{m}^{-2}$, if following the definition of Γ' in Joos (1999), there will be a dimensional inconsistency of eq. 2-7, which indicates that the definition of Γ' given by Joos (1999) is not correct. Therefore, in the remainder of the analysis in this section, the definition of Γ' given above will be used.

As a result of the surface excess oscillations, the bulk concentration also changes as

$$c = c_0 + H e^{-nz} e^{i\omega t} \quad (2-8)$$

where c_0 is equilibrium bulk concentration; H is a constant of integration; n is a variable and satisfies $n^2 = \frac{i\omega}{D}$, where D is diffusion coefficient; z is the distance from the interface, upon which the bulk concentration oscillations are dependent. The boundary condition for conservation of mass at the surface is

$$\frac{d\Gamma}{dt} + \theta\Gamma = D \left(\frac{\partial c}{\partial z} \right)_{z=0} \quad (2-9)$$

where θ is surface dilatation and it is defined as $\theta = \frac{d \ln A}{dt}$. Substitution of eqs. 2-5, 2-7 and 2-8 into eq. 2-9 gives

$$i\omega\Gamma'e^{i\omega t} + i\omega A'\Gamma_e e^{i\omega t} + i\omega A'\Gamma'e^{2i\omega t} = -DnHe^{i\omega t} \quad (2-10)$$

Note that in Joos (1999), instead of eq. 2-10, the substitution of equations that just described above gives

$$i\omega\Gamma'e^{i\omega t} + H\omega A'\Gamma_e e^{i\omega t} + H\omega A'\Gamma'e^{2i\omega t} = -DnHe^{i\omega t} \quad (2-11)$$

By comparison between eqs. 2-10 and 2-11, it can be seen that in the second and third terms of eq. 2-11, there should be an 'i' rather than an 'H'. In fact, this is caused by the incorrect calculation of differentiation $\frac{d \ln A}{dt}$ in Joos (1999). Therefore, in the following analysis, eq. 2-10 will be used.

In eq. 2-10, the higher harmonic term $i\omega A'\Gamma'e^{2i\omega t}$ can be neglected, as the amplitudes A' and Γ' are small and their product is even smaller. Therefore, eq. 2-10 can be simplified as

$$i\omega\Gamma' + i\omega A'\Gamma_e = -DnH \quad (2-12)$$

For a diffusion-controlled surfactant adsorption to an interface, there is equilibrium between the surface excess and the subsurface concentration, the relationship of which is called an ‘adsorption isotherm’. Note that the subsurface is an imaginary surface in the bulk solution with a thickness of several molecular diameters that directly next to the surface (Ward *et al.*, 1946). Since the fluctuations are small, the linear adsorption isotherm, i.e. the Henry’s law isotherm, can be applied herein, which is

$$\Gamma = K_H c \quad (2-13)$$

where K_H is the surface Henry’s law constant.

After association of eqs. 2-7, 2-8 and 2-13 gives:

$$\frac{c_s - c_0}{\Gamma - \Gamma_e} = \frac{H}{\Gamma'} = \frac{dc}{d\Gamma} = \frac{1}{K_H} \quad (2-14)$$

where c_s is subsurface concentration.

The constant of integration H can be eliminated between eqs. 2-12 and 2-14, thereby yielding the amplitude of the surface excess oscillations Γ' as a function of the amplitude of relative surface area disturbance A' :

$$\Gamma' = \frac{-i\omega A'\Gamma_e}{i\omega + Dn \frac{dc}{d\Gamma}} = -\frac{A'\Gamma_e}{1 + \frac{Dn}{i\omega} \frac{dc}{d\Gamma}} \quad (2-15)$$

Since the relaxation frequency ω_0 that related to the diffusion relaxation time is defined as

$$\omega_0 = D \left(\frac{dc}{d\Gamma} \right)^2 \quad (2-16)$$

Considering the definition of n as mentioned above and the relaxation frequency ω_0 , eq. 2-15 can be written as

$$\Gamma' = - \frac{A' \Gamma_e}{1 + \left(\frac{\omega_0}{i\omega} \right)^{1/2}} \quad (2-17)$$

In fact, the variation in surface excess due to periodic disturbance in surface area results in associated variation in surface tension, which can be written as

$$\sigma = \sigma_e + \sigma^* e^{i(\omega t + \varphi)} \quad (2-18)$$

The same mathematic simplification as mentioned above is also applied herein, thus eq. 2-18 can be simplified as

$$\sigma = \sigma_e + \sigma' e^{i\omega t} \quad (2-19)$$

where $\sigma' = \sigma^* e^{i\varphi}$, which is a complex quantity.

The amplitude of surface tension variations σ' is related to the amplitude of the surface excess oscillations Γ' :

$$\sigma' = \frac{d\sigma}{d\Gamma} \Gamma' = - \frac{d\sigma}{d\Gamma} \Gamma_e \frac{A'}{1 + \left(\frac{\omega_0}{i\omega} \right)^{1/2}} \quad (2-20)$$

Considering the definition of surface visco-elasticity ε and Gibbs elasticity ε_0 as given in eqs. 2-1 and 2-3, finally, eq. 2-20 becomes

$$\varepsilon = \frac{\varepsilon_0}{1 + \left(\frac{\omega_0}{i\omega}\right)^{1/2}} \quad (2-21)$$

In order to simplify eq. 2-21, ξ is introduced and defined by Joos (1999) as

$$\xi = \left(\frac{\omega_0}{2\omega}\right)^{1/2} \quad (2-22)$$

after rearrangement, eq. 2-21 becomes

$$\varepsilon = \frac{\varepsilon_0}{1 + \xi - i\xi} \quad (2-23)$$

Multiplying by the complex conjugate $(1 + \xi + i\xi)$, eq. 2-23 becomes

$$\varepsilon = \frac{\varepsilon_0(1 + \xi + i\xi)}{1 + 2\xi + 2\xi^2} = \frac{\varepsilon_0(1 + \xi)}{1 + 2\xi + 2\xi^2} + i \frac{\varepsilon_0\xi}{1 + 2\xi + 2\xi^2} \quad (2-24)$$

This equation was first derived by Lucassen and van den temple (1972a & b).

According to eq. 2-24, the real part ε_r (i.e. surface elasticity) and the imaginary part ε_i are

$$\varepsilon_r = \frac{\varepsilon_0(1 + \xi)}{1 + 2\xi + 2\xi^2}; \varepsilon_i = \frac{\varepsilon_0\xi}{1 + 2\xi + 2\xi^2} \quad (2-25)$$

Therefore, the modulus of visco-elasticity $|\varepsilon|$ and the phase angle φ between surface area disturbance and surface tension variation are given by

$$|\varepsilon| = (\varepsilon_r^2 + \varepsilon_i^2)^{1/2} = \frac{\varepsilon_0}{(1 + 2\xi + 2\xi^2)^{1/2}}; \tan \varphi = \frac{\varepsilon_i}{\varepsilon_r} = \frac{\xi}{1 + \xi} \quad (2-26)$$

It also follows that

$$\varepsilon_r = |\varepsilon| \cos \varphi; \varepsilon_i = |\varepsilon| \sin \varphi \quad (2-27)$$

According to eq. 2-1, the modulus of visco-elasticity can be calculated as the quotient of the amplitude of surface tension variation σ^* and the relative amplitude of surface area disturbance A' :

$$|\varepsilon| = \frac{\sigma^*}{A'} \quad (2-28)$$

Thus, these theoretical derivations provide a theoretical method to calculate surface rheological properties including surface elasticity, surface dilatational viscosity and Gibbs elasticity, which is applied in the oscillating pendent droplet method to obtain the values of surface elasticity and surface dilatational viscosity. In this current work, the oscillating pendent droplet method is applied to measure surface elasticity and surface dilatational viscosity of different surfactant solutions. Moreover, Gibbs elasticity is inferred from the results of surface elasticity and surface dilatational viscosity according to the mathematical description given above.

In fact, with the oscillating pendant droplet method, the amplitude of surface tension variation σ^* , the relative amplitude of surface area disturbance A' , the phase angle φ between surface area disturbance and surface tension variation, and the angular frequency of oscillation ω can be measured by the software

controlling the apparatus. Typical experimental results of surface tension variation and surface area disturbance obtained by the oscillating pendent droplet method are shown in Figure 2-1 as an example.

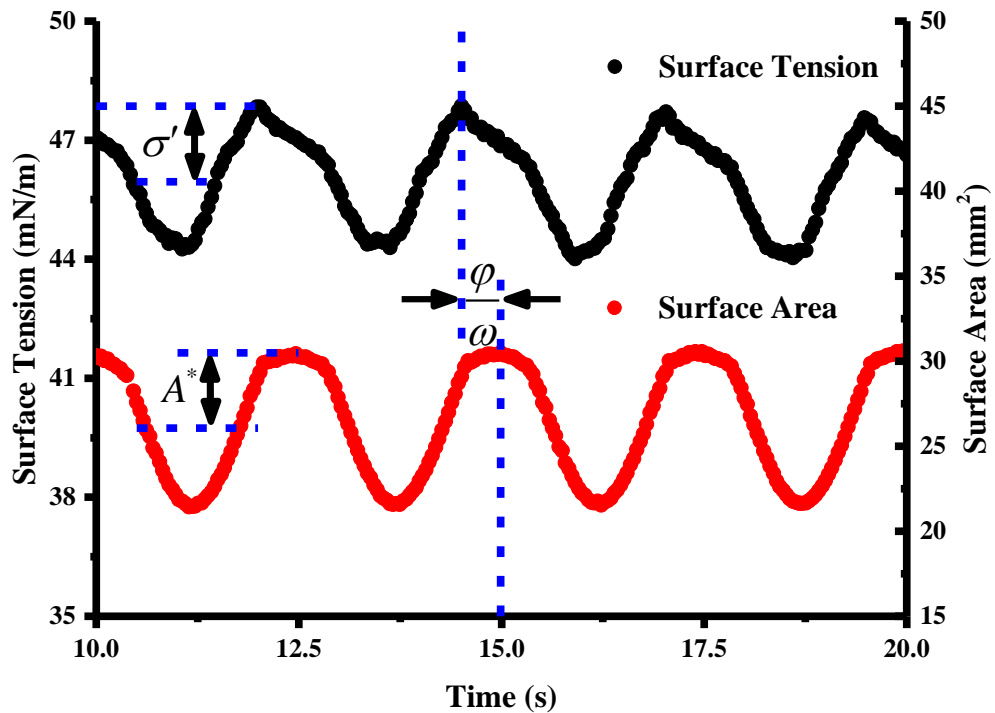


Figure 2-1. Typical experimental results of surface tension variation and surface area disturbance obtained by the oscillating pendent droplet method. These results are from surface rheological properties measurements of sodium dodecyl sulfate (SDS) solution at the concentration of 0.087 g/L (in 8.766 g/L NaCl aqueous solution) with the oscillation frequency and amplitude at 0.4 Hz and 0.25, respectively.

Via the values of these four parameters, surface elasticity and surface dilatational viscosity can be autogenously inferred according to eqs. 2-2, 2-27 and 2-28 by the software controlling the apparatus. Furthermore, Gibbs elasticity can be obtained through eq. 2-26. The flow chart of the oscillating pendant droplet method to obtain surface elasticity, surface dilatational viscosity and Gibbs elasticity is shown in Figure 2-2.

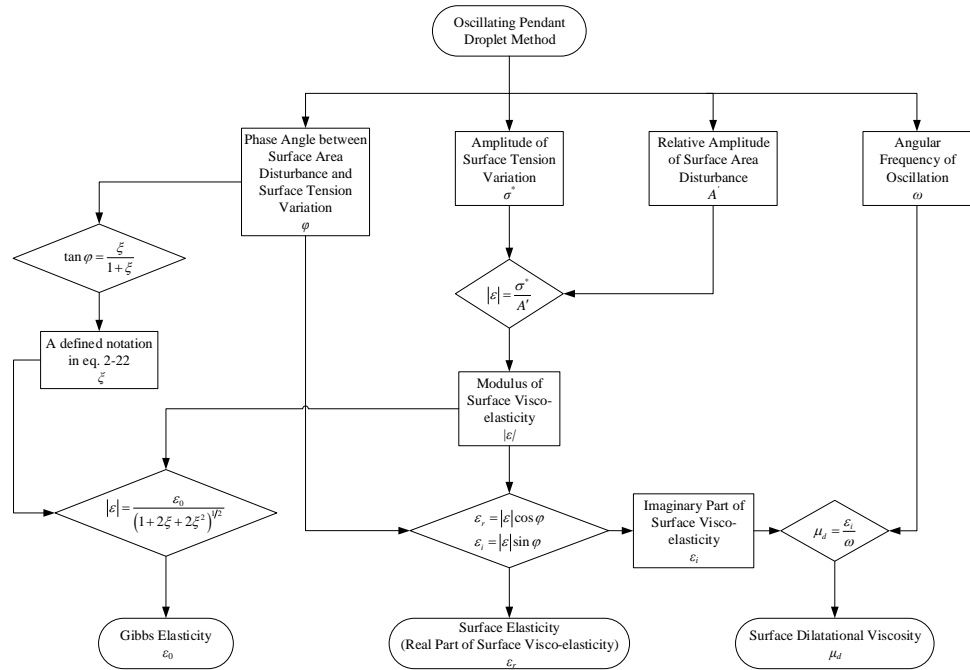


Figure 2-2. The flow chart of the oscillating pendant droplet method to obtain surface elasticity, surface dilatational viscosity and Gibbs elasticity

As can be seen from eqs. 2-1 and 2-21, surface visco-elasticity is related to the oscillation frequency and amplitude, and therefore, in the following sections (sections 2.3 and 2.4), measurements of surface rheological properties are performed to explore the dependency of surface rheological properties upon oscillation frequency and amplitude.

2.3 Experimental Details

The oscillating pendant droplet method is performed herein to measure surface rheological properties including surface elasticity and surface dilatational viscosity of sodium dodecyl sulfate (SDS) solution at the concentration of 0.087 g/L (in 8.766 g/L NaCl aqueous solution) with different oscillation frequencies and amplitudes. Note that this solution was used by the manufacturer of droplet shape analyser (Krüss, DSA100R) to test the function of this device after assembling and thus it is applied herein to explore the

dependency of surface rheological properties upon oscillation frequency and amplitude. The presence of this NaCl concentration (i.e. 8.766 g/L) in the SDS solution is to increase the SDS adsorption activity and to decrease the CMC to 0.404 g/L (Dutkiewicz *et al.*, 2002), thus this SDS solution (0.087 g/L in 8.766 g/L NaCl) is approximately at 21.5 % of the CMC. The Gibbs elasticity of this SDS solution with different oscillation frequencies and amplitudes as will be shown in Tables 2-1 and 2-2 is inferred from experimental results according to eq. 2-26. SDS is an anionic surfactant and was purchased from Fisher Scientific Co. with purity above 97.5%. It is used as received and deionised water is used. Note that SDS used herein is without further purification as the present study of surface rheological properties is prior to the study of stability of foams produced by surfactant solutions. Although it is possible to purify a small amount of surfactants in the study of surface rheological properties, it is difficult and time-consuming to purify a large amount of surfactants which are required in the study of foam stability. Due to this, in the current work, all the surfactants used are as received and without further purification. The SDS solution used herein is kept in a plastic container to minimise the hydrolysis rate of SDS, as it was demonstrated by Fainerman *et al.* (2010) that SDS solutions kept in a plastic container hydrolysed much slower than in a glass container.

A schematic diagram of the droplet shape analyser (Krüss, DSA100R) that has been used is shown in Figure 2-3. It consists primarily of 5 parts: (1) the dosing unit, (2) light source, (3) stage, (4) camera and (5) computer. In particular, the dosing unit includes 3 parts, which are the syringe, piezo pump

and the capillary. The capillary is used to suspend the pendant droplet. The syringe is controlled manually to produce a pendant droplet at the tip of the capillary. The piezo pump can be applied to oscillate the droplet at given amplitude and frequency. The droplet images are obtained using a digital camera which is mounted on the apparatus. The light source is also mounted on the apparatus to increase the image quality for accurate image analysis. The images are analysed and computed using droplet shape analysis software which is installed on the computer.

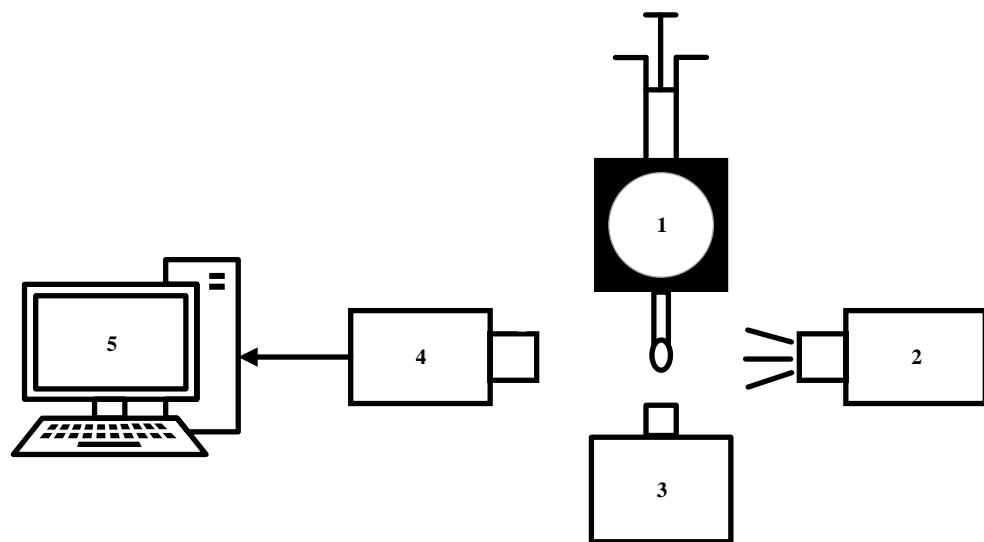


Figure 2-3. Schematic diagram of the droplet shape analyser (Krüss, DSA100R). 1. The dosing unit 2. Light source 3. Stage 4. Camera 5. Computer

All measurements are performed at the temperature of the laboratory, which is maintained at 22 ± 1 °C. A pendant droplet is suspended at the tip of the capillary and a video is recorded. The dilatational rheological measurements are performed by imposing a low frequency and low amplitude sinusoidal variation on the gas-liquid surface area. Note that the defined oscillation amplitude is a relative value which is related to the mean volume of the droplet and it is therefore dimensionless. Two sets of measurements are designed herein to test the dependency of surface rheological properties upon

oscillation frequency and amplitude. In one set of measurements, the oscillation frequency has been changed and the oscillation amplitude is held constant at 0.25, which ensures the oscillation of a droplet whilst readily retains the integrity of that droplet. The values of oscillation frequency tested herein are 0.1, 0.2, 0.4, 0.8 and 1 Hz. In the other set of measurements, the oscillation frequency is held constant at 0.5 Hz which is the intermediate value that the device can produce (the oscillation frequency that can be created by this device is 0-1 Hz), whereas the oscillation amplitude is varied. The values of oscillation amplitude are 0.1, 0.2, 0.3, 0.4 and 0.5. In both sets of measurements, the experiment is repeated 3 times at each value of oscillation frequency and amplitude. The accuracy of measurement using pendent droplet method can be affected by contamination, and therefore all the measurements performed herein are punctilious with respect to cleanliness. The dosing unit of the droplet shape analyser (Krüss, DSA100R) and all the glassware involved in the measurement are thoroughly flushed by deionised water and then by acetone to ensure the cleanliness. The capillary is mounted vertically to form an axisymmetric droplet to obtain accurate measurements of dynamic surface tension. The external diameter of the capillary used is 1.807 mm. All the measurements are performed with the droplet shape analyser mounted on a layer of polyfoam of depth 50 mm to reduce the droplet vibration induced by environmental vibration interference, which has been shown to be effective by taking Fourier series of the results. Details of the Fourier series analysis are given in Appendix A.

2.4 Dependency of Surface Rheological Properties upon Oscillation Frequency and Amplitude

The results of surface elasticity, surface dilatational viscosity and Gibbs elasticity of SDS solution at the concentration of 0.087 g/L (in 8.766 g/L NaCl aqueous solution) with different oscillation frequencies and amplitudes are shown in Tables 2-1 and 2-2, respectively. (The original results of surface rheological properties obtained by the oscillating pendent droplet method and the parameters inferred from the original data to obtain Gibbs elasticity in each independent measurement at different oscillation frequencies and amplitudes are shown in Appendix B.)

Table 2-1. Surface rheological properties of SDS solution at the concentration of 0.087 g/L in 8.766 g/L NaCl aqueous solution as a function of oscillation frequency. The oscillation amplitude is 0.25. The values in brackets represent the full range of observations.

Frequency (Hz)	Surface elasticity (mN/m)	Surface dilatational viscosity (mN·s/m)	Gibbs elasticity (mN/m)
0.1	4.58 (4.50 - 4.63)	4.80 (4.75 - 4.84)	19.24 (18.41 - 19.77)
0.2	6.19 (5.93 - 6.57)	3.62 (3.19 - 4.16)	37.99 (25.66 - 52.30)
0.4	7.87 (7.45 - 8.40)	2.23 (2.13 - 2.37)	41.03 (39.96 - 43.10)
0.8	9.85 (9.43 - 10.17)	1.37 (1.36 - 1.38)	49.04 (46.87 - 53.13)
1.0	10.53 (9.82 - 11.00)	1.24 (1.23 - 1.26)	64.48 (59.57 - 74.16)

Table 2-2. Surface rheological properties of SDS solution at the concentration of 0.087 g/L in 8.766 g/L NaCl aqueous solution as a function of oscillation amplitude. The oscillation frequency is 0.5 Hz. The values in brackets represent the full range of observations.

Amplitude (-)	Surface elasticity (mN/m)	Surface dilatational viscosity (mN·s/m)	Gibbs elasticity (mN/m)
0.1	8.99 (8.50 - 9.44)	1.95 (1.83 - 2.22)	44.17 (33.19 - 62.99)
0.2	9.58 (8.92 - 10.13)	1.89 (1.85 - 1.91)	35.36 (32.83 - 39.97)
0.3	9.86 (9.35 - 10.48)	1.96 (1.89 - 2.09)	36.67 (35.15 - 39.00)
0.4	9.47 (9.29 - 9.70)	1.88 (1.80 - 1.94)	35.21 (32.65 - 36.49)
0.5	9.27 (8.73 - 9.76)	1.84 (1.79 - 1.87)	34.26 (32.73 - 35.41)

The behaviour of surface elasticity, surface dilatational viscosity and Gibbs elasticity with increasing oscillation frequency and amplitude are shown in Figures 2-4 and 2-5, respectively. As can be seen from Figure 2-4, surface elasticity and Gibbs elasticity increase whereas surface dilatational viscosity decreases with increasing oscillation frequency. The dependency of surface rheological properties upon oscillation frequency are demonstrated. It is shown in Figure 2-5 that surface elasticity, surface dilatational viscosity and Gibbs elasticity approximately remain constant with increasing oscillation amplitude. Figure 2-5 also demonstrates that these surface rheological properties are approximately independent of oscillation amplitude. Note that in Figure 2-4, the Gibbs elasticity results at frequency of 0.2 and 1.0 Hz show relatively large errors compared with results at other frequencies. These large errors appear to result from the compromised method applied herein to infer Gibbs elasticity from measured results of surface elasticity and surface dilatational viscosity according to eq. 2-26. The details of this will be discussed later. The same reason accounts for the large error of Gibbs elasticity at amplitude of 0.1 in Figure 2-5.

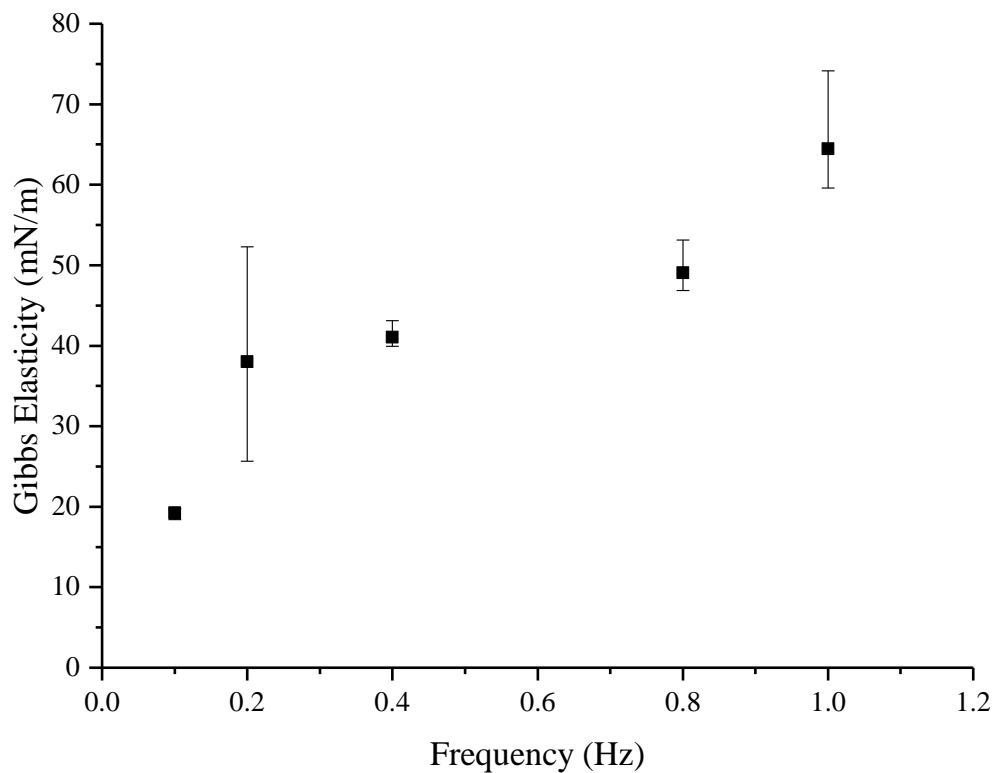
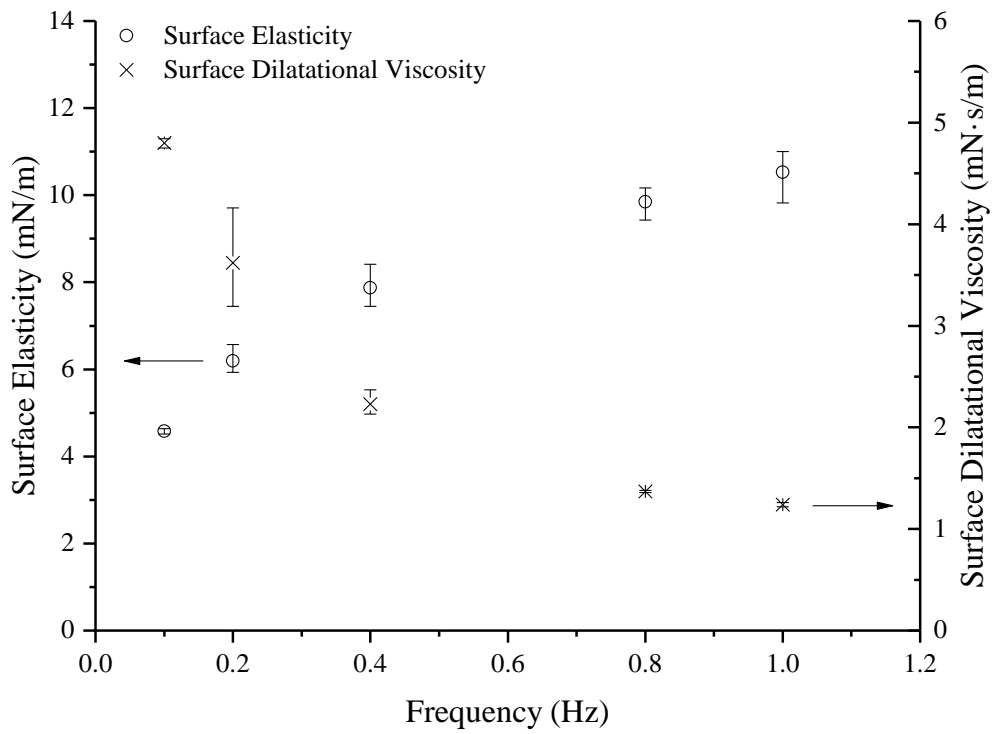


Figure 2-4. Surface elasticity, surface dilatational viscosity and Gibbs elasticity of SDS solution at the concentration of 0.087 g/L in 8.766 g/L NaCl aqueous solution as a function of oscillation frequency. The oscillation amplitude is 0.25. The error bars represent the full range of observations.

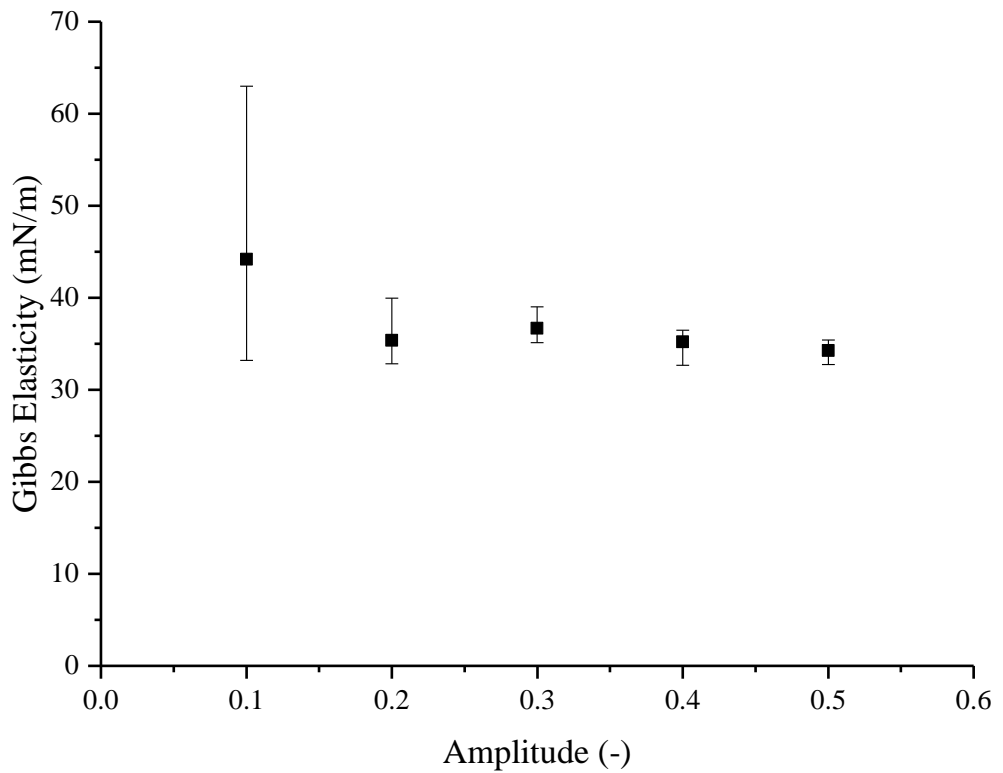
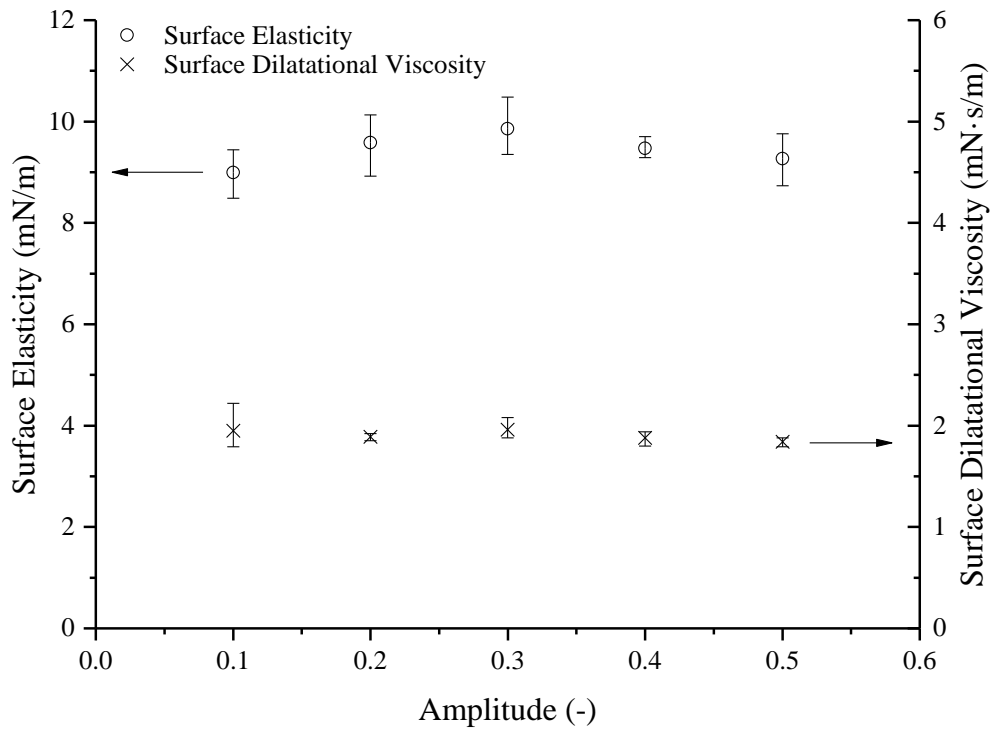


Figure 2-5. Surface elasticity, surface dilatational viscosity and Gibbs elasticity of SDS solution at the concentration of 0.087 g/L in 8.766 g/L NaCl aqueous solution as a function of oscillation amplitude. The oscillation frequency is 0.5 Hz. The error bars represent the full range of observations.

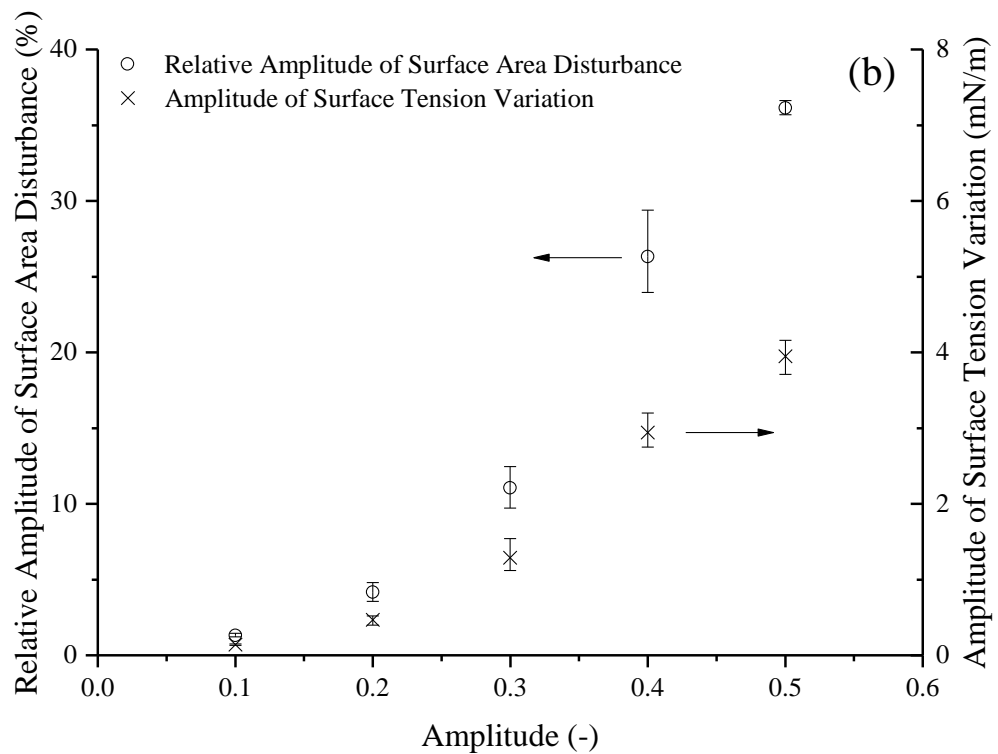
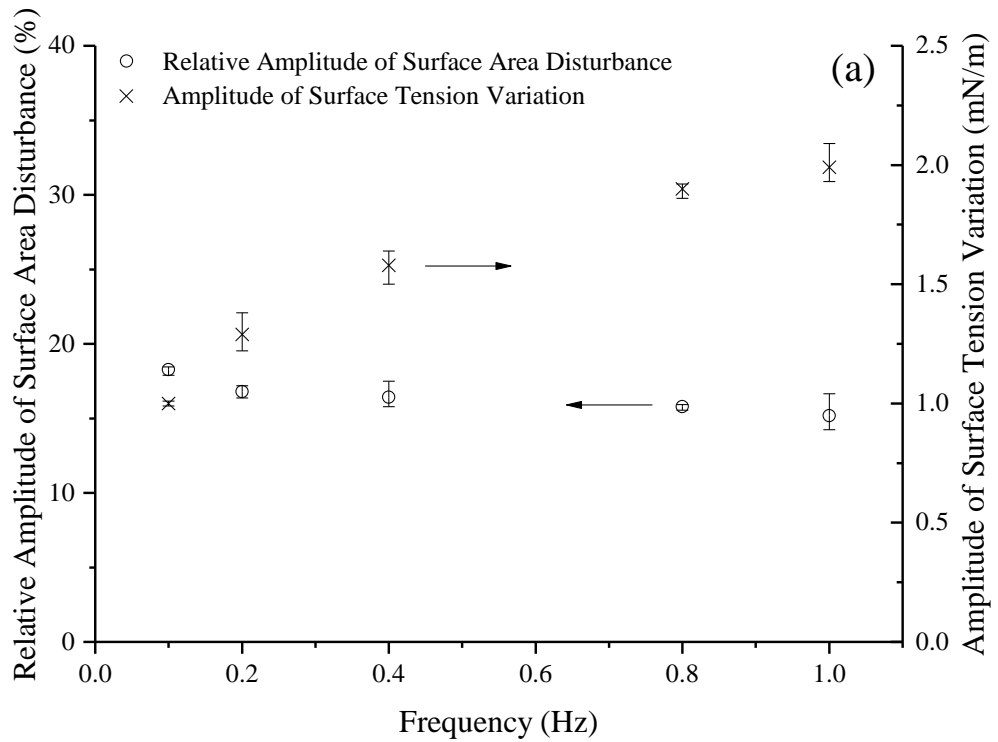


Figure 2-6. Relative amplitude of surface area disturbance and amplitude of surface tension variation of SDS solution at the concentration of 0.087 g/L in 8.766 g/L NaCl aqueous solution as a function of oscillation frequency and amplitude. (a) The results as a function of frequency. The oscillation amplitude is 0.25. (b) The results as a function of amplitude. The oscillation frequency is 0.5 Hz. The error bars represent the full range of observations.

The results of relative amplitude of surface area disturbance and amplitude of surface tension variation with different oscillation frequencies and amplitudes are shown in Figure 2-6. (The original results obtained in each independent measurement are shown in Appendix B.) It is seen from Figure 2-6(a) that the relative amplitude of surface area disturbance approximately remains constant whereas the amplitude of surface tension variation increases with the increase of oscillation frequency. As shown in Figure 2-6(b), the relative amplitude of surface area disturbance and the amplitude of surface tension variation increase approximately proportionally to the increase of oscillation amplitude. For the surface rheological properties with different oscillation frequencies, it is postulated that the characteristic time for diffusion of surfactants to the gas-liquid interface becomes progressively more significant with respect to the period of oscillation as frequency increases. Therefore, fewer molecules can adsorb in each cycle as the oscillation frequency increases. As a consequence, the absolute value of surface tension increases monotonically with the increase of oscillation frequency, which is shown in Figure 2-6(a). Since the relative amplitude of surface area disturbance is constant and the surface visco-elasticity is related to surface tension variation and surface area disturbance, the modulus of visco-elasticity increases with the increase of oscillation frequency. In addition, since the phase angle between surface area disturbance and surface tension oscillation decreases with the increase of oscillation frequency, according to eqs. 2-2 and 2-27, surface elasticity increases whereas surface dilatational viscosity decreases with increasing oscillation frequency. In fact, the dependency of surface elasticity and surface dilatational viscosity upon oscillation frequency have been observed by other researchers (Liggieri *et al.*,

2010; Karbaschi *et al.*, 2014). However, it is not expected to observe the dependency of Gibbs elasticity upon oscillation frequency, which is shown in Figure 2-4, since Gibbs elasticity is considered as a limiting surface elasticity at infinite oscillation frequency (Joos, 1999), thus it is supposed to be independent on the measuring oscillation frequency. This appears to be due to the fact that the method applied herein to obtain Gibbs elasticity is compromised. In our experiment, the values of Gibbs elasticity are inferred from the results of surface elasticity and surface dilatational viscosity which are measured at low frequency range (i.e. 0.1 - 1.0 Hz) according to eq. 2-26. However, it has been demonstrated by Wantke *et al.* (1998, 2001) that the theoretical model in eq. 2-24 is more applicable to obtain values of surface rheological properties at low frequency than at high frequency, as the calculated values of surface rheological properties according to the model in eq. 2-24 at high frequency exhibit large differences with the measured values. Furthermore, the large errors of Gibbs elasticity at some frequencies in our results also indicate the difficulties in using this method to infer Gibbs elasticity. However, it is still applied herein to provide an objective measurement for Gibbs elasticity.

With respect to the surface rheological properties with different oscillation amplitudes, the increase of oscillation amplitude results in the proportional increase of relative amplitude of surface area disturbance and amplitude of surface tension variation, which can be seen from Figure 2-6(b). Since the modulus of surface visco-elasticity is equivalent to the quotient of amplitude of surface tension variation and relative amplitude of surface area disturbance,

the modulus of surface visco-elasticity is independent of oscillation amplitude and approximately remains constant. Furthermore, as the oscillation frequency is also constant and therefore the phase angle between surface area disturbance and surface tension oscillation is constant as well, the surface rheological properties are independent of oscillation amplitude according to the relationship given in eq. 2-27. This observation shows agreement with the results of Georgieva *et al.* (2009) that surface tension shows a linear variation with relative change in surface area.

2.5 Summary

Since the results of surface rheological properties are dependent upon oscillation frequency, the measurement of surface rheological properties of different surfactant solutions in later chapters (chapter 5 and 6) should be performed at a fixed frequency which is dictated by the relevant experimental conditions. As for the oscillation amplitude, since the results of surface rheological properties are independent of it, a value that ensures droplet oscillation while retaining the integrity of the droplet can be assigned to the measurement of surface rheological properties in later chapters (chapter 5 and 6).

Chapter 3 Repeatability of Dynamic Surface Tension Measurement

3.1 Introduction

Besides surface rheological properties, surface tension is another fundamental property of gas-liquid interfaces that has relevance with foam stability (Kanokkarn *et al.*, 2017). Therefore, before relating foam stability to surface mechanical properties including surface rheological properties and surface tension, the method to measure surface tension needs to be studied as well. In this chapter, the repeatability of dynamic surface tension measurements of ionic surfactant solution using the static pendant droplet method is investigated. Firstly, an unexpected systematic change of dynamic surface tension of sodium alkyl sulfate solutions between different trials is described and then more measurements of dynamic surface tension of sodium alkyl sulfate solutions are performed to confirm that this unexpected observation is repeatable. Next, this unexpected systematic change of dynamic surface tension between different trials is attributed to the presence of trace amounts of highly surface-active impurities and this statement is verified by performing dynamic surface tension measurement of ionic surfactant solution without highly surface-active impurity. It is a consequence of the presence of highly surface-active impurity that the repeatability and precision of dynamic surface tension measurements are compromised. Finally, the method to determine the dynamic surface tension of ionic surfactant solution with highly surface-active impurity is explored. The large numbers of dynamic surface tension results of sodium alkyl sulfate solutions are statistically analysed and it is statistically demonstrated that the dynamic surface tension of individual trials of ionic surfactant solution with highly surface-active impurity can be considered as

the same and do not change significantly for a statistical perspective (i.e. considering large data population). Therefore, it is necessary to perform large numbers of independent trials of dynamic surface tension measurement to acquire the dynamic surface tension value by calculating the arithmetic mean.

3.2 Initial Measurement of Dynamic Surface Tension

3.2.1 Experimental Details

The static pendant droplet method is performed to measure dynamic surface tension of sodium tridecyl sulfate solution at the concentration of 1.301 g/L (i.e. 2.68% above the critical micelle concentration (CMC)) and sodium dodecyl sulfate (SDS) solution at the concentration of 0.288 g/L in 0.584 g/L NaCl aqueous solution (i.e. approximately 25% of the CMC) over time. The sodium tridecyl sulfate solution is prepared slightly above the CMC to ensure that the actual concentration of the prepared sodium tridecyl sulfate solution reaches the CMC and thus to avoid a possible smaller equilibrium surface tension if the actual concentration of the prepared sodium tridecyl sulfate solution is smaller than the CMC. The SDS solution is prepared in NaCl aqueous solutions since the dynamic surface tension of the same solution has been measured by Fainerman *et al.* (2010) using the pendant droplet method and it is designed to reproduce the dynamic surface tension measurement of this solution to compare the results of the current work with theirs. Sodium tridecyl sulfate is a homologue of SDS and was also purchased from Fisher Scientific Co. with purity above 98%. Sodium tridecyl sulfate and SDS are both used without further purification. Besides the reason explained in section

2.3, this is in particular due to that the present study of the surface tension of these surfactant solutions is prior to the study of stability of foams produced by these surfactant solutions. While relating foam stability to surface mechanical properties, the measured surfactant solutions need to be the same, however, the purification process would result in the change of surfactant concentrations (Fainerman *et al.*, 2010). This is the particular reason that the surfactants used herein are all as-received. Thus, trace amounts of tridecanol and dodecanol as inevitable impurities during synthesis process exist in sodium tridecyl sulfate and SDS, respectively (Mysels, 1986). Note that the sodium alkyl sulfate homologues are known to hydrolyse slowly to respective alkanols, which affects the purity of surfactant solutions (Varga *et al.*, 2007). However, it has been demonstrated by Vollhardt (1982) that the quality of SDS solution can be stable over one year at room temperature if it is kept in a hydrophobic container. Fainerman *et al.* (2010) has observed the similar phenomenon that SDS solutions kept in a plastic container hydrolysed much slower than in a glass container. Hence, in order to retard the hydrolysis rate, all the surfactant solutions used herein are kept in plastic containers. The deionised water is used to dilute the surfactants and the CMC of sodium tridecyl sulfate solution and SDS solution in 0.584 g/L NaCl aqueous solution are 1.267 g/L and 1.153 g/L, respectively. (Varga *et al.*, 2007; Fainerman *et al.*, 2010).

The same experimental device, the droplet shape analyser (Krüss, DSA100R) as shown in Figure 2-2, has also been used herein. All the measurements are static pendant droplet measurement and are performed at the temperature of

the laboratory, which is 22 ± 1 °C. (It has been demonstrated by Phongikaroon *et al.* (2005) that the equilibrium surface tension of surfactant solution decreases approximately linearly with increase of temperature, so that the equilibrium surface tension difference at this temperature range is insignificant. For instance, the equilibrium surface tension of SDS solution only decreases 0.31 mN/m from 21 to 23 °C. Thus the uncertainty of surface tension with respect to temperature is insignificant compared to the dispersion reported herein). A well-formed pendant droplet is suspended from a capillary for 2 minutes. The images of pendant droplet are acquired at a constant rate of 2.5 images per second for all measurements. A total of 300 images are obtained for each measurement. After 2 minutes, the old droplet is discarded and several droplets are formed and discarded to minimise the initial load of the old droplet before producing a new droplet, as the initial load of the old droplet affects the result of new droplet. By following this process, the initial load of old droplet is negligible and therefore the effect of initial load on surface tension measurement in the experiments performed herein is insignificant. When a new droplet is produced, a new measurement starts. The independent measurement is repeated 10 times. All the other experimental conditions are maintained the same as described in section 2.3.

3.2.2 Unexpected Systematic Change of Dynamic Surface Tension Results

Generally, it is expected that the dynamic surface tension results of independent trials will be consistent with only small random errors are observed between these trials. Then, the dynamic surface tension of each sample can be obtained by calculating the arithmetic mean of 10 trials, with a

reportable error. However, by inspection of the dynamic surface tension results of sodium tridecyl sulfate solution at the concentration of 1.301 g/L (i.e. 2.68% above the CMC) and SDS solution at the concentration of 0.288 g/L in 0.584 g/L NaCl aqueous solution (i.e. approximately 25% of the CMC), it is noticed that the dynamic surface tension results seem to change systematically with the proceeding of independent trials instead approximately remaining constant between measurements. The dynamic surface tension results of these two surfactant solutions are shown in Figure 3-1 and 3-2, respectively.

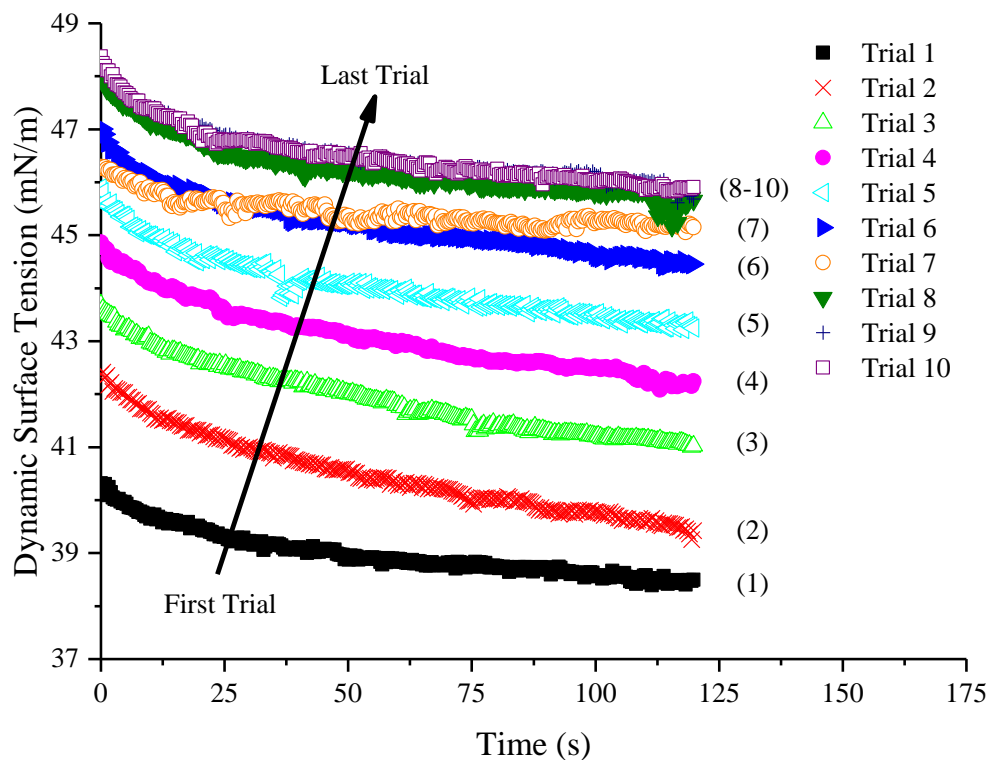


Figure 3-1. Dynamic surface tension results of sodium tridecyl sulfate solution at the concentration of 1.301 g/L (i.e. 2.68 % above the CMC). The number in bracket represents the sequential trial number.

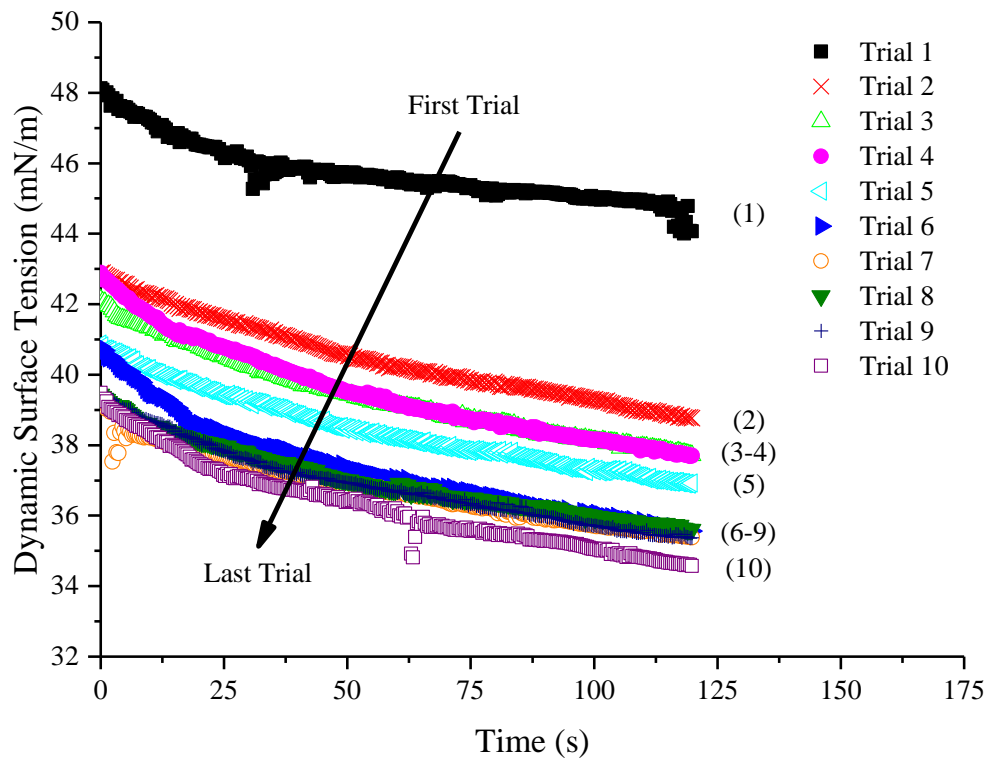


Figure 3-2. Dynamic surface tension results of SDS solution at the concentration of 0.288 g/L in 0.584 g/L NaCl aqueous solutions (i.e. approximately 25% of the CMC). The number in bracket represents the sequential trial number.

By inspection of Figure 3-1, it can be seen that there is poor agreement of dynamic surface tension results of sodium tridecyl sulfate solution (1.301 g/L) from trial to trial. The dynamic surface tension increases monotonically from trial 1 to trial 8 and then almost remains constant from trial 8 to trial 10. Due to the increase of dynamic surface tension throughout the course of the experiment, the repeatability of dynamic surface tension measurements is poor and therefore the precision of dynamic surface tension measurement is potentially compromised. Thus, the arithmetic mean of 10 trials cannot accurately represent the true value of the dynamic surface tension of sodium tridecyl sulfate solution (1.301 g/L). The equilibrium surface tension of sodium tridecyl sulfate solution (purified) at the concentration of 1.267 g/L (i.e. at the CMC) obtained by Varga *et al.* (2007) was approximate 38.00 mN/m (as shown in Table 2-1). By comparison of this value to the

observations of the current work, it indicates that the dynamic surface tension results of trial 1 show agreement with the observation of Varga *et al.* (2007), since the equilibrium surface tension inferred from the dynamic surface tension results of trial 1 is the closest value to 38.00 mN/m among the 10 trials.

As for SDS solution (0.288 g/L in 0.584 g/L NaCl), it can be seen from Figure 3-2 that the dynamic surface tension results of SDS solution (0.288 g/L in 0.584 g/L NaCl) also shows poor repeatability. However, contradictory to the observation of sodium tridecyl sulfate solution (1.301 g/L) that the dynamic surface tension increases as the measurement goes on, it is observed that the dynamic surface tension seems to decrease systematically from trial 1 to trial 10. Due to this systematic decrease of dynamic surface tension throughout the course of the experiment, the repeatability and precision of dynamic surface tension measurements of SDS solution (0.288 g/L in 0.584 g/L NaCl) are potentially compromised and therefore the accurate of dynamic surface tension measurement is poor if using the arithmetic mean of 10 trials to represent the true value of the dynamic surface tension of SDS solution (0.288 g/L in 0.584 g/L NaCl). Furthermore, the dynamic surface tension results of SDS solution (0.288 g/L in 0.584 g/L NaCl) obtained in the current work are compared with the results obtained by Fainerman *et al.* (2010). In their experiment, the dynamic surface tension of the same surfactant solution was measured using the pendant droplet method. The SDS used in the measurements of Fainerman *et al.* (2010) was also without further purification. After comparison of the results of Fainerman *et al.* (2010) with the results

obtained in this current work of 10 trials, it is demonstrated that the results they have obtained approximate to our observations obtained in trial 1.

These systematic changes of dynamic surface tension between different trials, either increase or decrease, are unexpected and they affect the accuracy of dynamic surface tension measurement. Thus, it is necessary to further explore these unexpected systematic changes of dynamic surface tension between different trials. First of all, it is a priority to ascertain that whether these unexpected observations are repeatable or not. Therefore, in the next section, more dynamic surface tension measurements of these two surfactant solutions are performed to investigate the repeatability of unexpected systematic change of dynamic surface tension between different trials.

3.3 Confirmation of the Unexpected Observation

In order to confirm the repeatability of above mentioned observation that dynamic surface tension changes systematically, the dynamic surface tension measurements of afore-mentioned two surfactant solutions are repeated more times using the same experiment method and under the same experiment conditions. In previous dynamic surface tension measurements of these two surfactant solutions, all the measurements are repeated 10 times and these 10 consecutive trials can be considered as a run. After one run, the apparatus is carefully cleaned and new surfactant solution is injected to perform another run. The dynamic surface tension measurements of each sample are repeated 10 runs in total, which means 100 independent measuring trials are performed. In order to compare the results between different runs, in each run, the

arithmetic mean of dynamic surface tension of 10 trials is calculated and then since this arithmetic mean result contains 300 data of dynamic surface tension over 2 minutes, the average of arithmetic mean result of dynamic surface tension over 2 minutes is calculated to represent the dynamic surface tension result of each run. The average of arithmetic mean result of dynamic surface tension over 2 minutes, σ_A , is defined as:

$$\sigma_A = \frac{1}{300} \sum_{i=1}^{300} \sigma_i \quad (3-1)$$

where i is the sequential image number and σ_i is the arithmetic mean result of dynamic surface tension between 10 trials of i^{th} image. Furthermore, in each run, the range of dynamic surface tension between 10 trials is calculated, and the average range of 300 images (i.e. over 2 minutes) is used to quantify the dispersion of the dynamic surface tension values obtained from 10 trials. Note that here the dispersion is represented by the range of data sets which is the difference between the largest and smallest values, as the range is most useful in representing the dispersion of small data sets (Viljoen, 2000). The average range of dynamic surface tension of 300 images, R_A , is defined as:

$$R_A = \frac{1}{300} \sum_{i=1}^{300} R_i \quad (3-2)$$

where R_i is the range of dynamic surface tension between 10 trials of i^{th} image. The smaller the average range is, the better the repeatability and precision of dynamic surface tension between different trials is. The average arithmetic mean, the average range and the changing trend of dynamic surface tension

between 10 trials in each run of afore-mentioned two surfactant solutions are shown in Table 3-1 (The detailed dynamic surface tension results of all 10 runs of these two surfactant solutions are shown in Appendix C). Note that the changing trend of dynamic surface tension between 10 trials in each run is marked by an arrow of different directions to indicate the systematic increase, fluctuation and systematic decrease. If the systematic increase of dynamic surface tension between 10 trials and a relatively large average range (larger than 3 mN/m, which is a pre-specified value that far larger than the average range value for measurements with good repeatability) have been observed, the changing trend will be marked by the ‘↑’ sign. If the systematic decrease of dynamic surface tension between 10 trials and a relatively large average range (larger than 3mN/m) have been observed, the changing trend will be marked by the ‘↓’ sign. Whereas for the measurements with fluctuation of dynamic surface tension between 10 trials and acceptable repeatability (i.e. the average range is smaller than 3 mN/m), the changing trend is marked by the ‘→’ sign.

Table 3-1. The average arithmetic mean, the average range and the changing trend of dynamic surface tension between different trials in each run of sodium tridecyl sulfate solution (1.301 g/L) and SDS solution (0.288 g/L in 0.584 g/L NaCl)

Run	Sodium tridecyl sulfate solution (1.301 g/L)			SDS solution (0.288 g/L in 0.584 g/L NaCl)		
	The average arithmetic mean (mN/m)	The average range (mN/m)	The changing trend (-)	The average arithmetic mean (mN/m)	The average range (mN/m)	The changing trend (-)
1	43.84	7.58	↑	38.77	9.48	↓
2	42.61	6.08	↑	43.71	6.52	↓
3	40.37	5.44	↑	46.89	5.00	↓
4	41.84	3.98	↑	48.73	2.36	→
5	37.47	0.47	→	49.66	0.94	→
6	37.33	0.31	→	50.02	1.22	→
7	37.34	1.56	→	50.24	2.11	→
8	37.53	0.51	→	51.01	0.72	→
9	37.57	0.63	→	49.25	1.79	→
10	36.70	0.96	→	49.66	1.81	→

The '↑' sign represents the systematic increase of dynamic surface tension as the measurement goes on. The '→' sign represents the dynamic surface tensions of 10 trials remain almost the same and only fluctuate with random errors. The '↓' sign represents the systematic decrease of dynamic surface tension as the measurement goes on.

It can be seen from Table 3-1 that, for sodium tridecyl sulfate solution (1.301 g/L), both unexpected systematic increase and expected fluctuation of dynamic surface tension between different trials have been observed and the unexpected systematic increase of dynamic surface tension between different trials occurs more than once. Whilst for SDS solution (0.288 g/L in 0.584 g/L NaCl), both unexpected systematic decrease and expected fluctuation of dynamic surface tension between different trials have been observed. For both surfactant solutions, it is noted that the systematic change of dynamic surface

tension between different trials can only be observed in the earlier runs (i.e. for sodium tridecyl sulfate solution (1.301 g/L), it is from run 1 to run 4, whilst for SDS solution (0.288 g/L in 0.584 g/L NaCl), it is from run 1 to run 3), whereas in the latter runs, it is the expected fluctuation of dynamic surface tension between different trials that have been observed.

The comparison between different runs of average arithmetic mean and average range of dynamic surface tension between different trials of sodium tridecyl sulfate solution (1.301 g/L) is shown in Figure 3-3 and that of SDS solution (0.288 g/L in 0.584 g/L NaCl) is shown in Figure 3-4. As can be seen from Figure 3-3, the average arithmetic mean of dynamic surface tension results obtained in the earlier runs (i.e. from run 1 to run 4) are much larger than those obtained in the rest of runs, which are approximately the same. In fact, this is due to the appreciable systematic increase of dynamic surface tension in the earlier runs. The average arithmetic mean of dynamic surface tension result generally decreases at first and then almost remains at constant through the course of performing different runs. It is also noted that if only considering the average dynamic surface tension result obtained in trial 1 of all the repeated runs, they are approximately the same.

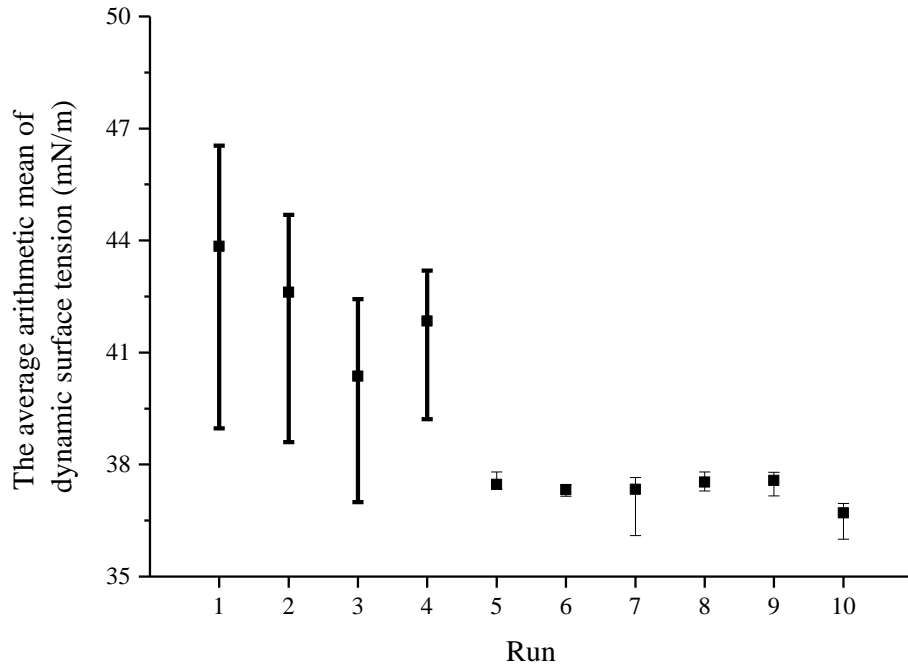


Figure 3-3. Comparison between different runs of average arithmetic mean and average range of dynamic surface tension between different trials of sodium tridecyl sulfate solution (1.301 g/L). The error bar of each run represents the average range of dynamic surface tension between different trials. The bold error bars indicate that the unexpected systematic increase of dynamic surface tension between different trials has been observed in this run, whereas the thin error bar indicates that the expected fluctuation of dynamic surface tension between different trials has been observed in this run.

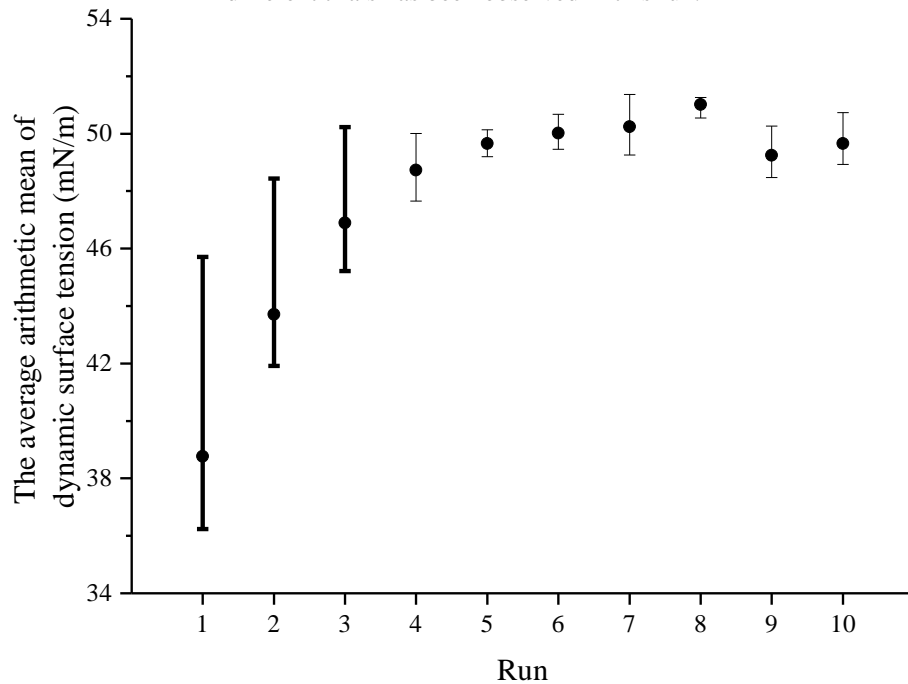


Figure 3-4. Comparison between different runs of average arithmetic mean and average range of dynamic surface tension between different trials of SDS solution (0.288 g/L in 0.584 g/L NaCl). The error bar of each run represents the average range of dynamic surface tension between different trials. The bold error bars indicate that the unexpected systematic decrease of dynamic surface tension between different trials has been observed in this run, whereas the thin error bar indicates that the fluctuation of dynamic surface tension between different trials has been observed in this run.

It is shown in Figure 3-4 that the dispersion of dynamic surface tension between different trials in the earlier runs (i.e. from run 1 to run 3) are much larger than that in the latter runs. This is due to the unexpected systematic decrease of dynamic surface tension between different trials in the earlier runs, which also accounts for the smaller average arithmetic mean of dynamic surface tension results obtained in the earlier runs (i.e. from run 1 to run 3), whereas the average arithmetic mean of dynamic surface tension results obtained in the other runs are much larger and approximately the same. The average arithmetic mean of dynamic surface tension result increases at first and then approximately maintains at the same throughout the course of performing different runs. However, if only considering the average dynamic surface tension result obtained in trial 1 of all the repeated runs, they are approximately the same.

To summarise, it appears that the considerable systematic change of dynamic surface tension between different trials are prone to occur in the earlier runs for both surfactant solutions. In the latter runs, it is more common to observe the expected fluctuation of dynamic surface tension between different trials. These observations demonstrate that the unexpected systematic changes are repeatable rather than random. Therefore, it is necessary to investigate the underlying cause for these unexpected systematic changes of dynamic surface tension between different trials. In the next section, these unexpected observations are ascribed to the presence of inevitable highly surface-active impurity and further measurements are performed to verify this statement.

3.4 Cause of the Unexpected Observation

3.4.1 Effect of Highly Surface-active Impurity on Dynamic Surface Tension Measurement

As described above, the surfactants including sodium tridecyl sulfate and SDS are both used as-received and without further purification. It has been demonstrated by Mysels (1986) that sodium alkyl sulfate homologues contained alkanol as inevitable highly surface-active impurities during synthesis process and they were difficult to remove. Thus, trace amounts of tridecanol and dodecanol as inevitable high surface-active impurities exist in the sodium tridecyl sulfate and SDS solutions, respectively. By inspecting the dynamic surface tension results of sodium tridecyl sulfate solution (1.301 g/L) and SDS solution (0.288 g/L in 0.584 g/L NaCl), it is believed in this current work that the presence of highly surface-active impurity accounts for the unexpected systematic change of dynamic surface tension between different trials.

It has been demonstrated by Lu *et al.* (1995) that the presence of trace amounts of dodecanol in SDS solution affected the adsorption of SDS to the air-liquid interface and the influence mechanism was different at various SDS concentrations (i.e. above the CMC or far below the CMC). For the SDS concentration above the CMC, most of the dodecanol molecules are solubilised by SDS micelles. Thus, the majority of dodecanol molecules which are encircled in SDS micelles remain in the bulk solution instead of adsorbing to the air-liquid interface. Due to the strong attractive interaction between

dodecanol and SDS molecules, the adsorption of SDS to the air-liquid interface is compromised by the presence of dodecanol. However, for the SDS concentration far below the CMC, as there is no SDS micelle to solubilise dodecanol molecules, the dodecanol molecules adsorb at the air-liquid interface. Because of the strong attractive interaction between dodecanol and SDS molecules, the SDS adsorption is enhanced by the presence of dodecanol. Since sodium tridecyl sulfate and SDS are homologues, the presence of trace amounts of tridecanol has the same effect on the adsorption of sodium tridecyl sulfate to the air-liquid interface. In fact, the unexpected observation of systematic change of dynamic surface tension between different trials as described above results from the effect of highly surface-active impurity on the adsorption of surfactant to the air-liquid interface.

In our experiments with sodium tridecyl sulfate solution (1.301 g/L), the concentration of sodium tridecyl sulfate solution is above the CMC, thus, the presence of trace amounts of tridecanol compromises the adsorption of sodium tridecyl sulfate to the air-liquid interface, which results in the increase of dynamic surface tension. In addition, due to the low concentration of tridecanol in the bulk solution, the diffusion rate of tridecanol from the bulk solution to the droplet is fairly slow. Therefore, in the earlier runs of dynamic surface tension measurement, the amount of tridecanol in the droplet increases trial-by-trial and thus tridecanol gradually acts more and more on compromising the adsorption of sodium tridecyl sulfate to the air-liquid interface with the measurement goes on. This results in the considerable systematic increase of dynamic surface tension between different trials in the

earlier runs as shown in Figure 3-3. Since the amount of tridecanol in the sodium tridecyl solution (1.301 g/L) is minor and distributed heterogeneously as highly surface-active impurity is preferentially enriched at the air-liquid interface (Lunkenheimer *et al.*, 2004), the majority of tridecanol in the sodium tridecyl sulfate solution (1.301 g/L) exist in the test samples of the earlier runs. Thus, for the latter runs, the amount of tridecanol in the test sample of sodium tridecyl sulfate solution (1.301 g/L) is negligible and therefore plays little role in affecting the adsorption of sodium tridecyl sulfate to the air-liquid interface, which accounts for the expected fluctuation of dynamic surface tension between different trials in the latter runs as shown in Figure 3-3.

As for the experiments with SDS solution (0.288 g/L in 0.584 g/L NaCl), since the SDS concentration is far below the CMC, the presence of trace amounts of dodecanol enhances the adsorption of SDS to the air-liquid interface, which results in the decrease of dynamic surface tension. Furthermore, the diffusion rate of dodecanol is also rather slow on account of the low concentration of dodecanol. Hence, in the earlier runs of measurement, the amount of dodecanol in the droplet increase gradually with the measurement goes on and therefore dodecanol plays an ever-increasing role upon the promotion of SDS adsorption to the air-liquid interface trial-by-trial, which accounts for the significant systematic decrease of dynamic surface tension between different trials in the earlier runs as shown in Figure 3-4. Due to the fact that dodecanol in SDS solution is limited and heterogeneously distributed, dodecanol mainly exists in the test samples of the earlier runs and becomes negligible in the test samples of the latter runs. Thus, the effect of dodecanol on the promotion of

adsorption of SDS to the air-liquid interface is insignificant in the measurements of the latter runs and therefore results in the expected fluctuation of dynamic surface tension between different trials in the latter runs as shown in Figure 3-4.

In this subsection, the unexpected systematic changes of dynamic surface tension between different trials in the earlier runs are attributed to the presence of trace amounts of highly surface-active impurities in the surfactant solutions. In order to verify this statement, more dynamic surface tension measurements of surfactant solution which is known without highly surface-active impurity are performed in the next subsection.

3.4.2 Verification of the Effect of Highly Surface-active Impurity on Dynamic Surface Tension Results

The surfactant considered in this subsection is dodecyl trimethyl ammonium bromide (DTAB) which is a cationic surfactant and was purchased from Fisher Scientific Co. with purity of 99%. It is used without further purification. Note that DTAB is much more chemically stable than sodium alkyl sulfate homologous and does not contain highly surface-active impurity (Ritacco *et al.*, 2011). This is the reason for choosing DTAB as tested surfactant to verify that whether the systematic change of dynamic surface tension between different trials can be observed or not. The dynamic surface tension of DTAB solution at the concentration of 4.954 g/L (i.e. 5.00 % above the CMC) is measured using the same experimental method and under the same experimental conditions as described in subsection 3.2.1. The CMC of DTAB

solution is 4.718 g/L (Atkin *et al.*, 2003). The measurements are also performed 10 trials in each run and are repeated 10 runs in total. The arithmetic mean and the dispersion of dynamic surface tension between 100 trials of DTAB solution (4.954 g/L) are shown in Figure 3-5 (The detailed dynamic surface tension results of all 10 runs of DTAB solution (4.954 g/L) are shown in Appendix C). Note that here the dispersion is represented by the standard deviation instead of the range, since the range is less useful in representing the dispersion of large data sets because it only depends on the largest and smallest values of the observations (Viljoen, 2000). The equilibrium surface tension of DTAB solution (4.954 g/L) is 37.40 ± 0.27 mN/m, which will be calculated in section 5.2 and shown in Table 5-1. This value obtained in the current work shows agreement with the equilibrium surface tension of DTAB solution at the concentration of 6.167 g/L (i.e. approximate 30% above the CMC) measured by Espert *et al.* (1998), which is approximate 38.00 mN/m (as shown in Table 2-1).

In order to compare the dispersion of dynamic surface tension results between different surfactant solutions, the arithmetic mean and the dispersion of dynamic surface tension between 100 trials of sodium tridecyl sulfate solution (1.301 g/L) and SDS solution (0.288 g/L in 0.584 g/L NaCl) are also shown in Figure 3-5. Furthermore, the average standard deviation of dynamic surface tension results over 2 minutes of these three surfactant solutions are also calculated. The average standard deviation of dynamic surface tension of 300 images, SD_A , is defined as:

$$SD_A = \frac{1}{300} \sum_{i=1}^{300} SD_i \quad (3-3)$$

where SD_i is the standard deviation of dynamic surface tension between different trials of i^{th} image.

The average standard deviation of dynamic surface tension over 2 minutes of sodium tridecyl sulfate solution (1.301 g/L), SDS solution (0.288 g/L in 0.584 g/L NaCl) and DTAB solution (4.954 g/L) are 2.97, 3.82 and 0.27 mN/m, respectively. The average standard deviation of DTAB solution (4.954 g/L) is much smaller than that of the other two surfactant solutions. By comparing the dispersion of dynamic surface tension results of these three surfactant solutions, for sodium tridecyl sulfate solution (1.301 g/L) and SDS solution (0.288 g/L in 0.584 g/L NaCl), the dispersion are very large as shown in Figure 3-5(a) & (b), which is due to the fact that the appreciable systematic change of dynamic surface tension between different trials has been observed. Whereas for DTAB solution (4.954 g/L), the dispersion is minor as shown in Figure 3-5(c) and therefore the dynamic surface tension results have demonstrable repeatability and precision between 100 trials. This indicates that the appreciable systematic change of dynamic surface tension between different trials has not been observed; neither the systematic increase nor the systematic decrease.

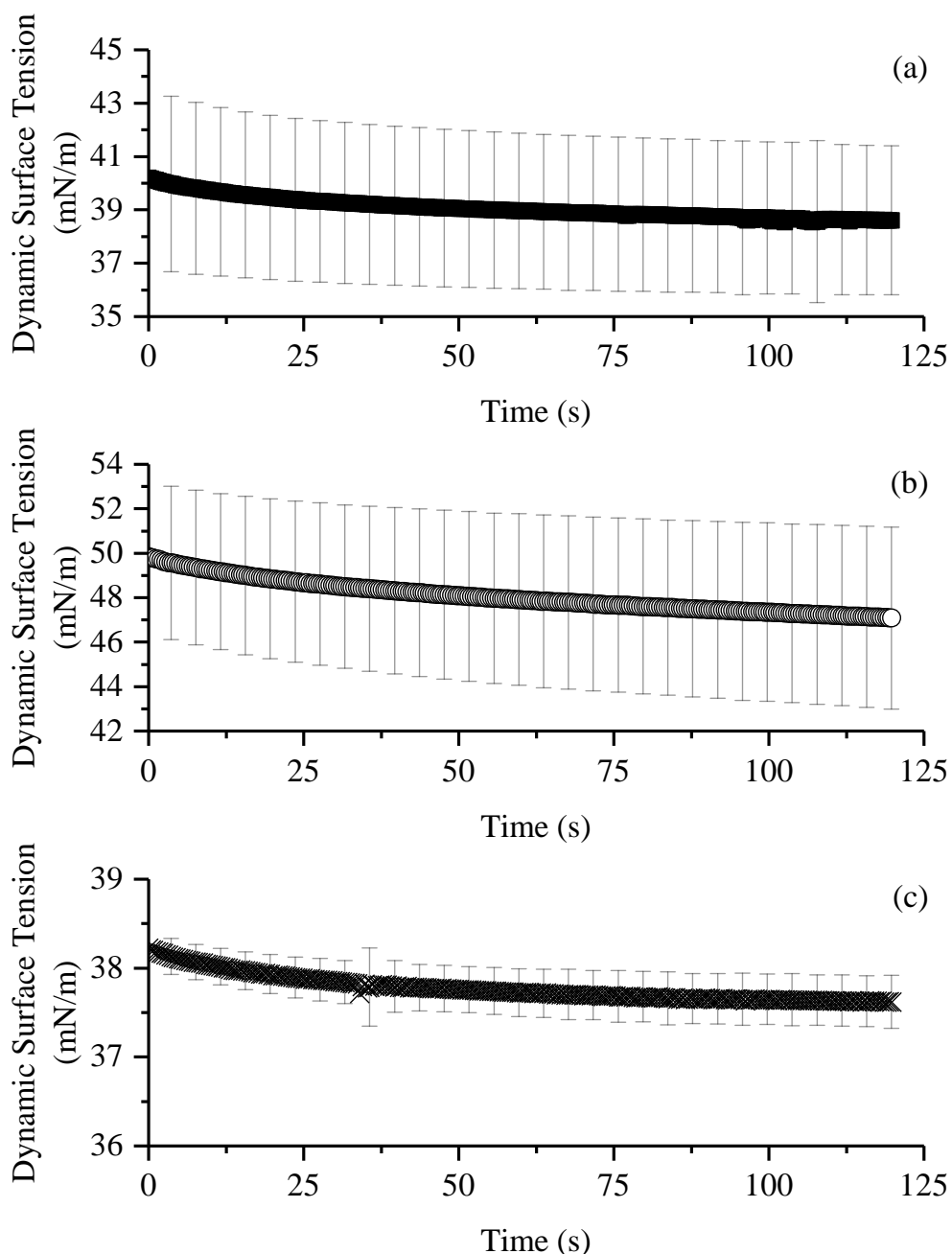


Figure 3-5. The arithmetic mean and the dispersion of dynamic surface tension between 100 trials of three surfactant solutions. Error bars represent the standard deviation of all the observations. All the errors of data over 2 minutes are calculated and only present 1 error bar in every 10 error bars for clarity. (a) The results of sodium tridecyl sulfate solution at the concentration of 1.301 g/L (i.e. 2.68% above the CMC). (b) The results of SDS solution at the concentration of 0.288 g/L in 0.584 g/L NaCl aqueous solution (i.e. approximately 25% of the CMC). (c) The results of DTAB solution at the concentration of 4.954 g/L (i.e. 5.00 % above the CMC).

To emphasise, it is demonstrated that the appreciable systematic change of dynamic surface tension between different trials does not occur at all in the dynamic surface tension measurements of DTAB solution (4.954 g/L). Since

DTAB does not contain highly surface-active impurity comparing with sodium alkyl sulfate homologues, this observation illustrates that the appreciable systematic change of dynamic surface tension between different trials is due to the presence of highly surface-active impurity. The effect of highly surface-active impurity on dynamic surface tension results has been demonstrated. Due to this effect, the repeatability and precision of dynamic surface tension measurements of surfactant solution with highly surface-active impurity is poor and thus it is difficult to decide the actual value of dynamic surface tension of surfactant solution with highly surface-active impurity. Therefore, it is necessary and important to determine a method by which to quantify the dynamic surface tension of surfactant solution with highly surface-active impurity. In the next section, statistical analysis of dynamic surface tension results of sodium tridecyl sulfate solution (1.301 g/L) and SDS solution (0.288 g/L in 0.584 g/L NaCl) is performed to achieve this goal.

3.5 Statistical Analysis of Dynamic Surface Tension Results

3.5.1 Proposal of a Hypothesis

As described above, the dynamic surface tension measurements of sodium tridecyl sulfate solution (1.301 g/L) and SDS solution (0.288 g/L in 0.584 g/L NaCl) have been repeated 10 runs and in each run 10 independent trials have been performed. Therefore, the dynamic surface tension measurements have been repeated many times and large amounts of dynamic surface tension data have been obtained. From these data, since both unexpected systematic change and expected fluctuation of dynamic surface tension between 10 trials have

been observed among 10 runs, it is not straightforward to decide whether there is a significant dynamic surface tension difference between independent trials or not from a statistical perspective (i.e. considering large data population). Thus, it is difficult to decide whether the arithmetic mean of large amount of dynamic surface tension data can be applied or not to represent the actual value of dynamic surface tension of surfactant solution with highly surface-active impurity from a statistical perspective (i.e. considering large data population). Therefore, the statistical hypothesis testing must be performed. The statistical hypothesis test is a method of statistical analysis to compare two statistical data sets to explore the statistical relationship between them. A statistical relationship between the data sets is proposed as a hypothesis and it is compared as an alternative to a null hypothesis that there is no such relationship between the data sets. This comparison is considered as statistically significant if the null hypothesis is not likely to realise according to a pre-specified threshold of probability, which is known as significance level that symbolised as α . In this case, the hypothesis that needs to be tested is that the dynamic surface tension changes significantly between independent trials. Since the largest dynamic surface tension differences can be observed are between trial 1 and trial 10 according to the experimental observations, the hypothesis that is going to be tested can be simplified as the dynamic surface tension change significantly between trial 1 and trial 10. In order to perform statistical hypothesis testing, the average of dynamic surface tension over 2 minutes are calculated to represent the result of individual trial. The average dynamic surface tension results of trial 1 and trial 10 of 10 runs of sodium

tridecyl sulfate solution (1.301 g/L) and SDS solution (0.288 g/L in 0.584 g/L NaCl) are shown in Table 3-2.

Table 3-2. The average dynamic surface tension results of trial 1 and trial 10 of 10 runs of sodium tridecyl sulfate solution (1.301 g/L) and SDS solution (0.288 g/L in 0.584 g/L NaCl)

		The average dynamic surface tension (mN/m)									
Sample	Trial										
		Run 1	Run 2	Run 3	Run 4	Run 5	Run 6	Run 7	Run 8	Run 9	Run 10
Sodium tridecyl sulfate solution (1.301 g/L)	1 st	38.99	38.60	36.99	39.21	37.42	37.21	36.44	36.00	35.73	36.17
	10 th	46.50	44.69	42.24	42.09	37.33	37.44	37.59	36.88	36.40	36.95
SDS solution (0.288 g/L in 0.584 g/L NaCl)	1 st	45.71	48.44	50.01	50.10	50.61	51.37	51.23	50.26	50.23	50.74
	10 th	36.27	42.98	49.03	49.61	49.46	50.53	50.98	49.99	48.68	49.53

For each surfactant solution, the average dynamic surface tension results of trial 1 and trial 10 can be considered as independent random variables. The average dynamic surface tension results of 10 runs of trial 1 can be regarded as one data set and that of trial 10 can be regarded as another data set. These two data sets are compared and the null hypothesis that symbolised as H_0 is proposed as the dynamic surface tension results of trial 1 can be considered as the same with the dynamic surface tension results of trial 10. Whereas the alternative hypothesis that symbolised as H_1 is the dynamic surface tension of trial 1 are significantly different from the dynamic surface tension results of trial 10. Mathematically, this is the difference between the mean of the

populations which the data sets are drawn from that is going to be compared to test this hypothesis. Therefore, the null hypothesis and the alternative hypothesis can be written as

$$H_0 : \mu_1 = \mu_2 ; H_1 : \mu_1 \neq \mu_2 \quad (3-4)$$

where μ_1 is the mean of the population which the data set 1 is drawn from; μ_2 is the mean of the population which the data set 2 is drawn from. The significant level is pre-specified as 0.01, which is a probability threshold below which the null hypothesis will be rejected. The reason for using 0.01 as the significance level is that this probability is a common value in statistics to represent unlikely realisation, which means the probability of an event less than 0.01 can be considered as small probability event (Nuzzo, 2014).

3.5.2 Method of Statistical Hypothesis Testing

The above-mentioned hypothesis can be tested using different methods and it is important to select appropriate test method to obtain reliable results. In each method, a test statistic which is calculated from data sets can be used to perform hypothesis test. Generally, the test statistic is defined to quantify behaviours that would distinguish the null hypothesis from the alternative hypothesis. The optimum test statistic is selected before performing statistical hypothesis testing. The flow chart of the whole process of selecting optimum test methods and performing statistic hypothesis test is shown in Figure 3-6.

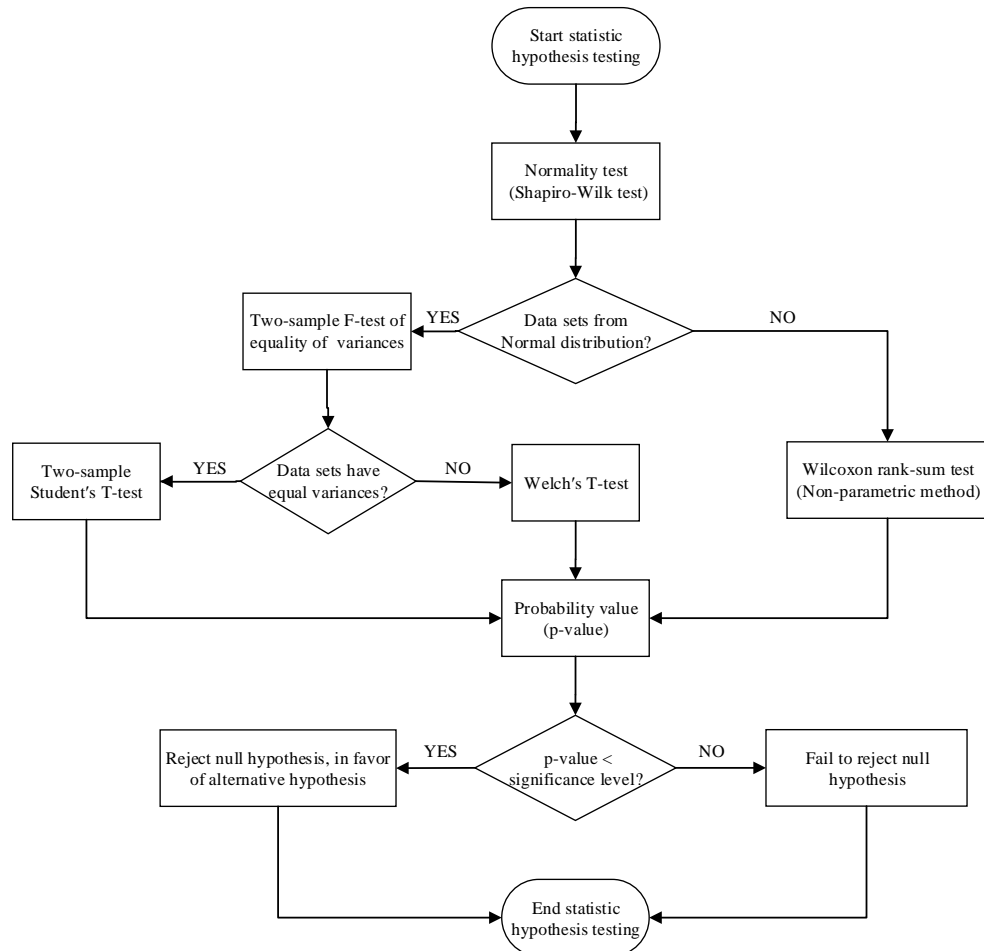


Figure 3-6. The flowchart for the statistical hypothesis testing

Firstly, it is necessary to decide whether the data sets are drawn from normally distributed populations, as the test methods for data from normal distribution and abnormal distribution are different: The common test methods are the parametric method and most of them are only suitable for data from normal distribution. As for data from abnormal distribution, a non-parametric method can be applied. The Shapiro-Wilk test (1965) is performed herein to test the normality of the data sets, since it is one of the most commonly used methods and it has been proved by Razali *et al.* (2011) that the Shapiro-Wilk test had the best utility for a given significance. It tests the null hypothesis that the data is normally distributed. The test statistic is

$$W = \frac{\sum_{j=1}^n a_j^2 x_{(j)}^2}{\sum_{j=1}^n (x_j - \bar{x})^2} \quad (3-5)$$

where $x_{(j)}$ (with parentheses enclosing the subscript index j) is the j^{th} order statistic, i.e., the j^{th} smallest number in the data set; x_j is the j^{th} statistic in the data set; \bar{x} is the arithmetic mean of the data set; a_j is a constant related to the standard normal distribution and is given by Shapiro and Wilk (1965). If the data sets are tested statistically not drawn from normal distribution population, the Wilcoxon rank sum test is applied to perform statistical hypothesis testing, as it is one of the most frequently used non-parametric tests (Mann *et al.*, 1947). The test statistic is

$$Z = \frac{r_1 - \frac{n_1(n_1 + n_2 + 1)}{2}}{\sqrt{\frac{n_1 n_2 (n_1 + n_2 + 1)}{12}}} \quad (3-6)$$

where r_1 is the sum of the ranks in data set 1; n_1 is the size of data set 1; n_2 is the size of data set 2. If the data sets are statistically proved to follow the normal distribution, another property that needs to be determined is the variance equality of two populations, as the test methods for data with equal variances and unequal variances are different. The test method used herein is the two-sample F-test of equality of variances. The test statistic is

$$F = \frac{S_1^2}{S_2^2} \quad (3-7)$$

where S_1^2 is the variance of data set 1; S_2^2 is the variance of data set 2. For data sets drawn from populations with equal variances, the two-sample Student's

T-test is applied to perform statistical hypothesis testing and for data sets drawn from populations with unequal variances, the Welch's test is used instead. The Welch's test is an adaptation of the Student's t-test, which is more reliable when the data sets are drawn from populations with unequal variances (Ruxton, 2006). The test statistic and the degree of freedom of test statistic of these two tests are different. The test statistic of the two-sample Student's T-test is

$$t = \frac{\bar{X}_1 - \bar{X}_2}{\sqrt{\frac{(n_1 - 1)S_1^2 + (n_2 - 1)S_2^2}{n_1 + n_2 - 2} \left(\frac{1}{n_1} + \frac{1}{n_2} \right)}} \quad (3-8)$$

where \bar{X}_1 is the arithmetic mean of data set 1; \bar{X}_2 is the arithmetic mean of data set 2. The degree of freedom of this test statistic is $n_1 + n_2 - 2$. As for the Welch's test, the test statistic is

$$t = \frac{\bar{X}_1 - \bar{X}_2}{\sqrt{\frac{S_1^2}{n_1} + \frac{S_2^2}{n_2}}} \quad (3-9)$$

and the degree of freedom of this test statistic is $\frac{\left(\frac{S_1^2}{n_1} + \frac{S_2^2}{n_2} \right)^2}{\left(\frac{\left(\frac{S_1^2}{n_1} \right)^2}{n_1 - 1} + \frac{\left(\frac{S_2^2}{n_2} \right)^2}{n_2 - 1} \right)}$. All of

these five test methods can provide the probability value (p-value), which is the probability that, when the null hypothesis is true, the test statistic would be the same as or of greater magnitude than the actual observed results. Then,

comparing the probability value with pre-specified significance level, if the probability value is less than the significance level, the null hypothesis will be rejected and the alternative hypothesis will be accepted, otherwise the null hypothesis will be accepted.

3.5.3 Results of Statistical Hypothesis Testing

The results of the normality test are shown in Table 3-3. It can be seen that the probability values of 2 trials of sodium tridecyl sulfate solution (1.301 g/L) are larger than the significance level ($\alpha = 0.01$), whereas those of SDS solution (0.288 g/L in 0.584 g/L NaCl) are smaller than the significance level. This indicates that the observed data of two trials of sodium tridecyl sulfate solution (1.301 g/L) are significantly drawn from normality distributed populations, whereas the data sets of two trials of SDS solution (0.288 g/L in 0.584 g/L NaCl) are not significantly drawn from normally distributed populations. Therefore, for SDS solution (0.288 g/L in 0.584 g/L NaCl), the Wilcoxon rank-sum test is applied directly to perform statistical hypothesis testing. While for sodium tridecyl sulfate solution (1.301 g/L), the equality of variances of the populations which the data sets are drawn from need to be tested next to select appropriate test method.

Table 3-3. Results of the normality test showing that whether the data sets are drawn from normally distributed populations

Sample	Trial	p-value	Decision at $\alpha=0.01$
Sodium tridecyl sulfate solution (1.301 g/L)	1 st	0.2866	Cannot reject normality
	10 th	0.0226	Cannot reject normality
SDS solution (0.288 g/L in 0.584 g/L NaCl)	1 st	0.0056	Reject normality
	10 th	0.0004	Reject normality

The two sample F-test for equality of variances is performed and the probability value of sodium tridecyl sulfate solution (1.301 g/L) is 0.0037, which is smaller than the pre-specified significance level. This illustrates that the variances of the two populations which the data sets of sodium tridecyl sulfate solution (1.301 g/L) drawn from are significantly different. Thus, for sodium tridecyl sulfate solution (1.301 g/L), Welch's T-test is the appropriate test method for performing statistical hypothesis testing. After conducting the normality test and the variance equality test, the optimum test method for each sample has been selected and then the statistical hypothesis testing for each sample has been conducted individually using corresponding optimum test method. The results of statistical hypothesis testing are shown in Table 3-4.

Table 3-4. Results of statistical hypothesis testing

Sample	Test method	p-value	Decision at $\alpha=0.01$
Sodium tridecyl sulfate solution (1.301 g/L)	Welch's T-test	0.0664	Cannot reject null hypothesis
SDS solution (0.288 g/L in 0.584 g/L NaCl)	Wilcoxon rank-sum test	0.0757	Cannot reject null hypothesis

It demonstrates that the probability values of these two surfactant solutions are both larger than the pre-specified significance level, which indicates that the null hypothesis cannot be rejected. The statement of null hypothesis is accepted and statistically proved, which indicates that, for both sodium tridecyl sulfate solution (1.301 g/L) and SDS solution (0.288 g/L in 0.584 g/L NaCl), the dynamic surface tension results of trial 1 can be considered as the same with the dynamic surface tension results of trial 10. Furthermore, this demonstrates that the dynamic surface tension of individual trials can be considered as the same and do not change significantly for a statistical perspective (i.e. considering large data population). Due to this, the arithmetic mean of the dynamic surface tension results of all 100 trials can be applied to represent the dynamic surface tension of these two surfactant solutions. In addition, this indicates that performing large numbers of independent trials of dynamic surface tension measurement using the static pendant droplet method is necessary to obtain the dynamic surface tension value of ionic surfactant solution with highly surface-active impurity, which can be quantified by the arithmetic mean of dynamic surface tension results between different trials.

3.6 Summary

Dynamic surface tension measurements of ionic surfactant solution using the static pendant droplet method are performed statistically sufficient independent trials. The observable differences of dynamic surface tension results are noted, and it is demonstrated that these differences are due to the presence of trace amounts of highly surface-active impurities, which compromises the repeatability and precision of dynamic surface tension

measurement of ionic surfactant solution using the static pendant droplet method. For ionic surfactant solution without highly surface-active impurity, the considerable differences of dynamic surface tension have not been observed and the dynamic surface tension results show acceptable repeatability and precision. Furthermore, it is proved that, with respect to the static pendant droplet method, obtaining the dynamic surface tension value of ionic surfactant solutions with highly surface active impurity from a single trial or a small quantity of trials is not necessarily accurate and therefore not reliable. It is necessary to perform large numbers of independent trials of dynamic surface tension measurement to acquire the dynamic surface tension values of ionic surfactant solution with highly surface-active impurity by calculating the arithmetic mean.

**Chapter 4 Effect of Environmental
Relative Humidity on Foam Stability**

4.1 Introduction

It is essential to characterise foam stability accurately when relating foam stability to surface mechanical properties, otherwise the conclusion obtained from the inaccurate foam stability results will be compromised. Therefore, it is important and necessary to study the accurate measurement of foam stability. In this chapter, measurements of foam stability at different environmental relative humidities are performed to confirm and extend the observation of the dependency of foam stability upon environmental relative humidity obtained by Li *et al.* (2010).

4.2 Experimental Details

The modified Bikerman foam stability test of Li *et al.* (2010) is performed herein to measure foam stability of SDS solution at the concentration of 2.402 g/L (i.e. 1.56% above the CMC) with different environmental relative humidities in the freeboard (which is the space between the foam surface and the top of the column). Note that the SDS solution is prepared slightly above the CMC to ensure that the actual concentration of the prepared SDS solution reaches the CMC and thus to avoid a possible smaller equilibrium surface tension if the actual concentration of the prepared SDS solution is smaller than the CMC. The CMC of SDS solution is 2.365 g/L (Varga *et al.*, 2007). In this modified method, a non-overflowing pneumatic foam is created in a column by supplying compressed air into SDS solution. The foam will reach an equilibrium height when the collapse rate at the top of the foam is equal to the formation rate at the bottom of the foam. In comparison to the original test of

Bikerman (1938, 1973), the modification is that the environmental relative humidity at the top of the column is controlled and recorded when producing the foam. In the original Bikerman foam stability test, foam stability was quantified as the quotient of equilibrium foam height and superficial air velocity, which was defined by Bikerman (1973) as

$$\Sigma = \frac{H_e}{j_a} \quad (4-1)$$

where Σ is the quotient of equilibrium foam height and superficial air velocity which has unit of time. H_e is the equilibrium foam height and j_a is the superficial air velocity. In the current experiment, foam stability is characterised by the equilibrium foam height when all the experimental conditions are specified, including temperature, superficial air velocity, and bubble size.

A representative photograph and a schematic diagram of the whole experimental system are shown in Figure 4-1 and 4-2, respectively. The Perspex column of circular section is 1.2 m tall and the internal and external diameters of the Perspex column are 52 mm and 60 mm, respectively. The column consists of two parts: the upper one is 1 m tall with a scale fitted to the side to record the foam height and the lower one is 0.2 m tall. They are connected by a flange. A glass frit is clamped between the two parts and the porosity of the glass frit is 40-100 μm . Humid air is pumped into the column from the bottom via this glass frit. A needle valve and a flowmeter are connected in series with the humid air tubing to control and measure the superficial velocity of humid air. Dry air is supplied into the column and

mixed with environmental air from the top via a specially constructed distribution tubing located 0.1 m below the top to control the relative humidity at the top of the column. Another needle valve/ flowmeter set is connected with the dry air tubing to control and measure the superficial velocity of dry air. Self-indicating silica gel (Fisher Scientific) is employed herein as drying agent, which turns from orange to colourless when water is adsorbed (The effectiveness of drying agent to dry compressed air is demonstrated in Appendix D). The relative humidity is measured at the top of the column by a thermohygrometer (Rotronic, HC2-WIN-USB) which reports to a computer. The relative humidity is recorded every minute and the arithmetic mean of all relative humidity results during the measurement is calculated as the value of relative humidity of the measurement. During the measurement, photographs are taken at the bottom of the foam layer by a digital camera (Canon, IXUS 275) with illumination (LED Torch, HILIGHT 2000).

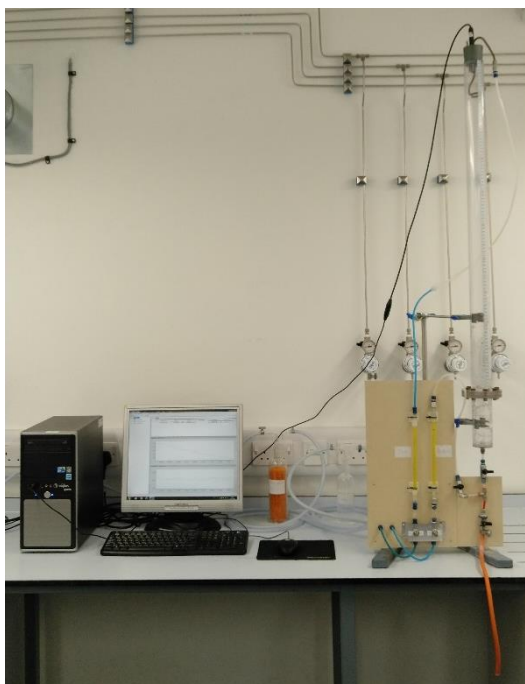


Figure 4-1. The representative photograph of the experimental system for measuring foam stability under conditions of controlled-humidity

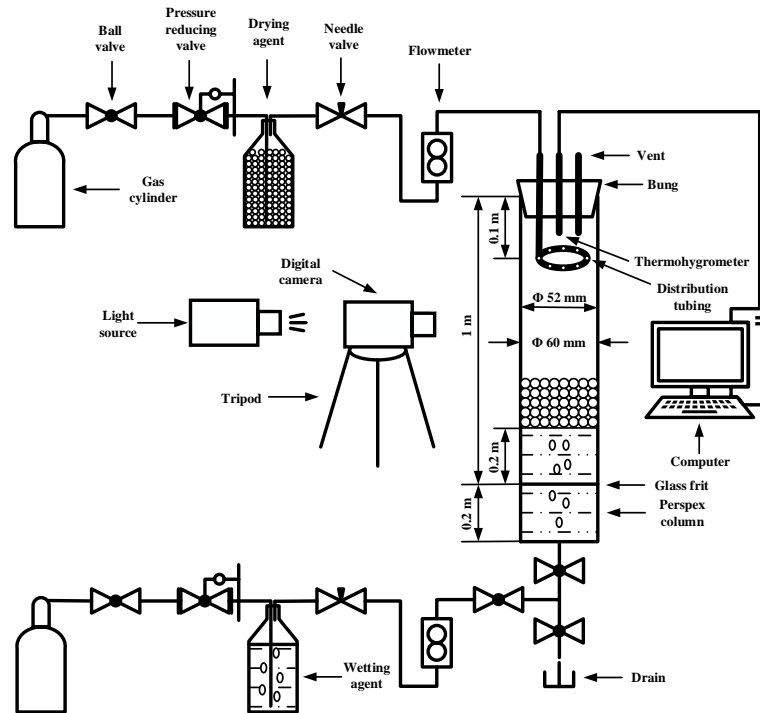


Figure 4-2. The schematic diagram of the experimental system for measuring foam stability under conditions of controlled-humidity

All measurements are performed at the temperature of the laboratory, which is controlled at 22 ± 1 °C. The values of environmental relative humidity controlled herein are 93.9 ± 1.0 , 71.1 ± 2.6 , 51.3 ± 1.2 , 30.5 ± 1.2 and $10.0 \pm 1.5\%$ (The corresponding superficial velocities of dry air to maintain these environmental relative humidities are 0 (The dry air is not delivered), 0.30 ± 0.03 , 0.35 ± 0.01 , 0.39 ± 0.01 , 0.42 ± 0.01 mm/s, respectively). The foam stability measurements are repeated 3 times at each environmental relative humidity value. 1 litre SDS solution at the concentration of 2.402 g/L is used and the foam-liquid interface is kept 0.8 m below the top of the column in each trial. The superficial velocity of humid air is kept constant at 0.075 ± 0.015 mm/s for each trial. (It has been demonstrated by Li *et al.* (2010) that the evolution of foam height was a function of superficial velocity of humid air and they have performed the foam stability measurement at humid air

superficial velocities of 0.027, 0.053, 0.080, 0.107 and 0.133 mm/s. In the current work, the superficial velocity of humid air is maintained constant at a relatively intermediate value to ensure the air flow is steady and non-overflowing foam is obtained). The foam height is recorded every 5 minutes after delivering humid air into SDS solution. For each trial, 3 photographs are taken of the foam and an image processing software (ImageJ) is applied to provide an estimation of the arithmetic mean bubble diameter of the foam. Note that due to the curved nature of the column and the refraction of light, the quality of photographs obtained herein is compromised because of the optical distortion issue and therefore affects the estimation of the arithmetic mean bubble diameter of the foam. However, these photographs are still analysed to provide an objective estimation of the arithmetic mean bubble diameter of the foam. By means of the programme, the photograph is expanded and a square with 100 mm² area is drawn upon it, then the number of bubbles covered in the square is counted. It is assumed that the shape of a bubble in the photograph is circle and the area of all bubbles covered in the square is approximately equal to the area of the square, which gives

$$n\pi\left(\frac{D_A}{2}\right)^2 = 100 \quad (4-2)$$

where n is the number of bubbles covered in the square and D_A is the arithmetic mean bubble diameter. According to eq. 4-2, the arithmetic mean bubble diameter can be calculated through the number of bubbles covered in the square. A representative photograph of produced foams with a square of 100 mm² area is shown in Figure 4-3.

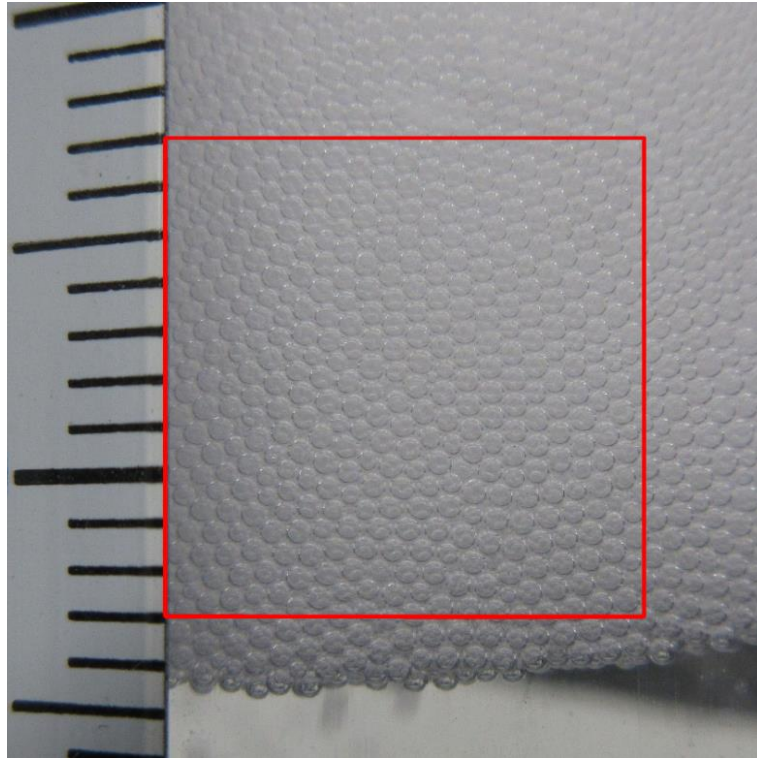


Figure 4-3. Representative photograph of produced foams with a square of 100 mm^2 area. This foam is produced by SDS solution at the concentration of 2.402 g/L with the environmental relative humidity at the top of the column controlled at $93.9 \pm 1.0 \%$. The minimum graduation of this scale is 1 mm .

Note that this method is not an actual measurement of the bubble diameter, instead it just provides an indication of bubble diameter. In the current work, it is used to estimate the arithmetic mean bubble diameter of produced foams. For all measurements, the estimation of arithmetic mean bubble diameter is $0.53 \pm 0.11 \text{ mm}$. The error is the standard deviation of all arithmetic mean bubble diameters calculated from all photographs.

4.3 Effect of Environmental Relative Humidity on Foam Stability

The evolution of foam height of SDS solution with different values of environmental relative humidity at the top of the column is shown in Figure 4-4 (The detailed results of each independent measurement are shown in Appendix E). It is seen that the foam height increases approximately linearly

when the environmental relative humidity at the top of the column is 93.9%. It indicates that the foam continues to grow linearly and does not reach an equilibrium height during the measurement period when the air at the top of the column is nearly saturated with water. For lower values of environmental relative humidity, it is seen that the foam heights also grow approximately linearly at first before attaining an equilibrium height. The equilibrium foam height and the Bikerman's Σ value with different environmental relative humidities at the top of the column are shown in Table 4-1 and the equilibrium foam height plotted against environmental relative humidity is shown in Figure 4-5. As can be seen, the equilibrium foam height grows monotonically with the increase of environmental relative humidity at the top of the column. This indicates that the equilibrium foam height is a function of environmental relative humidity, thereby confirming and extending the observations of Li *et al.* (2010). Furthermore, this result also shows agreement with the observation obtained by Champougny *et al.* (2018), who have experimentally investigated the influence of environmental relative humidity on soap film stability and have found that the film length at rupture increased continuously with the environmental relative humidity.

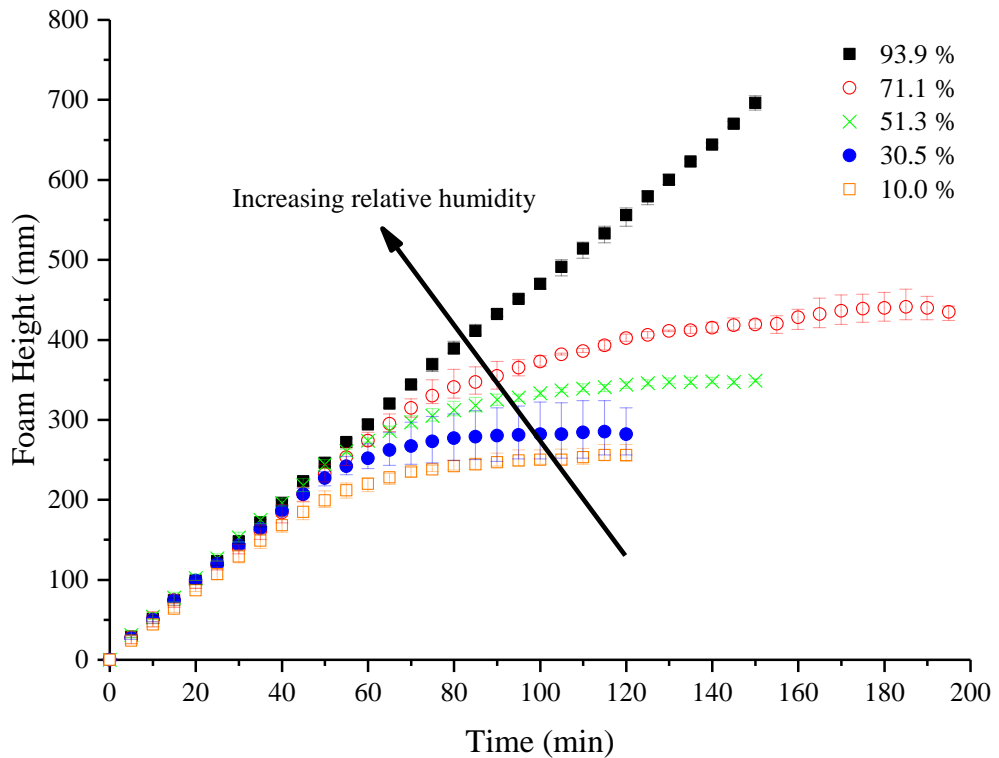


Figure 4-4. The foam height of SDS solution with different environmental relative humidities at the top of the column. The error bars represent the full range of independent observations. The legend indicates the environmental relative humidity in the freeboard of the column. This result shows agreement with the observation of Li *et al.* (2010)

Table 4-1. The equilibrium foam height with different environmental relative humidities at the top of the column. The error of the environmental relative humidity is the standard deviation of all recorded environmental relative humidity results. The values in brackets of equilibrium foam height represent the full range of observations. The values in brackets of Bikerman's Σ value represent the full range of calculations.

Relative Humidity (%)	Equilibrium Foam Height (mm)	Bikerman's Σ value (s)
93.9 ± 1.0	696 (687 - 705) (the highest value that was recorded)	9280 (7633 - 11750)
71.1 ± 2.6	435 (424 - 442)	5800 (4711 - 7367)
51.3 ± 1.2	349 (347 - 351)	4653 (3856 - 5850)
30.5 ± 1.2	282 (256 - 315)	3760 (2844 - 5250)
10.0 ± 1.5	256 (248 - 269)	3413 (2756 - 4483)

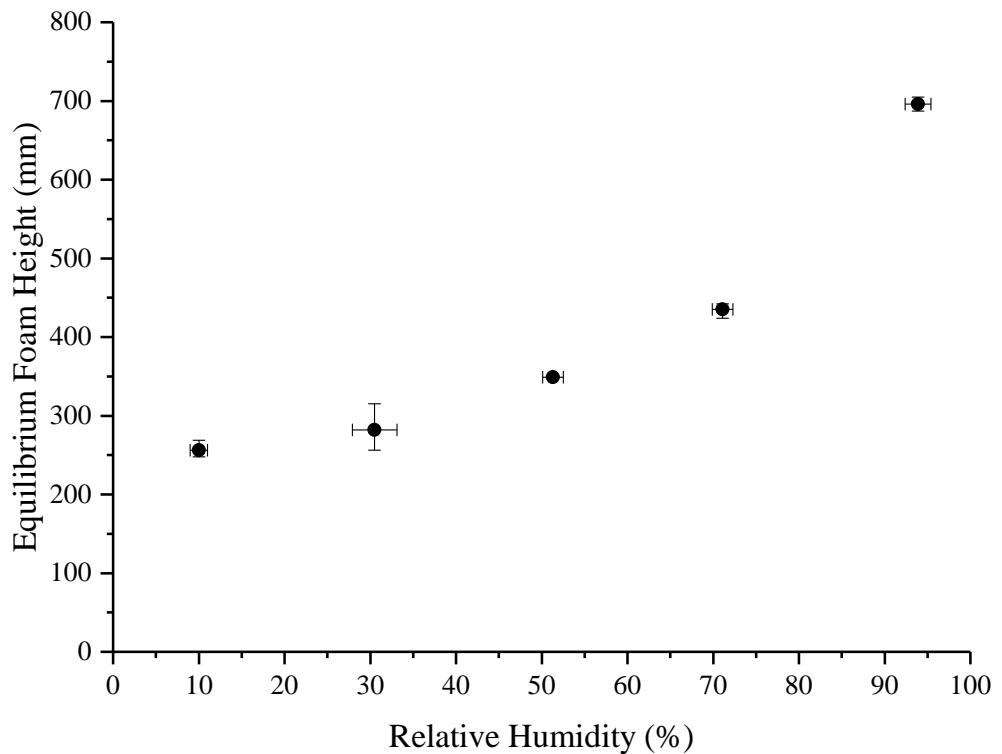


Figure 4-5. The equilibrium foam height as a function of environmental relative humidity. Note that the foam height at environmental relative humidity of 93.9% is the highest value that was recorded rather than an equilibrium value. The error bars of the environmental relative humidity represent the standard deviation of all observations. The error bars of equilibrium foam height represent the full range of independent observations (because the independent foam stability measurements at each environmental relative humidity are only repeated 3 times).

Since foam stability is characterised by the equilibrium foam height, it is reasonable to conclude that foam stability is a function of environmental relative humidity at the top of the column and the foam becomes more stable with the increase of the environmental relative humidity at the top of the column. Thus, foam stability can be manipulated by changing the environmental relative humidity at the top of the column. This indicates that the environmental relative humidity is also an important element that affects foam stability and it has to be controlled and measured when using equilibrium foam height or similar parameters to quantify foam stability. It is only meaningful to compare foam stability which is measured at the same environmental relative humidity, as well as other experimental conditions. Li

et al. (2010) have emphasised that environmental relative humidity should be controlled in foam stability measurement and the observation obtained by Champougny *et al.* (2018) has also suggested the importance of environmental relative humidity in foam stability measurement. However, this factor has still been largely overlooked by researchers who perform foam stability measurement and the environmental relative humidity has not been controlled with high precision. For instance, Wang *et al.* (2016) have studied the stability of foams stabilised by SDS solution with and without dodecanol. In their experiment, the environmental relative humidity was kept at 50-60% and it was considered as constant. Nevertheless, it can be seen from Figure 4-5 that the equilibrium foam height difference between the environmental relative humidity of 50% and 60% is still material, with a difference in foam height of approximately 50 mm being observed in the current experiment. This indicates that the environmental relative humidity of 50-60% cannot be regarded as the same and the conclusions obtained in their study are potentially compromised, as the difference of foam stability could result from the difference of environmental relative humidity. Therefore, it is important to control the environmental relative humidity with high accuracy when measuring foam stability. Note that in the current work, the observations of foam stability have not been compared directly with the results of foam stability measurement of Wang *et al.* (2016), since the experimental systems and conditions of their work are different with those of the current work, which results in the direct comparison impracticable.

4.4 Summary

In this chapter, foam stability is measured with a modified Bikerman foam stability test at different environmental relative humidities. It is confirmed that foam stability is dependent upon environmental relative humidity. With regards to relating foam stability to surface mechanical properties, foam stability of different surfactant solutions need to be measured at the same environmental relative humidity. In the experiments of later chapters (chapters 5 and 6), all the foam stability measurements are performed at consistent values of environmental relative humidity. In the next chapter (Chapter 5), the relationship between foam stability and surface mechanical properties, including surface tension and surface rheological properties, are studied. It is precisely to facilitate an investigation of this relationship that the environmental relative humidity has to be controlled at a constant value.

**Chapter 5 Dependency of Foam
Stability upon Surface Tension and
Surface Dilatational Properties**

5.1 Introduction

After a detailed exploration of the measurement of surface rheological properties, surface tension and foam stability, in this chapter, foam stability will be correlated to surface rheological properties including surface elasticity, surface dilatational viscosity and Gibbs elasticity under the condition that the effect of surface tension on foam stability is kept constant and therefore eliminated. Firstly, the static pendent droplet method is performed to measure dynamic surface tension of different surfactant solutions in order to find out the different surfactant solutions with approximately the same equilibrium surface tension. Then, the measurements of foam stability and surface rheological properties of these surfactant solutions are performed to correlate foam stability with surface rheological properties.

5.2 Different Surfactant Solutions with Approximately the Same Equilibrium Surface Tension

As described above (in subsection 1.4.2), it is important to eliminate the effect of surface tension on foam stability when relating foam stability to surface rheological properties. Therefore, surface rheological properties have to be varied independently of surface tension, which means that surface rheological properties are changed whilst maintaining an approximately constant equilibrium surface tension. This is achieved by changing the surfactant type and manipulating the concentration of surfactant solutions so that the equilibrium surface tension is approximately the same.

In order to find different surfactant solutions with approximately the same equilibrium surface tension, the static pendant droplet method is performed herein to measure dynamic surface tension of different surfactant solutions with different concentrations. The equilibrium surface tension can be obtained by linear extrapolation of the dynamic surface tension to infinite time *via* the method of Makievski *et al.* (1997), who suggested that as a long time approximation, the dynamic surface tension is a linear function of $t^{-1/2}$, which can be written as

$$\sigma = \frac{RT\Gamma_e^2}{2c} \left(\frac{\pi}{D} \right)^{1/2} t^{-1/2} + \sigma_e \quad (5-1)$$

where R is universal gas constant; T is absolute temperature; c is bulk concentration of surfactant solution; π is circular constant; D is diffusion coefficient; t is time and σ_e is equilibrium surface tension. When plotting eq. 5-1 into coordinate system with σ vs. $t^{-1/2}$, the intercept at ordinate is an estimation of equilibrium surface tension. In fact, to simplify the estimation process, the results of dynamic surface tension are plotted against $t^{-1/2}$, then a tangent of the curve is plotted and the intercept at ordinate can be considered as the estimation of equilibrium surface tension. Note that this method is originally proposed for non-ionic surfactants and the estimated equilibrium surface tension by this method is typically smaller than the real equilibrium surface tension, which can amount to 0.5-2 mN/m (Makievski *et al.*, 1997). However, it is applied herein to provide an objective criterion for the determination of equilibrium surface tension.

The surfactants used for the experiment are TX-100 which is a non-ionic surfactant, sodium tridecyl sulfate and dodecyl trimethyl ammonium bromide (DTAB). TX-100 was also purchased from Fisher Scientific Co. with purity above 95% and these three surfactants are all used without further purification. The CMC of these three surfactant solutions are 0.175 g/L, 1.267 g/L, and 4.718 g/L, respectively (Soria-Sanchez *et al.*, 2010; Varga *et al.*, 2007; Atkin *et al.*, 2003). The same apparatus as shown in Figure 2-2 has been applied to this set of experiments and the static pendent dropt method has been performed under the same experimental conditions as described in subsection 3.2.1. Independent measurements are repeated 100 times and the arithmetic mean of dynamic surface tension results obtained from all independent trials is calculated to obtain the value of dynamic surface tension. This set of experiments are repeated with above three surfactants at different concentrations until approximately the same equilibrium surface tension of these three surfactant solutions at different concentrations have been obtained. Finally, the determined concentrations for TX-100, sodium tridecyl sulfate and DTAB solutions are 0.066 g/L (i.e. 37.50% of the CMC of TX-100), 1.301 g/L (i.e. 2.68% above the CMC of sodium tridecyl sulfate) and 4.954 g/L (i.e. 5.00% above the CMC of DTAB), individually. Note that the equilibrium surface tension of TX-100 solution at the concentration of 0.066 g/L is actually slightly higher than the equilibrium surface tension of the other two surfactant solutions which are almost the same. However, it is the closest value can be obtained to the equilibrium surface tension of the other two surfactant solutions in the current experiments. The detailed results of equilibrium

surface tension of TX-100 solution at different concentrations are shown in Appendix F.

The dynamic surface tension results of these three surfactant solutions are shown in Figure 5-1 and the method of linear extrapolation of dynamic surface tension to estimate equilibrium surface tension is shown in Figure 5-2. It can be seen in Figure 5-1 that the dynamic surface tension of TX-100 solution at the concentration of 0.066 g/L is larger than that of sodium tridecyl sulfate solution at the concentration of 1.301 g/L which is larger than that of DTAB solution at the concentration of 4.954 g/L.

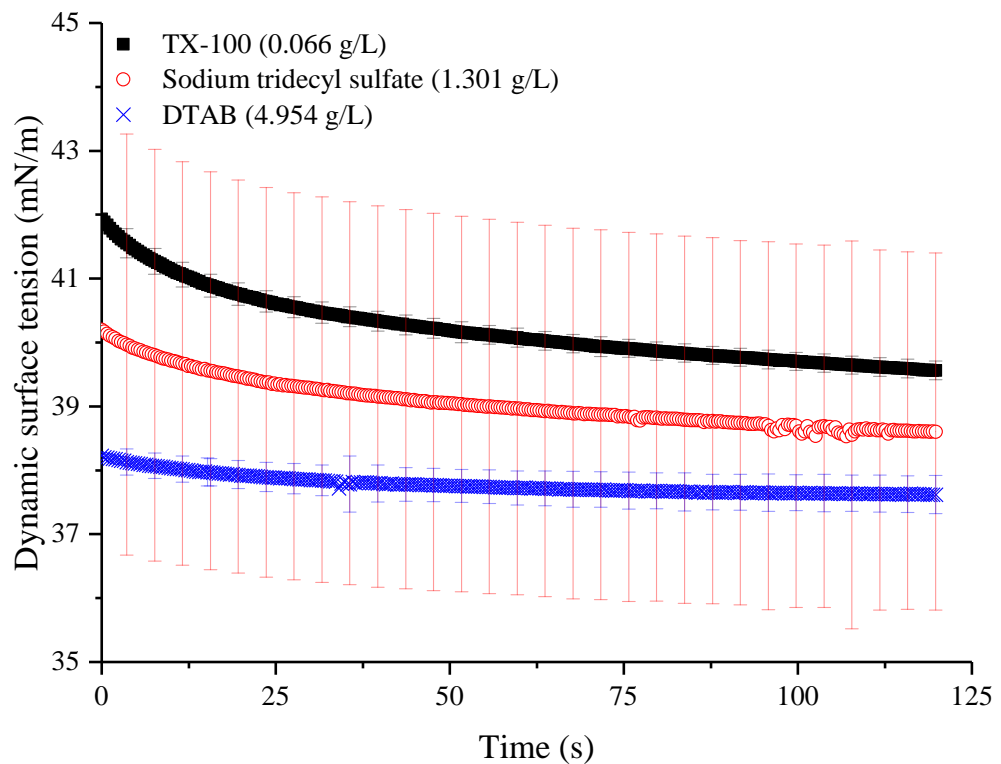


Figure 5-1. Dynamic surface tension results of TX-100 solution (0.066 g/L), sodium tridecyl sulfate solution (1.301 g/L) and DTAB solution (4.954 g/L). The error bars represent the standard deviation of the observations. All the errors of obtained data are calculated and only present 1 error bar in every 10 error bars for clarity.

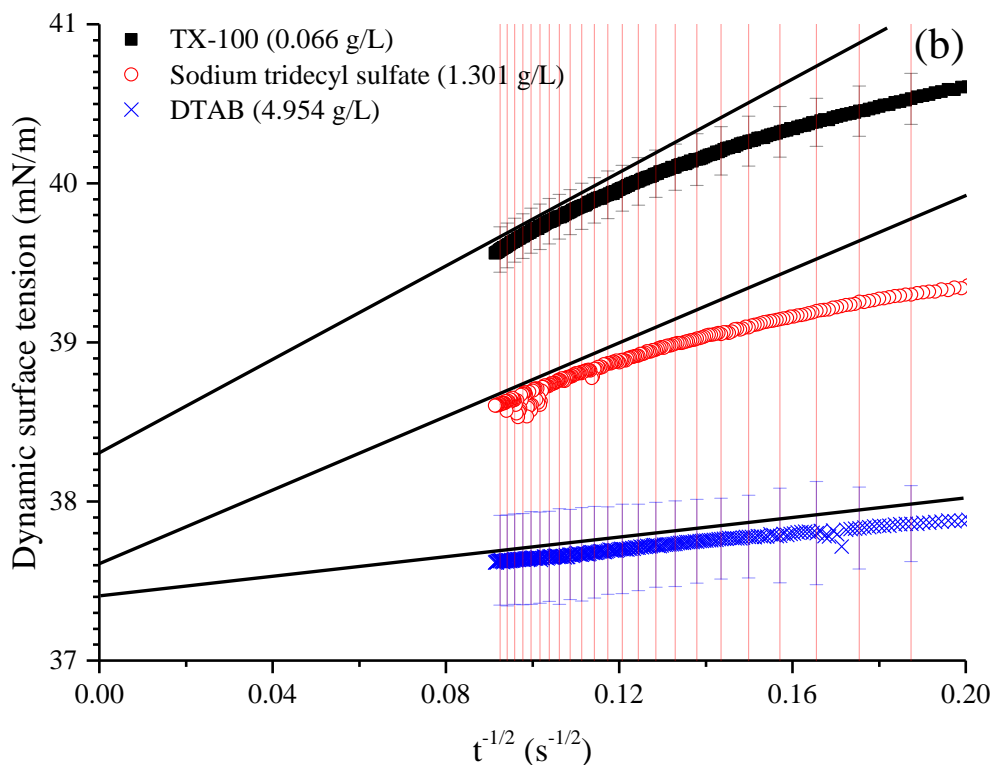
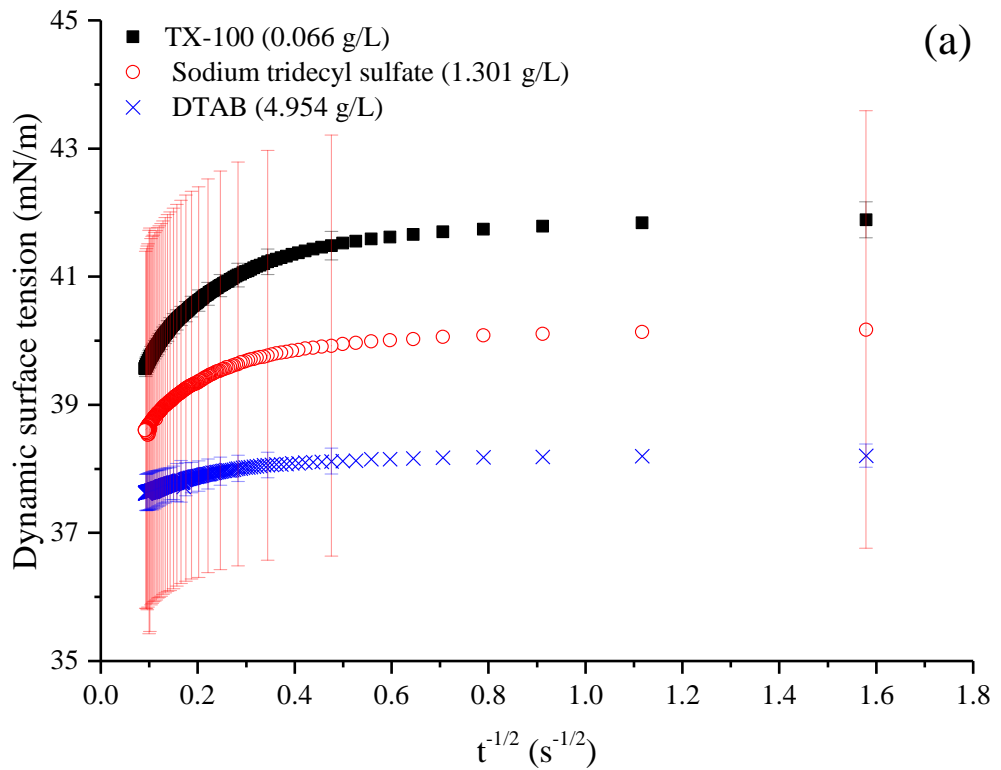


Figure 5-2. Dynamic surface tension results of TX-100 solution (0.066 g/L), sodium tridecyl sulfate solution (1.301 g/L) and DTAB solution (4.954 g/L) against $t^{-1/2}$. (a) Full range of results. (b) Partial enlarged view. The straight line represents a tangent and a linear extrapolation of dynamic surface tension to infinite time. The intercept at ordinate represents the estimated equilibrium surface tension. The error bars represent the standard deviation of the observations. All the errors of obtained data are calculated and only present 1 error bar in every 10 error bars for clarity.

After plotting the dynamic surface tension results of these three surfactant solutions against $t^{-1/2}$ as shown in Figure 5-2(a), a tangent to the curve is applied as linear extrapolation of dynamic surface tension and the intercepts at ordinate are the estimated equilibrium surface tensions of these three surfactant solutions, which are shown in Figure 5-2(b). The estimated equilibrium surface tensions of these three surfactant solutions are shown in Table 5-1. The error of equilibrium surface tension is calculated by the average of errors of dynamic surface tension of 300 images (i.e. over 2 minutes).

Table 5-1. Results of equilibrium surface tension, surface rheological properties and equilibrium foam height of TX-100 solution (0.066 g/L), DTAB solution (4.954 g/L) and sodium tridecyl sulfate solution (1.301 g/L). The errors of equilibrium surface tension and surface rheological properties are the standard deviation of the independent observations. The values in brackets represent the full range of observations.

Sample	Equilibrium surface tension (mN/m)	Surface elasticity (mN/m)	Surface dilatational viscosity (mN·s/m)	Gibbs elasticity (mN/m)	Equilibrium foam height (mm)
TX-100 (0.066 g/L)	38.30 ± 0.16	15.32 ± 0.27	2.46 ± 0.11	39.02 ± 2.45	164 (162 - 166)
DTAB (4.954 g/L)	37.40 ± 0.27	2.51 ± 0.43	0.05 ± 0.04	2.70 ± 0.42	288 (280 - 302)
Sodium tridecyl sulfate (1.301 g/L)	37.60 ± 2.97	3.53 ± 0.16	0.34 ± 0.02	5.50 ± 0.26	314 (307 - 320)

It can be seen from Figure 5-2(b) and Table 5-1 that the equilibrium surface tension of TX-100 solution at the concentration of 0.066 g/L, DTAB solution at the concentration of 4.954 g/L and sodium tridecyl sulfate solution at the concentration of 1.301 g/L are 38.30, 37.40 and 37.60 mN/m, respectively. This indicates that the equilibrium surface tension of DTAB solution at the concentration of 4.954 g/L and sodium tridecyl sulfate solution at the concentration of 1.301 g/L are approximately the same, whilst the equilibrium

surface tension of TX-100 solution at the concentration of 0.066 g/L is slightly higher than that of the other two solutions. This statement will be confirmed by the observation of bubble size of foams produced from these three surfactant solutions in the next section (section 5.3).

In this section, two surfactant solutions with approximately the same equilibrium surface tension and one surfactant solution with slightly higher equilibrium surface tension are obtained. In the next section, foam stability of these three surfactant solutions are measured at the same environmental relative humidity and surface rheological properties of these three surfactant solutions are measured at the same oscillation frequency and amplitude. Then, the relationship between surface rheological properties and foam stability of these three surfactant solutions will be studied.

5.3 Relationship between Surface Rheological Properties and Foam Stability

In order to relate foam stability to surface rheological properties, the measurements of foam stability and surface rheological properties of different surfactant solutions as mentioned above are performed. The same methods as described in sections 2.3 and 4.2 are applied. The foam stability measurements are performed at environmental relative humidity of $70.0 \pm 0.3\%$, since a finite foam height of large depth can be obtained under this condition. The superficial velocity of dry air is controlled at 0.30 ± 0.03 mm/s during the experiment to maintain this environmental relative humidity. All the other experimental conditions remain the same as mentioned in section 4.2 and the

same method to obtain the estimation of arithmetic mean bubble diameter as described in section 4.2 is applied herein as well to quantify the bubble size of produced foams. Also, the measurements of surface rheological properties are performed at the oscillation frequency of 0.5 Hz and the oscillation amplitude of 0.25. Note that 0.5 Hz is approximately the underlying frequency applied on bubbles in the foam stability measurement considering the superficial velocity of dry air (0.30 ± 0.03 mm/s) and the bubble size (i.e. arithmetic mean bubble diameter) of foams (for example, the estimation of arithmetic mean bubble diameter of foams produced from DTAB solution (4.954 g/L) is 0.59 ± 0.06 mm), since the quotient of superficial velocity of dry air and bubble size (i.e. arithmetic mean bubble diameter) indicates the value of underlying frequency applied on bubbles. The value of oscillation amplitude is chosen at 0.25, as this value ensures droplet oscillation whilst retaining the integrity of the droplet. The measurements are repeated 30 times with each of the surfactant solution. All the other experimental conditions are the same as in section 2.3.

Typical photographs of foams produced from TX-100 solution (0.066 g/L), DTAB solution (4.954 g/L) and sodium tridecyl sulfate solution (1.301 g/L) are shown in Figure 5-3. It can be seen from Figure 5-3 that the bubble size (i.e. arithmetic mean bubble diameter) of foam produced from TX-100 solution at the concentration of 0.066 g/L is larger than those of other foams, which are otherwise approximately the same. In fact, the bubble size (i.e. arithmetic mean bubble diameter) of these foams produced from TX-100 solution (0.066 g/L), DTAB solution (4.954 g/L) and sodium tridecyl sulfate

solution (1.301 g/L) are 0.77 ± 0.08 , 0.59 ± 0.06 and 0.59 ± 0.11 mm, respectively. The error of the bubble size is the standard deviation of bubble sizes calculated from all photographs of each surfactant solution. Note that the difference of bubble sizes between foam produced by TX-100 solution at the concentration of 0.066 g/L and the other two foams only results from the different equilibrium surface tension, as the foams of different surfactant solutions are produced at the same conditions (i.e. the porosity of glass frit, superficial air velocity, environmental temperature and relative humidity are all the same). Therefore, the observation of bubble size (i.e. arithmetic mean bubble diameter) of different foams confirms that the equilibrium surface tension of TX-100 solution at the concentration of 0.066 g/L is higher than those of DTAB solution at the concentration of 4.954 g/L and sodium tridecyl sulfate solution at the concentration of 1.301 g/L, which are approximately the same. This shows agreement with the observation of estimated equilibrium surface tension of these three surfactant solutions.

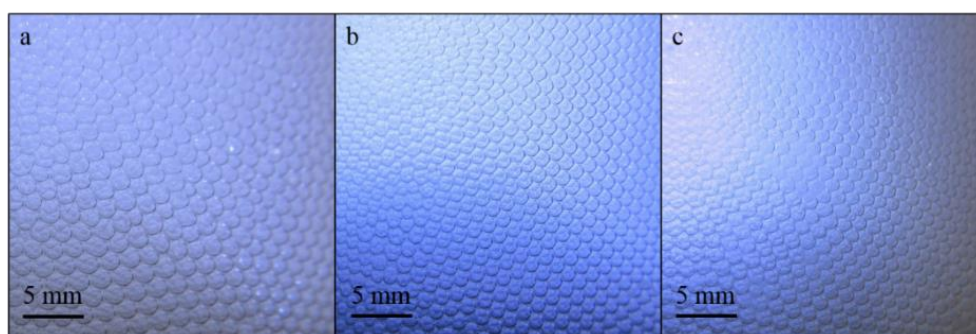


Figure 5-3. The representative photo of foams produced from TX-100 solution (0.066 g/L), DTAB solution (4.954 g/L) and sodium tridecyl sulfate solution (1.301 g/L). (a) Foam produced from TX-100 solution at the concentration of 0.066 g/L. (b) Foam produced from DTAB solution at the concentration of 4.954 g/L. (c) Foam produced from sodium tridecyl sulfate solution at the concentration of 1.301 g/L. The proportional scale is 5 mm.

The evolution of foam height of these three surfactant solutions are shown in Figure 5-4 (The detailed results of each independent measurement are shown

in Appendix F). It is shown in Figure 5-4 that the foam heights of these three surfactant solutions grow approximately linearly at first until reaching an equilibrium height, which confirms the observation that is shown in section 4.3.

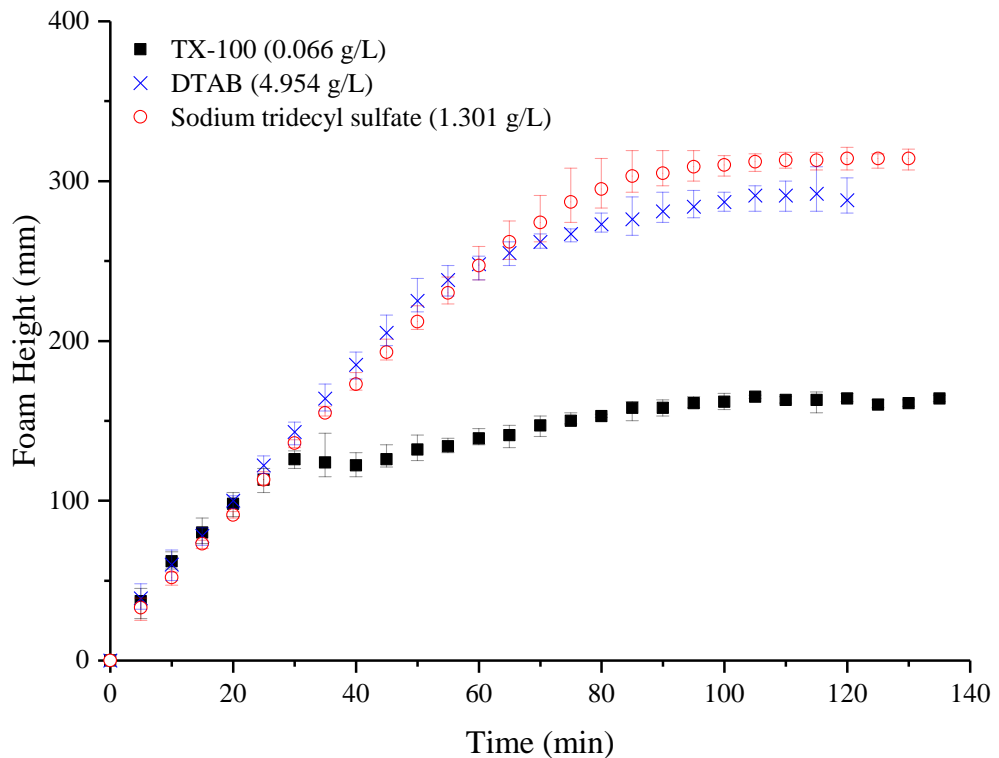


Figure 5-4. The evolution of foam height of TX-100 solution (0.066 g/L), DTAB solution (4.954 g/L) and sodium tridecyl sulfate solution (1.301 g/L) with environmental humidity at 70%. The error bars represent the full range of independent observations.

The equilibrium foam heights of these three surfactant solutions are shown in Table 5-1. As can be seen, the equilibrium foam height of TX-100 solution at the concentration of 0.066 g/L is lower than that of DTAB solution at the concentration of 4.954 g/L which is lower than that of sodium tridecyl sulfate solution at the concentration of 1.301 g/L. This demonstrates that the foam stability of sodium tridecyl sulfate solution at the concentration of 1.301 g/L is the best among foams produced by these three surfactant solutions, whilst the foam stability of DTAB solution at the concentration of 4.954 g/L is at the

intermediate value and the foam stability of TX-100 solution at the concentration of 0.066 g/L is the lowest.

The results of surface rheological properties of these three surfactant solutions are also shown in Table 5-1 (The detailed results of surface rheological properties in each independent measurement of these three surfactant solutions are shown in Appendix F). The surface rheological properties of TX-100 solution (0.066 g/L) obtained in the current work are compared with the values reported by Hunter *et al.* (2009) (the surface elasticity value) and Fruhner *et al.* (1999) (the surface dilatational viscosity and Gibbs elasticity values) of TX-100 solution at a similar concentration of 0.065 g/L, which are shown in Table 1-2. The difference in the surface elasticity value obtained in the current work (which is 15.32 ± 0.27 mN/m) and by Hunter *et al.* (2009) (which is 11.00 mN/m) is due to the different oscillation frequencies in the measurements, which are 0.5 Hz in the current work and 0.04 Hz in Hunter *et al.* (2009). The different values of Gibbs elasticity obtained in the current work (which is 39.02 ± 2.45 mN/m) and by Fruhner *et al.* (1999) (48.50 mN/m) could result from the slight difference in the solution concentration, since larger surfactant concentration results in smaller surface dilatational properties as demonstrated by Shrestha *et al.* (2008). It is worth noting that the surface dilatational viscosity of TX-100 solution (0.065 g/L) obtained by Fruhner *et al.* (1999) is actually an intrinsic value, which explains why it is much smaller than the value obtained in the current work, since the surface dilatational viscosity obtained in the current work is the apparent value.

Furthermore, the surface elasticity and surface dilatational viscosity of DTAB solution (4.954 g/L) obtained in the current work are compared with those values of DTAB solution at the concentration of 6.167 g/L reported by Monroy *et al.* (1998) which are shown in Table 1-2. The reason that these two DTAB solutions are comparable is the concentrations of these two DTAB solutions are both above the CMC, which is 4.718 g/L (Atkin *et al.*, 2003). The values of surface elasticity and surface dilatational viscosity obtained in the current work and in Monroy *et al.* (1998) are in the same range and the difference is due to the different oscillation frequencies in the measurements, which are 0.5 Hz in the current work and 800 Hz in Monroy *et al.* (1998).

It also can be seen from Table 5-1 that surface elasticity, surface dilatational viscosity and Gibbs elasticity of TX-100 solution at the concentration of 0.066 g/L are much larger than those of sodium tridecyl sulfate solution at the concentration of 1.301 g/L which are slight larger than those of DTAB solution at the concentration of 4.954 g/L. In fact, the much larger surface rheological properties of TX-100 solution (0.066 g/L) is due to the much lower surfactant concentration compared to sodium tridecyl sulfate solution (1.301 g/L) and DTAB solution (4.954 g/L), which is approximate 20-75 times lower to these two surfactant solutions. This is because lower surfactant concentration results in lower surface excess and thus surface tension changes more appreciably compared to surface area in response to the surface expansion, which leads to larger surface rheological properties (Shrestha *et al.*, 2008). In order to highlight the effect of surfactant concentration on surface rheological properties, the surface rheological properties of SDS solution

(0.087 g/L in 8.766 g/L NaCl, which has been studied in chapter 2) at the oscillation frequency of 0.5 Hz and the oscillation amplitude of 0.25 are shown in Table 5-2 as a reference to the surface rheological properties data shown in Table 5-1. Note that the measurement of surface rheological properties of this SDS solution at the oscillation frequency of 0.5 Hz is not actually performed in chapter 2 and the values of surface rheological properties at this oscillation frequency are inferred from Figure 2-4, thus these values should be considered as approximate. Furthermore, the equilibrium surface tension result of SDS solution (0.288 g/L in 0.584 g/L NaCl, which has been studied in chapter 3) and the equilibrium foam height of foams produced from SDS solution (2.402 g/L, which has been studied in chapter 4) at the environmental relative humidity of $71.1 \pm 2.6\%$ are also presented in Table 5-2 for a comparison with the data of equilibrium surface tension and equilibrium foam height shown in Table 5-1.

Table 5-2 Results of equilibrium surface tension, surface rheological properties and equilibrium foam height of SDS solution at different concentrations. The error of equilibrium surface tension is the standard deviation of the independent observations. The values in brackets represent the full range of observations.

Concentration of SDS solution (g/L)	Equilibrium surface tension (mN/m)	Surface elasticity (mN/m)	Surface dilatational viscosity (mN·s/m)	Gibbs elasticity (mN/m)	Equilibrium foam height (mm)
0.087 (in 8.766 g/L NaCl)	—	8.40	1.94	42.80	—
0.288 (in 0.584 g/L NaCl)	44.70 ± 3.82	—	—	—	—
2.402	—	—	—	—	435 (424 - 442)

It can be seen from Table 5-2 that surface elasticity, surface dilatational viscosity and Gibbs elasticity of SDS solution (0.087 g/L in 8.766 g/L NaCl)

are also much larger compared to those of sodium tridecyl sulfate solution (1.301 g/L) and DTAB solution (4.954 g/L). As explained above, this is also caused by the much lower surfactant concentration of SDS solution (0.087 g/L in 8.766 g/L NaCl) in comparison with that of sodium tridecyl sulfate solution (1.301 g/L) and DTAB solution (4.954 g/L), which is approximate 15-57 times lower to these two surfactant solutions.

By comparison between equilibrium foam height, equilibrium surface tension, surface elasticity, surface dilatational viscosity and Gibbs elasticity of these three surfactant solutions as shown in Table 5-1, it is indicated that TX-100 solution at the concentration of 0.066 g/L exhibits the largest equilibrium surface tension and surface rheological properties among these surfactant solutions whereas the foam stability is the lowest. As for DTAB solution at the concentration of 4.954 g/L, the equilibrium surface tension is approximately the same with that of sodium tridecyl sulfate solution at the concentration of 1.301 g/L but smaller than that of TX-100 solution at the concentration of 0.066 g/L, whilst the surface rheological properties are the smallest and the foam stability is at intermediate value among these three surfactant solutions. With regards to sodium tridecyl sulfate solution at the concentration of 1.301 g/L, the equilibrium surface tension is approximately the same with that of DTAB solution at the concentration of 4.954 g/L but smaller than that of TX-100 solution at the concentration of 0.066 g/L, whilst the surface rheological properties are at intermediate values and the foam stability is the best among these three surfactant solutions. In fact, the differences of foam stability among these three surfactant solutions result from both differences of surface

tension and surface rheological properties between these three surfactant solutions. Although, it is worth mentioning that the lowest foam stability of TX-100 solution (0.066 g/L) also results from the much lower surfactant concentration compared to the other two surfactant solutions, and the potential depletion of TX-100 surfactant from the bulk solution during the foaming process plays a role as well. However, the difference in surfactant concentration actually affects the surface mechanical properties and thus leads to different foam stability. Therefore, surface mechanical properties can be considered as a proxy of surfactant concentration to influence foam stability.

By comparison of DTAB solution at the concentration of 4.954 g/L to sodium tridecyl sulfate solution at the concentration of 1.301 g/L, since the equilibrium surface tension of these two surfactant solutions are approximately the same, the effect of surface tension on foam stability can be eliminated. As can be seen from Table 5-1, foam stabilised by sodium tridecyl sulfate solution at the concentration of 1.301 g/L has larger surface rheological properties and better stability, which indicates that surface rheological properties and foam stability are related and the larger surface rheological properties account for the better foam stability. This demonstrates that surface rheological properties also play a material role in foam stability. It is worth mentioning, that although the similar conclusions have been drawn by other researchers (Fruhner *et al.*, 1999; Wang *et al.*, 2016; Hofmann *et al.*, 2017), the effect of surface tension on foam stability has not been eliminated by them whereas it is eliminated in the current work.

With respect to a comparison of TX-100 solution at the concentration of 0.066 g/L and DTAB solution at 4.954 g/L, it can be seen from Table 5-1 that the foam stability of TX-100 solution at the concentration of 0.066 g/L is even worse than that of DTAB solution at the concentration of 4.954 g/L in spite of the much larger surface rheological properties of TX-100 solution at the concentration of 0.066 g/L. This is believed to be due to the larger equilibrium surface tension of TX-100 solution at the concentration of 0.066 g/L which deteriorates foam stability. This indicates that surface tension appears to play a more important role than surface rheological properties at foam stability. The comparison of TX-100 solution at the concentration of 0.066 g/L and sodium tridecyl sulfate solution at the concentration of 1.301 g/L demonstrates the same principle. The larger equilibrium surface tension of TX-100 solution at the concentration of 0.066 g/L results in the worse foam stability, regardless of the larger surface rheological properties. This implies that the dependency of foam stability on surface tension is stronger than on surface rheological properties. If the surface tension of different surfactant solutions are the same, the one with larger surface rheological properties have better foam stability. However, if the surface tension of different surfactant solutions are different, the surface tension governs the foam stability comparing with surface rheological properties that the lower surface tension, the better foam stability, in spite of the values of surface rheological properties. To summarise, the above observations demonstrate that both surface tension and surface rheological properties have an influence upon foam stability and surface tension appears to play a more important role than surface rheological properties.

In fact, the current observations are in partial agreement with other research results. Georgieva *et al.* (2009) have compared the foam stability of C₁₂G₂ solution at the concentration of 0.070 g/L and C₁₂E₆ solution at the concentration of 0.032 g/L. They demonstrated that the foam produced from C₁₂G₂ solution at the concentration of 0.070 g/L is more stable, which is attributed to the larger surface elasticity of C₁₂G₂ solution at the concentration of 0.070 g/L than that of C₁₂E₆ solution at the concentration of 0.032 g/L. However, the conclusion of Georgieva *et al.* is drawn under the presupposition that the surface tension of these two surfactant solutions are approximately the same. The equilibrium surface tension of C₁₂G₂ solution at the concentration of 0.070 g/L is 33.00 mN/m (Santini *et al.*, 2007) and that of C₁₂E₆ solution at the concentration of 0.032 g/L is 32.50 mN/m (Mulqueen *et al.*, 1999). Note that these two equilibrium surface tensions are obtained from published graphs and therefore should be considered as approximate values. It is seen that the equilibrium surface tension of these two surfactant solutions are approximately the same. Therefore, their results support the conclusion obtained herein that both surface tension and surface rheological properties including surface elasticity, surface dilatational viscosity and Gibbs elasticity affect foam stability, but the dependency of foam stability on surface tension is stronger than on surface rheological properties.

5.4 Summary

The surface rheological properties and foam stability of TX-100, DTAB and sodium tridecyl sulfate solutions at different concentrations are related under the condition that the surface rheological properties of these three surfactant

solutions are adjusted independently of the equilibrium surface tension. The surface rheological properties of different surfactant solutions are measured at the same oscillation frequency and amplitude, as the surface rheological properties are a function of oscillation frequency whereas independent of oscillation amplitude. Further, the foam stability of different surfactant solutions are measured at the same environmental relative humidity, as foam stability is strongly dependent upon environmental relative humidity. It is demonstrated that both surface tension and surface rheological properties including surface elasticity, surface dilatational viscosity and Gibbs elasticity affect foam stability, however, surface tension appears to play a more important role, with respect to the stability of surfactant-stabilised foams.

Chapter 6 Particle-stabilised Foams

6.1 Introduction

After investigating the relationship between surface mechanical properties and the stability of surfactant-stabilised foams, in this chapter, there is a focus upon exploring the effect of particles on foam stability and surface rheological properties. The stability of foams stabilised by the mixtures of particles and surfactants, as well as the relationship between surface mechanical properties and the stability of particle-stabilised foams, will be investigated in this chapter. Firstly, the effect of silica particles (at a fixed particle concentration) on stability of foams stabilised by cationic surfactant at different surfactant concentrations is described. Subsequently, the effect of particle concentration on stability of foams stabilised by mixtures of cationic surfactant and silica particles is studied. Finally, the stability of particle-stabilised foams to surface mechanical properties are correlated.

6.2 Effect of Silica Particles (at Fixed Particle Concentration) on the Stability of Foams Stabilised by Cationic Surfactant at Different Concentrations

6.2.1 Hydrophobicity of Silica Particles

Since the hydrophobicity of silica particles affects the ability of silica particles to stabilise foams, it is important to measure the hydrophobicity of silica particles with the adsorption of cationic surfactants at different concentrations. The hydrophobicity of silica particle in aqueous colloidal dispersions in the presence of cationic surfactants with different concentrations at high pH is investigated. At high pH, silica particles are negatively charged due to the

dissociation of surface silanol groups of silica particles (Binks *et al.*, 2008), which is conducive to the adsorption of cationic surfactants at the particle surface. The hydrophobicity of silica particles is quantified in terms of the amount of sediments in the mixture of silica particles and cationic surfactants, which has been demonstrated practicable by Binks *et al.* (2008). Since hydrophobic particles tend to aggregate, and the aggregation increases with the hydrophobicity of particles, the amount of sediments in mixtures can be applied to represent the hydrophobicity of silica particles. Note that in Binks *et al.* (2008), the particle hydrophobicity was also quantified by the contact angle of surfactant drops in air on a planar wafer which had similar composition to the particle. However, it has been demonstrated by Wenzel (1936) that the contact angle was proportional to the roughness of the surface. Therefore, the contact angle of planar surface is different with the contact angle of particle, and thus the quantification of particle hydrophobicity by using the contact angle of planar surface is potentially compromised. Although the direct determination of the contact angle of particle using ellipsometry has been proposed by Hunter *et al.* (2007), it is impracticable in the current work since the particles studied herein are generally partial hydrophobic so that they do not fulfil one of the criteria proposed by Hunter *et al.* (2009) to utilise the ellipsometric method that the colloidal particle dispersions should be highly stable. Thus, in the current work, the particle hydrophobicity is only quantified by the amount of sediments in the mixture of silica particles and cationic surfactants. The silica particle used herein is LUDOX HS-30 colloidal silica dispersions, which was purchased from Sigma-Aldrich. The concentration of colloidal silica dispersions is 30 wt% and the pH is 9.8. The surface area and

the average diameter of silica particle are approximately 220 nm and 12 nm, which are parameters quoted by the manufacturer. The cationic surfactant used is dodecyl trimethyl ammonium bromide (DTAB), which was purchased from Fisher Scientific with purity of 99%. It is used without further purification and the CMC of DTAB solution is 4.718 g/L (Atkin *et al.*, 2003). Sodium hydroxide (purchased from Fisher Scientific and with purity above 99%) is used to make concentrated sodium hydroxide solution to adjust the pH of aqueous dispersions and the deionised water is applied to dilute colloidal silica dispersions.

The as-received colloidal silica dispersions is diluted to the concentration of 3 wt% at pH = 10. The different concentrations of DTAB solutions are selected as 0, 0.1, 0.25, 0.5, 1.05, 2.5, 5, 10, 20 × CMC. Note that for the value of concentration around the CMC, the DTAB solution is prepared slightly above the CMC to ensure that the actual concentration of the prepared DTAB solution reaches the CMC and thus to avoid a possible smaller equilibrium surface tension if the actual concentration of the prepared DTAB solution is smaller than the CMC. The volume of diluted colloidal silica dispersions at different surfactant concentrations is 10 mL and corresponding amounts of DTAB at different concentrations are added to the diluted colloidal silica dispersions. The concentrated sodium hydroxide solution is added subsequently to maintain the pH at 10. Since it is just a few drops of concentrated sodium hydroxide solution added to the mixture, the concentration change of silica particles and DTAB is negligible. After preparation of these aqueous dispersions, they are stirred thoroughly and left

for 24 hours to let sedimentation finishes. Photographs of mixtures of colloidal silica particles (3 wt%) and DTAB solutions at different concentrations after 24 hours are shown in Figure 6-1.

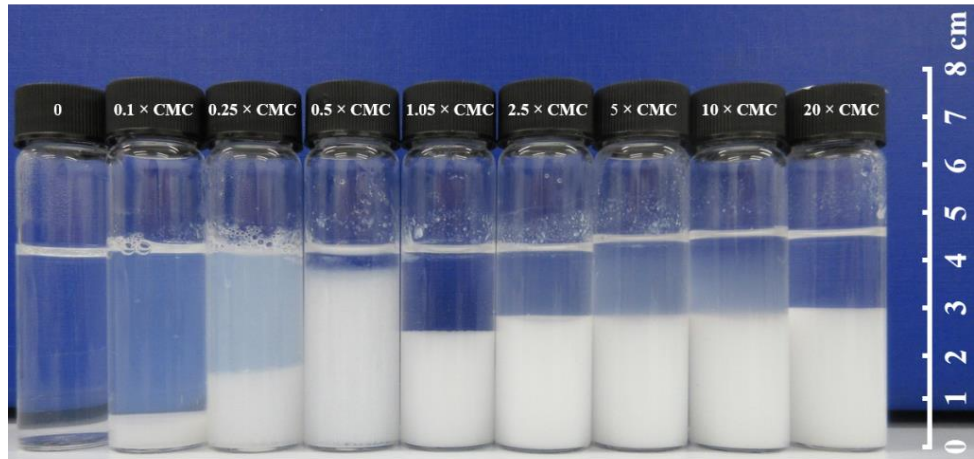


Figure 6-1. Photos of mixtures of colloidal silica particles (3 wt%) and DTAB solutions at different concentrations after 24 hours. The concentration of DTAB solution in each mixture is shown at the top of the vial.

It can be seen from Figure 6-1 that the mixtures of colloidal silica particles (3 wt%) and DTAB solutions at different concentrations possess different degrees of sedimentation. The amount of sediments increases with increasing surfactant concentration at first and reaches a peak value at the surfactant concentration of $0.5 \times \text{CMC}$. After that the amount of sediments drops and then approximately remains constant above the surfactant concentration of CMC. This observation demonstrates that the hydrophobicity of silica particles in different mixtures changes from hydrophilic to hydrophobic and then back to less hydrophobic with the increase of DTAB concentration. This observation shows an agreement with the results of Binks *et al.* (2008) in a similar system, which is a mixture of colloidal silica particles (2 wt%) and di-decyl dimethyl ammonium bromide (di- C_{10}DMAB) at different concentrations. The colloidal silica particles used by them is precisely the same as applied

herein. They ascribed the variation of particle hydrophobicity to the adsorption of cationic surfactant at silica particles. In the current work, silica particles are inherently hydrophilic as containing surface silanol groups and appreciably negatively charged at pH of 10 because of the dissociation of surface silanol groups (Binks *et al.*, 2008). The oppositely charged cationic surfactants DTAB adsorb at particle surface by electrostatic adsorption and render the silica particle from hydrophilic to hydrophobic, as the hydrophilic head of surfactant adsorbing on particle surface and the hydrophobic tail pointing to solutions. Due to this, silica particles start to aggregate progressively as the hydrophobic tails of adsorbed surfactants on particle surface attract to each other by van der Waals force (Binks *et al.*, 2008). With the increase of surfactant concentration, more DTAB surfactants adsorb on particle surface and thus make the silica particle more hydrophobic, therefore the amount of sediments also increases, as shown in Figure 6-1 from surfactant concentration at 0 to $0.5 \times \text{CMC}$. As a monolayer forms, silica particles show the most hydrophobic and the amount of sediments is the largest, as shown in Figure 6-1 at the surfactant concentration of $0.5 \times \text{CMC}$. Above this concentration, further adsorption of extra surfactants on particle surface by the tail-tail interaction results in the partial bilayer with some hydrophilic head groups pointing to solutions, which makes silica particles less hydrophobic and therefore causes the decrease of sediment amount as can be seen in Figure 6-1 from $0.5 \times \text{CMC}$ to $1.05 \times \text{CMC}$. Further increase of surfactant concentration leads to more adsorption of surfactants on particle surface to form bilayer with all hydrophilic head groups exposed to solutions rendering silica particles hydrophilic again. This should have resulted in the decrease of sediment amount, however, it can be seen in

Figure 6-1 from $1.05 \times \text{CMC}$ to $20 \times \text{CMC}$ that the amount of sediments approximately keeps constant. This is likely due to the potential flocculation of silica particles because of the electrical double layer reduction at high electrolyte levels (Derjaguin *et al.*, 1941; Verwey *et al.*, 1948), since the surfactant concentrations in these mixtures are relatively high. A schematic diagram which illustrates the variation of particle hydrophobicity with increasing surfactant concentration caused by the adsorption of surfactant as described above is shown in Figure 6-2.

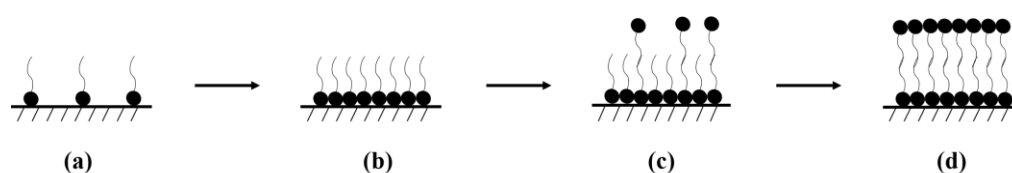


Figure 6-2. A schematic diagram of variation of particle hydrophobicity with increasing surfactant concentration caused by the surfactant adsorption at the particle surface. The surfactant concentration increases from (a) to (d). (a) The adsorbed surfactants form partial monolayer which renders the particle from hydrophilic to less hydrophobic. (b) The adsorbed surfactants form monolayer which makes the particle the most hydrophobic. (c) The adsorbed surfactants form partial bilayer which makes the particle less hydrophobic. (d) The adsorbed surfactants form bilayer which changes the particle to hydrophilic again.

Therefore, due to the adsorption of DTAB surfactant at the particle surface, the hydrophobicity of silica particles first increases and then decreases with increasing surfactant concentration. This confirms the observation of Binks *et al.* (2008) that the hydrophobicity of silica particles was affected by the concentration of surfactant and the most hydrophobic particles were obtained at the intermediate surfactant concentrations. It was suggested by Binks *et al.* (2008) that the most hydrophobic particles obtained at the intermediate surfactant concentrations yielded the most stable foams. However, the observations obtained by Zhu *et al.* (2015) appeared to suggest that the most hydrophobic particles have not resulted in the best foam stability. Thus, in the

next subsection (subsection 6.2.2), foam stability of DTAB solutions with and without 3 wt% colloidal silica particles at different surfactant concentrations are measured to ascertain the optimum particle hydrophobicity which gives the best foam stability.

6.2.2 Foam Stability Measurement

Since the sediments in mixtures at relatively high DTAB concentrations (i.e. $5-20 \times \text{CMC}$) are likely due to the potential flocculation of silica particles at high electrolyte levels rather than the hydrophobic interaction between silica particles, such high concentrations are not considered in the foam stability measurement. The foam stability measurements of DTAB solutions with and without 3 wt% colloidal silica dispersions at concentrations of 0.1, 0.25, 0.5, 1.05, and $2.5 \times \text{CMC}$ are performed. DTAB solutions in the absence of silica particles are prepared with 1 litre of deionised water and the corresponding amounts of DTAB at different concentrations, whereas mixtures of silica particles and DTAB are prepared with 1 litre colloidal silica dispersions (3 wt%) and the same amounts of DTAB at those different concentrations. The pH of all these samples is kept at 10 as well to ensure that the silica particles are negatively charged, which is conducive to the adsorption of DTAB at silica particles. The same method of foam stability measurement as described in section 4.2 is also used herein. This method is reproducible and maintains a constant environmental relative humidity in the freeboard of the column. The environmental relative humidity is controlled at $70.4 \pm 0.5\%$, since a finite foam height of large depth can be obtained under this condition. All the other experimental conditions are remained the same as described in section 4.2.

Furthermore, the same method to obtain the estimation of arithmetic mean bubble diameter as described in section 4.2 is also applied herein to quantify the bubble size of produced foams. It is reiterated that this method just provides an indication of bubble diameter rather than an actual value of bubble diameter.

The bubble size (i.e. arithmetic mean bubble diameter) of foams produced by DTAB solutions with and without 3 wt% colloidal silica dispersions at different surfactant concentrations are shown in Figure 6-3. As can be seen, the bubble size (i.e. arithmetic mean bubble diameter) of foams produced by DTAB solutions with silica particles is larger than that of foams produced without silica particles at the same DTAB concentration. This is attributed to the increase of surface tension caused by the decrease of DTAB concentration in solutions as DTAB surfactants adsorbed on silica particle surface. In fact, it was known that bubble size had an influence on foam stability (Cho *et al.*, 2002). However, in the current case, bubble size works as a proxy of surface tension to affect foam stability and the change of surface tension results from the existence of silica particles. Thus, the change of foam stability herein all accounts for the presence of silica particles. The surface tension changes caused by the presence of silica particles are described in subsection 6.4.1.

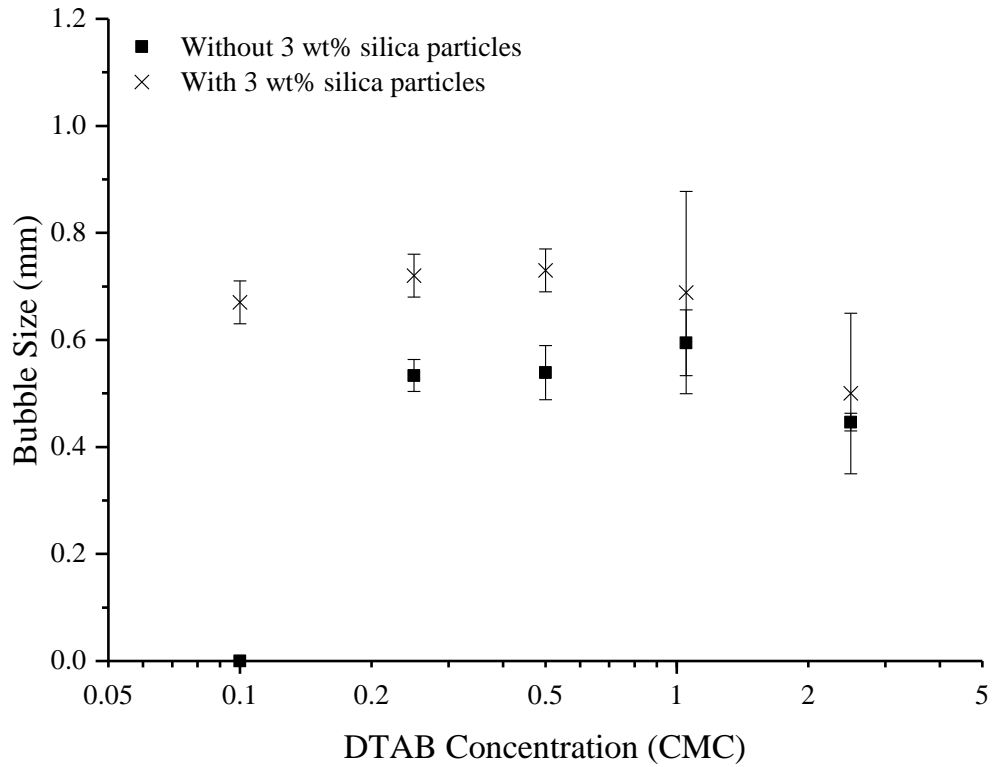
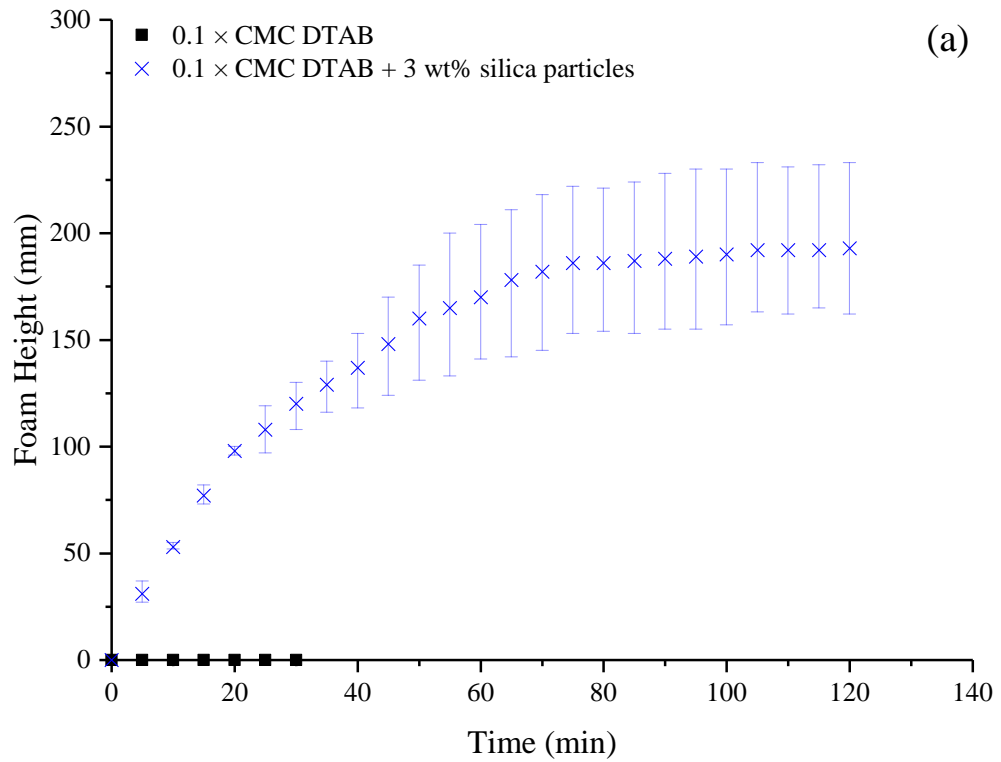
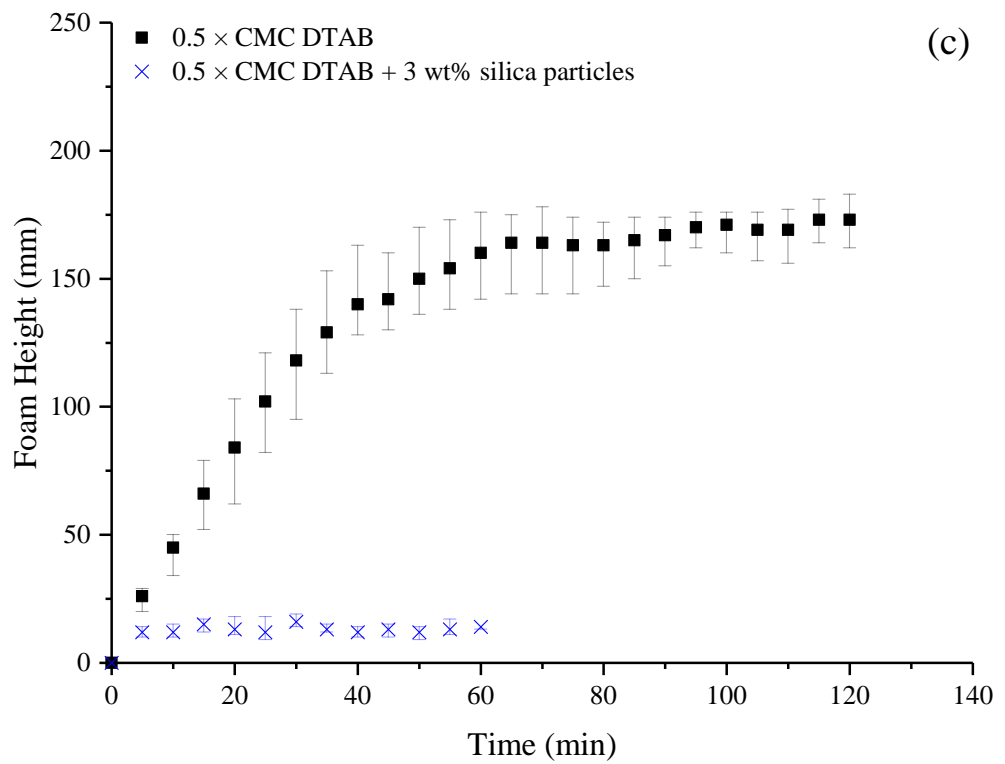
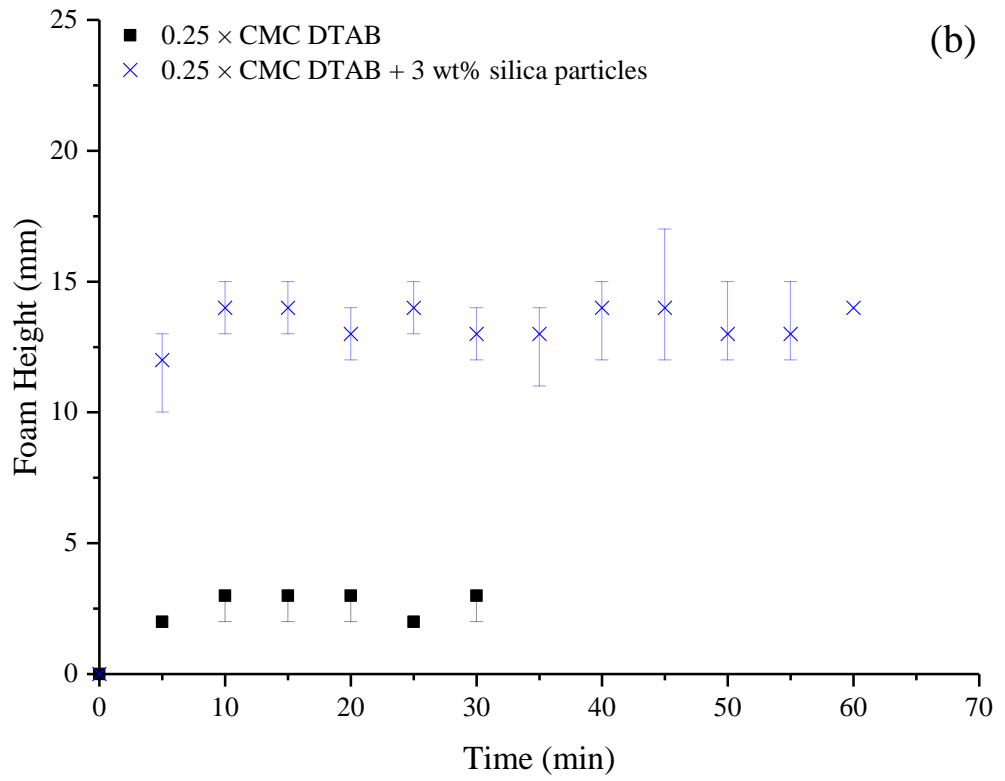
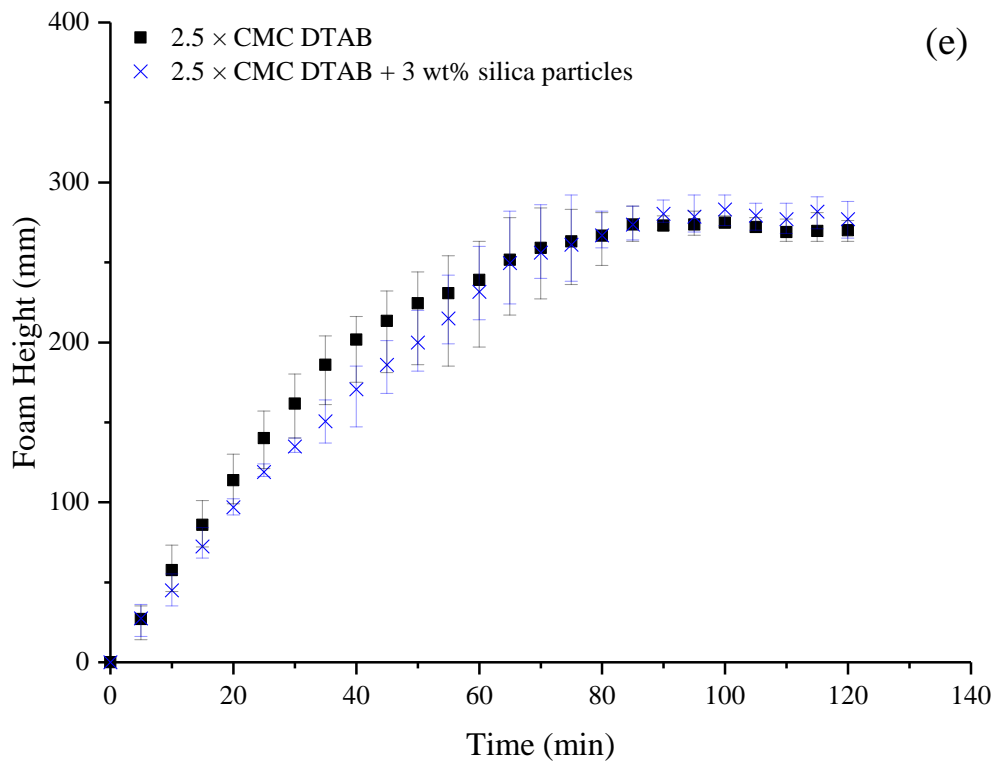
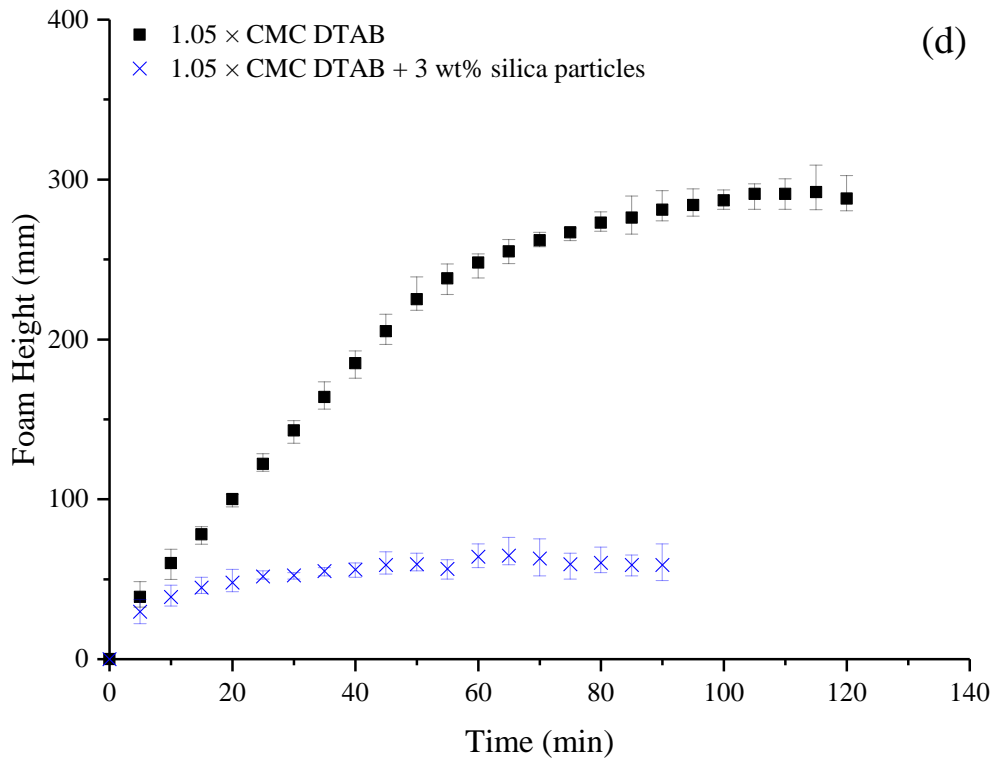


Figure 6-3. The bubble size (i.e. arithmetic mean bubble diameter) of DTAB surfactant solutions with and without 3 wt% colloidal silica dispersions at different surfactant concentrations. The error bars represent the standard deviation of all observations. The point on the abscissa represents that there is no foam produced in this set of measurements.







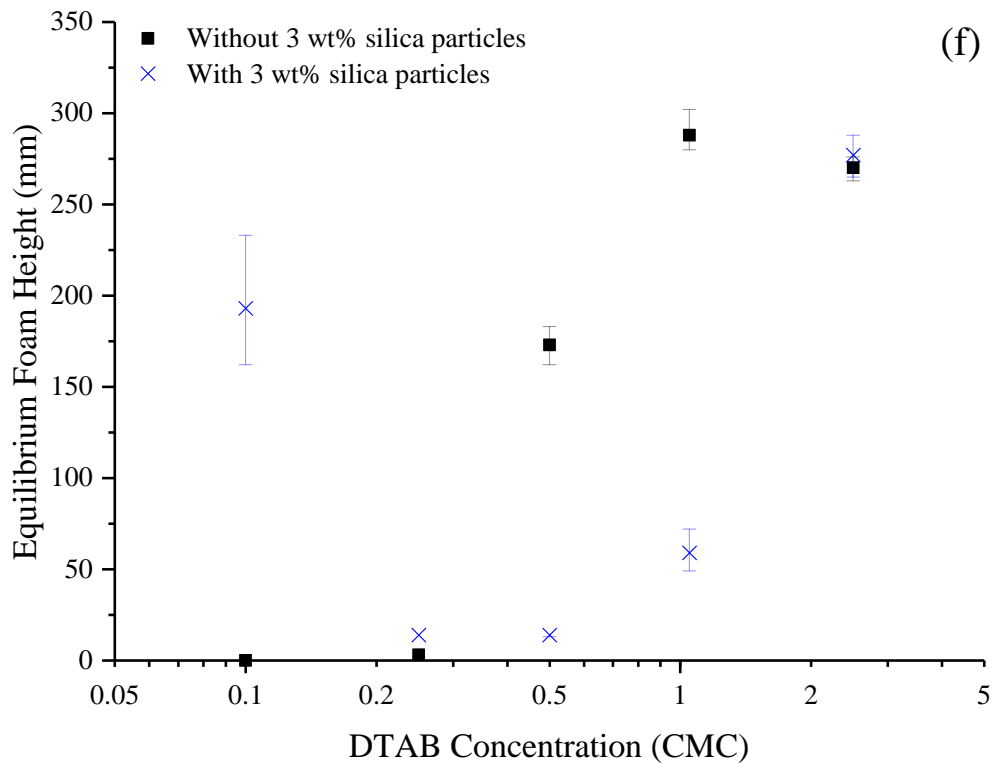


Figure 6-4. The foam height comparison of foams produced by DTAB solutions with and without 3 wt% colloidal silica dispersions at different surfactant concentrations. (a) The comparison at surfactant concentration of $0.1 \times \text{CMC}$. (b) The comparison at surfactant concentration of $0.25 \times \text{CMC}$. (c) The comparison at surfactant concentration of $0.5 \times \text{CMC}$. (d) The comparison at surfactant concentration of $1.05 \times \text{CMC}$. (e) The comparison at surfactant concentration of $2.5 \times \text{CMC}$. (f) The comparison of equilibrium foam height. The error bars represent the full range of all observations.

The foam height comparison of foams produced by DTAB solutions with and without 3 wt% colloidal silica dispersions at different surfactant concentrations are shown in Figure 6-4 (The detailed results of each independent measurement are shown in Appendix G). As can be seen from Figure 6-4(a), a stable foam cannot be formed solely by DTAB solution at the concentration of $0.1 \times \text{CMC}$, whereas foam is much more stable when producing from mixture of DTAB solution ($0.1 \times \text{CMC}$) and colloidal silica dispersions (3 wt%). This demonstrates that foam stability is increased markedly by adding silica particles to DTAB solution at the concentration of $0.1 \times \text{CMC}$. It is shown in Figure 6-4(b) that foams produced from DTAB solutions at the concentration of $0.25 \times \text{CMC}$ with and without silica particles

show approximately the same instability, although the foam produced with silica particles are slightly more stable. It appears that silica particles do not have a significant effect on foam stability in this case. Figure 6-4(c) and 6-4(d) show that foams produced from DTAB solutions without silica particles at concentrations of 0.5 and $1.05 \times \text{CMC}$ are much more stable than those produced with silica particles at the same surfactant concentration, which indicates that silica particles in these cases act as antifoaming agent and diminish foam stability. As shown in Figure 6-4(e), foams produced from DTAB solutions at the concentration of $2.5 \times \text{CMC}$ with and without silica particles are both stable and exhibit approximately the same stability. This demonstrates that silica particles on this occasion also play little role on foam stability, which is the same as shown in Figure 6-4(b). Figure 6-4 (f) shows the equilibrium foam height of foams produced by DTAB solutions with and without silica particles at different surfactant concentrations. It is seen that foam stabilised solely by DTAB solutions increases first and then approximately remains constant with increasing DTAB concentration, whereas the stability of foam stabilised by the mixture of DTAB solutions and colloidal silica dispersions decreases first and then increases with the increase of DTAB concentration. With silica particles, stable foams can be obtained at both low and high surfactant concentrations.

By comparison of foam stability of DTAB solutions with and without silica particles at different surfactant concentrations, it is demonstrated that the presence of silica particles plays different roles on foam stability at different surfactant concentrations, as the promotion, deterioration and maintaining

consistency of foam stability after adding silica particles to DTAB solutions have all been observed. Foam stability can only be improved by adding silica particles to DTAB solution at the concentration of $0.1 \times \text{CMC}$, whereas at higher concentrations, foam stability either remains the same or decreases after adding silica particles. This indicates that the effect of silica particles on foam stability depends on the surfactant concentration which affects the hydrophobicity of silica particles. The silica particles can only increase foam stability at low surfactant concentrations, which makes the silica particles intermediately hydrophobic as discussed in subsection 6.2.1. Therefore, it is demonstrated that silica particles can only increase foam stability when the particles have intermediate hydrophobicity. This observation shows agreement with the results of Binks *et al.* (2005) obtained from foams stabilised solely by hydrophobic silica particles (hydrophobised by *ex-situ* method). It has been demonstrated by them that particles of intermediate hydrophobicity were the only ones capable of stabilising foams. However, this observation differs to the results of Binks *et al.* (2008) obtained from foams stabilised by mixture of cationic surfactant and hydrophilic silica particles (*in-situ* method to hydrophobise silica particles), which showed that foam stability was enhanced with particles being maximally hydrophobic at the intermediate surfactant concentration. It appears that the observations of Binks *et al.* (2005, 2008) are different in respect of the optimal hydrophobicity range of solid particles for foam stabilisation, and that the present results are in favour of the observation of Binks *et al.* (2005) that only intermediate hydrophobic particles are capable of increasing foam stability. The current observation seems to suggest that foam stability can only be improved by intermediate hydrophobic silica

particles regardless the method applied (either *ex-situ* chemisorption method or *in-situ* physisorption method) to obtain hydrophobic silica particles. The difference between results of current work and the observation of Binks *et al.* (2008) appears to be due to the different methods to measure and quantify foam stability. Binks *et al.* (2008) have applied the ‘hand shaking’ method to produce foam and monitored the foam volume change during a certain time to quantify foam stability. However, the ‘hand shaking’ method to produce foam is not a reproducible method as the energy created by shaking hand to form bubble is difficult to maintain constant. Furthermore, the environmental relative humidity in the measuring vessel, which has been demonstrated by Li *et al.* (2010, 2012) and Champougny *et al.* (2018) to be a determining factor on foam stability, has not been controlled and measured, although it could be approximately considered to be close to the saturation condition in the ‘hand shaking’ method. Therefore, the reproducibility of the quantification of foam stability in Binks *et al.* (2008) is likely to be compromised and thus results in the different observations of the optimum particle hydrophobicity to increase foam stability compared to the results obtained herein. It is reiterated that the method of foam stability measurement used in the current work is reproducible and maintains a constant environmental relative humidity in the freeboard of the column.

In this subsection, foam stability of DTAB solutions with and without 3 wt% colloidal silica dispersions at different surfactant concentrations has been studied. However, it is noted that, in these measurements, the concentration of colloidal silica particles is kept at a fixed value. Therefore, the effect of silica

particle concentration on the hydrophobicity of silica particles and then on the foam stability has not been explored in the above study. Thus, in the next section (section 6.3), the effect of silica particle concentration on the stability of foams produced from mixtures of DTAB solutions and colloidal silica dispersions will be studied.

6.3 Effect of Particle Concentration on the Stability of Foams Stabilised by Mixtures of Cationic Surfactant and Silica Particles

6.3.1 Foam Stability Measurement

Since foam stability can only be promoted by adding silica particles to DTAB solution at the surfactant concentration of $0.1 \times \text{CMC}$ (0.472 g/L) as demonstrated above, the concentration of DTAB solution studied herein is chosen as $0.1 \times \text{CMC}$. The values of silica particle concentration are chosen as 0.1, 0.3, 1, 3, 9 wt%. The pH of all these mixtures are also controlled at 10 to create negatively charged silica particles. The foam stability measurements of mixtures of DTAB solutions at the concentration of $0.1 \times \text{CMC}$ and colloidal silica dispersions at different particle concentrations are performed. The method and the experimental conditions are the same as described in subsection 6.2.2. The results of bubble size (i.e. arithmetic mean bubble diameter) and equilibrium foam height of foams produced from mixtures of DTAB solutions at the concentration of $0.1 \times \text{CMC}$ and colloidal silica dispersions at different particle concentrations are shown in Figure 6-5 (The detailed results of evolution of foam height in each independent measurement are shown in Appendix G). It can be seen that the bubble size (i.e. arithmetic

mean bubble diameter) of foams approximately remains constant with increasing silica particle concentration, whereas the equilibrium foam height increases first reaches a maximum at silica particle concentration of 3 wt% and then decreases with increasing silica particle concentration. This indicates that foams produced from mixtures of DTAB solutions ($0.1 \times \text{CMC}$) and colloidal silica dispersions at intermediate silica particle concentrations (i.e. 3 wt% in this case) are the most stable. Since it has been demonstrated in section 6.2 that foam stability can only be increased by silica particles with intermediate hydrophobicity, it is pertinent to explore whether the most stable foam obtained herein is stabilised by the intermediately hydrophobic silica particles as well. Therefore, in order to verify the validity of the observation obtained in section 6.2, the hydrophobicity of silica particle with the presence of DTAB solutions ($0.1 \times \text{CMC}$) in aqueous colloidal dispersions at different silica particle concentrations is investigated in the next subsection (subsection 6.3.2). This aims to determine whether the mixture of colloidal silica particles at intermediate concentration (i.e. 3 wt% in this case) and DTAB solution at the concentration of $0.1 \times \text{CMC}$ generates the intermediately hydrophobic particles.

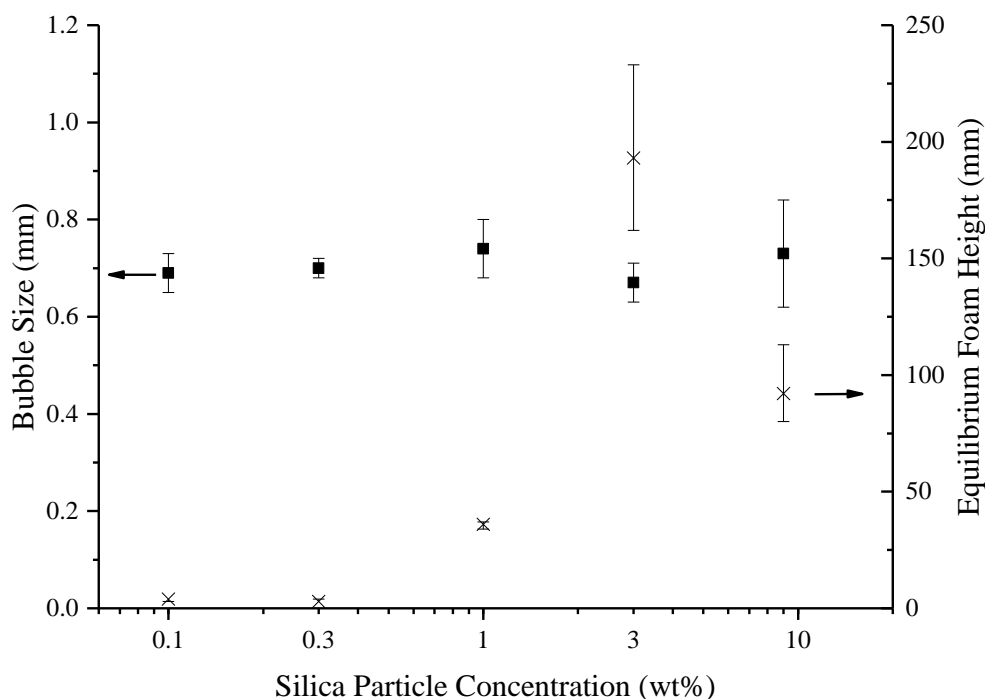


Figure 6-5. The bubble size (i.e. arithmetic mean bubble diameter) and equilibrium foam height of foams produced from mixtures of DTAB solutions at the concentration of $0.1 \times$ CMC and colloidal silica dispersions at different particle concentrations. The error bars of bubble size represent the standard deviation of all observations. The error bars of equilibrium foam height represent the full range of all observations (because the independent foam stability measurements for each mixture are only repeated 3 times).

6.3.2 Hydrophobicity of Silica Particles

The same method and materials as described in section 6.2.1 are also applied to the experiments reported herein. The ‘as-received’ colloid silica dispersions (30 wt%) are diluted to different concentrations of 0.1, 0.3, 1, 3, 9 wt%. The volume of each diluted colloidal silica dispersions is 10 mL and 0.005 g DTAB is added to each diluted colloidal silica dispersions, which makes the DTAB concentration at $0.1 \times$ CMC. The pH of mixtures is maintained at 10 by adding concentrated sodium hydroxide solution. All these prepared aqueous dispersions are stirred thoroughly and left for 24 hours to allow for sedimentation. Photographs of mixtures of DTAB solutions at the concentration of $0.1 \times$ CMC and colloidal silica particles at different concentrations after 24 hours are shown in Figure 6-6.

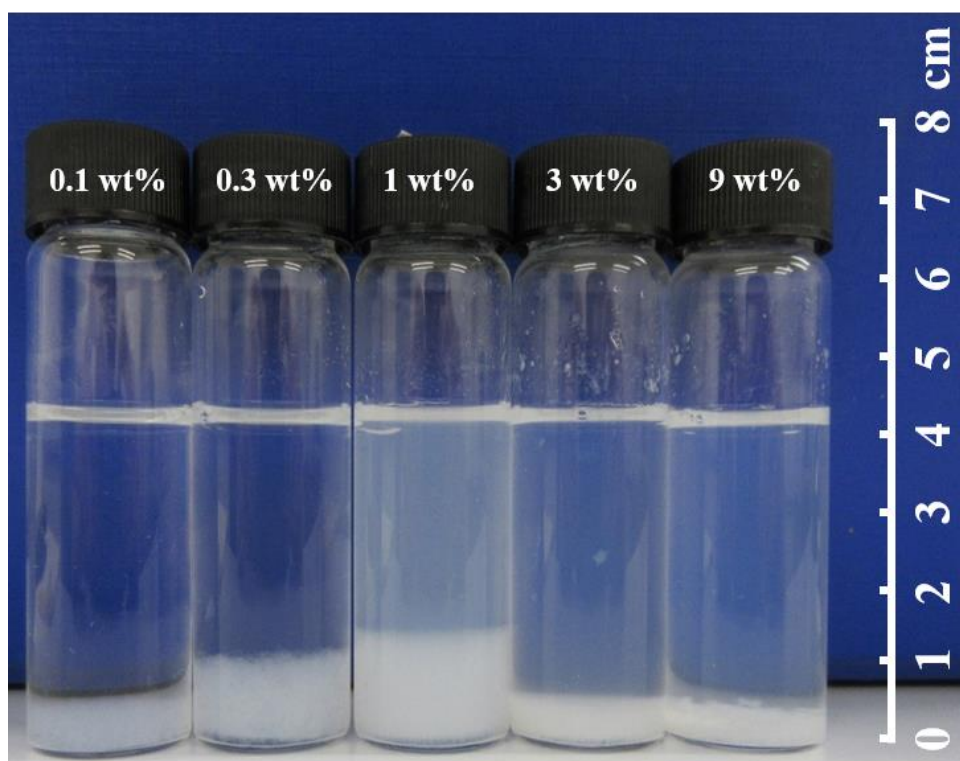


Figure 6-6. Photographs of mixtures of DTAB solutions ($0.1 \times \text{CMC}$) and colloidal silica particles at different concentrations after 24 hours. The concentration of silica particles in each mixture is shown at the top of the vial.

It can be seen that the amount of sediments increases first and then decreases with the increase of silica particle concentration. The peak value of sediment amount is observed at the particle concentration of 1 wt%. Since it has been shown in subsection 6.2.1 that the amount of sediments represents the hydrophobicity of silica particles, this variation of sediment amount indicates that silica particles vary from less hydrophobic to the most hydrophobic and then changes back to less hydrophobic again. In fact, the change of hydrophobicity of silica particles herein is also due to the adsorption of DTAB to silica particles as demonstrated in subsection 6.2.1. However, in this case, it is a reverse process of the surfactant adsorption on silica particles with increasing surfactant concentration as described in subsection 6.2.1.

At a fixed DTAB concentration (e.g. $0.1 \times \text{CMC}$ in this case), if the particle concentration is extremely low, the amount of surfactants is abundant compared to the quantity of particles and thus surfactants adsorb on particle surface to form a bilayer of adsorbed surfactants with hydrophilic heads pointing towards solutions, which makes particles remain hydrophilic. With the increase of particle concentration, the amount of adsorbed surfactants on a single particle decreases, which forms a partial bilayer of adsorbed surfactants on a particle surface with some hydrophobic tails of surfactants pointing to solutions and therefore renders the particle from hydrophilic to less hydrophobic. Further increasing particle concentration keeps reducing the amount of adsorbed surfactants on a particle surface and therefore increasing the hydrophobicity of silica particles until a monolayer is formed and the hydrophobicity of silica particles reaches the maximum value, as shown in Figure 6-6 from 0.1 to 1 wt%. Above a particle concentration of 1 wt%, increasing particle concentration results in further decrease of adsorbed surfactants on a particle surface and thus forms a partial monolayer, which leads to still less hydrophobic silica particles as can be seen from 1 to 9 wt% in Figure 6-6. This variation of particle hydrophobicity with increasing particle concentration caused by the adsorption of surfactant is illustrated in a schematic diagram as shown in Figure 6-7.

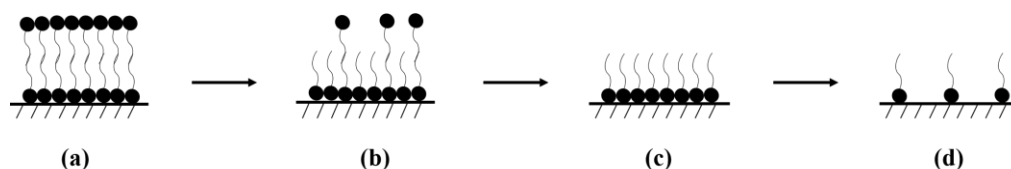


Figure 6-7. A schematic diagram of variation of particle hydrophobicity with increasing particle concentration caused by the surfactant adsorption at particle surface. The particle concentration increases from (a) to (d). (a) The adsorbed surfactants form bilayer which makes the particle still remain hydrophilic. Note that this step has not been observed in the current experiment. (b) The adsorbed surfactants form partial bilayer which renders the particle from hydrophilic to less hydrophobic. (c) The adsorbed surfactants form monolayer which makes the particle the most hydrophobic. (d) The adsorbed surfactants form partial monolayer which makes the particle less hydrophobic.

Therefore, it is demonstrated that mixtures of DTAB solutions ($0.1 \times \text{CMC}$) and colloidal silica dispersions at intermediate particle concentration (i.e. 3 wt% in this case) result in intermediately hydrophobic silica particles. Thus, it is explained why that the most stable foams obtained in subsection 6.3.1 is stabilised by silica particles possess intermediate hydrophobicity. This agrees with the observation obtained in section 6.2 that the intermediately hydrophobic silica particles are the only ones capable of increasing foam stability.

However, it is worth exploring why it is that intermediately hydrophobic silica particles can increase foam stability. Therefore, in the next section (section 6.4), surface mechanical properties of the samples used in sections 6.2 and 6.3 are investigated to correlate them with the stability of particle-stabilised foams.

6.4 Relationship between the Stability of Particle-stabilised Foams and Surface Mechanical Properties

6.4.1 Surface Mechanical Properties of DTAB Solutions with and without Colloidal Silica Dispersions (3 wt%) at Different Surfactant Concentrations

The oscillating and static pendant droplet methods as described in chapters 2 and 3 are performed herein to obtain surface rheological properties and equilibrium surface tension, respectively, of samples used in section 6.2.2. The Gibbs elasticity of these samples are inferred from experimental results of surface elasticity and surface dilatational viscosity according to eq. 2-26. Independent measurements are repeated 25 times for each sample and all the other experimental conditions are maintained the same as described in section 5.3. The equilibrium surface tension can be obtained by linear extrapolation of the dynamic surface tension to infinite time according to the method of Makievski *et al.* (1997) that has been described in section 5.2. The independent measurement of dynamic surface tension of each sample is repeated 25 times as well and all the other experimental conditions are the same as described in section 5.2.

The results of surface rheological properties and equilibrium surface tension of DTAB solutions with and without 3 wt% colloidal silica dispersions at different surfactant concentrations are shown in Table 6-1 (The detailed results of surface rheological properties and equilibrium surface tension in each independent measurement of these samples are shown in Appendix G). The equilibrium foam heights of these samples are also presented in Table 6-1 to

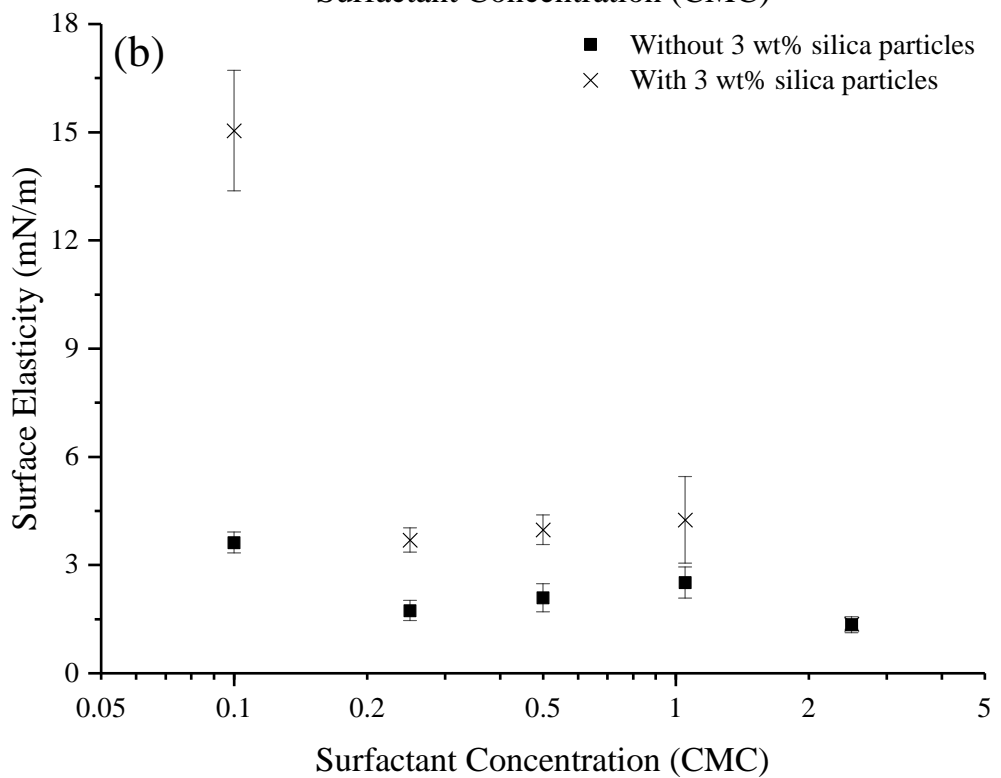
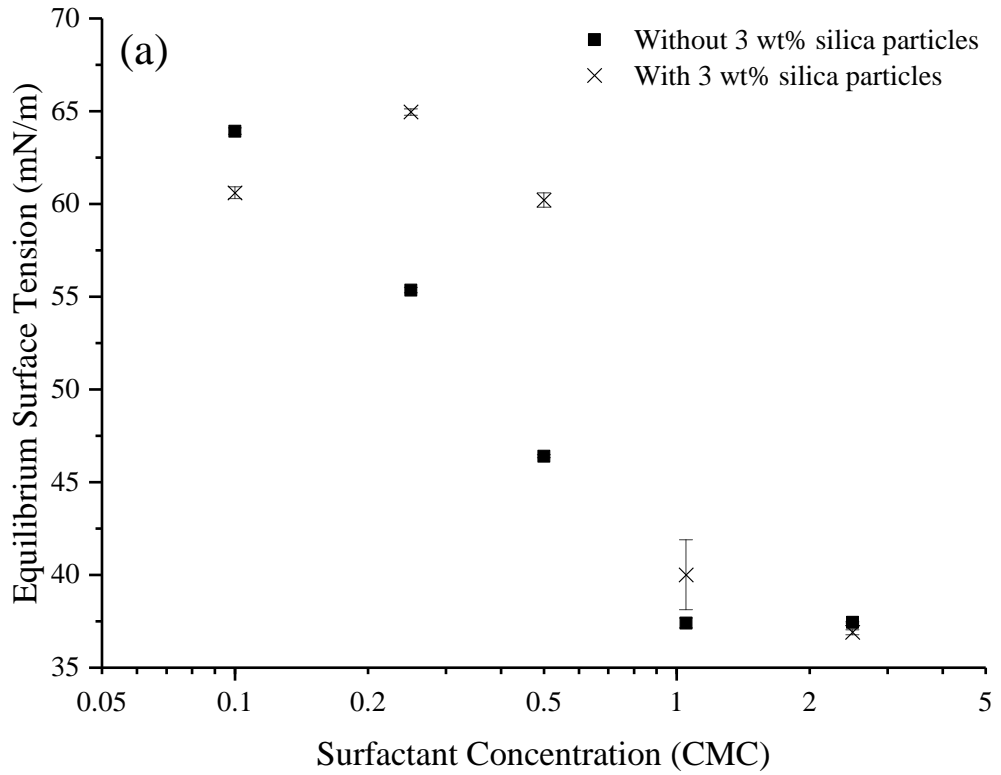
enable reference to surface mechanical properties. As can be seen from Table 6-1, stable foams can be produced by mixtures of 3 wt% colloidal silica dispersions and DTAB solutions at concentrations of 0.1 and $2.5 \times \text{CMC}$. By inspection of the surface mechanical properties of mixtures of 3 wt% colloidal silica dispersions and DTAB solutions at concentrations of 0.1 and $2.5 \times \text{CMC}$, it is shown that surface elasticities of these two samples are smaller than half of equilibrium surface tensions of these two samples. This indicates that the prediction criterion of stable particle-stabilised foams proposed by Stocco *et al.* (2009, 2011), that particle-stabilised foams become stable if surface elasticity is greater than half of equilibrium surface tension is not supported by the current measurements, since the prediction criterion has not been fulfilled whereas stable foams are apparent. It is demonstrated that the criterion for particle-stabilisation proposed by Stocco *et al.* (2009, 2011) is not universally valid, according to the current measurements. This is due to the fact that the measured value of surface elasticity is dependent upon the oscillation frequency (Liggieri *et al.*, 2010) and a larger oscillation frequency results in larger surface elasticity. Although this proposed prediction criterion relating surface elasticity and surface tension is not always valid, surface elasticity and surface tension both play important roles on the stability of particle-stabilised foams.

Table 6-1. The comparison of surface rheological properties, equilibrium surface tension and equilibrium foam height of DTAB solutions with and without 3 wt% colloidal silica dispersions at different surfactant concentration. The errors are the standard deviation of all observations and the values in the brackets represent the full range of observations.

Samples	Surface elasticity (mN/m)	Surface dilatational viscosity (mN·s/m)	Gibbs elasticity (mN/m)	Equilibrium surface tension (mN/m)	Equilibrium foam height (mm)
0.1 × CMC DTAB	3.62 ± 0.29	0.15 ± 0.04	4.25 ± 0.38	63.92 ± 0.17	Zero in all cases
0.1 × CMC DTAB + 3 wt% silica particles	15.04 ± 1.67	0.06 ± 0.05	15.25 ± 1.74	60.60 ± 0.32	193 (162 - 233)
0.25 × CMC DTAB	1.73 ± 0.28	0.14 ± 0.07	2.56 ± 0.99	55.35 ± 0.14	3 (2 - 3)
0.25 × CMC DTAB + 3 wt% silica particles	3.69 ± 0.34	0.20 ± 0.04	4.57 ± 0.32	64.95 ± 0.18	14 (14 - 14)
0.5 × CMC DTAB	2.09 ± 0.39	0.09 ± 0.02	2.47 ± 0.39	46.40 ± 0.08	173 (162 - 183)
0.5 × CMC DTAB + 3 wt% silica particles	3.97 ± 0.41	0.38 ± 0.03	6.18 ± 0.45	60.20 ± 0.39	14 (13 - 14)
1.05 × CMC DTAB	2.51 ± 0.43	0.05 ± 0.04	2.70 ± 0.42	37.40 ± 0.27	288 (280 - 302)
1.05 × CMC DTAB + 3 wt% silica particles	4.25 ± 1.20	0.19 ± 0.04	5.05 ± 1.16	40.00 ± 1.88	59 (49 - 72)
2.5 × CMC DTAB	1.34 ± 0.22	0.06 ± 0.04	1.66 ± 0.38	37.43 ± 0.04	270 (263 - 276)
2.5 × CMC DTAB + 3 wt% silica particles	1.36 ± 0.15	0.05 ± 0.02	1.59 ± 0.20	36.90 ± 0.13	277 (265 - 288)

The surface mechanical properties of DTAB solutions both with and without 3 wt% colloidal silica dispersions at different concentrations are shown in Figure 6-8. They are correlated with data for foam stability which are shown in Figure 6-4(f). As previously demonstrated in section 6.2, foam stability can only be improved by adding colloidal silica dispersions (3 wt%) to DTAB solution at the concentration of 0.1 × CMC (which produces intermediately hydrophobic silica particles), whereas for higher DTAB concentrations, foam

stability either remains approximately the same (at DTAB concentration of 0.25 and $2.5 \times \text{CMC}$) or decreases (at DTAB concentration of 0.5 and $1.05 \times \text{CMC}$) after the addition of silica particles.



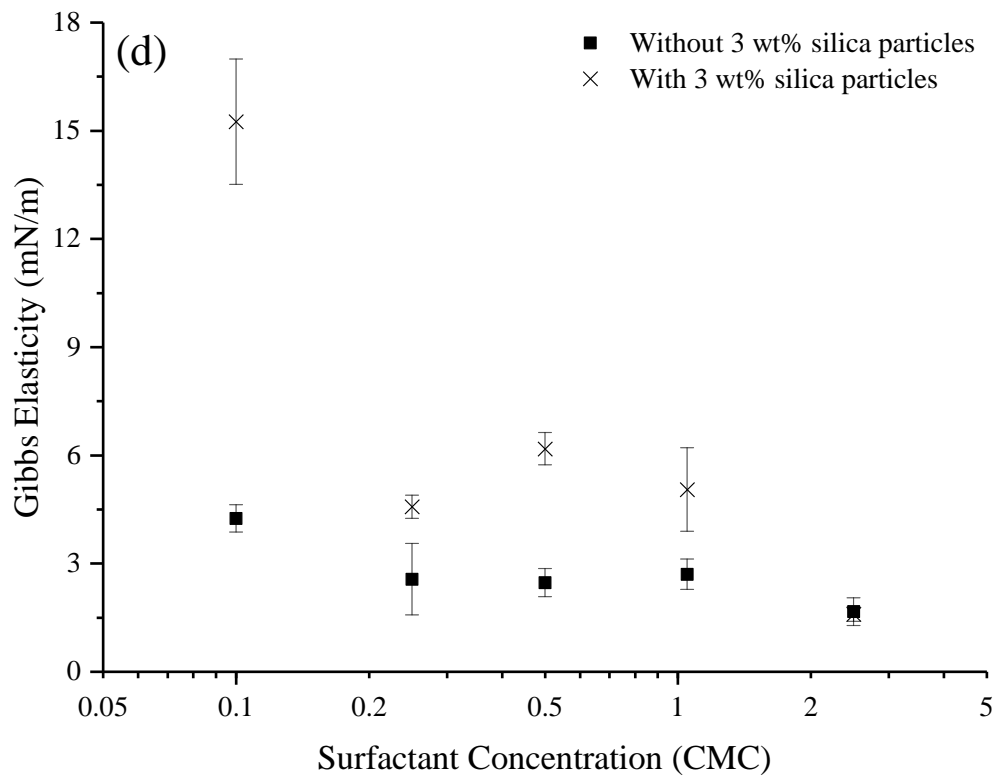
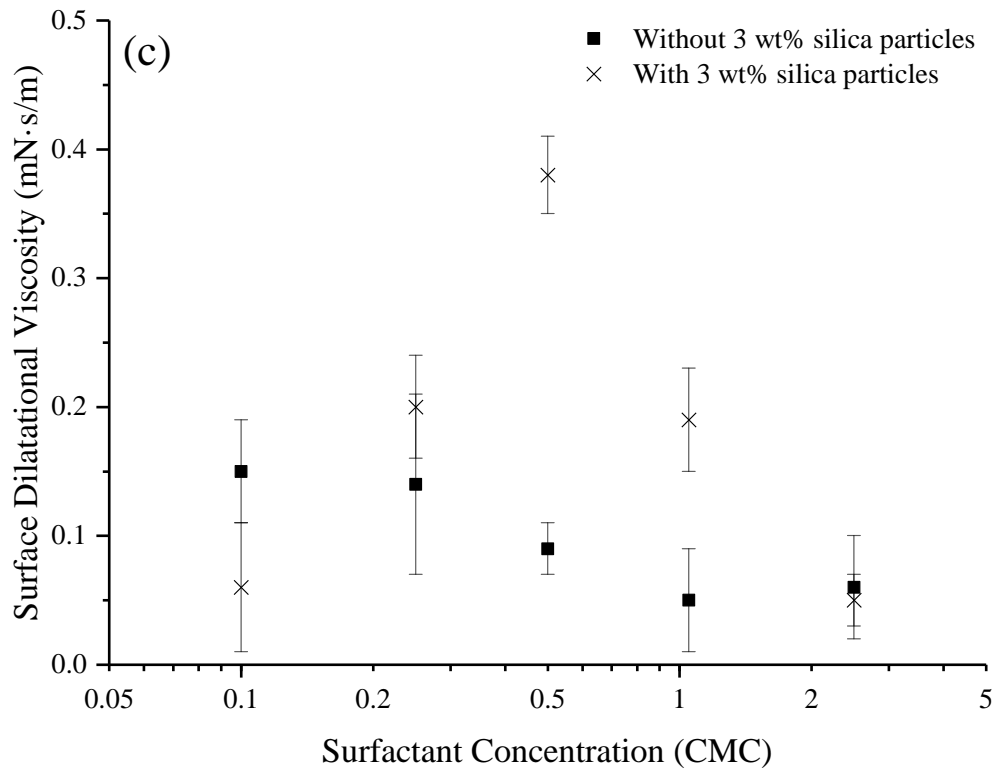


Figure 6-8. The surface mechanical properties of DTAB solutions both with and without 3 wt% colloidal silica dispersions at different surfactant concentrations. (a) Equilibrium surface tension results. (b) Surface elasticity results. (c) Surface dilatational viscosity results. (d) Gibbs elasticity results. The error bars represent the standard deviation of all observations.

For the case that foam stability are improved (i.e. at DTAB concentration of $0.1 \times \text{CMC}$), it can be seen in Figure 6-8 that equilibrium surface tension and surface dilatational viscosity are smaller whereas surface elasticity and Gibbs elasticity are larger with addition of silica particles. All these changes of surface mechanical properties result in the promotion of foam stability since the surface is more elastic and surface tension is lower. In fact, these changes of surface mechanical properties are due to the interaction of surfactants and silica particles. The adsorption of surfactants on particle surfaces is supposed to result in the increase of surface tension as fewer surfactants are remained to adsorb at the air-liquid interface to lower surface tension, however, the adsorption of silica particles on the air-liquid interface decreases surface tension. Therefore, there is a synergistic effect on surface tension due to surfactant adsorption on particle surfaces and particle adsorption on air-liquid interface, which ultimately results in the decrease of surface tension if the silica particles are at intermediate hydrophobicity. Furthermore, the adsorption of silica particles to the air-liquid interface accounts for the increase of surface elasticity and Gibbs elasticity and the decrease of surface dilatational viscosity if there is no excess interaction between adsorbed silica particles and silica particles in bulk solution.

For the cases that foam stability is compromised after adding silica particles (i.e. at DTAB concentrations of 0.5 and $1.05 \times \text{CMC}$), it is noted that, although surface elasticity and Gibbs elasticity increase slightly (in favour of foam stability), surface tension and surface dilatational viscosity also increase (deteriorating foam stability), which ultimately causes a decrease of foam

stability. In fact, the increase of surface elasticity and Gibbs elasticity is due to the adsorption of silica particles on air-liquid interface whereas the increase of surface dilatational viscosity results from the excess interaction between silica particles on the air-liquid interface and silica particles in bulk solution as the silica particles obtained in these cases are more hydrophobic and therefore more likely to aggregate, which makes the air-liquid interface more viscous. In addition, the increase of surface tension is due to a synergistic effect of surfactant adsorption on particle surface and particle adsorption on air-liquid interface. Furthermore, the more hydrophobic particles obtained in these cases increase the probability of particle interaction in bulk solution instead of particle adsorption at the air-liquid interface, which generally affects the surface mechanical properties of the air-liquid interface. For cases in which foam stability approximately remains the same after the addition of silica particles (i.e. at DTAB concentrations of 0.25 and $2.5 \times \text{CMC}$), surface mechanical properties either remain the same (as shown in Figure 6-8 at DTAB concentration of $2.5 \times \text{CMC}$) or have been changed, but the competing effects of changed surface mechanical properties on foam stability are likely counteracted (as shown at DTAB concentration of $0.25 \times \text{CMC}$). Thus, foam stability maintains the same after the addition of silica particles.

Therefore, it is demonstrated that the variation of surface mechanical properties affects the stability of particle-stabilised foams and the changes of surface mechanical properties are governed by two competing effects: One is the competition of adsorption of surfactants upon the solid-liquid interface *versus* the air-liquid interface. The other one is the competition between the

adsorption of silica particles on air-liquid interface *versus* the interaction between silica particles in bulk solution. These two effects are combined together to influence surface tension, surface elasticity, surface dilatational viscosity and Gibbs elasticity. Foams can be stabilised by adding silica particles if surface tension and surface dilatational viscosity are reduced and surface elasticity and Gibbs elasticity are promoted. This is the reason for that intermediately hydrophobic particles are capable of increasing foam stability. In this subsection, the effect of silica particles on surface mechanical properties and the reason why intermediately hydrophobic particles can increase foam stability have been explored. In the next subsection (subsection 6.4.2), the effect of particle concentration on surface mechanical properties are investigated to verify whether the most stable foam obtained with different particle concentrations possesses the best surface mechanical properties which are conducive to foam stability.

6.4.2 Surface Mechanical Properties of Mixtures of DTAB Solutions ($0.1 \times$ CMC) and Colloidal Silica Dispersions at Different Particle Concentrations

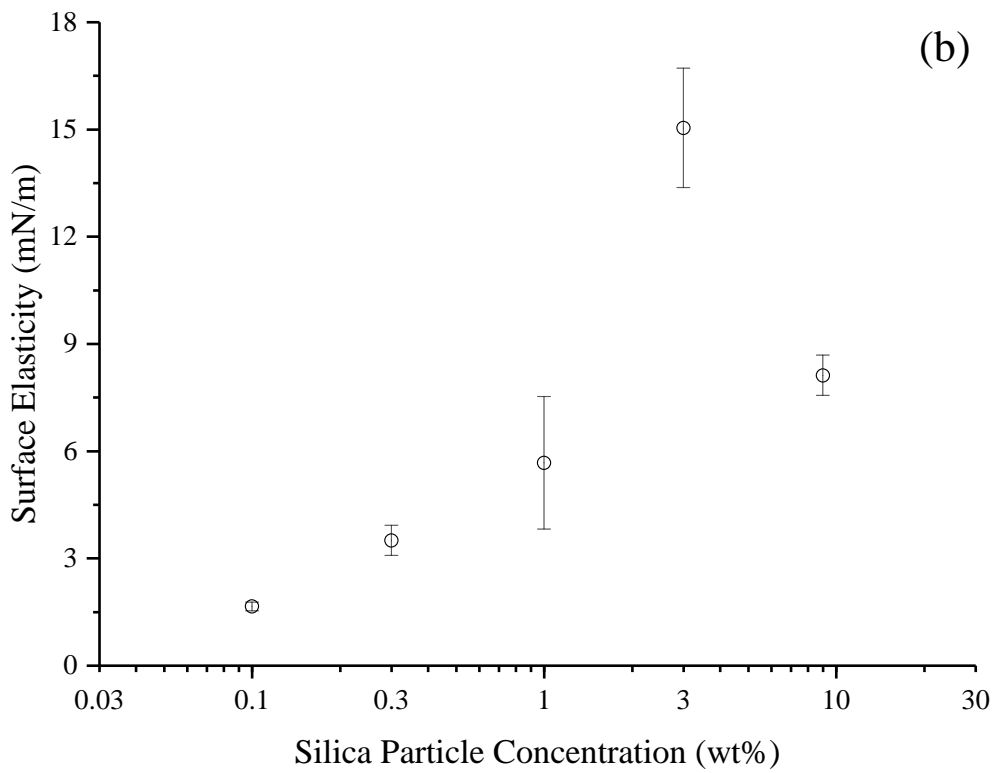
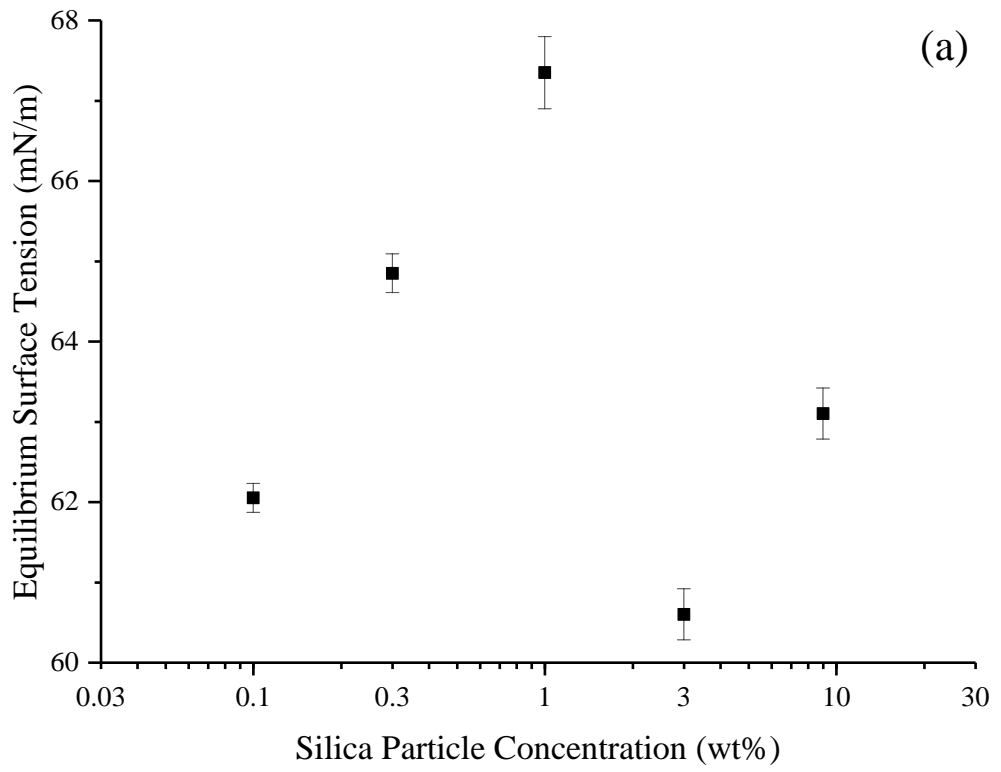
Surface rheological properties and equilibrium surface tension of the samples used as described in subsection 6.3.1 are measured. The same methods as described in subsection 6.4.1 have been applied and the results of surface rheological properties and equilibrium surface tension of mixtures of DTAB solutions at the concentration of $0.1 \times$ CMC and colloidal silica dispersions at different particle concentrations are shown in Table 6-2 (The detailed results of surface rheological properties and equilibrium surface tension in each independent measurement of these samples are shown in Appendix G). The

equilibrium foam heights of these samples are also shown in Table 6-2 in order to enable a comparison with surface mechanical properties. As can be seen from Table 6-2, for all samples, surface elasticity is smaller than half of equilibrium surface tension, however, both stable and unstable foams stabilised by these samples have been observed. This shows agreement with the observation obtained in subsection 6.4.1 that the prediction criterion for stable particle-stabilised foams proposed by Stocco *et al.* (2009, 2011) is not universally valid.

Table 6-2. The comparison of surface rheological properties, equilibrium surface tension and equilibrium foam height of mixtures of DTAB solutions at the concentration of $0.1 \times \text{CMC}$ and colloidal silica dispersions at different particle concentrations. The errors are the standard deviation of all observations and the values in the brackets represent the full range of observations.

Samples	Surface elasticity (mN/m)	Surface dilatational viscosity (mN·s/m)	Gibbs elasticity (mN/m)	Equilibrium surface tension (mN/m)	Equilibrium foam height (mm)
$0.1 \times \text{CMC}$ DTAB + 0.1 wt% silica particles	1.65 ± 0.12	0.11 ± 0.02	2.22 ± 0.18	62.05 ± 0.18	4 (3 - 4)
$0.1 \times \text{CMC}$ DTAB + 0.3 wt% silica particles	3.50 ± 0.42	0.14 ± 0.07	4.15 ± 0.51	64.85 ± 0.24	3 (3 - 4)
$0.1 \times \text{CMC}$ DTAB + 1 wt% silica particles	5.67 ± 1.85	0.48 ± 0.26	8.53 ± 3.37	67.35 ± 0.45	36 (34 - 37)
$0.1 \times \text{CMC}$ DTAB + 3 wt% silica particles	15.04 ± 1.67	0.06 ± 0.05	15.25 ± 1.74	60.60 ± 0.32	193 (162 - 233)
$0.1 \times \text{CMC}$ DTAB + 9 wt% silica particles	8.12 ± 0.56	0.06 ± 0.03	8.30 ± 0.56	63.10 ± 0.32	92 (80 - 113)

The surface mechanical properties of mixtures of DTAB solutions at the concentration of $0.1 \times \text{CMC}$ and colloidal silica dispersions at different concentrations are shown in Figure 6-9. They are compared with foam stability results of these samples as can be seen in Figure 6-5. It has already been demonstrated in subsection 6.3.1 that foam stability increases first and then decreases with increasing particle concentration. The most stable foams are obtained at a particle concentration of 3 wt%. It can be seen from Figure 6-9 that equilibrium surface tension increases first and then decreases, and afterwards increases again with increasing particle concentration. The maximum and minimum values of equilibrium surface tension are at 1 and 3 wt% respectively. As for the surface rheological properties, they increase first and then decrease with increasing particle concentration. The maximum values of surface elasticity and Gibbs elasticity are at the concentration of 3 wt%, whereas that of surface dilatational viscosity is at 1 wt%. The variations of surface mechanical properties are actually due to the competitive adsorption of surfactants on solid-liquid interface and air-liquid interface, and the competition between particle adsorption on air-liquid interface and inter-particle interaction in bulk solution. Furthermore, it is worth mentioning that the decrease of equilibrium surface tension from silica particle concentration of 1 wt% to 3 wt% as shown in Figure 6-9(a) is also likely to be driven by the elongation of droplet shape due to the weight of silica particles collecting at the bottom of the droplet (Manga *et al.*, 2016).



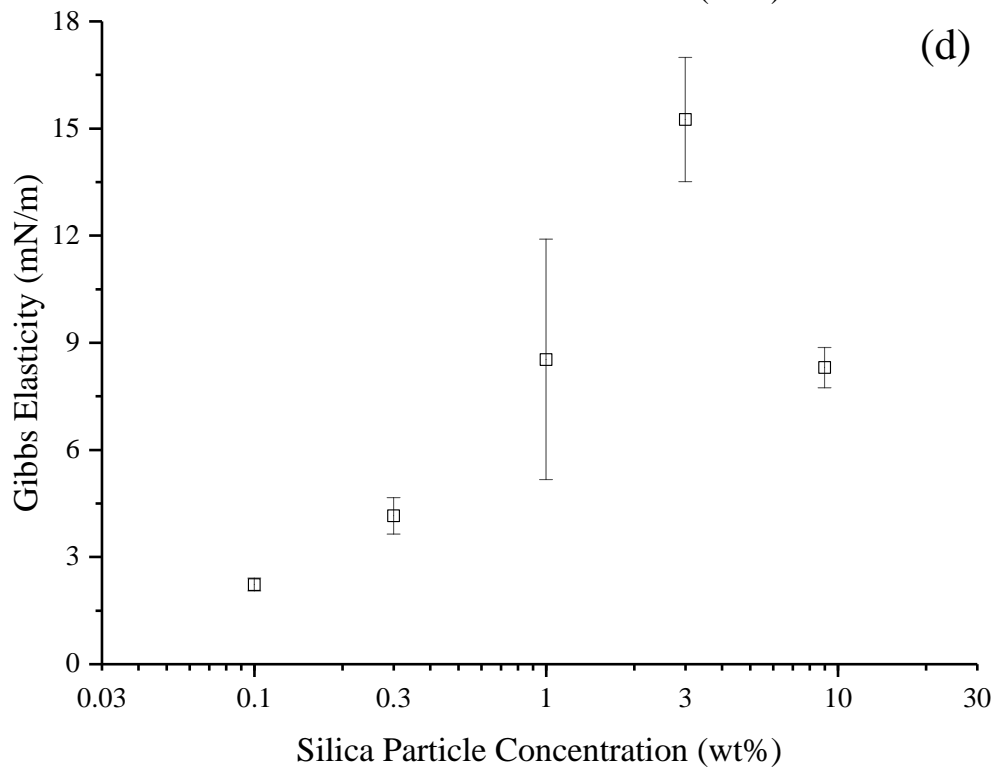
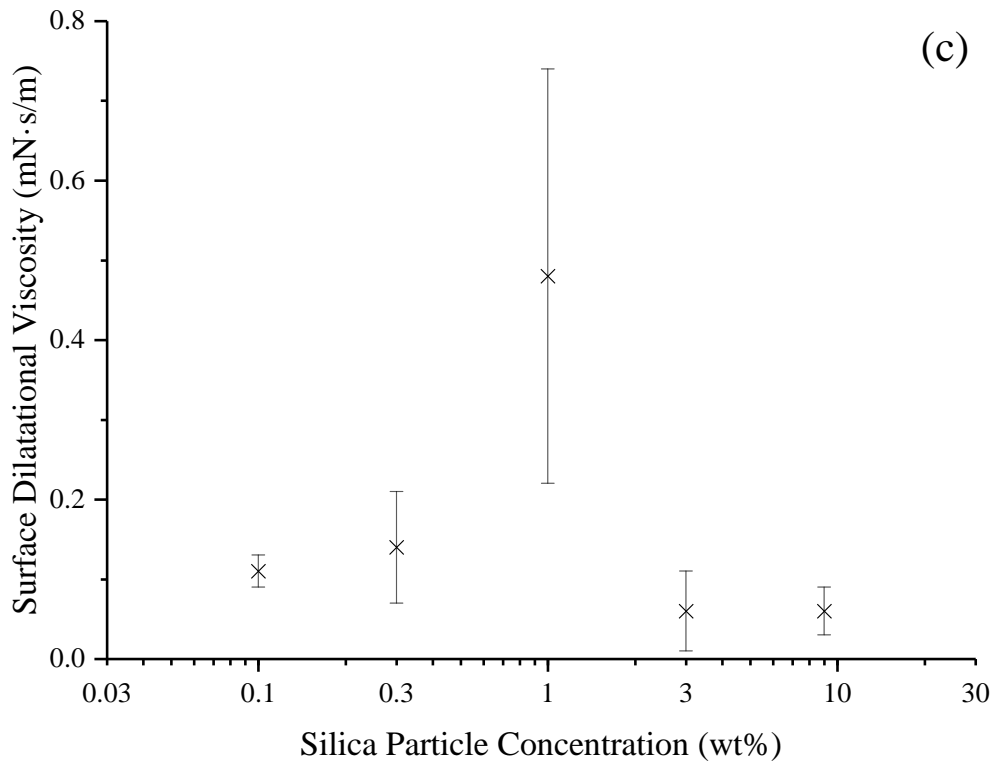


Figure 6-9. The surface mechanical properties of mixtures of DTAB solutions at the concentration of $0.1 \times \text{CMC}$ and colloidal silica dispersions at different concentrations. (a) Equilibrium surface tension results. (b) Surface elasticity results. (c) Surface dilatational viscosity results. (d) Gibbs elasticity results. The error bars represent the standard deviation of all observations.

By relating surface mechanical properties to foam stability, it is demonstrated that the most stable foams (at the particle concentration of 3 wt%) are obtained at the smallest equilibrium surface tension and surface dilatational viscosity, whereas surface elasticity and Gibbs elasticity are at their greatest. The foams stabilised by mixtures at other particle concentrations are less stable due to larger equilibrium surface tension and surface dilatation viscosity and smaller surface elasticity and Gibbs elasticity, which is a synergistic effect to compromise foam stability. This shows agreement with the observation in subsection 6.4.1 that the stability of particle-stabilised foams is governed by the synergism of surface mechanical properties. Foam stability can be improved by adding intermediately hydrophobic silica particles because surface tension and surface dilatational viscosity are diminished whereas surface elasticity and Gibbs elasticity are increased.

6.5 Summary

In this chapter, the link between foam stability and surface mechanical properties of mixtures of DTAB solutions and silica particles is investigated. The effect of silica particles (at a fixed particle concentration) on the stability of foams produced by DTAB solutions at different concentrations and the effect of particle concentration on the stability of foams stabilised by mixtures of DTAB solutions and silica particles are described. It is experimentally demonstrated that different surfactant and particle concentrations affect the particle hydrophobicity due to the adsorption of surfactant at particle surface and only intermediately hydrophobic particles can enhance foam stability. Furthermore, the stability of particle-stabilised foams and the surface

mechanical properties of air-liquid interfaces of these foams are compared, which demonstrates that the reason why silica particle with intermediate hydrophobicity is capable of improving foam stability is due to its effect on surface mechanical properties which increases surface elasticity and Gibbs elasticity whilst decreases surface tension and surface dilatational viscosity. All these changes in surface mechanical properties have a synergistic effect on the stability of particle-stabilised foams. The variations of surface mechanical properties are due to the competitive adsorption of surfactants on solid-liquid interface and air-liquid interface, and the competition between the adsorption of silica particles on air-liquid interface and the interaction between silica particles in bulk solution.

**Chapter 7 Conclusions and
Recommendations for Future Work**

7.1 Conclusions

In this chapter, the achievements of this thesis in the context of the objectives as described in subsection 1.1.2 are reviewed. Then, the recommendations for future works are presented.

1. It has been confirmed that the theoretical equations which describe the oscillatory mechanical properties of a gas-liquid interface (presented in section 2.2) have been applied autogenously in the oscillating pendent droplet method to measure surface elasticity and surface dilatational viscosity. Therefore, according to these theoretical equations, the values of Gibbs elasticity were able to be obtained by inference from the results of surface elasticity and surface dilatational viscosity in the current work. Subsequently, the dependency of surface rheological properties on oscillation frequency and amplitude has been observed in section 2.4 and this dependency indicated that, in order to obtain convincing observations of the relationship between surface mechanical properties and foam stability (which is the first objective as described in subsection 1.1.2), the measurement of surface rheological properties of different surfactant solutions should be performed at a fixed oscillation frequency and amplitude.

2. The observable differences of dynamic surface tension results of ionic surfactant solutions (obtained by the static pendant droplet method) between different trials have been noted in sections 3.2 and 3.3, and then this unexpected systematic change of dynamic surface tension between different trials has been found to be due to the presence of trace amounts of highly

surface-active impurities in section 3.4. It was a consequence of the presence of highly surface-active impurities that the repeatability and precision of dynamic surface tension measurements were compromised. It has also been statistically demonstrated in section 3.5 that, with respect to the static pendant droplet method, performing large numbers of independent trials of dynamic surface tension measurement and then calculating the arithmetic mean of all dynamic surface tension results is necessary to obtain the dynamic surface tension value of ionic surfactant solutions with highly surface-active impurity.

3. The measurements of foam stability using the modified Bikerman test of Li *et al.* (2010), that controls the environmental relative humidity at the top of column, were performed at different environmental relative humidities (ranging from 10% to 90 %) in chapter 4 to confirm and extend the observation of the dependency of foam stability upon environmental relative humidity that foam stability increases with an increase of environmental relative humidity. With regards to relating foam stability to surface mechanical properties (the first objective), foam stability of different surfactant solutions need to be measured at the same environmental relative humidity.

4. Three different surfactant solutions have been prepared in section 5.2 by changing the surfactant type and manipulating the concentration of surfactant solutions so that two of them had approximately the same equilibrium surface tension whereas the other one had slightly higher equilibrium surface tension. The measurements of foam stability (at constant relative humidity) and surface rheological properties (at the same oscillation frequency and amplitude) of

these three surfactant solutions were performed in section 5.3 to correlate foam stability to surface rheological properties (the first objective). It has been demonstrated that both surface tension and surface rheological properties affected the stability of surfactant-stabilised foams, however, surface tension appeared to play a more important role, with respect to the stability of surfactant-stabilised foams.

5. The stability of foams stabilised by the mixtures of particles and surfactants, as well as the relationship between the surface mechanical properties of air-liquid interfaces and the stability of particle-stabilised foams, has also been studied in this thesis (which is the second objective as described in subsection 1.1.2). The stability of particle-stabilised foams has been measured by the modified Bikerman test of Li *et al.* (2010) as well, which was more reproducible than other methods to produce foam and to quantify foam stability such as ‘hand-shaking’ method which has been applied in Binks *et al.* (2008). It has been experimentally demonstrated in sections 6.2 and 6.3 that only intermediately hydrophobic particles could enhance foam stability by the addition of particles to surfactant solutions, since these particles affected the surface mechanical properties of air-liquid interfaces of particle-stabilised foams by increasing surface elasticity and Gibbs elasticity whereas decreasing equilibrium surface tension and surface dilatational viscosity, which had a synergistically positive affect on the stability of particle-stabilised foams. The variations of surface mechanical properties of air-liquid interfaces of particle-stabilised foams were ascribed, in section 6.4, to the competitive adsorption of surfactants on solid-liquid interface and air-liquid interface, and the

competition between the adsorption of silica particles on air-liquid interface and the interaction between silica particles in bulk solution. However, this observation of the optimum range of particle hydrophobicity to stabilise foam did not agree with the results of Binks *et al.* (2008) which concluded that the most hydrophobic particles were more successful at increasing foam stability. This difference in the experimental observations was attributed to the different methods to produce foam and quantify foam stability, since it was the ‘hand-shaking’ method applied in Binks *et al.* (2008) that could compromise the reproducibility of the quantification of foam stability.

7.2 Recommendations for Future Work

In the current work to obtain surface rheological properties of air-liquid interfaces of foams, Gibbs elasticity (which can be considered as the limiting surface elasticity at infinite oscillation frequency) was inferred from the results of surface elasticity and surface dilatational viscosity which were measured at the relative low oscillation frequency (less than 1 Hz), since the device of droplet shape analyser applied in this study is not available to perform the measurement at relatively high frequency (for example, several hundred Hertz). Thus, the values of Gibbs elasticity obtained in this thesis could be potentially compromised. The recommendation is, in the future, to obtain Gibbs elasticity at higher frequency directly.

In the exploration of foam stability measurement, the representative photographs of foams were obtained from normal digital camera, which could result in poor quality and optical distortion of photographs, and thus

compromises the estimation of bubble distribution of a foam. Therefore, in the future, it is recommended to use high resolution camera to increase photograph quality and to apply corrections on photographs by software to eliminate optical distortion issue, in order to obtain an accurate estimation of bubble distribution of a foam.

In the study of the relationship between surface mechanical properties and foam stability, the determined surfactant solutions with similar equilibrium surface tension were limited, which were sodium tridecyl sulfate (anionic surfactant), DTAB (cationic surfactant) and TX-100 (non-ionic surfactant). In the future, more surfactant solutions will be tested to confirm and extend the observation obtained in the current work that surface tension plays a more important role than surface rheological properties in governing the stability of surfactant-stabilised foams. Furthermore, the effect of potential surfactant depletion during foaming process on surface mechanical properties and then on foam stability has been noticed in this thesis, it is suggested to measure the surface tension of surfactant solution before and after foaming process to test the depletion of surfactant in the future.

In the investigation of the stability of particle-stabilised foams and the relationship between the surface mechanical properties of air-liquid interfaces and the stability of particle-stabilised foams, the foam was actually stabilised by the mixture of particles and surfactants. The work concerning the foam stabilised solely by particles has not been performed in this thesis, which is worth exploring in the future. Thus, the stability of foams stabilised solely by particles should be studied with the reproducible method of controlling

environmental relative humidity during foam stability measurements. Furthermore, the surface mechanical properties of liquid-air interfaces of foams stabilised solely by particles should be investigated as well.

Finally, in the current work, the study focused either on microscale (the investigation of surface mechanical properties of air-liquid interfaces) or on mesoscale (the exploration of the stability of foams stabilised by surfactants or mixtures of surfactants and particles). However, none of the work in this thesis was related to industrial applications (i.e. the study in macroscale). In fact, foams have great potential in various industrial applications including consumer products (such as home and personal care or food and drink products), flotation, fire-fighting, and in particular, enhanced oil recovery. In the future, it is expected to apply stable foams, which are obtained by the modification of surface mechanical properties of gas-liquid interfaces, in the oil field to improve oil sweep efficiency.

References

Alvarez, N. J., Walker, L. M., Anna, S. L., 2009. A non-gradient based algorithm for the determination of surface tension from a pendant drop: Application to low Bond number drop shapes. *Journal of Colloid and Interface Science*, 333, 557-562.

AlYousef, Z. A., Almobarky, M. A., Schechter, D. S., 2018. The effect of nanoparticle aggregation on surfactant foam stability. *Journal of Colloid and Interface Science*, 511, 365-373.

Anazadehsayed, A., Rezaee, N., Naser, J., Nguyen, A. V., 2018. A review of aqueous foam in microscale. *Advances in Colloid and Interface Science*, 256, 203-229.

Atkin, R., Craig, V. S. J., Wanless, E. J., Biggs, S., 2003. Mechanism of cationic surfactant adsorption at the solid-aqueous interface. *Advances in Colloid and Interface Science*, 103, 219-304.

Bain, C. D., Davies, P. B., Ward, R. N., 1994. In-situ sum-frequency spectroscopy of sodium dodecyl sulfate and dodecanol co-adsorbed at a hydrophobic surface. *Langmuir*, 10, 2060-2063.

Barbian, N., Ventura-Medina, E., Cilliers, J. J., 2003. Dynamic froth stability in froth flotation. *Minerals Engineering*, 16, 1111-1116.

Barbian, N., Hadler, K., Ventura-Medina, E., Cilliers, J. J., 2005. The froth stability column: Linking froth stability and flotation performance. *Minerals Engineering*, 18, 317-324.

Barbian, N., Hadler, K., Cilliers, J. J., 2006. The froth stability column: Measuring froth stability at an industrial scale. *Minerals Engineering*, 19, 713-718.

Berry, J. D., Neeson, M. J., Dagastine, R. R., Chan, D. Y. C., Tabor, R. F., 2015. Measurement of surface and interface tension using pendant drop tensiometry. *Journal of Colloid and Interface Science*, 454, 226-237.

Bikerman, J. J., 1938. The unit of foaminess. *Transactions of the Faraday Society*, 34, 634-638.

Bikerman, J. J., 1973. *Foams*. New York: Springer-Verlag.

Binks, B. P., Lumsdon, S. O., 2000. Influence of particle wettability on the type and stability of surfactant-free emulsions. *Langmuir*, 16, 8622-8631.

Binks, B. P., 2002. Particles as surfactants—similarities and differences. *Current Opinion in Colloid and Interface Science*, 7, 21-41.

Binks, B. P., Clint, J. H., 2002. Solid wettability from surface energy components: relevance to Pickering emulsions. *Langmuir*, 18, 1270-1273.

Binks, B. P., Horozov, T. S., 2005. Aqueous foams stabilised solely by silica nanoparticles. *Angewandte Chemie International Edition*, 44, 3722-3725.

Binks, B. P., Horozov, T. S. (editors), 2006. *Colloidal Particles at Liquid Interfaces*. New York: Cambridge University Press.

Binks, B. P., Kirkland, M., Rodrigues, J. A., 2008. Origin of stabilisation of aqueous foams in nanoparticle-surfactant mixtures. *Soft Matter*, 4, 2373-2382.

Blanco-Gomis, D., Mangas-Alonso, J. J., Junco-Corujedo, S., Gutierrez-Alvarez, M. D., 2009. Characterisation of sparkling cider by the yeast type used in taking foam on the basis of polypeptide content and foam characteristics. *Food Chemistry*, 115, 375-379.

Borwankar, R. P., Wasan, D. T., 1988. Equilibrium and dynamics of adsorption of surfactants at fluid-fluid interfaces. *Chemical Engineering Science*, 43, 1323-1337.

Bournival, G., Ata, S., Karakashev, S. I., Jameson, G. J., 2014. An investigation of bubble coalescence and post-rupture oscillation in non-ionic surfactant solutions using high-speed cinematography. *Journal of Colloid and Interface Science*, 414, 50-58.

Bournival, G., Ata, S., Wanless, E. J., 2015. The roles of particles in multiphase processes: particles on bubble surfaces. *Advances in Colloid and Interface Science*, 225, 114-133.

Bournival, G., Ata, S., Jameson, G. J., 2017. Bubble and froth stabilising agents in froth flotation. *Mineral Processing and Extractive Metallurgy Review*, 38, 366-387.

Briceño-Ahumada, Z., Langevin, D., 2017. On the influence of surfactant on the coarsening of aqueous foams. *Advances in Colloid and Interface Science*, 244, 124-131.

Canny, J., 1986. Computational approach to edge detection. *IEEE Transactions on Pattern Analysis and Machine Intelligence*, PAMI-8, 679-698.

Cantat, I., Cohen-Addad, S., Elias, F., Graner, F., Hohler, R., Pitois, O., Rouyer, F., Saint-Jalmes, A., Flatman, R., Cox, S., 2013. *Foams: structure and dynamics*. Oxford, New York: Oxford University Press.

Carrier, V., Colin, A., 2003. Coalescence in draining foams. *Langmuir*, 19, 4535-4538.

Cervantes Martinez, A., Rio, E., Delon, G., Saint-Jalmes, A., Langevin, D., Binks, B. P., 2008. On the origin of the remarkable stability of aqueous foams stabilised by nanoparticles: link with microscopic surface properties. *Soft Matter*, 4, 1531-1535.

Champougny, L., Miguët, J., Henaff, R., Restagno, F., Boulogne, F., Rio, E., 2018. Influence of evaporation on soap film rupture. *Langmuir*, 34, 3221-3227.

Chen, M., Sala, G., van Valenberg, H. J. F., van Hooijdonk, A. C. M., van der Linden, E., Meinders, M. B. J., 2018. Foam and thin films of hydrophilic silica particles modified by β -casein. *Journal of Colloid and Interface Science*, 513, 357-366.

Cheng, P., Li, D., Boruvka, L., Rotenberg, Y., Neumann, A. W., 1990. Automation of Axisymmetric Drop Shape Analysis for measurements of interfacial tensions and contact angles. *Colloids and Surfaces*, 43, 151-167.

Cho, Y. S., Laskowski, J. S., 2002. Effect of flotation frothers on bubble size and foam stability. *International Journal of Mineral Processing*, 64, 69-80.

Choung, J., Walker, J., Xu, Z. H., Masliyah, J., 2004. Effect of temperature on the stability of froth formed in the recycle process water of oil sands extraction. *The Canadian Journal of Chemical Engineering*, 82, 801-806.

Clunie, S. J., Ingram, B. T., 1983. Adsorption of non-ionic surfactants. In Parfitt, G. D., Rochester, C. H. (editors). *Adsorption from Solution at the Solid/Liquid Interface*. London: Academic Press, 105-149.

Colin, A., 2012. Coalescence in foams. In Stevenson, P. (editor). *Foam engineering: fundamentals and applications*. Chichester: John Wiley & Sons, 75-90.

De Gennes, P. G., 2001. Some remarks on coalescence in emulsions or foams. *Chemical Engineering Science*, 56, 5449-5450.

Del Rio, O. I., Neumann, A. W., 1997. Axisymmetric Drop Shape Analysis: computational methods for the measurement of interfacial properties from the shape and dimensions of pendant and sessile drops. *Journal of Colloid and Interface Science*, 196, 136-147.

Derjaguin, B., Landau, L. D., 1941. Theory of the stability of strongly charged lyophobic sols and of the adhesion of strongly charged particles in solutions of electrolytes. *Acta Physico Chemica URSS*, 14, 633-662.

Dickinson, E., Ettelaie, R., Kostakis, T., Murray, B. S., 2004. Factors controlling the formation and stability of air bubbles stabilised by partially hydrophobic silica nanoparticles. *Langmuir*, 20, 8517-8525.

Drenckhan, W., Hutzler, S., 2015. Structure and energy of liquid foams. *Advances in Colloid and Interface Science*, 224, 1-16.

Dutkiewicz, E., Jakubowska, A., 2002. Effect of electrolytes on the physicochemical behaviour of sodium dodecyl sulphate micelles. *Colloid and Polymer Science*, 280, 1009-1014.

Eastoe, J., Dalton, J. S., 2000. Dynamic surface tension and adsorption mechanisms of surfactants at the air-water interface. *Advances in Colloid and Interface Science*, 85, 103-144.

Edwards, D. A., Brenner, H., Wasan, D. T., 1991. *Interfacial Transport Processes and Rheology*. Boston: Butterworth-Heinemann.

Einstein, A., 1905. On the movement of small particles suspended in a stationary liquid demanded by the molecular-kinetic theory of heat. *Annals of Physics*, 322, 549-560.

Espert, A., Klitzing, R. V., Poulin, P., Colin, A., Zana, R., Langevin, D., 1998. Behaviour of soap films stabilised by a cationic dimeric surfactant. *Langmuir*, 14, 4251-4260.

Evertett, D. H., 1988. *Basic Principles of Colloid Science*. London: Royal Society of Chemistry.

Fainerman, V. B., Vollhardt, D., Emrich, G., 2001. Dynamics and phases transition in adsorbed monolayers of sodium dodecyl sulfate/dodecanol mixtures. *Journal of Physical Chemistry B*, 105, 4324-4330.

Fainerman, V. B., Lylyk, S. V., Aksenenko, E. V., Petkov, J. T., Yorke, J., Miller, R., 2010. Surface tension isotherms, adsorption dynamics and

dilatational visco-elasticity of sodium dodecyl sulphate solutions. . Colloids and Surfaces A: Physicochemical and Engineering Aspects, 354, 8-15.

Fameau, A. L., Carl, A., Saint-Jalmes, A., von Klitzing, R., 2015. Responsive aqueous foams. Chemphyschem, 16, 66-75.

Fang, J. P., Joos, P., 1992a. The dynamic surface tension of SDS-dodecanol mixtures 1. The submicellar systems. Colloids and Surfaces, 65, 113-120.

Fang, J. P., Joos, P., 1992b. The dynamic surface tension of SDS-dodecanol mixtures 2. Micellar SDS-dodecanol mixtures. Colloids and Surfaces, 65, 121-129.

Farrokhpay, S., 2011. The significance of froth stability in mineral flotation: A review. Advances in Colloid and Interface Science, 166, 1-7.

Ferrera, C., Montanero, J. M., Cabezas, M. G., 2007. An analysis of the sensitivity of pendant drops and liquid bridges to measure the interfacial tension. Measurement Science and Technology, 18, 3713-3723.

Fruhner, H., Wantke, K. D., Lunkenheimer, K., 1999. Relationship between surface dilatational properties and foam stability. Colloids and Surfaces A: Physicochemical and Engineering Aspects, 162, 193-202.

Gao, Y., Du, J., Gu, T., 1987. Hemimicelle formation of cationic surfactants at the silica gel-water interface. Journal of the Chemical Society, Faraday Transactions 1: Physical Chemistry in Condensed Phases, 83, 2671-2679.

Garrett, P. R., 2015. Defoaming: Antifoams and mechanical methods. Current Opinion in Colloid and Interface Science, 20, 81-91.

Georgieva, D., Cagna, A., Langevin, D., 2009. Link between surface elasticity and foam stability. Soft Matter, 5, 2063-2071.

Gibbs, J. W., 1928. The Collected Works of J. Willard Gibbs. New York: Longman.

Glazier, J. A., Weaire, D., 1992. The kinetics of cellular-patterns. *Journal of Physics: Condensed Matter*, 4, 1867-1894.

Guzmán, E., Tajuelo, J., Pastor, J. M., Rubio, M. A., Ortega, F., Rubio, R. G., 2018. Shear rheology of fluid interfaces: Closing the gap between macro- and micro-rheology. *Current Opinion in Colloid and Interface Science*, 37, 33-48.

Hansen, B. B., Kiil, S., Johnsson, J. E., Sonder, K. B., 2008. Foaming in wet flue gas desulfurization plants: The influence of particles, electrolytes, and buffers. *Industrial and Engineering Chemistry Research*, 47, 3239-3246.

Hartley, G. S., 1936. *Aqueous Solutions of Paraffin Chain Salts*. Paris: Hermann and Cie.

Heller, J. P., 1994. CO₂ foams in enhanced oil recovery. In Schramm, L. L. (editor). *Foams: Fundamentals and Applications in the Petroleum Industry*. Washington: American Chemical Society, 201-234.

Hilgenfeldt, S., Koehler, S. A., Stone, H. A., 2001. Dynamics of coarsening foams: accelerated and self-limiting drainage. *Physical Review Letters*, 86, 4704-4707.

Hill, C., Eastoe, J., 2017. Foams: From nature to industry. *Advances in Colloid and Interface Science*, 247, 496-513.

Hofmann, M. J., Motschmann, H., 2017. Surface rheology and its relation to foam stability in solutions of sodium decyl sulfate. *Colloids and Surfaces A: Physicochemical and Engineering Aspects*, 532, 472-475.

Holmberg, K., Jonsson, B., Kronberg, B., Lindman, B., 2003. *Surfactants and Polymers in Aqueous Solution*. USA: John Wiley & Sons.

Hoorfar, M., Neumann, A. W., 2004. Axisymmetric drop shape analysis (ADSA) for the determination of surface tension and contact angle. *The Journal of Adhesion*, 80, 727-743.

Hoorfar, M., Neumann, A. W., 2006. Recent progress in axisymmetric drop shape analysis (ADSA). *Advances in Colloid and Interface Science*, 121, 25-49.

Horozov, T. S., 2008. Foams and foam films stabilised by solid particles. *Current Opinion in Colloid and Interface Science*, 13, 134-140.

Hunter, R. J., 1993. *Introduction to Modern Colloid Science*. New York: Oxford University Press.

Hunter, T. N., Jameson, G. J., Wanless, E. J., 2007. Determination of contact angles of nanosized silica particles by multi-angle single-wavelength ellipsometry. *Australian Journal of Chemistry*, 60, 651-655.

Hunter, T. N., Pugh, R. J., Franks, G. V., Jameson, G. J., 2008. The role of particles in stabilising foams and emulsions. *Advances in Colloid and Interface Science*, 137, 57-81.

Hunter, T. N., Wanless, E. J., Jameson, G. J., 2009. Effect of esterically bonded agents on the monolayer structure and foamability of nano-silica. *Colloids and Surfaces A: Physicochemical and Engineering Aspects*, 334, 181-190.

Hunter, T. N., Wanless, E. J., Jameson, G. J., Pugh, R. J., 2009. Non-ionic surfactant interactions with hydrophobic nanoparticles: impact on foam stability. *Colloids and Surfaces A: Physicochemical and Engineering Aspects*, 347, 81-89.

Hunter, T. N., Jameson, G. J., Wanless, E. J., Dupin, D., Armes, S. P., 2009. Adsorption of submicrometer-sized cationic sterically stabilised polystyrene latex at the air-water interface: contact angle determination by ellipsometry. *Langmuir*, 25, 3440-3449.

Jaensson, N., Vermant, J., 2018. Tensiometry and rheology of complex interfaces. *Current Opinion in Colloid and Interface Science*, 37, 136-150.

Joos, P., 1999. Periodic surface deformation. In Fainerman, V. B., Loglio, G., Lucassen-Reynders, E. H., Miller, R., Petrov, P. (editors). *Dynamic Surface Phenomena*. Utrecht: VSP, 223-257.

Kalantarian, A., David, R., Chen, J., Neumann, A. W., 2011. Simultaneous measurement of contact angle and surface tension using Axisymmetric Drop Shape Analysis - No Apex (ADSA-NA). *Langmuir*, 27, 3485-3495.

Kalantarian, A., Saad, S. M. I., Neumann, A. W., 2013. Accuracy of surface tension measurement from drop shapes: the role of image analysis. *Advances in Colloid and Interface Science*, 199-200, 15-22.

Kanner, B., Glass, J. E., 1969. Surface viscosity and elasticity — significant parameters in industrial processes. *Industrial and Engineering Chemistry*, 61, 31-41.

Kanokkarn, P., Shiina, T., Santikunaporn, M., Chavadej, S., 2017. Equilibrium and dynamic surface tension in relationship to diffusivity and foaming properties: effects of surfactant type and structure. *Colloids and Surfaces A: Physicochemical and Engineering Aspects*, 524, 135-142.

Karbaschi, M., Lotfi, M., Krägel, J., Javadi, A., Bastani, D., Miller, R., 2014. Rheology of interfacial layers. *Current Opinion in Colloid and Interface Science*, 19, 514-519.

Khristov, K., Exerowa, D., Minkov, G., 2002. Critical capillary pressure for destruction of single foam films and foam: effect of foam film size. *Colloids and Surfaces A: Physicochemical and Engineering Aspects*, 210, 159-166.

Koehler, S. A., Hilgenfeldt, S., Stone, H. A., 1999. Liquid flow through aqueous foams: the node-dominated foam drainage equation. *Physical Review Letters*, 82, 4232-4235.

Koehler, S. A., Hilgenfeldt, S., Stone, H. A., 2000. A generalised view of foam drainage: experiment and theory. *Langmuir*, 16, 6327-6341.

Koehler, S. A., Hilgenfeldt, S., Stone, H. A., 2004. Foam drainage on the microscale. part 1: Modelling flow through single plateau borders. *Journal of Colloid and Interface Science*, 276, 420-438.

Koehler, S. A., 2012. Foam drainage. In Stevenson, P. (editor). *Foam engineering: fundamentals and applications*. Chichester: John Wiley & Sons, 27-58.

Kovalchuk, V. I., Krägel, J., Makievski, A. V., Loglio, G., Ravera, F., Liggieri, L., Miller, R., 2002. Frequency characteristics of amplitude and phase of oscillating bubble systems in a closed measuring cell. *Journal of Colloid and Interface Science*, 252, 433-442.

Kovalchuk, V. I., Krägel, J., Makievski, A. V., Ravera, F., Liggieri, L., Loglio, G., Fainerman, V. B., Miller, R., 2004. Rheological surface properties of C₁₂DMPO solution as obtained from amplitude- and phase-frequency characteristics of an oscillating bubble system. *Journal of Colloid and Interface Science*, 280, 498-505.

Kovalchuk, V. I., Miller, R., Fainerman, V. B., Loglio, G., 2005. Dilatational rheology of adsorbed surfactant layers — role of the intrinsic two-dimensional compressibility. *Advances in Colloid and Interface Science*, 114-115, 303-312.

Krägel, J., Derkach, S. R., 2010. Interfacial shear rheology. *Current Opinion in Colloid and Interface Science*, 15, 246-255.

Kruglyakov, P. M., Exerowa, D. R., 1997. Foams and foam films. In Möbius, D., Miller, R. (editors). *Studies of Interface Science*, vol. 5. Amsterdam: Elsevier.

Kruglyakov, P. M., Karakashev, S. I., Nguyen, A. V., Vilkova, N. G., 2008. Foam drainage. *Current Opinion in Colloid and Interface Science*, 13, 163-170.

Kruglyakov, P. M., Elaneva, S. I., Vilkova, N. G., 2011. About mechanism of foam stabilisation by solid particles. *Advances in Colloid and Interface Science*, 165, 108-116.

Lambert, J., Cantat, I., Delannay, R., Mokso, R., Cloetens, P., Glazier, J., Graner, F., 2007. Experimental growth law for bubbles in a moderately “wet” 3D liquid foam. *Physical Review Letters*, 99, 058304.

Langevin, D., 2000. Influence of interfacial rheology on foam and emulsion properties. *Advances in Colloid and Interface Science*, 88, 209-222.

Langevin, D., 2014. Surface shear rheology of monolayers at the surface of water. *Advances in Colloid and Interface Science*, 207, 121-130.

Langevin, D., 2015. Bubble coalescence in pure liquids and in surfactant solutions. *Current Opinion in Colloid and Interface Science*, 20, 92-97.

Langevin, D., 2017. Aqueous foams and foam films stabilised by surfactants. Gravity-free studies. *Comptes Rendus Mecanique*, 345, 47-55.

Lemlich, R., 1978. Prediction of changes in bubble size distribution due to inter-bubble gas diffusion in foam. *Industrial & Engineering Chemistry Fundamentals*, 17, 89-93.

Leonard, R. Lemlich, R., 1965. A study of interstitial liquid flow in foam. *A. I. Ch. E. Journal*, 11, 18-25.

Levitz, P. E., 2002. Adsorption of non-ionic surfactants at the solid/water interface. *Colloids and Surfaces A: Physicochemical and Engineering Aspects*, 205, 31-38.

Li, X, Shaw, R., Stevenson, P., 2010. Effect of humidity on dynamic foam stability. *International Journal of Mineral Processing*, 94, 14-19.

Li, X., Karakashev, S. I., Evans, G. M., Stevenson, P., 2012. Effect of environmental humidity on static foam stability. *Langmuir*, 28, 4060-4068.

Li, X., 2012. Transport Phenomena in Foam Fractionation. PhD thesis, The University of Newcastle (Australia).

Lifshitz, I. M., Slyozov, V. V., 1961. The kinetics of precipitation from supersaturated solid solutions. *Journal of Physics and Chemistry of Solids*, 19, 35-50.

Liggieri, L., Miller, R., 2010. Relaxation of surfactants adsorption layers at liquid interfaces. *Current Opinion in Colloid and Interface Science*, 15, 256-263.

Lin, S. Y., Chen, L. J., Xu, J. W., Wang, W. J., 1995. An examination on the accuracy of interfacial tension measurement from pendant drop profiles. *Langmuir*, 11, 4159-4166.

Lin, S. Y., Wang, W. J., Lin, L. W., Chen, L. J., 1996. Systematic effects of bubble volume on the surface tension measured by pendant bubble profiles. *Colloids and Surfaces A: Physicochemical and Engineering Aspects*, 114, 31-39.

Lindman, B., Wennerström, H., 1980. Micelles: Amphiphile Aggregation in Aqueous Solution, In *Micelles (Topic in Current Chemistry)*. Berlin: Springer-Verlag.

Lu, J. R., Purcell, I. P., Lee, E. M., Simister, E. A., Thomas, R. K., Rennie, A. R., Penfold, J., 1995. The composition and structure of sodium dodecyl sulfate-dodecanol mixtures adsorbed at the air-water interface: a neutron reflection study. *Journal of Colloid and Interface Science*, 174, 441-455.

Lucassen, J., Van Den Tempel, M., 1972a. Dynamic measurements of dilatational properties of a liquid interface. *Chemical Engineering Science*, 27, 1283-1291.

Lucassen, J., Van Den Tempel, M., 1972b. Longitudinal waves on visco-elastic surfaces. *Journal of Colloid and Interface Science*, 41, 491-498.

Lucassen-Reynders, E. H., 1981. *Anionic Surfactants - Physical Chemistry of Surfactant Action*. New York: Marcel Dekker.

Lunkenheimer, K., Czichocki, G., Hirte, R., Barzyk, W., 1995. Novel results on the adsorption of ionic surfactants at the air/water interface — sodium-n-alkyl sulphates. *Colloids and Surfaces A: Physicochemical and Engineering Aspects*, 101, 187-197.

Lunkenheimer, K., Wienskol, G., Prosser, J., 2004. Automated high-performance purification of surfactant solutions: study of convective-enhanced adsorption. *Langmuir*, 20, 5738-5744.

MacPherson, P. D., Srolovitz, D. J., 2007. The von Neumann relation generalised to coarsening of three-dimensional microstructures. *Nature*, 446, 1053-1055.

Makievski, A. V., Fainerman, V. B., Miller, R., Bree, M., Liggieri, L., Ravera, F., 1997. Determination of equilibrium surface tension values by extrapolation via long time approximations. *Colloids and Surfaces A: Physicochemical and Engineering Aspects*, 122, 269-273.

Malysa, K., Lunkenheimer, K., 2008. Foams under dynamic conditions. *Current Opinion in Colloid and Interface Science*, 13, 150-162.

Manev, E. D., Nguyen, A. V., 2005. Critical thickness of microscopic thin liquid films. *Advances in Colloid and Interface Science*, 114-115, 133-146.

Manga, M. S., Hunter, T. N., Cayre, O. J., York, D. W., Reichert, M. D., Anna, S. L., Walker, L. M., Williams, R. A., Biggs, S. R., 2016. Measurements of submicron particle adsorption and particle film elasticity at oil-water interfaces. *Langmuir*, 32, 4125-4133.

Mann, H. B., Whitney, D. R., 1947. On a test of whether one of two random variables is stochastically larger than the other. *Annals of Mathematical Statistics*, 18, 50-60.

Mcbain, J. W., 1913. Colloids and Their Viscosity: Discussion. *Transactions of the Faraday Society*, 9, 99-101.

Meinders, M. B. J., van Vliet, T., 2004. The role of interfacial rheological properties on Ostwald ripening in emulsions. *Advances in Colloid and Interface Science*, 108, 119-126.

Mendoza, A. J., Guzmán, E., Martínez-Pedrero, F., Ritacco, H., Rubio, R. G., Ortega, F., Starov, V. M., Miller, R., 2014. Particle laden fluid interfaces: dynamics and interfacial rheology. *Advances in Colloid and Interface Science*, 206, 303-319.

Miller, R., Liggieri, L. (editors), 2009. *Interfacial Rheology*. Progress in Colloid and Interface Science. Brill: Leiden.

Miller, R., Ferri, J. K., Javadi, A., Krägel, J., Mucic, N., Wüstneck, R., 2010. Rheology of interfacial layers. *Colloid and Polymer Science*, 288, 937-950.

Monroy, F., Kahn, J. G., Langevin, D., 1998. Dilatational viscoelasticity of surfactant monolayers. *Colloids and Surfaces A: Physicochemical and Engineering Aspects*, 143, 251-260.

Morita, A. T., Carastan, D. J., Demarquette, N. R., 2002. Influence of drop volume on surface tension evaluated using the pendant drop method. *Colloid Polymer Science*, 280, 857-864.

Mulqueen, M., Blankschtein, D., 1999. Prediction of equilibrium surface tension and surface adsorption of aqueous surfactant mixtures containing ionic surfactants. *Langmuir*, 15, 8832-8848.

Mysels, K. J., 1986. Surface tension of solutions of pure sodium dodecyl sulfate. *Langmuir*, 2, 423-428.

Nelder, J., Mead, R., 1965. A simplex method for function minimization. *The Computer Journal*, 7, 308-313.

Nguyen, A. V., Pugh, R. J., Jameson, G. J., 2006. Collection and attachment of particles by air bubbles in froth flotation. In Binks, B. P., Horozov, T. S.

(editors). *Colloidal Particles at Liquid Interfaces*. New York: Cambridge University Press.

Noskov, B. A., 2002. Kinetics of adsorption from micellar solutions. *Advances in Colloid and Interface Science*, 95, 237-293.

Noskov, B. A., Akentiev, A. V., Bilibin, A. Y., Zorin, I. M., Miller, R., 2003. Dilatational surface viscoelasticity of polymer solutions. *Advances in Colloid and Interface Science*, 104, 245-271.

Nuzzo, R., 2014. Scientific method: statistical errors. *Nature*, 506, 150-152.

Paria, S., Khilar, K. C., 2004. A review on experimental studies of surfactant adsorption at the hydrophilic solid-water interface. *Advances in Colloid and Interface Science*, 110, 75-95.

Pernell, C. W., Foegeding, E. A., Luck, P. J., Davis, J. P., 2002. Properties of whey and egg white protein foams. *Colloids and Surfaces A: Physicochemical and Engineering Aspects*, 204, 9-21.

Phongikaroon, S., Hoffmaster, R., Judd, K. P., Smith, G. B., Handler, R. A., 2005. Effect of temperature on the surface tension of soluble and insoluble surfactants of hydrodynamical importance. *Journal of Chemical and Engineering Data*, 50, 1602-1607.

Pitois, O., 2012. Foam ripening. In Stevenson, P. (editor). *Foam engineering: fundamentals and applications*. Chichester: John Wiley & Sons, 59-73.

Plateau, J. A. F., 1873. *Experimental and theoretical statics of liquids subject to molecular forces only*. Paris: Gauthier-Villars.

Porter, M. R., 1994. *Handbook of Surfactants*. Glasgow: Blackie Academic and Professional.

Preston, W. C., 1948. Some Correlating Principles of Detergent Action. *Journal of Physical Colloid Chemistry*, 52, 84-97.

- Ravera, F., Loglio, G., Kovalchuk, V. I., 2010. Interfacial dilatational rheology by oscillating bubble/drop methods. *Current Opinion in Colloid and Interface Science*, 15, 217-228.
- Razali, N., Wah, Y. B., 2011. Power comparisons of Shapiro-Wilk, Kolmogorov-Smirnov, Lilliefors and Anderson-Darling tests. *Journal of Statistical Modelling and Analytics*, 2, 21-33.
- Rio, E., Drenckhan, W., Salonen, A., Langevin, D., 2014. Unusually stable liquid foams. *Advances in Colloid and Interface Science*, 205, 74-86.
- Ritacco, H., Langevin, D., Diamant, H., Andelman, D., 2011. Dynamic surface tension of aqueous solutions of ionic surfactants: Role of electrostatics. *Langmuir*, 27, 1009-1014.
- Rosen, M. J., Kunjappu J. P., 2012. *Surfactants and Interfacial Phenomena*. New Jersey: John Wiley & Sons.
- Ross, J., Miles, G., 1941. An apparatus for comparison of foaming properties of soaps and detergents. *Journal of the American Oil Chemists' Society*, 18, 99-102.
- Rotenberg, Y., Boruvka, L., Neumann, A. W., 1983. Determination of surface tension and contact angle from the shapes of axisymmetric fluid interfaces. *Journal of Colloid and Interface Science*, 93, 169-183.
- Ruxton, G. D., 2006. The unequal variance t-test is an underused alternative to Student's t-test and the Mann-Whitney U test. *Behavioural Ecology*, 17, 688-690.
- Saad, S. M. I., Policova, Z., Neumann, A. W., 2011. Design and accuracy of pendant drop methods for surface tension measurement. *Colloids and Surfaces A: Physicochemical and Engineering Aspects*, 384, 442-452.
- Saad, S. M. I., Neumann, A. W., 2016. Axisymmetric drop shape analysis (ADSA): an outline. *Advances in Colloid and Interface Science*, 238, 62-87.

Safouane, M., Langevin, D., Binks, B. P., 2007. Effect of particle hydrophobicity on the properties of silica particle layers at the air-water interface. *Langmuir*, 23, 11546-11553.

Saint-Jalmes, A., Langevin, D., 2002. Time evolution of aqueous foams: drainage and coarsening. *Journal of Physics: Condensed Matter*, 14, 9397-9412.

Saint-Jalmes, A., 2006. Physical chemistry in foam drainage and coarsening. *Soft Matter*, 2, 836-849.

Santini, E., Ravera, F., Ferrari, M., Stubenrauch, C., Makievski, A., Kragel, J., 2007. A surface rheological study of non-ionic surfactants at the water-air interface and the stability of the corresponding thin foam films. *Colloids and Surfaces A: Physicochemical and Engineering Aspects*, 298, 12-21.

Schramm, L. L., 2005. *Emulsions, Foams, and Suspensions*. Weinheim: WILEY-VCH Verlag GmbH & Co. KGaA.

Schramm, L. L., Isaacs, E. E., 2012. Foams in enhancing petroleum recovery. In Stevenson, P. (editor). *Foam engineering: fundamentals and applications*. Chichester: John Wiley & Sons, 283-305.

Shapiro, S. S., Wilk, M. B., 1965. An analysis of variance test for normality (complete samples). *Biometrika*, 52, 591-611.

Shaw, D. J., 1991. *Introduction to Colloid and Surface Science*. Oxford: Butterworth-Heinemann.

Shrestha, L. K., Matsumoto, Y., Ihara, K., Aramaki, K., 2008. Dynamic surface tension and surface dilatational elasticity properties of mixed surfactant/protein systems. *Journal of Oleo Science*, 57, 485-494.

Singh, R., Mohanty, K. K., 2015. Synergy between nanoparticles and surfactants in stabilising foams for oil recovery. *Energy Fuels*, 29, 467-479.

- Smith, S. M., Brady, J. M., 1997. SUSAN: a new approach to low level image processing. *International Journal of Computer Vision*, 23, 45-78.
- Somasundaran, P., Fuerstenau, D. W., 1966. Mechanisms of alkyl sulfonate adsorption at the alumina-water interface. *Journal of Physical Chemistry*, 70, 90-96.
- Somasundaran, P., Huang, L., 2000. Adsorption/aggregation of surfactants and their mixtures at solid-liquid interfaces. *Advances in Colloid and Interface Science*, 88, 179-208.
- Soria-Sanchez, M., Maroto-Valiente, A., Guerrero-Ruiz, A., Nevskaja, D. M., 2010. Adsorption of non-ionic surfactants on hydrophobic and hydrophilic carbon surfaces, 343, 194-199.
- Stevenson, P., 2005. Remarks on the shear viscosity of surface stabilised with soluble surfactants. *Journal of Colloid and Interface Science*, 290, 603-606.
- Stevenson, P., 2006. Dimensional analysis of foam drainage. *Chemical Engineering Science*, 61, 4503-4510.
- Stevenson, P., 2007. On the forced drainage of foam. *Colloids and Surfaces A: Physicochemical and Engineering Aspects*, 305, 1-9.
- Stevenson, P., 2010. Inter-bubble gas diffusion in liquid foam. *Current Opinion in Colloid and Interface Science*, 15, 374-381.
- Stevenson, P., Li, X., 2010. A viscous-inertial model of foam drainage. *Chemical Engineering Research and Design*, 88, 928-935.
- Stevenson, P., Li, X., 2014. *Foam Fractionation Principles and Process Design*. Boca Raton: CRC Press.
- Stocco, A., Drenckhan, W., Rio, E., Langevin, D., Binks, B. P., 2009. Particle-stabilised foams: an interfacial study. *Soft Matter*, 5, 2215-2222.

Stocco, A., Rio, E., Binks, B. P., Langevin, D., 2011. Aqueous foams stabilised solely by particles. *Soft Matter*, 7, 1260-1267.

Stubenrauch, C., Miller, R., 2004. Stability of foam films and surface rheology: an oscillating bubble study at low frequencies. *Journal of Physical Chemistry B*, 108, 6412-6421.

U. S. Department of Energy, 2019. Enhanced Oil Recovery [online]. U. S. Department of Energy. [Viewed 30 July 2019]. Available from: <https://www.energy.gov/fe/science-innovation/oil-gas-research/enhanced-oil-recovery>

Tadros, T. F., 2005. *Applied Surfactants*. Weinheim: WILEY-VCH Verlag GmbH & Co. KGaA.

Tambe, D. E., Sharma, M. M., 1994. The effect of colloidal particles on fluid-fluid interfacial properties and emulsion stability. *Advances in Colloid and Interface Science*, 52, 1-65.

Thomson, W., 1887. On the division of space with minimum partitional area. *Philosophical Magazine letters*, 24, 503-514.

Vandewalle, N., Lentz, J. F., Dorbolo, S., Brisbois, F., 2001. Avalanche of draining foams. *Physical Review Letters*, 86, 179-182.

Varga, I., Meszaros, R., Gilanyi, T., 2007. Adsorption of sodium alkyl sulfate homologues at the air/solution interface. *Journal of Chemistry B*, 111, 7160-7168.

Verbist, G., Weaire, D., 1994. A soluble model for foam drainage. *Europhysics Letters*, 26, 631-634.

Verwey, E. J. W., Overbeek, J. Th. G., 1948. *Theory of the Stability of Lyophobic Colloids*. New York: Elsevier.

Viljoen, C., van der Merwe, L., 2000. *Applied Elementary Statistics*. South Africa: Pearson Education.

Vlahovska, P. M., Danov, K. D., Mehreteab, A., Broze, G., 1997. Adsorption kinetics of ionic surfactants with detailed account for the electrostatic interactions. *Journal of Colloid and Interface Science*, 192, 194-206.

Vollhardt, D., 1982. Studies of structure and molecular interactions in amphiphilic monolayers at the air/water interface. Berlin: Academic of Science.

Vollhardt, D., Czichocki, G., 1984. Influence of small quantities of isomeric alcohols on the surface tension behaviour of aqueous sodium alkyl sulfate solutions. *Colloids and Surfaces*, 11, 209-217.

Vollhardt, D., Czichocki, G., 1990. Effect of isomeric alcohols as a minor component on the adsorption properties of aqueous sodium alkyl sulfate solutions. *Langmuir*, 6, 317-322.

Vollhardt, D., Emrich, G., 2000. Co-adsorption of sodium dodecyl sulfate and medium-chain alcohols at the air-water interface. *Colloids and Surfaces A: Physicochemical and Engineering Aspects*, 161, 173-182.

von Neumann, 1952. Discussion: shape of metal grains. In Herring, C. (editor). *Metal Interfaces*. Cleveland: American Society for Metals, 108-110.

Wagner, C., 1961. Theorie der Alterung von Niederschlägen durch Umlösen (Ostwald-Reifung). *Zeitschrift für Elektrochemie*, 65, 581-591.

Wang, H., Gong, Y., Lu, W., Chen, B., 2008. Influence of nano-SiO₂ on dilatational viscoelasticity of liquid/air interface of cetyltrimethyl ammonium bromide. *Applied Surface Science*, 254, 3380-3384.

Wang, J., Nguyen, A. V., Farrokhpay, S., 2016. Effects of surface rheology and surface potential on foam stability. *Colloids and Surfaces A: Physicochemical and Engineering Aspects*, 488, 70-81.

- Wang, H., Guo, W., Zheng, C., Wang, D., Zhan, H., 2017. Effect of temperature on foaming ability and foam stability of typical surfactants used for foaming agent. *Journal of Surfactants and Detergents*, 20, 615-622.
- Wantke, K. D., Fruhner, H., Fang, J., Lunkenheimer, K., 1998. Measurements of the surface elasticity in medium frequency range using the oscillating bubble method. *Journal of Colloid and Interface Science*, 208, 34-48.
- Wantke, K. D., Fruhner, H., 2001. Determination of surface dilatational viscosity using the oscillating bubble method. *Journal of Colloid and Interface Science*, 237, 185-199.
- Wantke, K. D., Fruhner, H., Örtengren, J., 2003. Surface dilatational properties of mixed sodium dodecyl sulfate/dodecanol solutions. *Colloids and Surfaces A: Physicochemical and Engineering Aspects*, 221, 185-195.
- Ward, A. F. H., Tordai, L., 1946. Time-dependence of boundary tensions of solutions I. The role of diffusion in time-effects. *Journal of Chemical Physics*, 14, 453-461.
- Ward, R. N., Davies, P. B., Bain, C. D., 1997. Co-adsorption of sodium dodecyl sulfate and dodecanol at a hydrophobic surface. *Journal of Physical Chemistry*, 101, 1594-1601.
- Weaire, D., Phelan R., 1994. A counterexample to Kelvin's conjecture on minimal surfaces. *Philosophical Magazine Letters*, 69, 107-110.
- Weaire, D., Hutzler, S., 1999. *The Physics of Foams*. Oxford: Clarendon Press.
- Weaire, D., Tobin, S. T., Meagher, A. J., Hutzler, S., 2012. Foam morphology. In Stevenson, P. (editor). *Foam engineering: fundamentals and applications*. Chichester: John Wiley & Sons, 7-26.
- Wenzel, R. N., 1936. Resistance of solid surfaces to wetting by water. *Industrial and Engineering Chemistry*, 28, 988-994.

Winsor, P. A., 1968. Binary and multicomponent solutions of amphiphilic compounds. Solubilisation and the formation, structure, and theoretical significance of liquid crystalline solutions. *Chemical Reviews*, 68, 1-40.

Zhang, R., Somasundaran, P., 2006. Advances in adsorption of surfactants and their mixtures at solid/solution interfaces. *Advances in Colloid and Interface Science*, 123-126, 213-229.

Zholob, S. A., Makievski, A. V., Miller, R., Fainerman, V. B., 2007. Optimisation of calculation methods for determination of surface tensions by drop profile analysis tensiometry. *Advances in Colloid and Interface Science*, 134-135, 322-329.

Zhu, Y., Jiang, J., Cui, Z., Binks, B. P., 2014. Responsive aqueous foams stabilised by silica nanoparticles hydrophobised in situ with a switchable surfactant. *Soft Matter*, 10, 9739-9745.

Zhu, Y., Pei, X., Jiang, J., Cui, Z., Binks, B. P., 2015. Responsive aqueous foams stabilised by silica nanoparticles hydrophobised in situ with a conventional surfactant. *Langmuir*, 31, 12937-12943.

Zuo, Y. Y., Ding, M., Bateni, A., Hoorfar, M., Neumann, A. W., 2004. Improvement of interfacial tension measurement using a captive bubble in conjunction with Axisymmetric Drop Shape Analysis (ADSA). *Colloids and Surfaces A: Physicochemical and Engineering Aspects*, 250, 233-246.

Appendices

Appendix A Influence of Noise upon Results Obtained by Droplet Shape Analyser

It is supposed herein that potentially poor signal-to-noise ratios could have a detrimental impact upon results obtained by the oscillating pendant droplet method, and therefore the method of noise elimination should be further studied before performing measurements of surface rheological properties. The noise caused herein is mainly due to the environmental vibration interference. In order to reduce the droplet vibration induced by the environmental vibration interference, the droplet shape analyser is mounted on a layer of polyfoam of depth 50 mm.

The oscillating pendant droplet method is applied to measure dynamic surface tension for effectiveness evaluation of the environmental vibration reduction of the polyfoam. The measurements are performed by imposing a low frequency and amplitude sinusoidal variation on the air-liquid surface area. The dynamic surface tension of an oscillating droplet of SDS solution at the concentration of 0.087 g/L is measured over time. The frequency of oscillation is 0.5 Hz and the relative amplitude of the disturbance is 0.1. Note that the defined amplitude is related to the mean volume of the droplet and it is a dimensionless parameter. The oscillation of the droplet lasts for 20 seconds. In order to test the effectiveness of the polyfoam to reduce the environmental vibration, two sets of measurement are designed. In one set of measurements,

the experiment is performed with the droplet shape analyser placed on a standard laboratory bench directly; in the other, the same experiment is repeated with the apparatus mounted on the polyfoam. The dynamic surface tension results obtained from the oscillating pendant droplet method with and without the polyfoam is shown in Figure A-1.

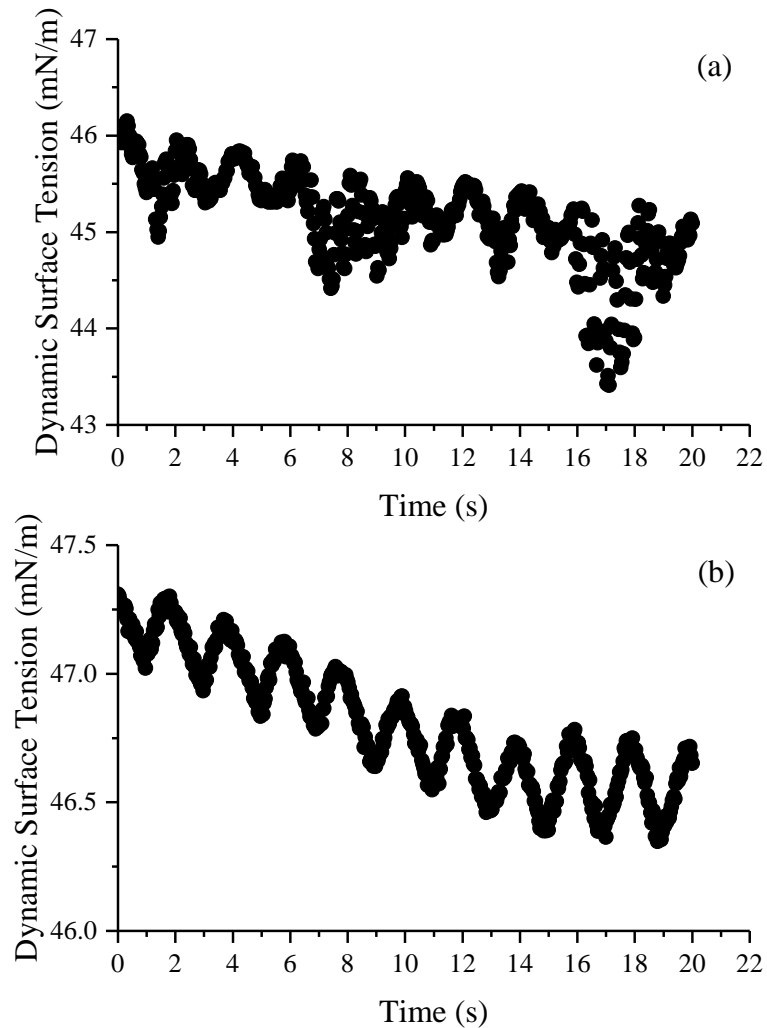


Figure A-1. The dynamic surface tension results obtained from the oscillating pendant droplet method with and without the polyfoam. (a) The dynamic surface tension measurement is performed without the polyfoam. (b) The dynamic surface tension measurement is performed with the polyfoam.

After comparison, it can be seen that the dynamic surface tension results measured without polyfoam show certain degree of noise, while the dynamic surface tension results obtained with polyfoam have less noise. This

demonstrates that the environmental vibration influences the accuracy of dynamic surface tension measurement and the polyfoam applied herein can reduce the environmental vibration effectively. A Fourier analysis of dynamic surface tension results has been performed to confirm the reduction of environmental vibration by employing the polyfoam. The comparison of Fourier analyses of dynamic surface tension results obtained with and without the polyfoam is shown in Figure A-2.

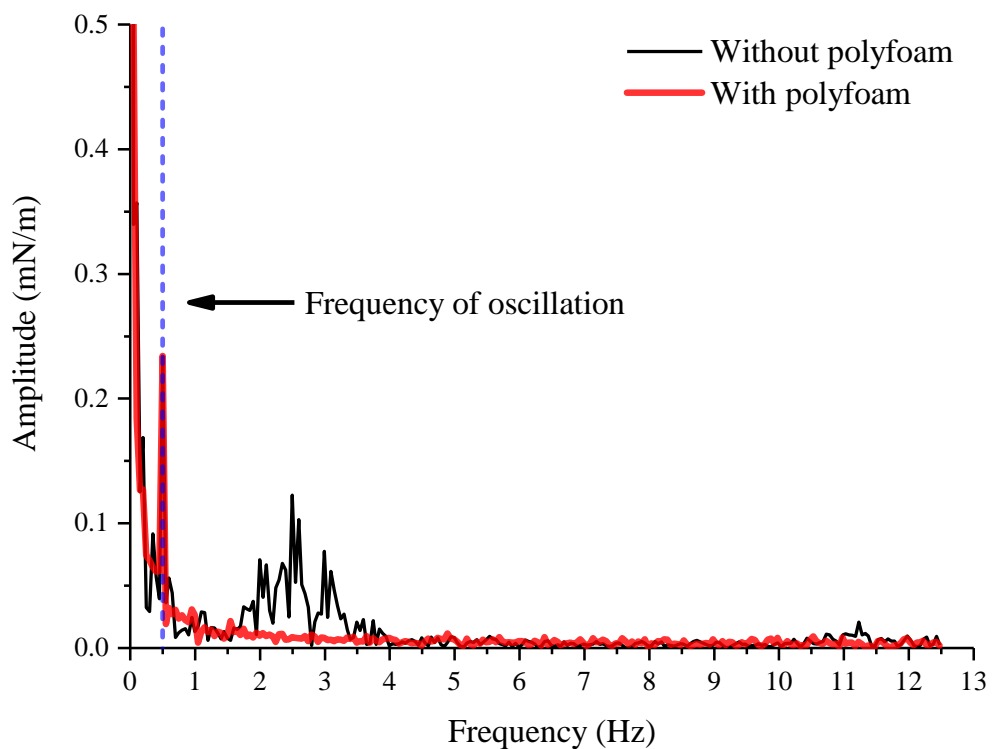


Figure A-2. Fourier analyses of dynamic surface tension results obtained with and without the polyfoam

As can be seen, the dash line indicates the oscillation frequency of the droplet imposed by the apparatus, which is 0.5 Hz. For the dynamic surface tension measurement without the polyfoam, obvious noise exists except for the oscillation frequency, which varies from 1.5 Hz to 3.5 Hz, whereas for the dynamic surface tension measurement with the polyfoam, the noise has been reduced and almost only the oscillation frequency exists. It is believed that

applying polyfoam can filter environmental vibration effectively and the polyfoam should be applied under the apparatus as a routine to increase the accuracy of dynamic surface tension measurement. It is noted that an even better reduction of noise could probably be achieved if the equipment were to be mounted upon an optical bench.

Appendix B Original Results and Inferred Parameters of Surface Rheological Properties Measurements in Chapter 2

The original experimental data for surface rheological properties obtained by the oscillating pendent droplet method in each independent measurement at different oscillation frequencies are shown in Table B-1. Elastic modulus (also known as surface elasticity or the real part of visco-elasticity), loss modulus (i.e. the imaginary part of visco-elasticity), modulus of visco-elasticity and surface dilatational viscosity can be measured directly. The parameters inferred from the original data to obtain Gibbs elasticity in each independent measurement at different oscillation frequencies are shown in Table B-2. The original results of relative amplitude of surface area disturbance and amplitude of surface tension variation in each trial at different oscillation frequencies are shown in Table B-3.

Table B-1. Original results of surface rheological properties in each trial at different oscillation frequencies

Frequency (Hz)	Trial	Elastic modulus (mN/m)	Loss modulus (mN/m)	Modulus of visco-elasticity (mN/m)	Surface dilatational viscosity (mN·s/m)
0.1	(1)	4.63	2.98	5.51	4.75
	(2)	4.50	3.02	5.42	4.80
	(3)	4.59	3.04	5.51	4.84
0.2	(1)	6.57	5.23	8.40	4.16
	(2)	6.08	4.01	7.28	3.19
	(3)	5.93	4.41	7.39	3.51
0.4	(1)	7.45	5.35	9.18	2.13
	(2)	7.75	5.49	9.50	2.19
	(3)	8.40	5.95	10.29	2.37
0.8	(1)	9.43	6.87	11.67	1.37
	(2)	10.17	6.94	12.31	1.38
	(3)	9.96	6.86	12.09	1.36
1.0	(1)	11.00	7.92	13.55	1.26
	(2)	9.82	7.72	12.49	1.23
	(3)	10.77	7.80	13.30	1.24

Table B-2. Parameters inferred from results given in Table B-1 to obtain Gibbs elasticity in each trial at different oscillation frequencies

Frequency (Hz)	Trial	$\sin(\varphi)$	$\cos(\varphi)$	$\tan(\varphi)$	ξ	Gibbs elasticity (mN/m)
0.1	(1)	0.54	0.84	0.64	1.81	18.41
	(2)	0.56	0.83	0.67	2.03	19.77
	(3)	0.55	0.83	0.66	1.96	19.54
0.2	(1)	0.62	0.78	0.79	3.87	52.30
	(2)	0.55	0.83	0.66	1.94	25.66
	(3)	0.60	0.80	0.74	2.91	36.00
0.4	(1)	0.58	0.81	0.72	2.55	40.04
	(2)	0.58	0.82	0.71	2.435	39.96
	(3)	0.58	0.82	0.71	2.42	43.10
0.8	(1)	0.59	0.81	0.73	2.68	53.13
	(2)	0.56	0.83	0.68	2.15	46.87
	(3)	0.57	0.82	0.69	2.21	47.12
1.0	(1)	0.58	0.81	0.72	2.58	59.72
	(2)	0.62	0.79	0.79	3.67	74.16
	(3)	0.59	0.81	0.72	2.63	59.57

Table B-3. Original results of relative amplitude of surface area disturbance and amplitude of surface tension variation in each trial at different oscillation frequencies

Frequency (Hz)	Trial	Relative amplitude of surface area disturbance (%)	Amplitude of surface tension variation (mN/m)
0.1	(1)	17.90	0.99
	(2)	18.45	1.00
	(3)	18.43	1.01
0.2	(1)	16.37	1.37
	(2)	16.81	1.22
	(3)	17.18	1.27
0.4	(1)	17.50	1.61
	(2)	15.78	1.50
	(3)	15.94	1.64
0.8	(1)	15.93	1.86
	(2)	15.54	1.91
	(3)	15.88	1.92
1.0	(1)	14.24	1.93
	(2)	16.66	2.08
	(3)	14.63	1.95

The original results of surface rheological properties obtained by the oscillating pendent droplet method in each independent measurement at different oscillation amplitudes are shown in Table B-4. The parameters inferred from the original data to obtain Gibbs elasticity in each independent measurement at different oscillation amplitudes are shown in Table B-5. The

original results of relative amplitude of surface area disturbance and amplitude of surface tension variation in each trial at different oscillation amplitudes are shown in Table B-6.

Table B-4. Original results of surface rheological properties in each trial at different oscillation amplitudes

Amplitude (-)	Trial	Elastic modulus (mN/m)	Loss modulus (mN/m)	Modulus of visco-elasticity (mN/m)	Surface dilatational viscosity (mN·s/m)
0.1	(1)	9.44	5.76	11.06	1.83
	(2)	9.04	6.97	11.42	2.22
	(3)	8.50	5.63	10.19	1.79
0.2	(1)	9.69	5.80	11.29	1.85
	(2)	8.92	6.02	10.76	1.91
	(3)	10.13	5.98	11.76	1.90
0.3	(1)	9.75	6.02	11.46	1.91
	(2)	10.48	6.56	12.36	2.09
	(3)	9.35	5.93	11.08	1.89
0.4	(1)	9.29	5.66	10.88	1.80
	(2)	9.70	6.10	11.46	1.94
	(3)	9.43	6.00	11.18	1.91
0.5	(1)	9.76	5.82	11.36	1.85
	(2)	9.32	5.89	11.03	1.87
	(3)	8.73	5.62	10.38	1.79

Table B-5. Parameters inferred from results given in Table B-4 to obtain Gibbs elasticity in each trial at different oscillation amplitudes

Amplitude (-)	Trial	$\sin(\varphi)$	$\cos(\varphi)$	$\tan(\varphi)$	ξ	Gibbs Elasticity (mN/m)
0.1	(1)	0.52	0.85	0.61	1.56	33.19
	(2)	0.61	0.79	0.77	3.37	62.99
	(3)	0.55	0.83	0.66	1.97	36.32
0.2	(1)	0.51	0.86	0.60	1.49	32.83
	(2)	0.56	0.83	0.68	2.08	39.97
	(3)	0.51	0.86	0.59	1.44	33.29
0.3	(1)	0.53	0.85	0.62	1.61	35.15
	(2)	0.53	0.85	0.63	1.67	39.00
	(3)	0.54	0.84	0.63	1.74	35.87
0.4	(1)	0.52	0.85	0.61	1.56	32.65
	(2)	0.53	0.85	0.63	1.69	36.49
	(3)	0.54	0.84	0.64	1.75	36.48
0.5	(1)	0.51	0.86	0.60	1.48	32.73
	(2)	0.53	0.85	0.63	1.72	35.41
	(3)	0.54	0.84	0.64	1.81	34.65

Table B-6. Original results of relative amplitude of surface area disturbance and amplitude of surface tension variation in each trial at different oscillation amplitudes

Amplitude (-)	Trial	Relative amplitude of surface area disturbance (%)	Amplitude of surface tension variation (mN/m)
0.1	(1)	1.25	0.14
	(2)	1.21	0.14
	(3)	1.46	0.15
0.2	(1)	3.55	0.40
	(2)	4.80	0.52
	(3)	4.20	0.49
0.3	(1)	9.73	1.12
	(2)	12.47	1.54
	(3)	10.95	1.21
0.4	(1)	29.39	3.20
	(2)	23.95	2.75
	(3)	25.66	2.87
0.5	(1)	36.63	4.16
	(2)	36.06	3.98
	(3)	35.69	3.70

Appendix C Detailed Results of Dynamic Surface Tension Measurement in Chapter 3

The detailed dynamic surface tension results of sodium tridecyl sulfate solution (1.301 g/L) from run 2 to run 10 are shown in Figure C-1 to C-9, respectively.

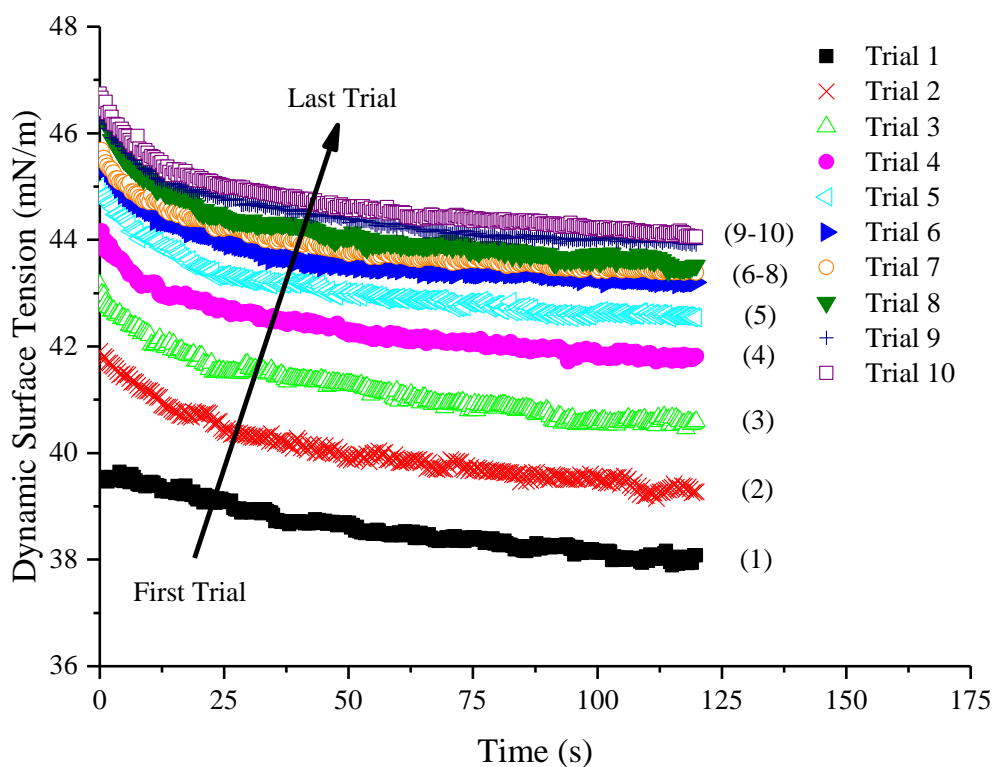


Figure C-1. Dynamic surface tension results of sodium tridecyl sulfate solution (1.301 g/L) of run 2. The number in bracket represents the sequential trial number.

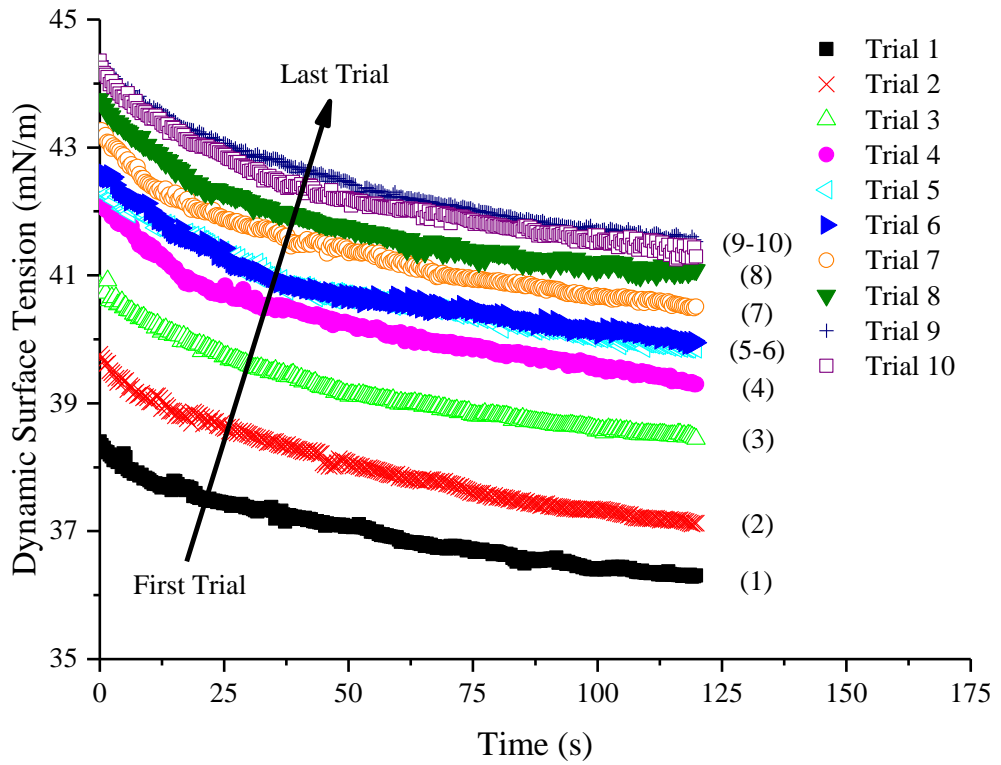


Figure C-2. Dynamic surface tension results of sodium tridecyl sulfate solution (1.301 g/L) of run 3. The number in bracket represents the sequential trial number.

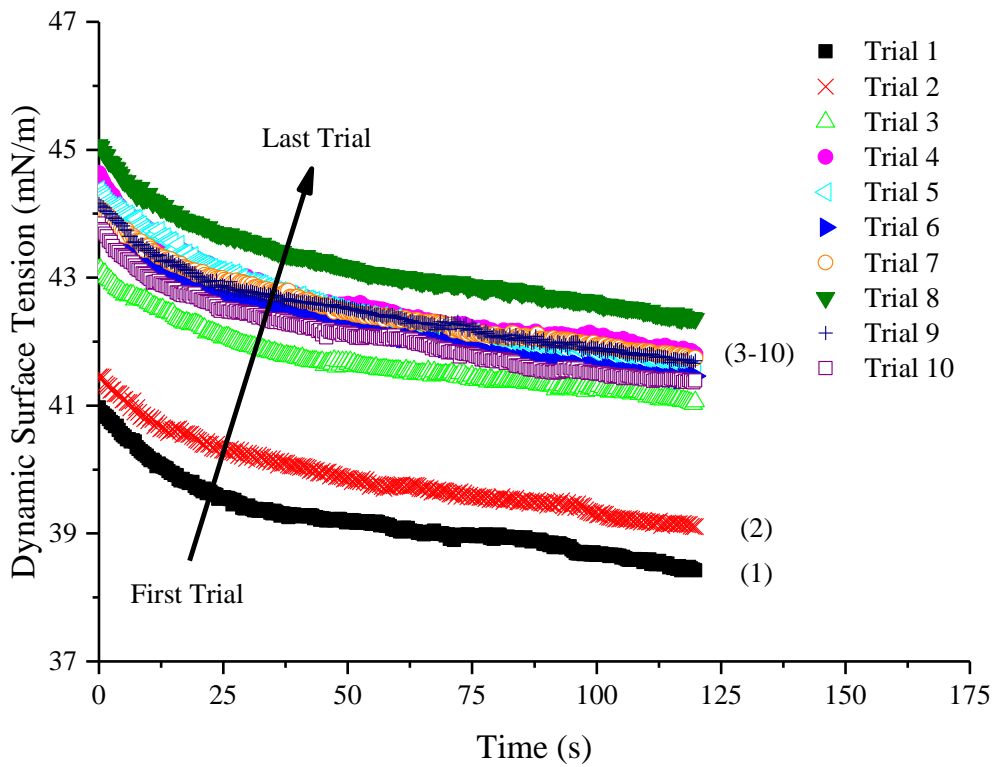


Figure C-3. Dynamic surface tension results of sodium tridecyl sulfate solution (1.301 g/L) of run 4. The number in bracket represents the sequential trial number.

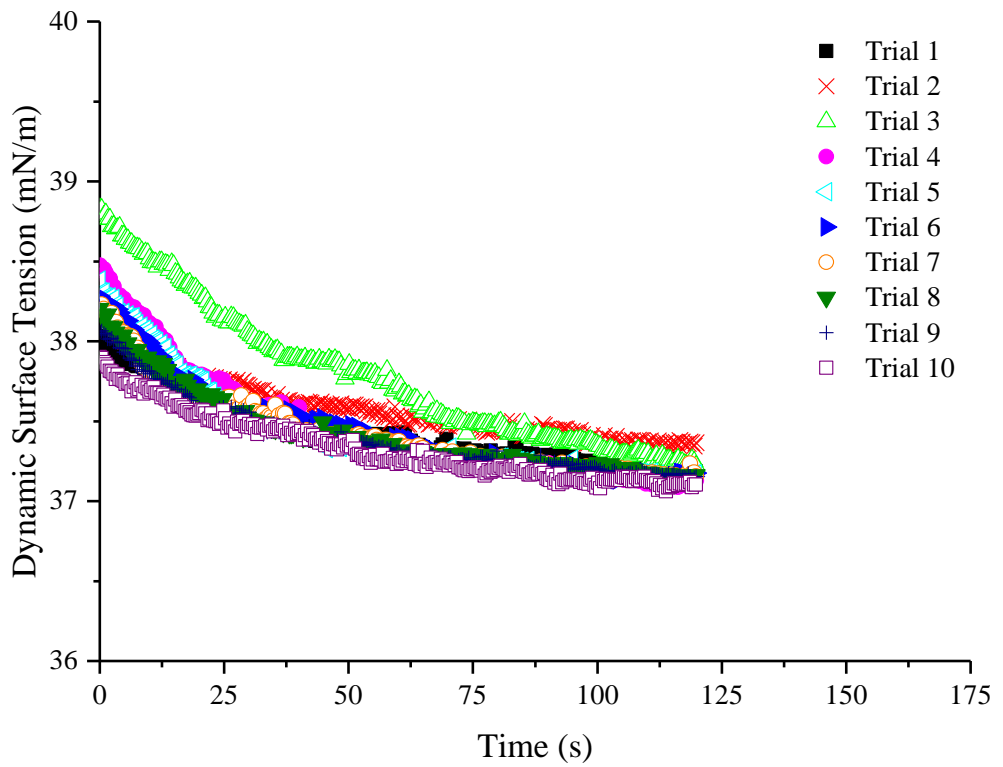


Figure C-4. Dynamic surface tension results of sodium tridecyl sulfate solution (1.301 g/L) of run 5.

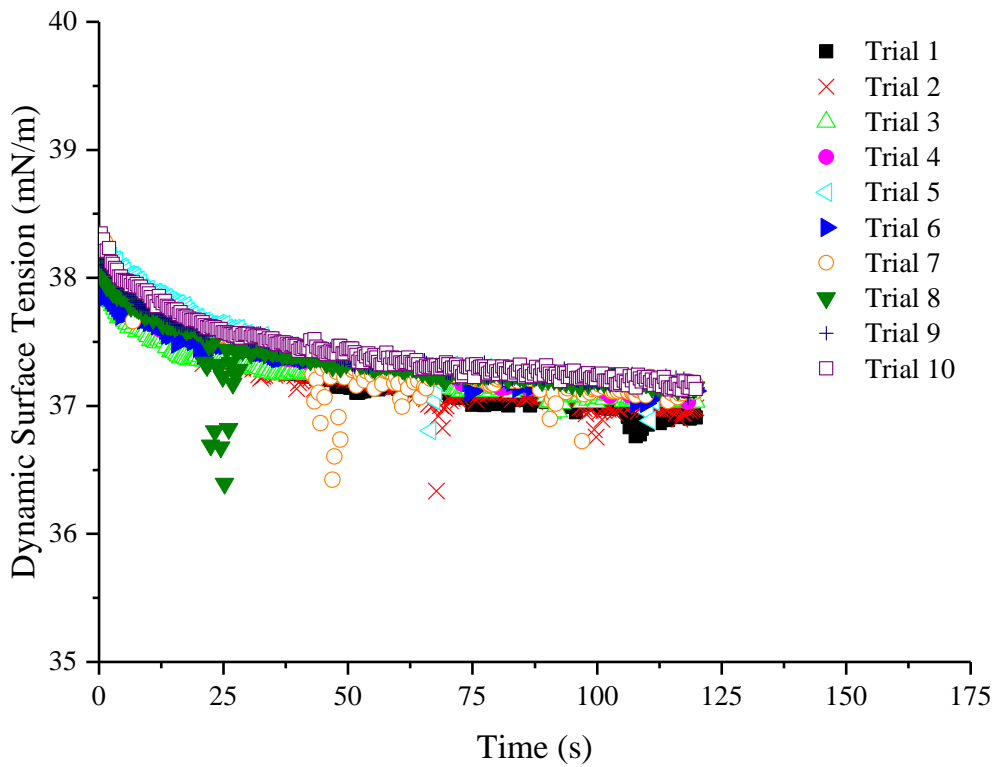


Figure C-5. Dynamic surface tension results of sodium tridecyl sulfate solution (1.301 g/L) of run 6.

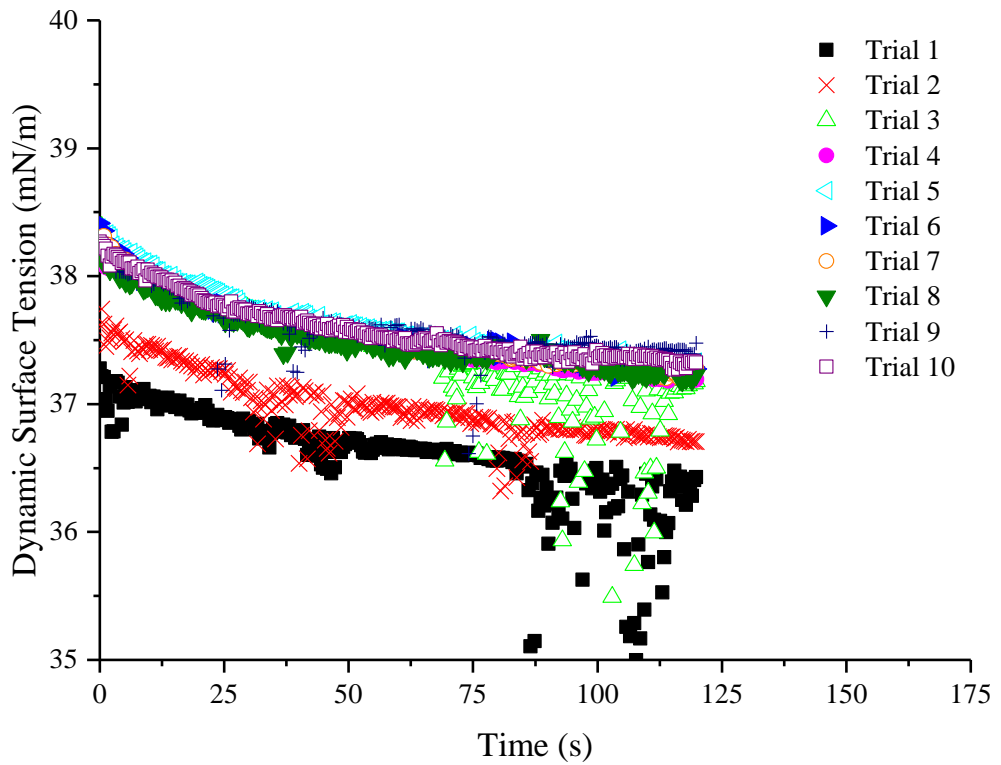


Figure C-6. Dynamic surface tension results of sodium tridecyl sulfate solution (1.301 g/L) of run 7.

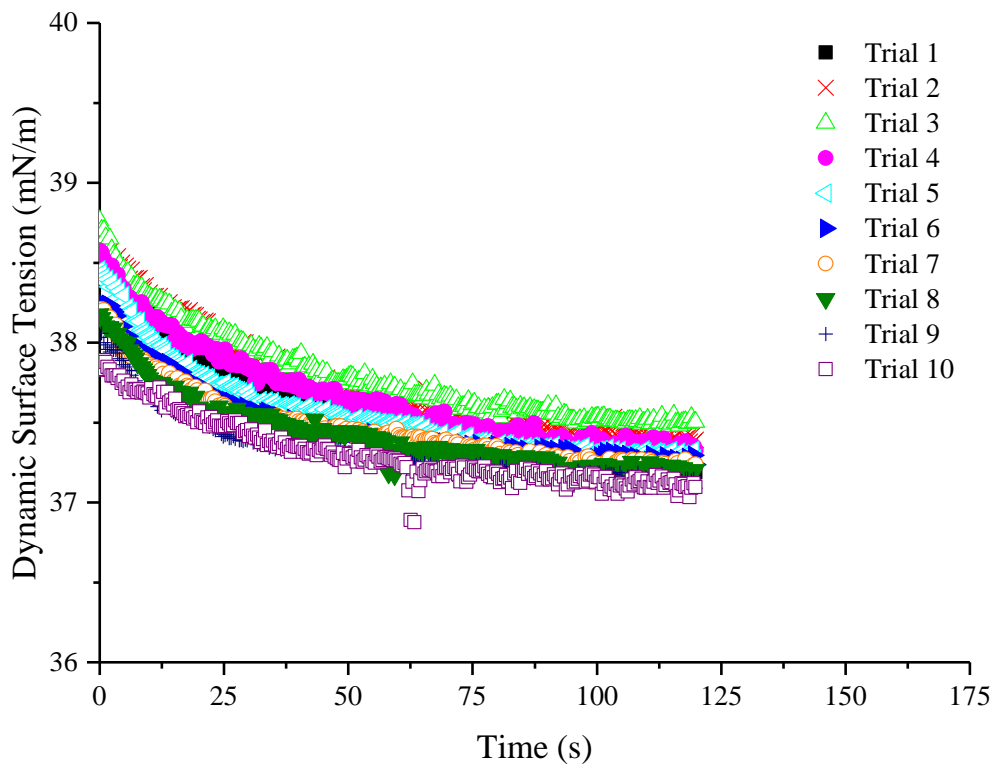


Figure C-7. Dynamic surface tension results of sodium tridecyl sulfate solution (1.301 g/L) of run 8.

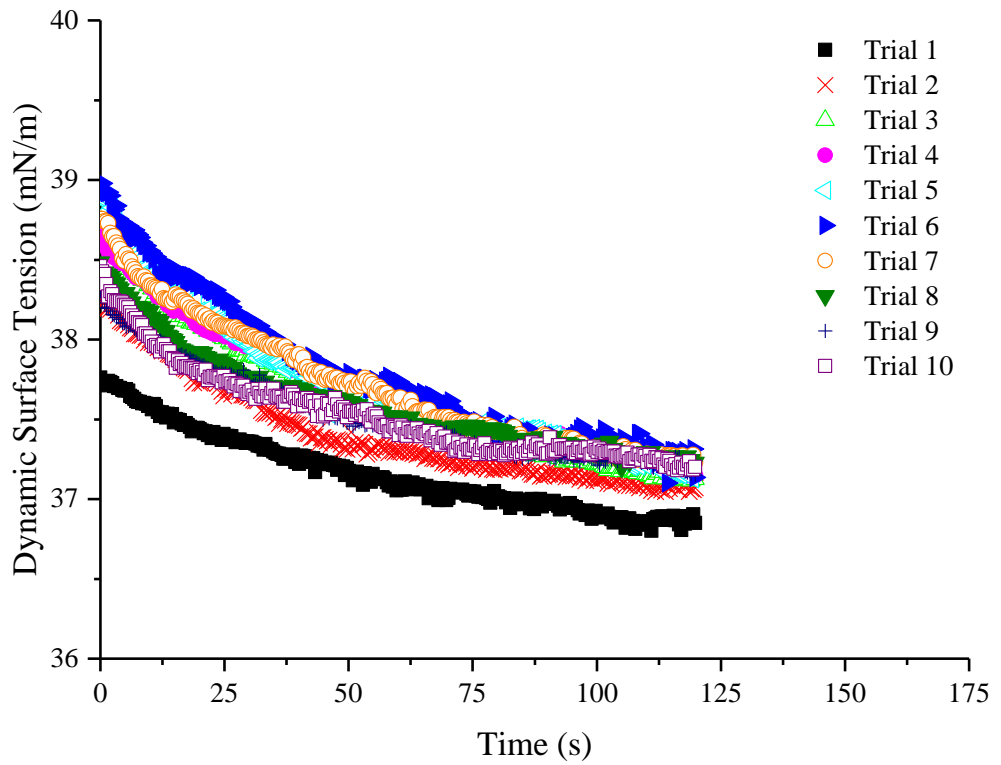


Figure C-8. Dynamic surface tension results of sodium tridecyl sulfate solution (1.301 g/L) of run 9.

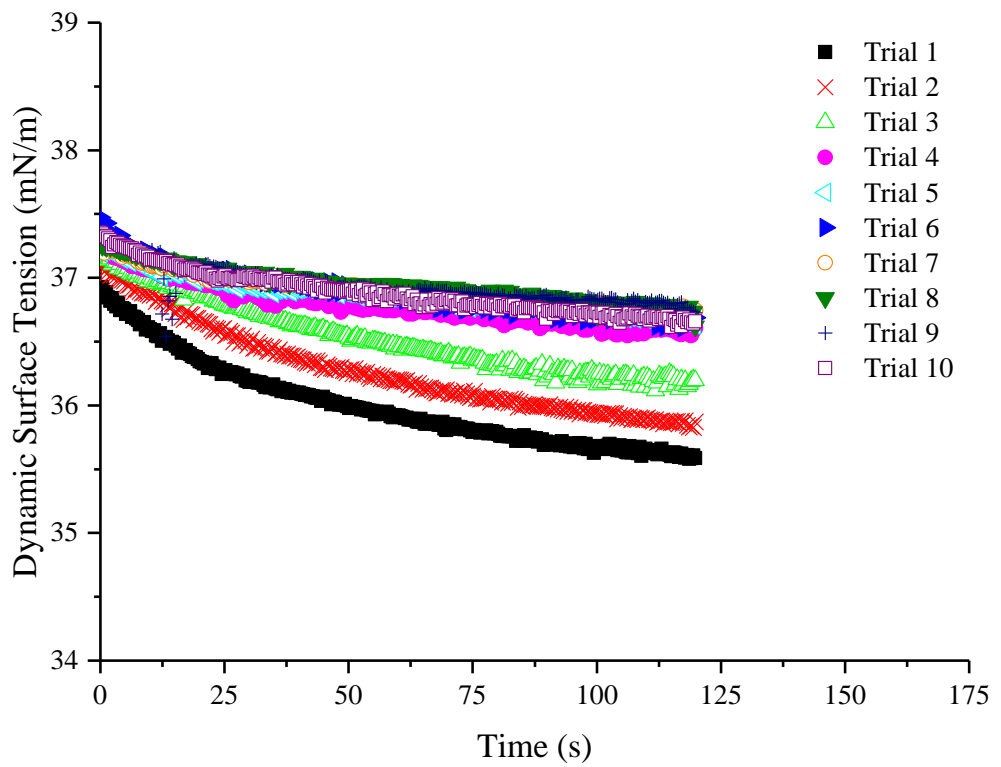


Figure C-9. Dynamic surface tension results of sodium tridecyl sulfate solution (1.301 g/L) of run 10.

The detailed dynamic surface tension results of SDS solution (0.288 g/L in 0.584 g/L NaCl) from run 2 to run 9 are shown in Figure C-10 to C-18, respectively.

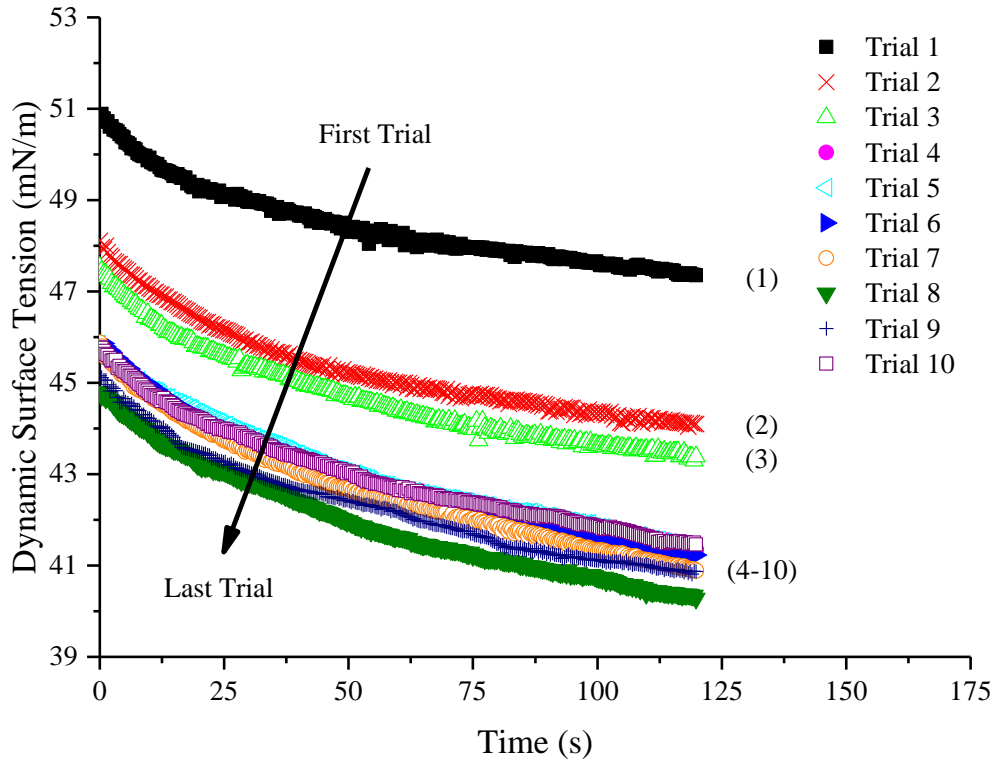


Figure C-10. Dynamic surface tension results of SDS solution (0.288 g/L in 0.584 g/L NaCl) of run 2. The number in bracket represents the sequential trial number.

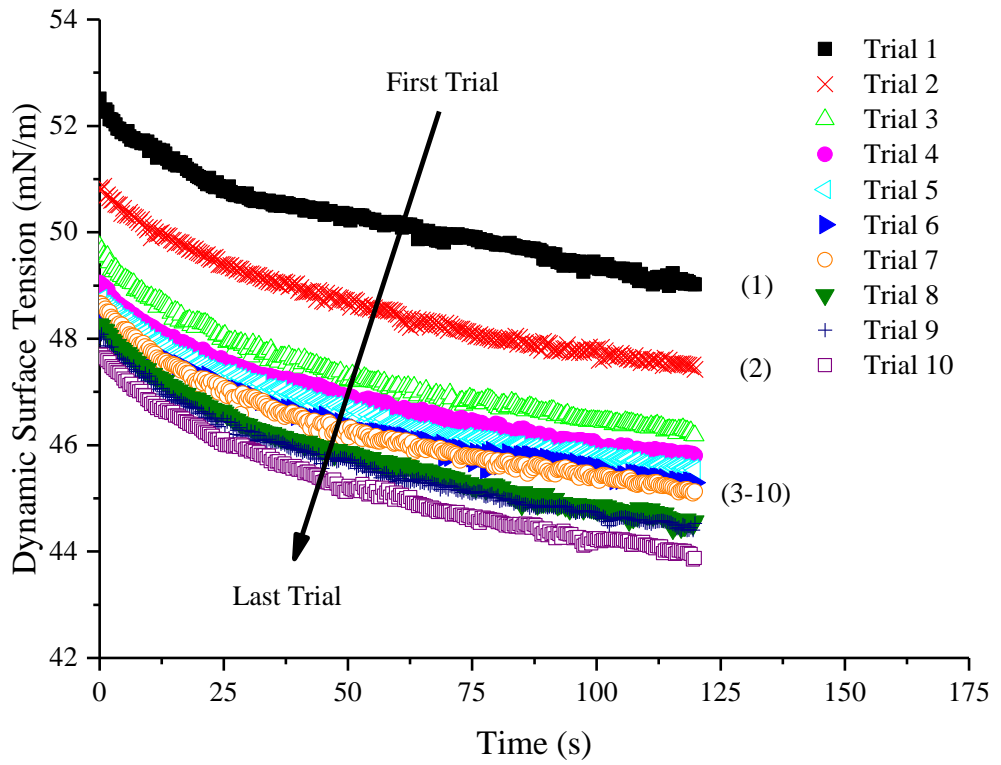


Figure C-11. Dynamic surface tension results of SDS solution (0.288 g/L in 0.584 g/L NaCl) of run 3. The number in bracket represents the sequential trial number.

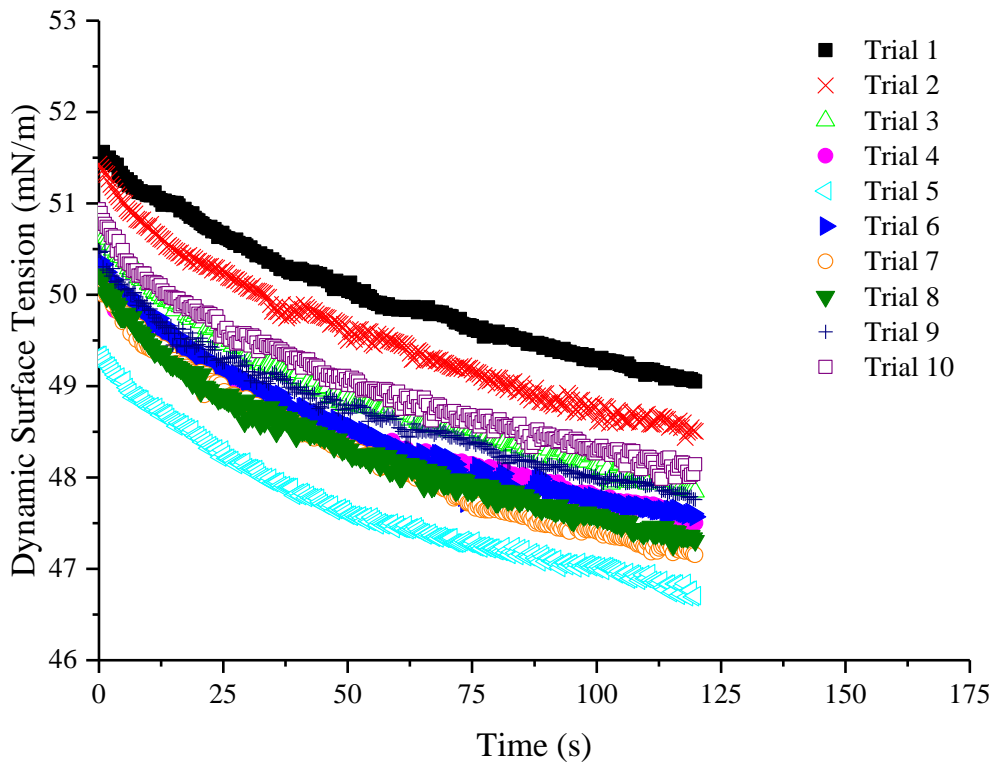


Figure C-12. Dynamic surface tension results of SDS solution (0.288 g/L in 0.584 g/L NaCl) of run 4.

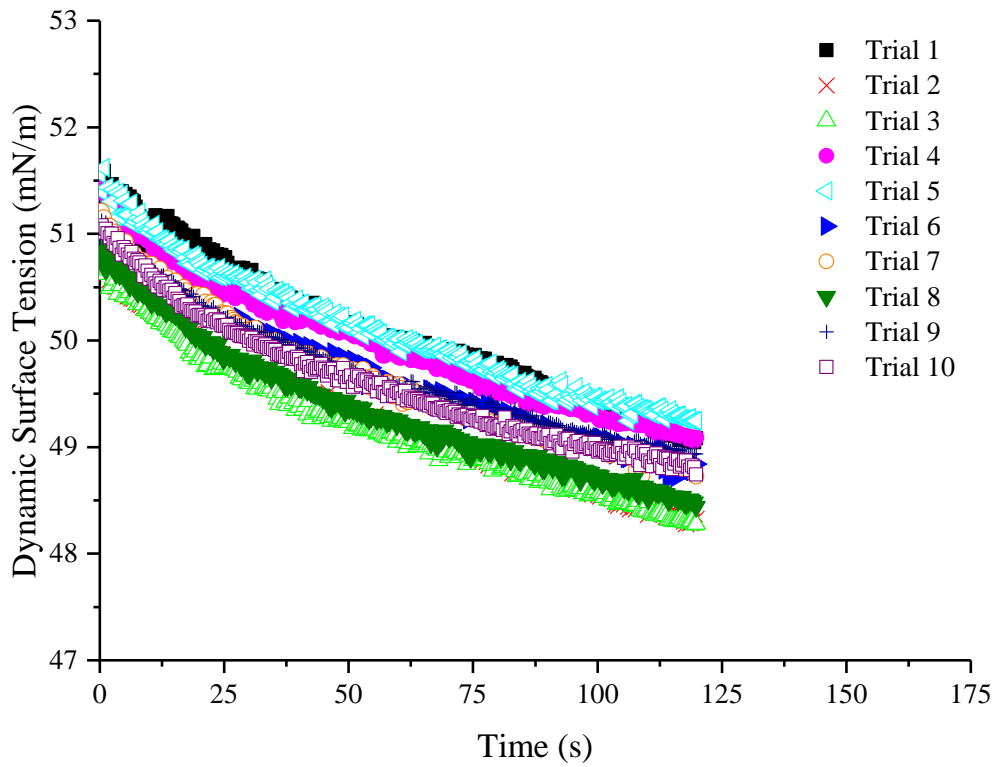


Figure C-13. Dynamic surface tension results of SDS solution (0.288 g/L in 0.584 g/L NaCl) of run 5.

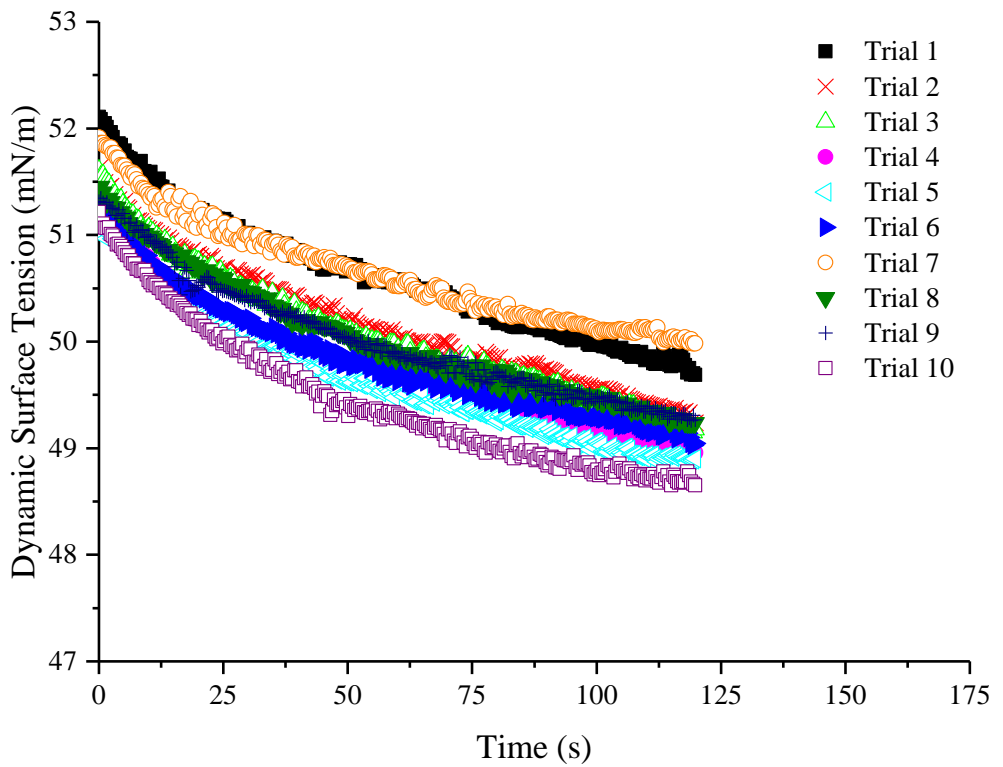


Figure C-14. Dynamic surface tension results of SDS solution (0.288 g/L in 0.584 g/L NaCl) of run 6.

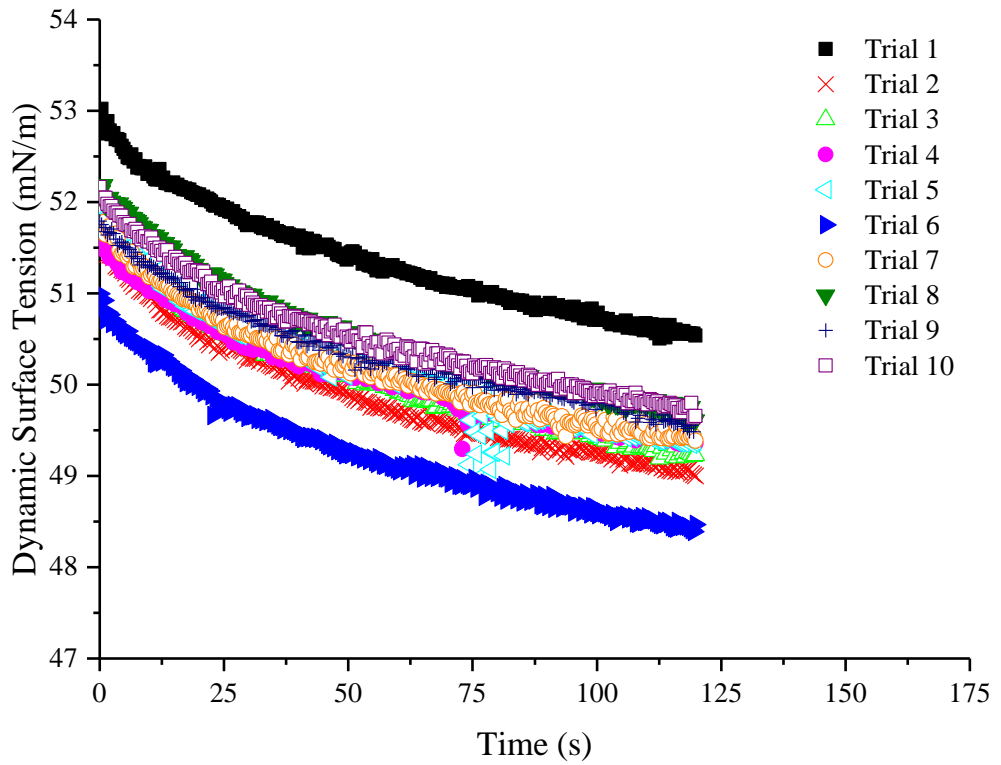


Figure C-15. Dynamic surface tension results of SDS solution (0.288 g/L in 0.584 g/L NaCl) of run 7.

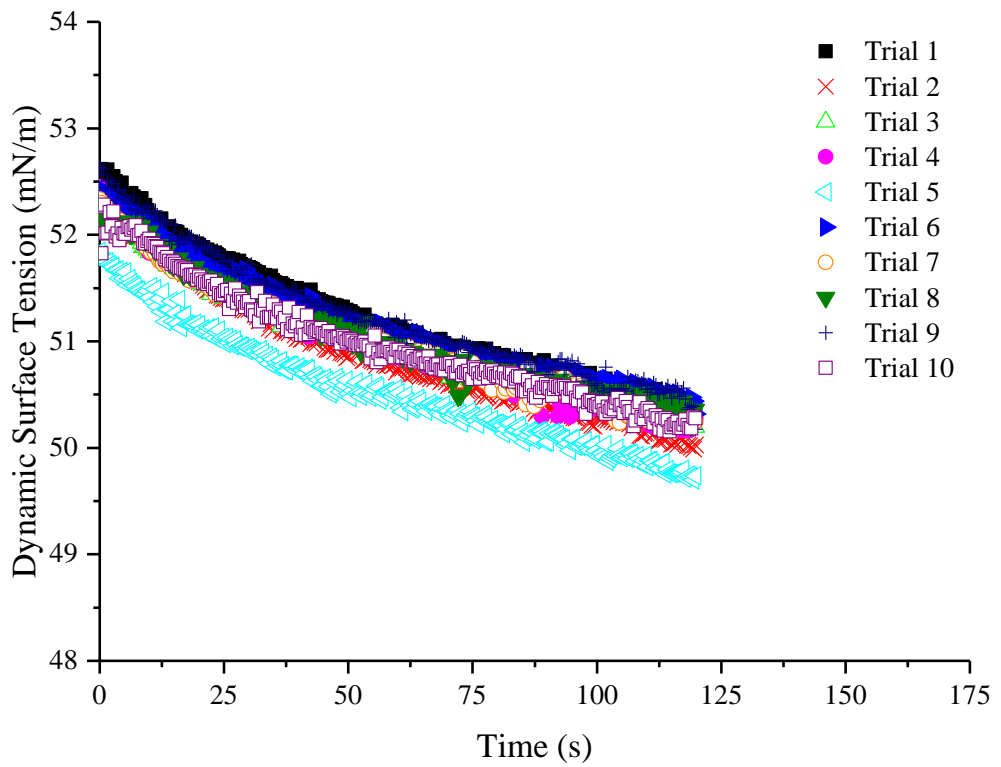


Figure C-16. Dynamic surface tension results of SDS solution (0.288 g/L in 0.584 g/L NaCl) of run 8.

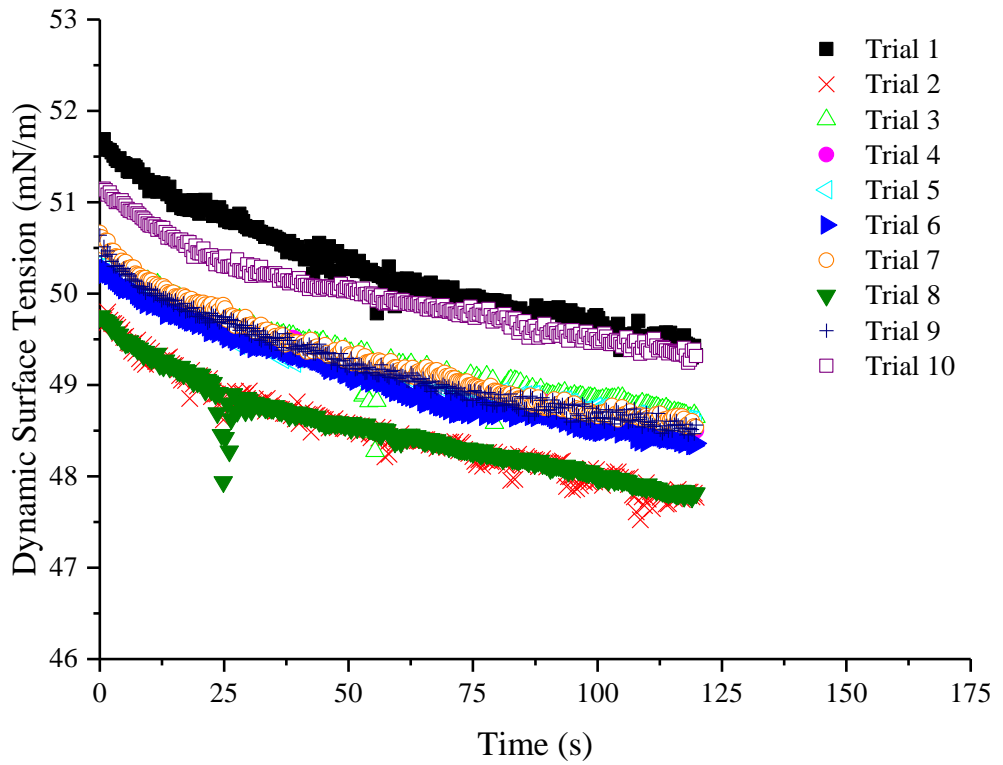


Figure C-17. Dynamic surface tension results of SDS solution (0.288 g/L in 0.584 g/L NaCl) of run 9.

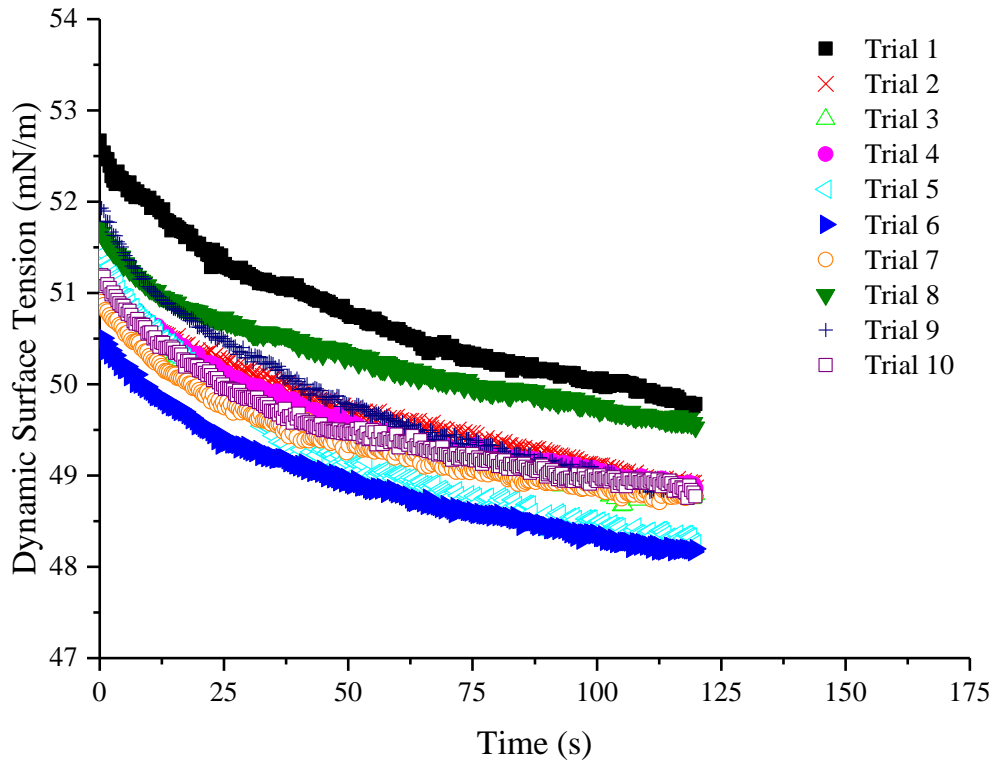


Figure C-18. Dynamic surface tension results of SDS solution (0.288 g/L in 0.584 g/L NaCl) of run 10.

The detailed dynamic surface tension results of DTAB solution (4.954 g/L) of all 10 runs are shown in Figure C-19 to C-28, respectively.

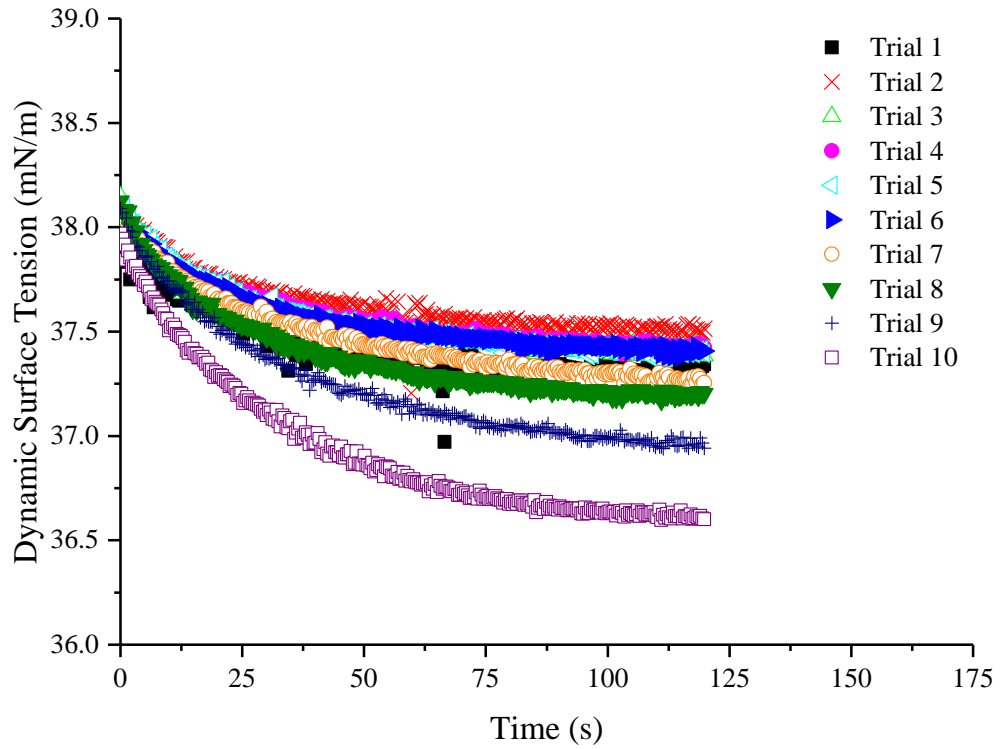


Figure C-19. Dynamic surface tension results of DTAB solution (4.954 g/L) of run 1.

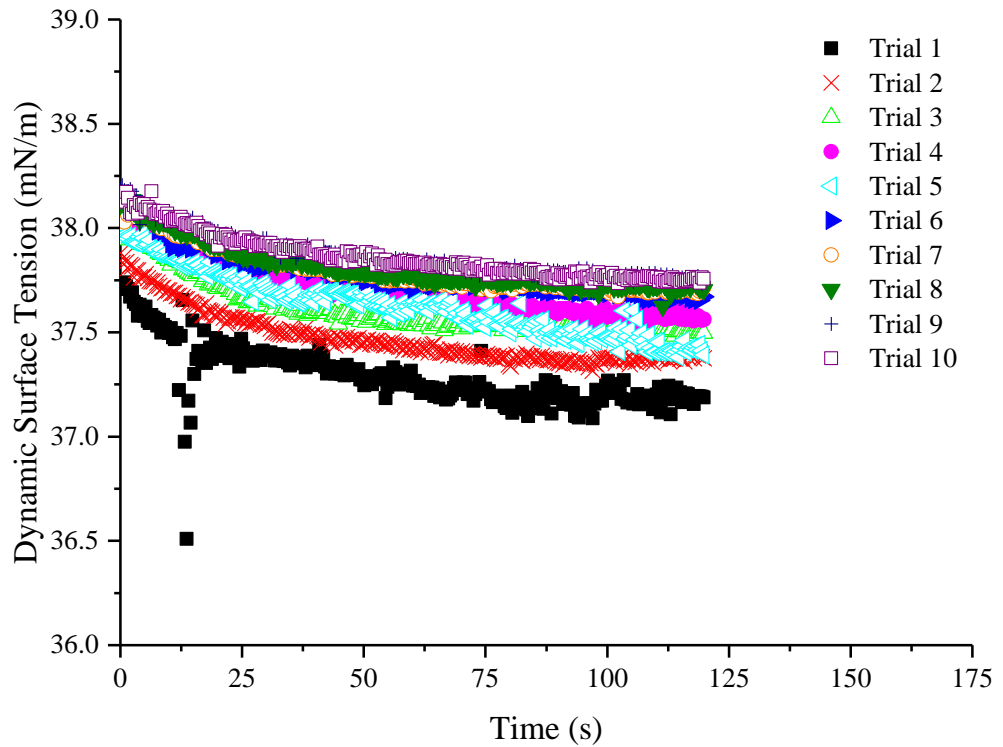


Figure C-20. Dynamic surface tension results of DTAB solution (4.954 g/L) of run 2.

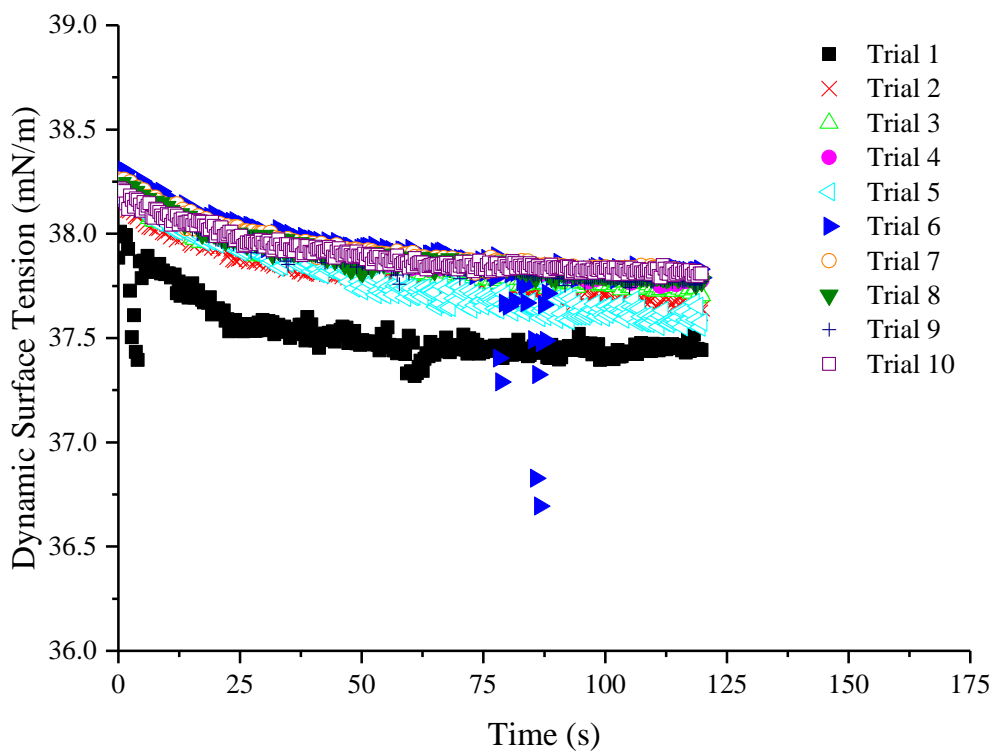


Figure C-21. Dynamic surface tension results of DTAB solution (4.954 g/L) of run 3.

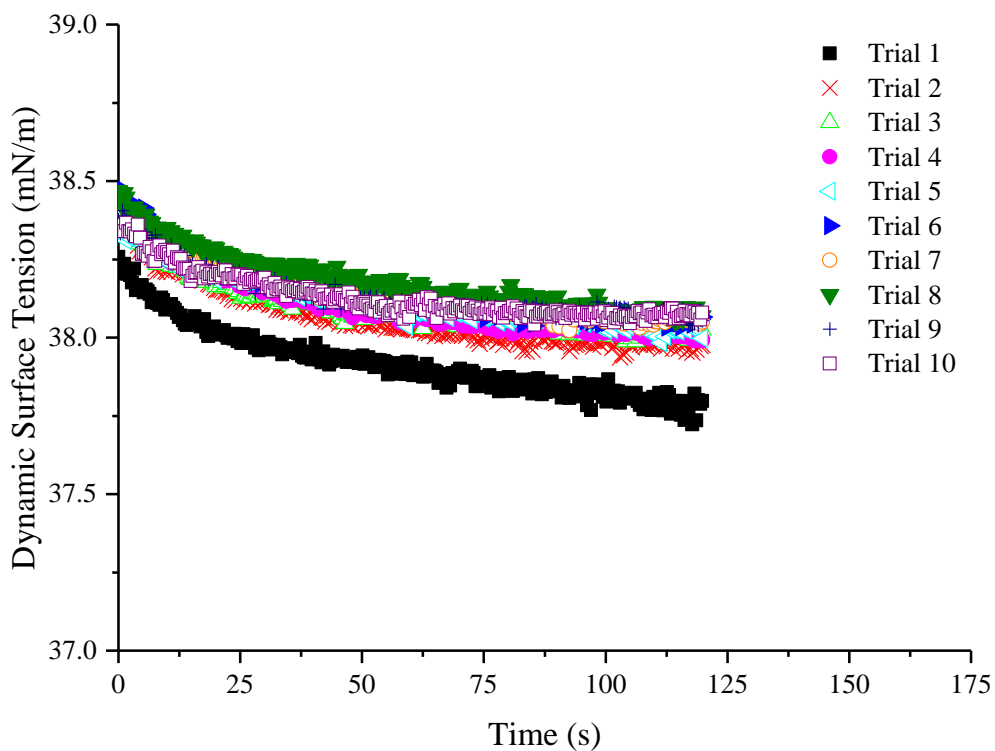


Figure C-22. Dynamic surface tension results of DTAB solution (4.954 g/L) of run 4.

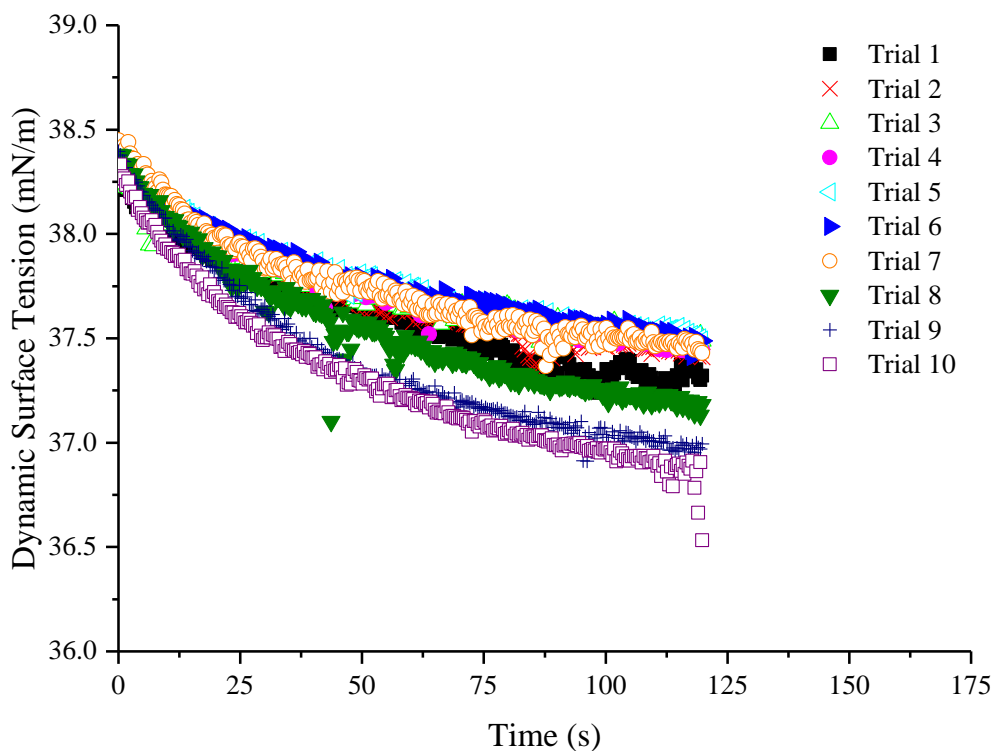


Figure C-23. Dynamic surface tension results of DTAB solution (4.954 g/L) of run 5.

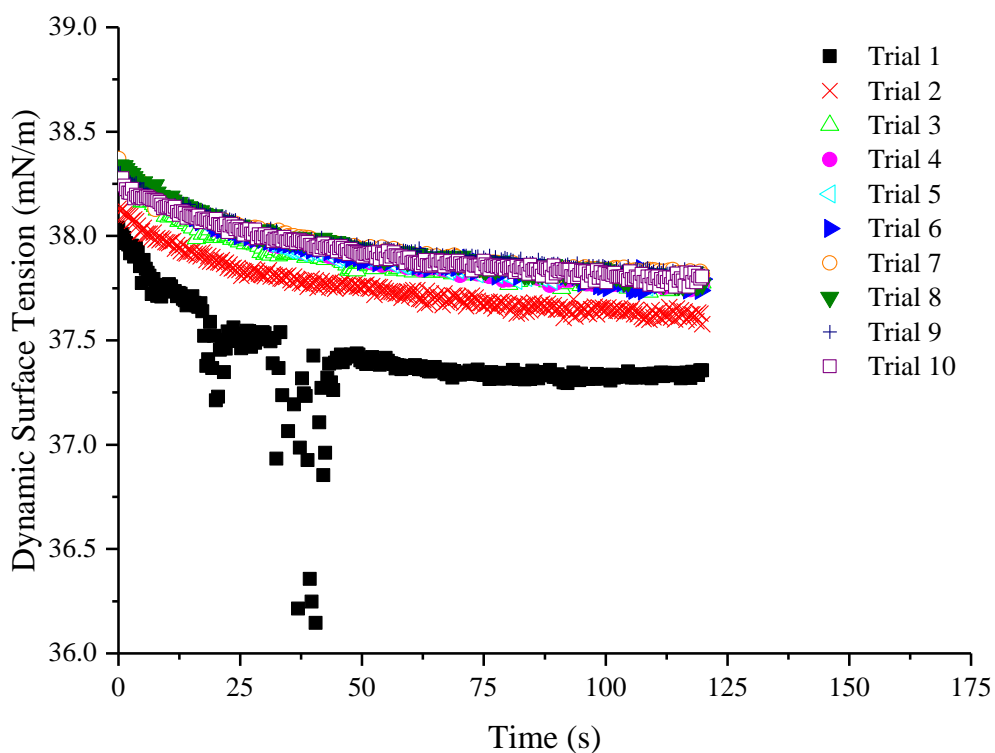


Figure C-24. Dynamic surface tension results of DTAB solution (4.954 g/L) of run 6.

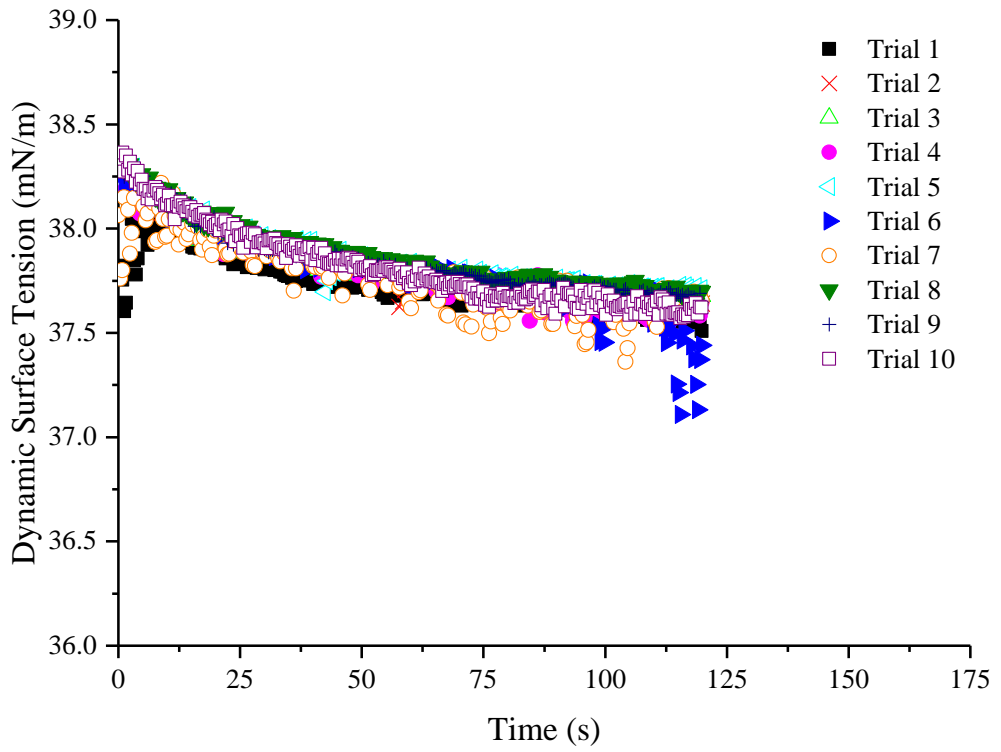


Figure C-25. Dynamic surface tension results of DTAB solution (4.954 g/L) of run 7.

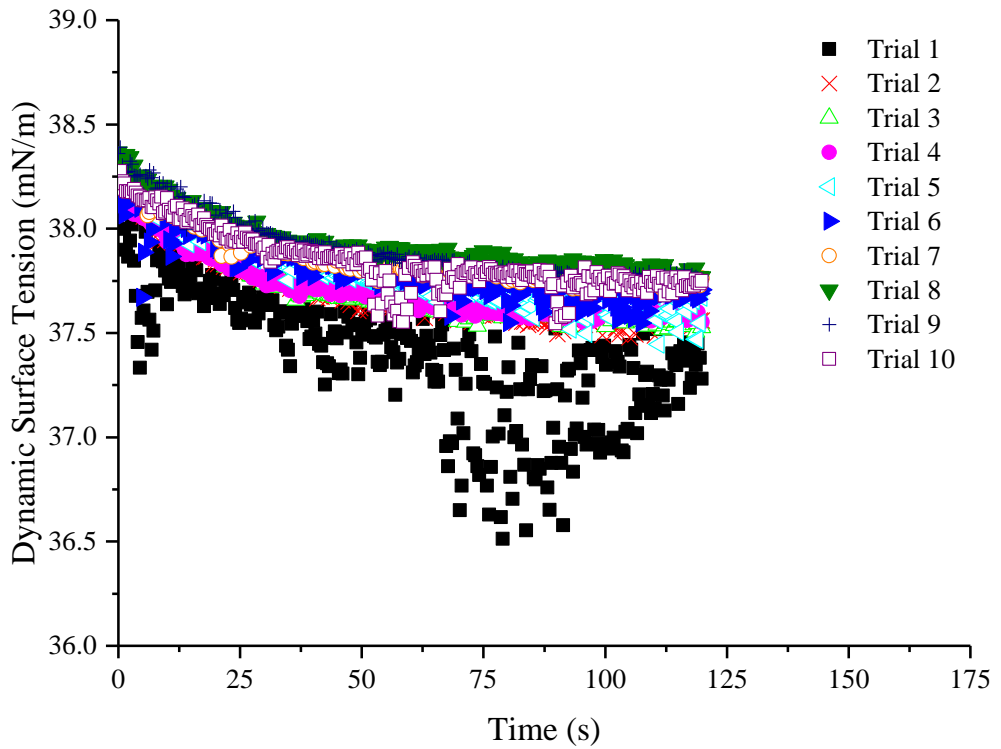


Figure C-26. Dynamic surface tension results of DTAB solution (4.954 g/L) of run 8.

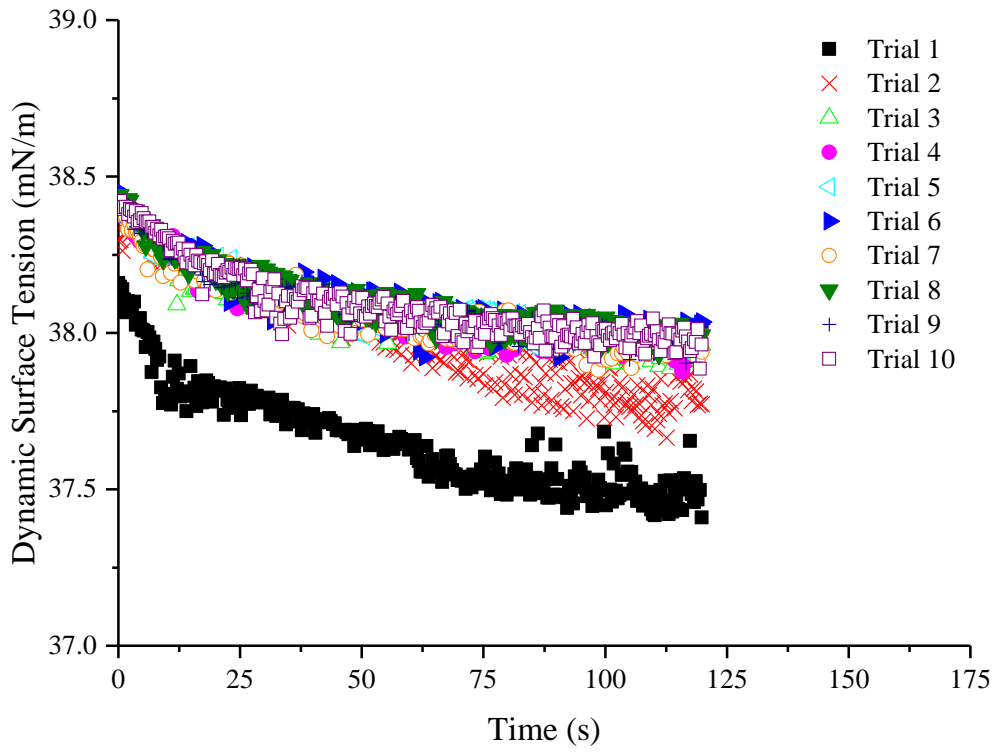


Figure C-27. Dynamic surface tension results of DTAB solution (4.954 g/L) of run 9.

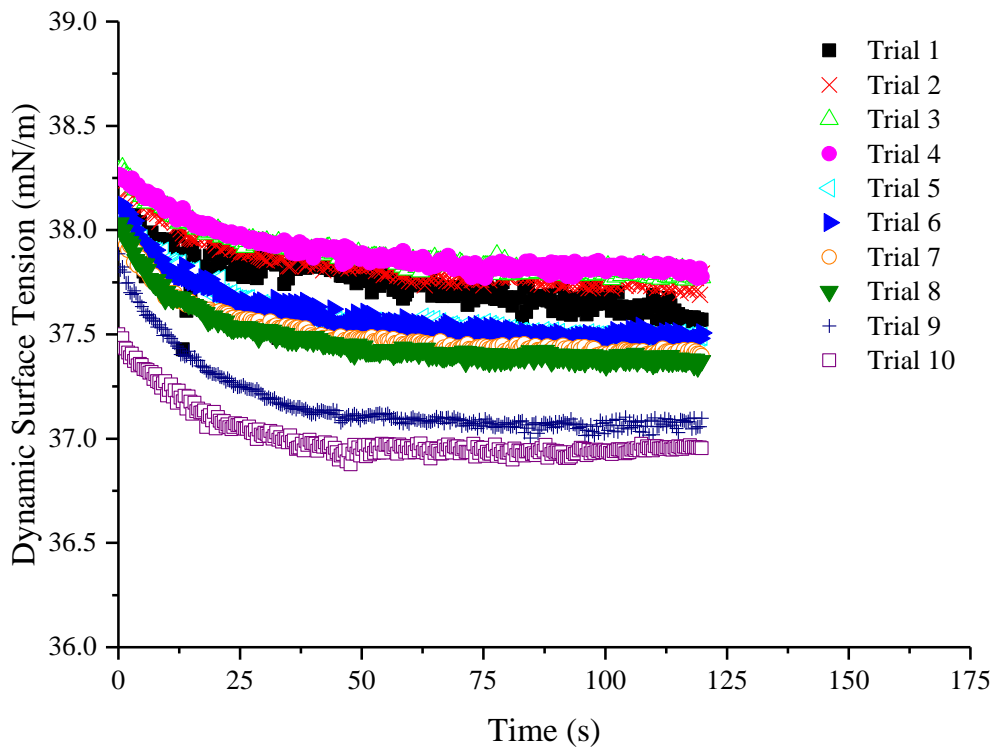


Figure C-28. Dynamic surface tension results of DTAB solution (4.954 g/L) of run 10.

Appendix D Effectiveness of Drying Agent to Dry Compressed Air

Prior to performing foam stability measurements, the effectiveness of the drying agent (which is self-indicating silica gel applied in the current work) is ascertained that whether there is effective drying of compressed air which is delivered from the top of the column as shown in Figure 4-2, since only mixing appreciable dry air with environmental air is capable of adjusting the relative humidity of the freeboard in a wide scope. The relative humidity of compressed air before and after going through the drying agent is measured.

The testing system is shown in Figure D-1. Compressed air is delivered into a Perspex column through two lines that one is going through the drying agent whereas another is not. The relative humidity in the Perspex column is measured and recorded every minute by a thermohygrometer (Rotronic, HC2-WIN-USB), which is directly linked with a computer. The flowrate of compressed air is kept at constant at 0.5 L/min. Firstly, all the valves in the system are closed, thus there is no compressed air delivered into the Perspex column and the relative humidity of environmental air in the Perspex column is measured for 30 minutes. Then, ball valves 1 & 2 and the pressure reducing valve are switched on and thus compressed air without going through the drying agent is delivered into the column. After the relative humidity in the column is stable, which means the column is fully filled with undried compressed air, the relative humidity of undried compressed air in the column is measured for 30 minutes as well. Finally, ball valve 2 is turned off and ball valves 3 & 4 are switched on, thus compressed air after going through the drying agent is delivered into the column. After the column is fully filled with

dried compressed air, the relative humidity of dried compressed air is also measured for 30 minutes. The arithmetic mean of the relative humidity observations in each 30-minute measurement is chosen to represent the relative humidity of that type of air.

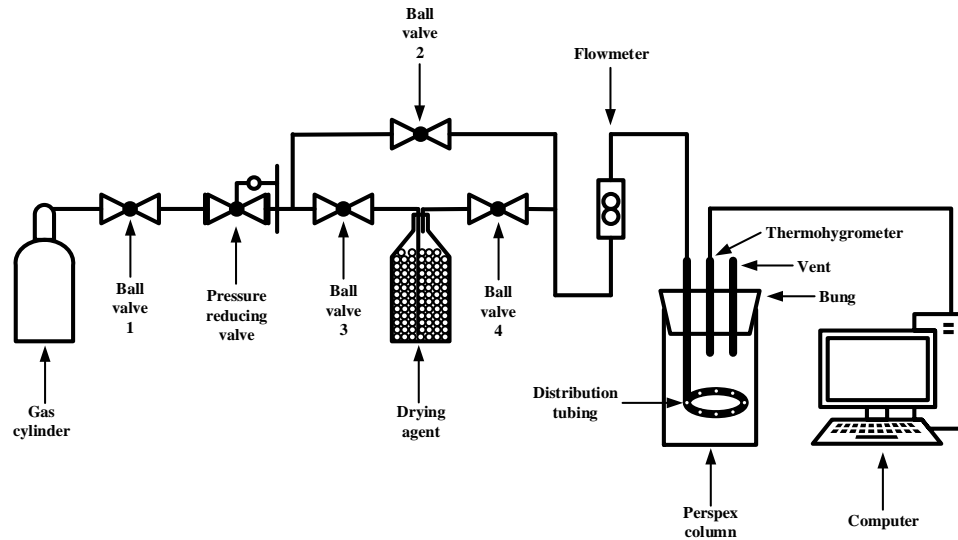


Figure D-1. Schematic diagram of the compressed air humidity measuring system

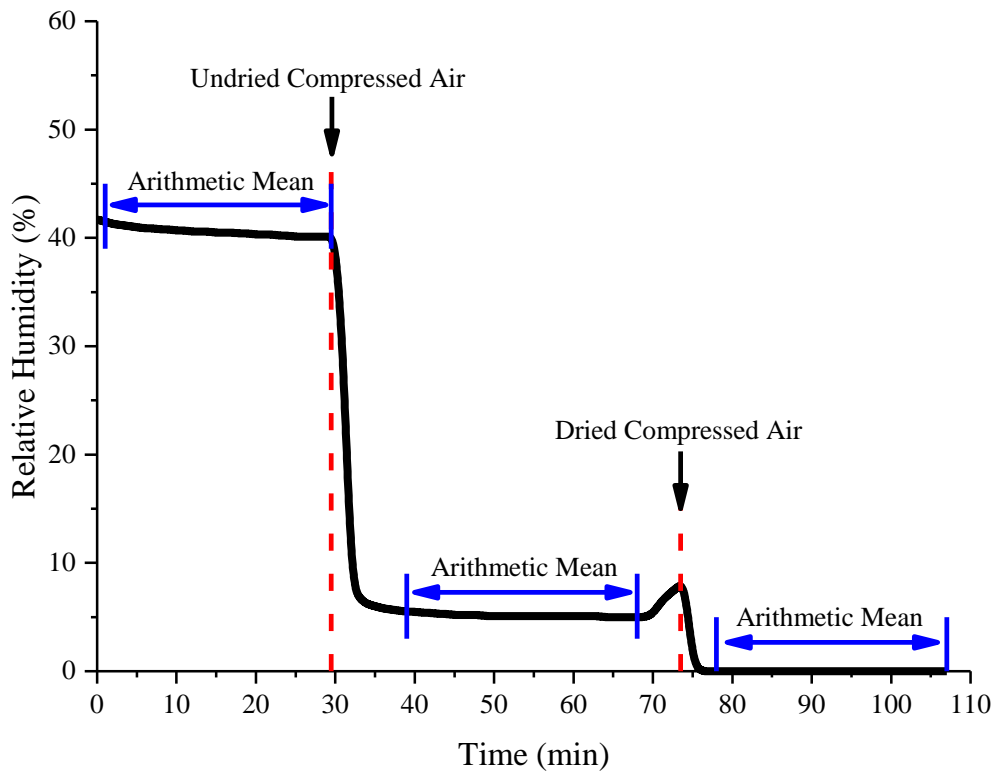


Figure D-2. The evolution of relative humidity in the column

Table D-1. The detailed results of relative humidity in the column. Note that the humidity values recorded by the thermohyrometer used in the current work are only to one decimal place.

Time (min)	Humidity (%)	Time (min)	Humidity (%)	Time (min)	Humidity (%)
0	41.7	36	5.8	72	7.1
1	41.5	37	5.7	73	7.7
2	41.3	38	5.6	74	8.3
3	41.2	39	5.5	75	0.8
4	41.1	40	5.5	76	0.0
5	41.0	41	5.4	77	0.0
6	40.9	42	5.4	78	0.0
7	40.9	43	5.3	79	0.0
8	40.8	44	5.3	80	0.0
9	40.8	45	5.2	81	0.0
10	40.7	46	5.2	82	0.0
11	40.7	47	5.2	83	0.0
12	40.6	48	5.2	84	0.0
13	40.6	49	5.1	85	0.0
14	40.6	50	5.1	86	0.0
15	40.5	51	5.1	87	0.0
16	40.5	52	5.1	88	0.0
17	40.5	53	5.1	89	0.0
18	40.4	54	5.1	90	0.0
19	40.4	55	5.1	91	0.0
20	40.3	56	5.1	92	0.0
21	40.3	57	5.1	93	0.0
22	40.3	58	5.1	94	0.0
23	40.2	59	5.1	95	0.0
24	40.2	60	5.1	96	0.0
25	40.1	61	5.1	97	0.0
26	40.1	62	5.1	98	0.0
27	40.1	63	5.1	99	0.0
28	40.1	64	5.0	100	0.0
29	40.1	65	5.0	101	0.0
30	40.1	66	5.0	102	0.0
31	29.5	67	5.0	103	0.0
32	8.2	68	5.0	104	0.0
33	6.7	69	5.0	105	0.0
34	6.2	70	5.3	106	0.0
35	6.0	71	6.4	107	0.0

The evolution of relative humidity in the column is shown in Figure D-2 and the detailed results of relative humidity in the column are shown in Table D-1. As can be seen from Figure D-2, the relative humidity of environmental air in the column is stable and maintains around 40 %. The arrows in Figure D-2 indicate the moments at which the undried and dried compressed air are delivered into the column. After delivering undried compressed air into the column, the relative humidity in the column decreases directly to about 5 %

and then keeps constant. Note that the slight increase of relative humidity in the column from 69 to 74 minutes is due to the switching off undried compressed air and the environmental air flows into the column from the vent. Whilst dried compressed air is delivered into the column, the relative humidity decreases immediately again to 0 % and remains at null value until the measurement stops.

The relative humidity of environmental air, undried compressed air and dried compressed air are shown in Table D-2. As can be seen, the relative humidity of undried compressed air is 5.2 % and the relative humidity of dried compressed air is 0.0 %. This demonstrates that the drying agent is effective and the compressed air after going through the drying agent is approximately completely dry, which allows adjusting the relative humidity of the freeboard in a wide scale.

Table D-2. The relative humidity of environmental air, undried compressed air and dried compressed air

Type of air	Relative humidity (%)
Environmental air	40.6
Undried compressed air	5.2
Dried compressed air	0.0

Appendix E Detailed Results of Foam Stability Measurement in Chapter 4

The detailed results of evolution of foam height of SDS solution in each independent measurement with different values of environmental relative humidity at the top of the column are shown in Tables E-1, E-2, E-3, E-4, and E-5.

Table E-1. The detailed results of evolution of foam height of SDS solution in each independent measurement with relative humidity of 93.4 % at the top of the column

Time (min)	Trial 1			Trial 2			Trial 3			Average	
	Foam Height (mm)			Foam Height (mm)			Foam Height (mm)			Foam Height (mm)	
	H ₁	H ₂	ΔH	H ₁	H ₂	ΔH	H ₁	H ₂	ΔH	ΔH	Error
0	200	200	0	200	200	0	200	200	0	0	0
5	200	228	28	200	231	31	200	229	29	29	3
10	200	252	52	200	255	55	200	245	45	51	10
15	200	277	77	200	277	77	200	268	68	74	9
20	200	303	103	200	300	100	200	294	94	99	9
25	200	327	127	200	324	124	200	318	118	123	9
30	200	349	149	200	349	149	200	345	145	148	4
35	200	375	175	200	374	174	200	366	166	172	9
40	200	399	199	200	398	198	200	392	192	196	7
45	200	428	228	200	423	223	200	417	217	223	11
50	200	453	253	200	445	245	200	441	241	246	12
55	200	476	276	200	470	270	200	469	269	272	7
60	200	500	300	200	491	291	200	492	292	294	9
65	200	526	326	200	518	318	200	515	315	320	11
70	200	547	347	200	547	347	200	538	338	344	9
75	200	570	370	200	577	377	200	560	360	369	17
80	200	587	387	200	598	398	200	583	383	389	15
85	200	609	409	200	619	419	200	606	406	411	13
90	200	630	430	200	638	438	200	629	429	432	9
95	200	650	450	200	655	455	200	647	447	451	8
100	200	672	472	200	676	476	200	663	463	470	13
105	200	694	494	200	700	500	200	680	480	491	20
110	200	718	518	200	722	522	200	702	502	514	20
115	200	742	542	200	737	537	200	721	521	533	21
120	200	765	565	200	762	562	200	742	542	556	23
125	200	786	586	200	783	583	200	769	569	579	17
130	200	807	607	200	800	600	200	794	594	600	13
135	200	826	626	200	825	625	200	817	617	623	9
140	200	845	645	200	846	646	200	840	640	644	6
145	200	873	673	200	872	672	200	866	666	670	7
150	200	905	705	200	895	695	200	887	687	696	18

Note: H₁ represents the height of foam-liquid interface. H₂ represents the top height of foam.

ΔH represents the foam height, which is the difference between H₁ and H₂. Error is the difference between largest and smallest foam height values of all independent measurements.

These definitions also apply to the other tables which are used for recording the detailed results of foam height evolution in all appendixes (Appendix E, F and G).

Table E-2. The detailed results of evolution of foam height of SDS solution in each independent measurement with relative humidity of 71.1 % at the top of the column

Time (min)	Trial 1 Foam Height (mm)			Trial 2 Foam Height (mm)			Trial 3 Foam Height (mm)			Average Foam Height (mm)	
	H ₁	H ₂	ΔH	H ₁	H ₂	ΔH	H ₁	H ₂	ΔH	ΔH	Error
0	200	200	0	200	200	0	275	275	0	0	0
5	200	235	35	200	230	30	275	295	20	28	15
10	200	260	60	200	253	53	275	316	41	51	19
15	200	282	82	200	275	75	275	340	65	74	17
20	200	299	99	200	297	97	275	364	89	95	10
25	200	323	123	200	319	119	275	387	112	118	11
30	200	344	144	200	342	142	275	407	132	139	12
35	200	368	168	200	364	164	275	425	150	161	18
40	200	394	194	200	388	188	275	446	171	184	23
45	200	416	216	200	407	207	275	473	198	207	18
50	200	444	244	200	429	229	275	497	222	232	22
55	200	465	265	200	451	251	275	518	243	253	22
60	200	484	284	200	471	271	275	542	267	274	17
65	200	507	307	200	493	293	275	560	285	295	22
70	200	526	326	200	516	316	275	578	303	315	23
75	200	550	350	200	521	321	275	595	320	330	30
80	200	563	363	200	527	327	275	609	334	341	36
85	200	566	366	200	532	332	275	619	344	347	34
90	200	573	373	200	538	338	275	630	355	355	35
95	200	575	375	200	555	355	275	639	364	365	20
100	200	580	380	200	567	367	275	648	373	373	13
105	200	583	383	200	581	381	275	658	383	382	2
110	200	584	384	200	586	386	275	664	389	386	5
115	200	587	387	200	599	399	275	669	394	393	12
120	200	600	400	200	607	407	275	673	398	402	9
125	200	607	407	200	610	410	275	677	402	406	8
130	200	610	410	200	612	412	275	686	411	411	2
135	200	608	408	200	617	417	275	685	410	412	9
140	200	609	409	200	622	422	275	689	414	415	13
145	200	616	416	200	627	427	275	687	412	418	15
150	200	618	418	200	625	425	275	689	414	419	11
155	200	622	422	200	630	430	275	683	408	420	22
160	200	638	438	200	633	433	275	688	413	428	25
165	200	652	452	200	630	430	275	690	415	432	37
170	200	656	456	200	634	434	275	694	419	436	37
175	200	657	457	200	638	438	275	697	422	439	35
180	200	659	459	200	638	438	275	698	423	440	36
185	200	663	463	200	636	436	275	700	425	441	38
190	200	654	454	200	640	440	275	700	425	440	29
195	200	642	442	200	640	440	275	699	424	435	18

Table E-3. The detailed results of evolution of foam height of SDS solution in each independent measurement with relative humidity of 51.3 % at the top of the column

Time (min)	Trial 1 Foam Height (mm)			Trial 2 Foam Height (mm)			Trial 3 Foam Height (mm)			Average Foam Height (mm)	
	H ₁	H ₂	ΔH	H ₁	H ₂	ΔH	H ₁	H ₂	ΔH	ΔH	Error
0	218	218	0	225	225	0	221	221	0	0	0
5	218	247	29	225	252	27	221	257	36	31	9
10	218	270	52	225	275	50	221	280	59	54	9
15	218	290	72	225	303	78	221	305	84	78	12
20	218	317	99	225	326	101	221	328	107	102	8
25	218	341	123	225	350	125	221	353	132	127	9
30	218	365	147	225	377	152	221	380	159	153	12
35	218	388	170	225	400	175	221	400	179	175	9
40	218	410	192	225	420	195	221	423	202	196	10
45	218	428	210	225	442	217	221	447	226	218	16
50	218	457	239	225	467	242	221	471	250	244	11
55	218	475	257	225	487	262	221	484	263	261	6
60	218	495	277	225	497	272	221	495	274	274	5
65	218	510	292	225	508	283	221	503	282	286	10
70	218	523	305	225	519	294	221	512	291	297	14
75	218	532	314	225	527	302	221	519	298	305	16
80	218	541	323	225	533	308	221	526	305	312	18
85	218	546	328	225	542	317	221	531	310	318	18
90	218	550	332	225	551	326	221	539	318	325	14
95	218	550	332	225	554	329	221	544	323	328	9
100	218	554	336	225	558	333	221	550	329	333	7
105	218	555	337	225	565	340	221	555	334	337	6
110	218	553	335	225	570	345	221	559	338	339	10
115	218	553	335	225	568	343	221	565	344	341	9
120	218	557	339	225	570	345	221	568	347	344	8
125	218	560	342	225	571	346	221	571	350	346	8
130	218	563	345	225	570	345	221	573	352	347	7
135	218	562	344	225	569	344	221	574	353	347	9
140	218	565	347	225	570	345	221	574	353	348	8
145	218	562	344	225	571	346	221	572	351	347	7
150	218	566	348	225	572	347	221	572	351	349	4

Table E-4. The detailed results of evolution of foam height of SDS solution in each independent measurement with relative humidity of 30.5 % at the top of the column

Time (min)	Trial 1 Foam Height (mm)			Trial 2 Foam Height (mm)			Trial 3 Foam Height (mm)			Average Foam Height (mm)	
	H ₁	H ₂	ΔH	H ₁	H ₂	ΔH	H ₁	H ₂	ΔH	ΔH	Error
0	221	221	0	215	215	0	208	208	0	0	0
5	221	251	30	215	240	25	208	234	26	27	5
10	221	274	53	215	265	50	208	255	47	50	6
15	221	300	79	215	287	72	208	279	71	74	8
20	221	324	103	215	312	97	208	305	97	99	6
25	221	345	124	215	332	117	208	326	118	120	7
30	221	366	145	215	354	139	208	352	144	143	6
35	221	386	165	215	378	163	208	373	165	164	2
40	221	405	184	215	398	183	208	400	192	186	9
45	221	424	203	215	420	205	208	422	214	207	11
50	221	438	217	215	444	229	208	443	235	227	18
55	221	452	231	215	457	242	208	462	254	242	23
60	221	460	239	215	463	248	208	478	270	252	31
65	221	464	243	215	473	258	208	492	284	262	41
70	221	465	244	215	476	261	208	505	297	267	53
75	221	467	246	215	483	268	208	512	304	273	58
80	221	470	249	215	490	275	208	515	307	277	58
85	221	471	250	215	490	275	208	519	311	279	61
90	221	469	248	215	492	277	208	523	315	280	67
95	221	472	251	215	490	275	208	525	317	281	66
100	221	472	251	215	488	273	208	530	322	282	71
105	221	473	252	215	487	272	208	529	321	282	69
110	221	473	252	215	490	275	208	532	324	284	72
115	221	477	256	215	489	274	208	532	324	285	68
120	221	477	256	215	491	276	208	523	315	282	59

Table E-5. The detailed results of evolution of foam height of SDS solution in each independent measurement with relative humidity of 10.0 % at the top of the column

Time (min)	Trial 1 Foam Height (mm)			Trial 2 Foam Height (mm)			Trial 3 Foam Height (mm)			Average Foam Height (mm)	
	H ₁	H ₂	ΔH	H ₁	H ₂	ΔH	H ₁	H ₂	ΔH	ΔH	Error
0	216	216	0	224	224	0	216	216	0	0	0
5	216	239	23	224	244	20	216	246	30	24	10
10	216	261	45	224	265	41	216	263	47	44	6
15	216	282	66	224	283	59	216	283	67	64	8
20	216	305	89	224	309	85	216	303	87	87	4
25	216	329	113	224	324	100	216	325	109	107	13
30	216	353	137	224	345	121	216	345	129	129	16
35	216	373	157	224	363	139	216	366	150	149	18
40	216	395	179	224	383	159	216	382	166	168	20
45	216	413	197	224	399	175	216	398	182	185	22
50	216	427	211	224	414	190	216	413	197	199	21
55	216	437	221	224	426	202	216	430	214	212	19
60	216	443	227	224	434	210	216	438	222	220	17
65	216	448	232	224	443	219	216	449	233	228	14
70	216	452	236	224	452	228	216	456	240	235	12
75	216	453	237	224	459	235	216	459	243	238	8
80	216	455	239	224	461	237	216	465	249	242	12
85	216	458	242	224	462	238	216	468	252	244	14
90	216	458	242	224	466	242	216	474	258	247	16
95	216	459	243	224	466	242	216	478	262	249	20
100	216	461	245	224	468	244	216	478	262	250	18
105	216	460	244	224	468	244	216	479	263	250	19
110	216	460	244	224	474	250	216	480	264	253	20
115	216	465	249	224	473	249	216	485	269	256	20
120	216	464	248	224	475	251	216	485	269	256	21

Appendix F Detailed Results of Equilibrium Surface Tension, Foam Stability and Surface Rheological Properties Measurements in Chapter 5

The estimation of equilibrium surface tension of TX-100 solution at the concentration of 0.175 g/L (i.e. at the CMC of TX-100) is shown in Figure F-1.

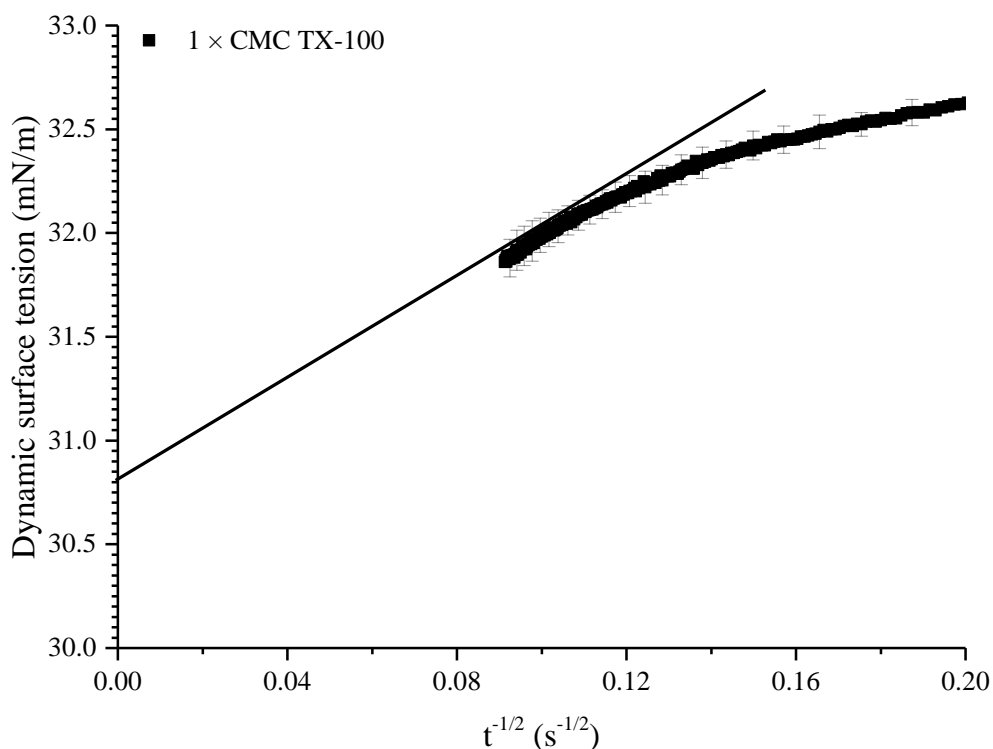


Figure F-1. Partial enlarged view of dynamic surface tension results of TX-100 solution at the concentration of 0.175 g/L (i.e. at the CMC of TX-100) against $t^{-1/2}$. The straight line represents a tangent and a linear extrapolation of dynamic surface tension to infinite time. The intercept at ordinate represents the estimated equilibrium surface tension. The error bars represent the standard deviation of the observations. All the errors of obtained data are calculated and only present 1 error bar in every 10 error bars for clarity.

The estimation of equilibrium surface tension of TX-100 solution at the concentration of 0.088 g/L (i.e. 50% of the CMC of TX-100) is shown in Figure F-2.

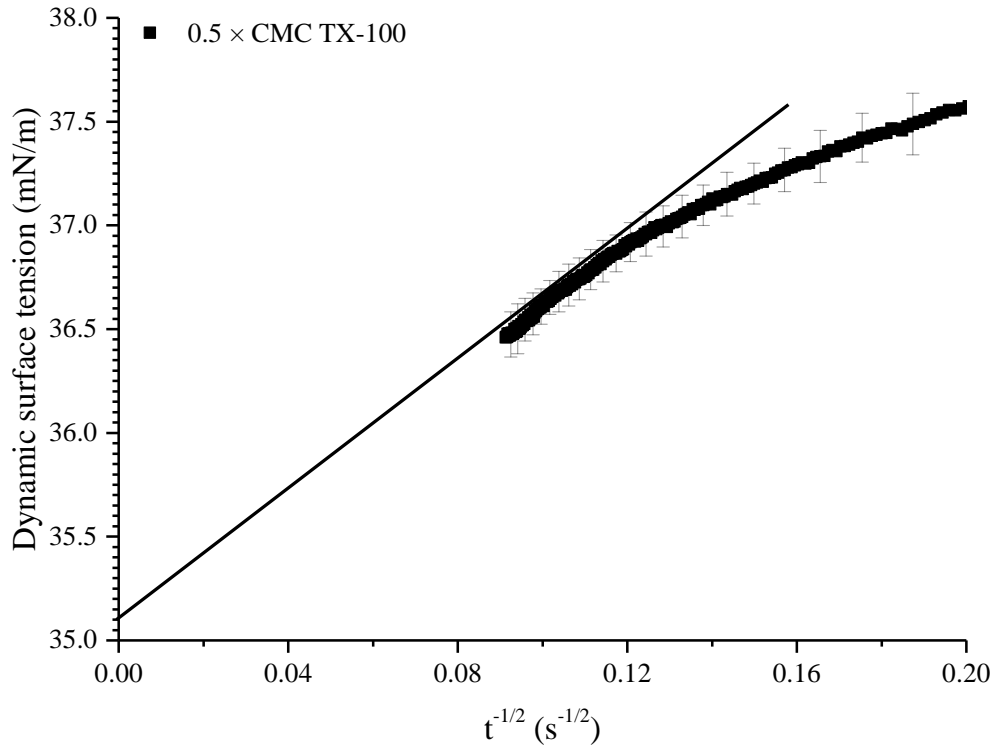


Figure F-2. Partial enlarged view of dynamic surface tension results of TX-100 solution at the concentration of 0.088 g/L (i.e. 50% of the CMC of TX-100) against $t^{-1/2}$. The straight line represents a tangent and a linear extrapolation of dynamic surface tension to infinite time. The intercept at ordinate represents the estimated equilibrium surface tension. The error bars represent the standard deviation of the observations. All the errors of obtained data are calculated and only present 1 error bar in every 10 error bars for clarity.

The estimation of equilibrium surface tension of TX-100 solution at the concentration of 0.070 g/L (i.e. 40% of the CMC of TX-100) is shown in Figure F-3.

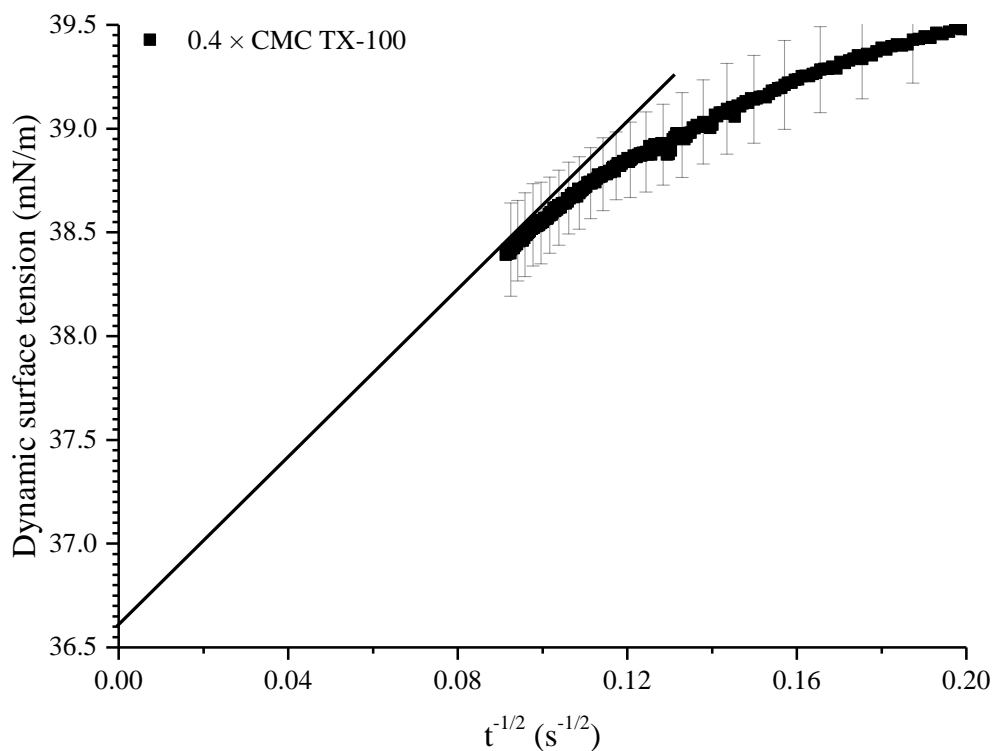


Figure F-3. Partial enlarged view of dynamic surface tension results of TX-100 solution at the concentration of 0.070 g/L (i.e. 40% of the CMC of TX-100) against $t^{-1/2}$. The straight line represents a tangent and a linear extrapolation of dynamic surface tension to infinite time. The intercept at ordinate represents the estimated equilibrium surface tension. The error bars represent the standard deviation of the observations. All the errors of obtained data are calculated and only present 1 error bar in every 10 error bars for clarity.

The estimation of equilibrium surface tension of TX-100 solution at the concentration of 0.044 g/L (i.e. 25% of the CMC of TX-100) is shown in Figure F-4.

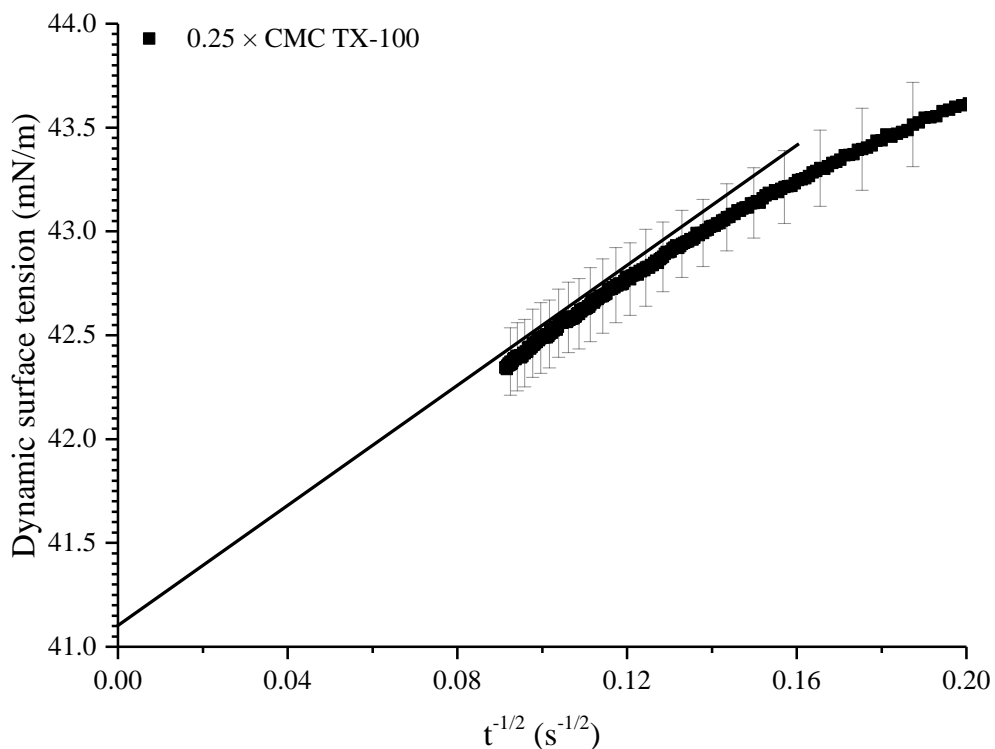


Figure F-4. Partial enlarged view of dynamic surface tension results of TX-100 solution at the concentration of 0.044 g/L (i.e. 25% of the CMC of TX-100) against $t^{-1/2}$. The straight line represents a tangent and a linear extrapolation of dynamic surface tension to infinite time. The intercept at ordinate represents the estimated equilibrium surface tension. The error bars represent the standard deviation of the observations. All the errors of obtained data are calculated and only present 1 error bar in every 10 error bars for clarity.

The results of equilibrium surface tension of TX-100 solution at different concentrations are shown in Table F-1.

Table F-1. Results of equilibrium surface tension of TX-100 solution at different concentrations. The errors of equilibrium surface tension are the standard deviation of the independent observations.

Concentration of TX-100 solution (g/L)	Equilibrium surface tension (mN/m)
0.175 (at the CMC)	30.80 ± 0.08
0.088 (50% of the CMC)	35.10 ± 0.11
0.070 (40% of the CMC)	36.60 ± 0.20
0.066 (37.5% of the CMC)	38.30 ± 0.16
0.044 (25% of the CMC)	41.10 ± 0.18

The detailed results of evolution of foam height of TX-100 solution (0.066 g/L) in each independent measurement at environmental relative humidity of $70.0 \pm 0.3\%$ are shown in Table F-2.

Table F-2. The detailed results of evolution of foam height of TX-100 solution (0.066 g/L) in each independent measurement at environmental relative humidity of $70.0 \pm 0.3\%$

Time (min)	Trial 1 Foam Height (mm)			Trial 2 Foam Height (mm)			Trial 3 Foam Height (mm)			Average Foam Height (mm)	
	H ₁	H ₂	ΔH	H ₁	H ₂	ΔH	H ₁	H ₂	ΔH	ΔH	Error
0	200	200	0	200	200	0	200	200	0	0	0
5	205	231	26	202	247	45	204	243	39	37	19
10	205	262	57	202	270	68	204	265	61	62	11
15	205	278	73	201	290	89	204	283	79	80	16
20	205	295	90	201	306	105	204	303	99	98	15
25	205	310	105	201	321	120	204	319	115	113	15
30	205	325	120	201	328	127	204	335	131	126	11
35	205	320	115	201	317	116	204	346	142	124	27
40	207	322	115	202	322	120	205	335	130	122	15
45	207	328	121	202	325	123	205	340	135	126	14
50	207	338	131	202	327	125	204	345	141	132	16
55	207	340	133	202	332	130	204	343	139	134	9
60	205	342	137	202	337	135	205	350	145	139	10
65	205	347	142	202	335	133	205	352	147	141	14
70	205	352	147	202	342	140	205	358	153	147	13
75	205	353	148	202	350	148	205	360	155	150	7
80	205	358	153	202	355	153	205	357	152	153	1
85	205	367	162	202	363	161	205	355	150	158	12
90	205	358	153	202	365	163	206	363	157	158	10
95	205	363	158	202	367	165	205	365	160	161	7
100	205	362	157	202	369	167	206	368	162	162	10
105	205	370	165	202	367	165	206	370	164	165	1
110	205	366	161	202	365	163	206	371	165	163	4
115	205	360	155	202	368	166	207	375	168	163	13
120	205	372	167	202	365	163	206	368	162	164	5
125	205	365	160	202	360	158	207	370	163	160	5
130	205	367	162	203	362	159	206	369	163	161	4
135	205	371	166	203	365	162	207	370	163	164	4

The detailed results of evolution of foam height of DTAB solution (4.954 g/L) in each independent measurement at environmental relative humidity of $70.0 \pm 0.3\%$ are shown in Table F-3.

Table F-3. The detailed results of evolution of foam height of DTAB solution (4.954 g/L) in each independent measurement at environmental relative humidity of $70.0 \pm 0.3\%$

Time (min)	Trial 1 Foam Height (mm)			Trial 2 Foam Height (mm)			Trial 3 Foam Height (mm)			Average Foam Height (mm)	
	H ₁	H ₂	ΔH	H ₁	H ₂	ΔH	H ₁	H ₂	ΔH	ΔH	Error
0	200	200	0	200	200	0	200	200	0	0	0
5	209	241	32	210	246	36	207	255	48	39	16
10	209	259	50	210	272	62	207	276	69	60	19
15	208	280	72	210	290	80	207	290	83	78	11
20	208	303	95	210	312	102	207	310	103	100	8
25	208	325	117	210	330	120	207	335	128	122	11
30	208	343	135	210	355	145	207	356	149	143	14
35	208	364	156	210	372	162	207	380	173	164	17
40	208	384	176	210	397	187	207	400	193	185	17
45	208	405	197	210	413	203	208	424	216	205	19
50	208	426	218	210	428	218	208	447	239	225	21
55	208	447	239	210	438	228	208	455	247	238	19
60	208	460	252	210	448	238	208	461	253	248	15
65	208	470	262	210	457	247	208	463	255	255	15
70	208	475	267	210	468	258	208	469	261	262	9
75	208	478	270	210	480	270	208	470	262	267	8
80	208	480	272	210	490	280	208	476	268	273	12
85	209	482	273	210	500	290	208	474	266	276	24
90	209	485	276	209	502	293	208	482	274	281	19
95	209	490	281	210	504	294	208	485	277	284	17
100	209	490	281	210	503	293	208	494	286	287	12
105	209	490	281	208	502	294	208	505	297	291	16
110	209	490	281	209	500	291	208	508	300	291	19
115	209	490	281	209	495	286	208	517	309	292	28
120	209	489	280	209	490	281	208	510	302	288	22

The detailed results of evolution of foam height of sodium tridecyl sulfate solution (1.301 g/L) in each independent measurement at environmental relative humidity of $70.0 \pm 0.3\%$ are shown in Table F-4.

Table F-4. The detailed results of evolution of foam height of sodium tridecyl sulfate solution (1.301 g/L) in each independent measurement at environmental relative humidity of $70.0 \pm 0.3\%$

Time (min)	Trial 1 Foam Height (mm)			Trial 2 Foam Height (mm)			Trial 3 Foam Height (mm)			Average Foam Height (mm)	
	H ₁	H ₂	ΔH	H ₁	H ₂	ΔH	H ₁	H ₂	ΔH	ΔH	Error
0	200	200	0	200	200	0	200	200	0	0	0
5	215	254	39	211	245	34	215	240	25	33	14
10	221	276	55	215	269	54	216	263	47	52	8
15	221	296	75	216	289	73	218	288	70	73	5
20	224	317	93	218	307	89	220	310	90	91	4
25	225	337	112	219	337	118	222	332	110	113	8
30	227	365	138	220	356	136	223	356	133	136	5
35	227	380	153	221	380	159	224	377	153	155	6
40	229	398	169	222	402	180	225	396	171	173	11
45	230	418	188	223	424	201	225	416	191	193	13
50	230	437	207	224	446	222	226	434	208	212	15
55	231	454	223	225	465	240	227	453	226	230	17
60	231	469	238	225	484	259	227	472	245	247	21
65	233	484	251	225	500	275	228	489	261	262	24
70	235	497	262	225	516	291	229	499	270	274	29
75	233	507	274	225	533	308	230	510	280	287	34
80	234	517	283	226	540	314	229	518	289	295	31
85	235	528	293	226	545	319	230	527	297	303	26
90	236	533	297	227	546	319	230	530	300	305	22
95	237	537	300	227	546	319	230	537	307	309	19
100	237	540	303	227	543	316	230	540	310	310	13
105	236	542	306	228	545	317	231	543	312	312	11
110	237	545	308	228	546	318	231	545	314	313	10
115	240	547	307	229	547	318	231	545	314	313	11
120	239	546	307	229	550	321	231	545	314	314	14
125	239	547	308	230	547	317	231	547	316	314	9
130	239	546	307	230	550	320	232	547	315	314	13

The detailed results of surface rheological properties in each independent measurement of TX-100 solution (0.066 g/L) at oscillation amplitude of 0.25 and oscillation frequency of 0.5 Hz are shown in Table F-5.

Table F-5. The detailed results of surface rheological properties in each independent measurement of TX-100 solution (0.066 g/L) at oscillation amplitude of 0.25 and oscillation frequency of 0.5 Hz.

Trial	Surface elasticity (mN/m)	Surface dilatational viscosity (mN·s/m)	Gibbs elasticity (mN/m)
1	15.00	2.45	38.88
2	15.34	2.27	34.94
3	15.53	2.63	42.62
4	15.64	2.41	37.57
5	15.08	2.44	38.60
6	15.30	2.41	37.83
7	14.54	2.40	38.32
8	15.39	2.33	35.95
9	15.22	2.51	40.02
10	15.92	2.45	38.00
11	15.40	2.53	40.43
12	15.29	2.43	38.18
13	15.38	2.43	38.01
14	15.25	2.33	36.14
15	15.29	2.60	42.30
16	15.26	2.44	38.35
17	15.34	2.44	38.44
18	14.87	2.54	41.50
19	15.38	2.30	35.49
20	15.25	2.49	39.55
21	15.79	2.52	39.68
22	15.20	2.47	39.13
23	15.55	2.63	42.56
24	15.38	2.47	38.90
25	15.54	2.41	37.64
26	14.96	2.48	39.73
27	15.47	2.30	35.33
28	15.20	2.69	44.88
29	15.45	2.67	43.75
30	15.31	2.42	37.87

The detailed results of surface rheological properties in each independent measurement of DTAB solution (4.954 g/L) at oscillation amplitude of 0.25 and oscillation frequency of 0.5 Hz are shown in Table F-6.

Table F-6. The detailed results of surface rheological properties in each independent measurement of DTAB solution (4.954 g/L) at oscillation amplitude of 0.25 and oscillation frequency of 0.5 Hz.

Trial	Surface elasticity (mN/m)	Surface dilatational viscosity (mN·s/m)	Gibbs elasticity (mN/m)
1	2.47	0.07	2.30
2	2.19	0.09	1.98
3	2.25	0.19	3.28
4	2.33	0.02	2.40
5	2.36	0.05	2.53
6	2.06	0.09	2.41
7	2.22	0.12	2.76
8	2.01	0.05	1.89
9	2.01	0.02	2.06
10	2.19	0.06	2.41
11	2.25	0.06	2.48
12	2.61	0.02	2.68
13	2.54	0.01	2.52
14	1.24	0.02	1.30
15	1.74	0.06	1.96
16	2.83	0.01	2.87
17	2.85	0.02	2.91
18	2.81	0.05	2.99
19	2.89	0.01	2.92
20	3.02	0.02	2.95
21	2.89	0.04	3.03
22	2.92	0.08	3.21
23	2.76	0.06	2.98
24	2.87	0.02	2.81
25	2.96	0.04	3.10
26	2.78	0.03	2.89
27	2.93	0.04	2.82
28	2.73	0.06	2.96
29	2.80	0.01	2.78
30	2.79	0.02	2.84

The detailed results of surface rheological properties in each independent measurement of sodium tridecyl sulfate solution (1.301 g/L) at oscillation amplitude of 0.25 and oscillation frequency of 0.5 Hz are shown in Table F-7.

Table F-7. The detailed results of surface rheological properties in each independent measurement of sodium tridecyl sulfate solution (1.301 g/L) at oscillation amplitude of 0.25 and oscillation frequency of 0.5 Hz

Trial	Surface elasticity (mN/m)	Surface dilatational viscosity (mN·s/m)	Gibbs elasticity (mN/m)
1	3.81	0.33	5.62
2	3.44	0.38	5.86
3	3.46	0.36	5.68
4	3.47	0.35	5.55
5	3.54	0.30	5.21
6	3.48	0.34	5.50
7	3.42	0.34	5.49
8	3.58	0.34	5.57
9	3.33	0.33	5.34
10	3.52	0.32	5.32
11	3.60	0.34	5.56
12	3.52	0.32	5.36
13	3.45	0.32	5.33
14	3.25	0.33	5.30
15	3.29	0.31	5.06
16	3.43	0.33	5.34
17	3.54	0.37	5.89
18	3.59	0.31	5.30
19	3.64	0.36	5.77
20	3.33	0.32	5.21
21	3.35	0.29	4.95
22	3.54	0.34	5.49
23	3.47	0.37	5.76
24	3.38	0.37	5.79
25	3.67	0.30	5.29
26	3.70	0.38	6.03
27	3.63	0.32	5.41
28	3.76	0.33	5.55
29	3.78	0.33	5.57
30	3.88	0.36	5.94

Appendix G Detailed Results of Foam Stability and Surface Rheological Properties Measurements in Chapter 6

The detailed results of evolution of foam height of DTAB solution at the concentration of $0.1 \times \text{CMC}$ in each independent measurement at environmental relative humidity of $70.4 \pm 0.5\%$ are shown in Table G-1.

Table G-1. The detailed results of evolution of foam height of DTAB solution at the concentration of $0.1 \times \text{CMC}$ in each independent measurement at environmental relative humidity of $70.4 \pm 0.5\%$

Time (min)	Trial 1 Foam Height (mm)			Trial 2 Foam Height (mm)			Trial 3 Foam Height (mm)			Average Foam Height (mm)	
	H ₁	H ₂	ΔH	H ₁	H ₂	ΔH	H ₁	H ₂	ΔH	ΔH	Error
0	200	200	0	215	215	0	215	215	0	0	0
5	217	217	0	215	215	0	215	215	0	0	0
10	217	217	0	215	215	0	215	215	0	0	0
15	216	216	0	215	215	0	215	215	0	0	0
20	216	216	0	215	215	0	215	215	0	0	0
25	216	216	0	216	216	0	215	215	0	0	0
30	216	216	0	215	215	0	215	215	0	0	0

The detailed results of evolution of foam height of mixture of DTAB solution ($0.1 \times \text{CMC}$) and colloidal silica dispersions (3 wt%) in each independent measurement at environmental relative humidity of $70.4 \pm 0.5\%$ are shown in Table G-2.

Table G-2. The detailed results of evolution of foam height of mixture of DTAB solution ($0.1 \times \text{CMC}$) and colloidal silica dispersions (3 wt%) in each independent measurement at environmental relative humidity of $70.4 \pm 0.5\%$

Time (min)	Trial 1 Foam Height (mm)			Trial 2 Foam Height (mm)			Trial 3 Foam Height (mm)			Average Foam Height (mm)	
	H ₁	H ₂	ΔH	H ₁	H ₂	ΔH	H ₁	H ₂	ΔH	ΔH	Error
0	202	202	0	202	202	0	203	203	0	0	0
5	211	240	29	210	237	27	211	248	37	31	10
10	212	264	52	210	263	53	213	268	55	53	3
15	212	285	73	210	292	82	214	290	76	77	9
20	213	312	99	210	310	100	214	310	96	98	4
25	213	310	97	211	319	108	215	334	119	108	22
30	212	320	108	211	332	121	215	345	130	120	22
35	214	330	116	211	342	131	215	355	140	129	24
40	214	332	118	212	353	141	217	370	153	137	35
45	215	339	124	211	362	151	216	386	170	148	46
50	214	345	131	210	373	163	215	400	185	160	54
55	215	348	133	210	373	163	215	415	200	165	67
60	214	355	141	213	379	166	216	420	204	170	63
65	214	356	142	210	390	180	216	427	211	178	69
70	214	359	145	212	394	182	216	434	218	182	73
75	214	367	153	212	394	182	215	437	222	186	69
80	214	368	154	212	394	182	215	436	221	186	67
85	215	368	153	210	393	183	216	440	224	187	71
90	215	370	155	211	393	182	215	443	228	188	73
95	215	370	155	210	392	182	215	445	230	189	75
100	214	371	157	210	392	182	215	445	230	190	73
105	215	378	163	211	392	181	213	446	233	192	70
110	215	377	162	210	392	182	215	446	231	192	69
115	215	380	165	213	392	179	214	446	232	192	67
120	215	377	162	212	395	183	215	448	233	193	71

The detailed results of evolution of foam height of DTAB solution at the concentration of $0.25 \times \text{CMC}$ in each independent measurement at environmental relative humidity of $70.4 \pm 0.5\%$ are shown in Table G-3.

Table G-3. The detailed results of evolution of foam height of DTAB solution at the concentration of $0.25 \times \text{CMC}$ in each independent measurement at environmental relative humidity of $70.4 \pm 0.5\%$

Time (min)	Trial 1 Foam Height (mm)			Trial 2 Foam Height (mm)			Trial 3 Foam Height (mm)			Average Foam Height (mm)	
	H ₁	H ₂	ΔH	H ₁	H ₂	ΔH	H ₁	H ₂	ΔH	ΔH	Error
0	209	209	0	209	209	0	207	207	0	0	0
5	209	211	2	208	210	2	207	209	2	2	0
10	209	212	3	208	210	2	207	210	3	3	1
15	209	211	2	208	211	3	207	210	3	3	1
20	209	212	3	208	211	3	208	210	2	3	1
25	209	211	2	208	210	2	208	210	2	2	0
30	209	211	2	208	211	3	207	210	3	3	1

The detailed results of evolution of foam height of mixture of DTAB solution ($0.25 \times \text{CMC}$) and colloidal silica dispersions (3 wt%) in each independent measurement at environmental relative humidity of $70.4 \pm 0.5\%$ are shown in Table G-4.

Table G-4. The detailed results of evolution of foam height of mixture of DTAB solution ($0.25 \times \text{CMC}$) and colloidal silica dispersions (3 wt%) in each independent measurement at environmental relative humidity of $70.4 \pm 0.5\%$

Time (min)	Trial 1			Trial 2			Trial 3			Average	
	Foam Height (mm)			Foam Height (mm)			Foam Height (mm)			Foam Height (mm)	
	H ₁	H ₂	ΔH	H ₁	H ₂	ΔH	H ₁	H ₂	ΔH	ΔH	Error
0	205	205	0	203	203	0	202	202	0	0	0
5	210	223	13	204	217	13	200	210	10	12	3
10	210	225	15	203	217	14	200	213	13	14	2
15	213	226	13	204	218	14	200	215	15	14	2
20	210	222	12	203	215	12	200	214	14	13	2
25	212	227	15	203	218	15	200	213	13	14	2
30	213	225	12	203	217	14	200	212	12	13	2
35	213	224	11	204	217	13	200	214	14	13	3
40	215	227	12	203	218	15	200	215	15	14	3
45	213	225	12	202	215	13	200	217	17	14	5
50	215	228	13	204	216	12	200	215	15	13	3
55	215	227	12	204	219	15	200	213	13	13	3
60	213	227	14	204	218	14	200	214	14	14	0

The detailed results of evolution of foam height of DTAB solution at the concentration of $0.5 \times \text{CMC}$ in each independent measurement at environmental relative humidity of $70.4 \pm 0.5\%$ are shown in Table G-5.

Table G-5. The detailed results of evolution of foam height of DTAB solution at the concentration of $0.5 \times \text{CMC}$ in each independent measurement at environmental relative humidity of $70.4 \pm 0.5\%$

Time (min)	Trial 1 Foam Height (mm)			Trial 2 Foam Height (mm)			Trial 3 Foam Height (mm)			Average Foam Height (mm)	
	H ₁	H ₂	ΔH	H ₁	H ₂	ΔH	H ₁	H ₂	ΔH	ΔH	Error
0	200	200	0	200	200	0	202	202	0	0	0
5	207	236	29	204	232	28	210	230	20	26	9
10	206	256	50	205	255	50	210	244	34	45	16
15	207	275	68	206	285	79	211	263	52	66	27
20	207	293	86	207	310	103	213	275	62	84	41
25	207	310	103	207	328	121	214	296	82	102	39
30	207	328	121	207	345	138	214	309	95	118	43
35	208	330	122	207	360	153	214	327	113	129	40
40	208	337	129	207	370	163	214	342	128	140	35
45	209	339	130	207	367	160	214	350	136	142	30
50	209	345	136	207	377	170	214	358	144	150	34
55	209	347	138	207	380	173	214	366	152	154	35
60	209	351	142	207	383	176	214	375	161	160	34
65	209	353	144	208	383	175	214	386	172	164	31
70	210	354	144	207	385	178	214	384	170	164	34
75	210	354	144	208	382	174	214	385	171	163	30
80	210	357	147	207	378	171	214	386	172	163	25
85	210	360	150	207	379	172	214	388	174	165	24
90	210	365	155	207	379	172	214	388	174	167	19
95	210	372	162	207	380	173	214	390	176	170	14
100	210	370	160	207	383	176	214	390	176	171	16
105	210	367	157	207	383	176	214	387	173	169	19
110	210	366	156	207	384	177	214	388	174	169	21
115	210	374	164	207	388	181	214	388	174	173	17
120	210	372	162	207	390	183	214	388	174	173	21

The detailed results of evolution of foam height of mixture of DTAB solution ($0.5 \times \text{CMC}$) and colloidal silica dispersions (3 wt%) in each independent measurement at environmental relative humidity of $70.4 \pm 0.5\%$ are shown in Table G-6.

Table G-6. The detailed results of evolution of foam height of mixture of DTAB solution ($0.5 \times \text{CMC}$) and colloidal silica dispersions (3 wt%) in each independent measurement at environmental relative humidity of $70.4 \pm 0.5\%$

Time (min)	Trial 1 Foam Height (mm)			Trial 2 Foam Height (mm)			Trial 3 Foam Height (mm)			Average Foam Height (mm)	
	H ₁	H ₂	ΔH	H ₁	H ₂	ΔH	H ₁	H ₂	ΔH	ΔH	Error
0	202	202	0	199	199	0	205	205	0	0	0
5	209	220	11	204	214	10	210	224	14	12	4
10	210	225	15	205	215	10	212	222	10	12	5
15	212	228	16	205	222	17	213	225	12	15	5
20	212	230	18	206	217	11	214	225	11	13	7
25	213	231	18	207	217	10	214	223	9	12	9
30	214	233	19	208	222	14	215	230	15	16	5
35	215	230	15	208	220	12	215	228	13	13	3
40	215	228	13	209	223	14	216	226	10	12	4
45	215	230	15	210	225	15	216	226	10	13	5
50	216	230	14	210	223	13	217	226	9	12	5
55	217	228	11	211	228	17	217	228	11	13	6
60	217	230	13	211	225	14	217	231	14	14	1

The detailed results of evolution of foam height of mixture of DTAB solution ($1.05 \times \text{CMC}$) and colloidal silica dispersions (3 wt%) in each independent measurement at environmental relative humidity of $70.4 \pm 0.5\%$ are shown in Table G-7.

Table G-7. The detailed results of evolution of foam height of mixture of DTAB solution ($1.05 \times \text{CMC}$) and colloidal silica dispersions (3 wt%) in each independent measurement at environmental relative humidity of $70.4 \pm 0.5\%$

Time (min)	Trial 1 Foam Height (mm)			Trial 2 Foam Height (mm)			Trial 3 Foam Height (mm)			Average Foam Height (mm)	
	H ₁	H ₂	ΔH	H ₁	H ₂	ΔH	H ₁	H ₂	ΔH	ΔH	Error
0	201	201	0	201	201	0	205	205	0	0	0
5	207	237	30	205	227	22	200	237	37	30	15
10	208	241	33	202	240	38	194	240	46	39	13
15	208	250	42	200	241	41	191	255	64	45	10
20	207	253	46	200	242	42	191	247	56	48	14
25	207	257	50	198	248	50	190	245	55	52	5
30	207	261	54	197	250	53	190	240	50	52	4
35	208	265	57	197	253	56	188	240	52	55	5
40	208	265	57	198	258	60	188	239	51	56	9
45	208	265	57	193	260	67	187	240	53	59	14
50	208	265	57	193	259	66	188	243	55	59	11
55	208	265	57	193	255	62	194	244	50	56	12
60	208	265	57	192	264	72	192	255	63	64	15
65	208	267	59	190	266	76	192	251	59	65	17
70	208	270	62	190	265	75	191	243	52	63	23
75	208	270	62	190	256	66	192	242	50	59	16
80	208	265	57	190	260	70	192	246	54	60	16
85	208	268	60	192	257	65	191	243	52	59	13
90	209	265	56	191	263	72	191	240	49	59	23

The detailed results of evolution of foam height of DTAB solution at the concentration of $2.5 \times \text{CMC}$ in each independent measurement at environmental relative humidity of $70.4 \pm 0.5\%$ are shown in Table G-8.

Table G-8. The detailed results of evolution of foam height of DTAB solution at the concentration of $2.5 \times \text{CMC}$ in each independent measurement at environmental relative humidity of $70.4 \pm 0.5\%$

Time (min)	Trial 1 Foam Height (mm)			Trial 2 Foam Height (mm)			Trial 3 Foam Height (mm)			Average Foam Height (mm)	
	H ₁	H ₂	ΔH	H ₁	H ₂	ΔH	H ₁	H ₂	ΔH	ΔH	Error
0	200	200	0	200	200	0	201	201	0	0	0
5	211	225	14	210	245	35	208	240	32	27	21
10	210	254	44	209	282	73	208	264	56	58	29
15	210	282	72	209	310	101	208	293	85	86	29
20	210	309	99	211	341	130	208	320	112	114	31
25	209	330	121	213	370	157	208	350	142	140	36
30	209	349	140	213	393	180	209	374	165	162	40
35	209	370	161	214	418	204	209	402	193	186	43
40	209	384	175	214	428	214	209	425	216	202	41
45	209	390	181	213	440	227	209	441	232	213	51
50	209	395	186	215	459	244	209	452	243	224	58
55	210	395	185	216	469	253	211	465	254	231	69
60	213	410	197	217	480	263	212	469	257	239	66
65	215	432	217	217	495	278	213	473	260	252	61
70	215	442	227	216	500	284	215	481	266	259	57
75	215	451	236	216	499	283	215	485	270	263	47
80	215	463	248	217	498	281	216	487	271	267	33
85	215	478	263	216	501	285	217	490	273	274	22
90	215	485	270	218	497	279	217	487	270	273	9
95	216	488	272	218	500	282	217	484	267	274	15
100	217	490	273	217	496	279	218	490	272	275	7
105	217	486	269	217	495	278	218	487	269	272	9
110	217	480	263	218	495	277	218	485	267	269	14
115	217	482	265	217	498	281	219	482	263	270	18
120	217	480	263	217	493	276	219	490	271	270	13

The detailed results of evolution of foam height of mixture of DTAB solution ($2.5 \times \text{CMC}$) and colloidal silica dispersions (3 wt%) in each independent measurement at environmental relative humidity of $70.4 \pm 0.5\%$ are shown in Table G-9.

Table G-9. The detailed results of evolution of foam height of mixture of DTAB solution ($2.5 \times \text{CMC}$) and colloidal silica dispersions (3 wt%) in each independent measurement at environmental relative humidity of $70.4 \pm 0.5\%$

Time (min)	Trial 1 Foam Height (mm)			Trial 2 Foam Height (mm)			Trial 3 Foam Height (mm)			Average Foam Height (mm)	
	H ₁	H ₂	ΔH	H ₁	H ₂	ΔH	H ₁	H ₂	ΔH	ΔH	Error
0	199	199	0	206	206	0	202	202	0	0	0
5	208	224	16	210	246	36	205	235	30	27	20
10	210	245	35	211	266	55	208	253	45	45	20
15	208	273	65	212	296	84	208	276	68	72	19
20	208	305	97	213	315	102	208	300	92	97	10
25	208	325	117	214	338	124	208	324	116	119	8
30	208	348	140	214	345	131	208	342	134	135	9
35	208	372	164	213	350	137	209	360	151	151	27
40	208	393	185	213	360	147	209	389	180	171	38
45	209	410	201	214	382	168	209	398	189	186	33
50	208	428	220	214	396	182	210	408	198	200	38
55	208	450	242	214	413	199	210	414	204	215	43
60	208	468	260	214	435	221	211	425	214	232	46
65	208	490	282	215	458	243	211	435	224	250	58
70	208	494	286	215	457	242	212	452	240	256	46
75	208	500	292	215	468	253	212	450	238	261	54
80	208	490	282	216	476	260	213	472	259	267	23
85	208	493	285	216	480	264	213	485	272	274	21
90	208	497	289	217	492	275	213	490	277	280	14
95	208	500	292	217	492	275	214	483	269	279	23
100	208	500	292	217	501	284	214	487	273	283	19
105	208	495	287	217	498	281	214	484	270	279	17
110	208	495	287	217	493	276	214	482	268	277	19
115	208	499	291	217	500	283	215	486	271	282	20
120	207	495	288	217	495	278	215	480	265	277	23

The evolutions of foam height of mixtures of DTAB solution ($0.1 \times \text{CMC}$) and colloidal silica dispersions at different particle concentrations with the environmental relative humidity of $70.4 \pm 0.5\%$ are shown in Figure G-1.

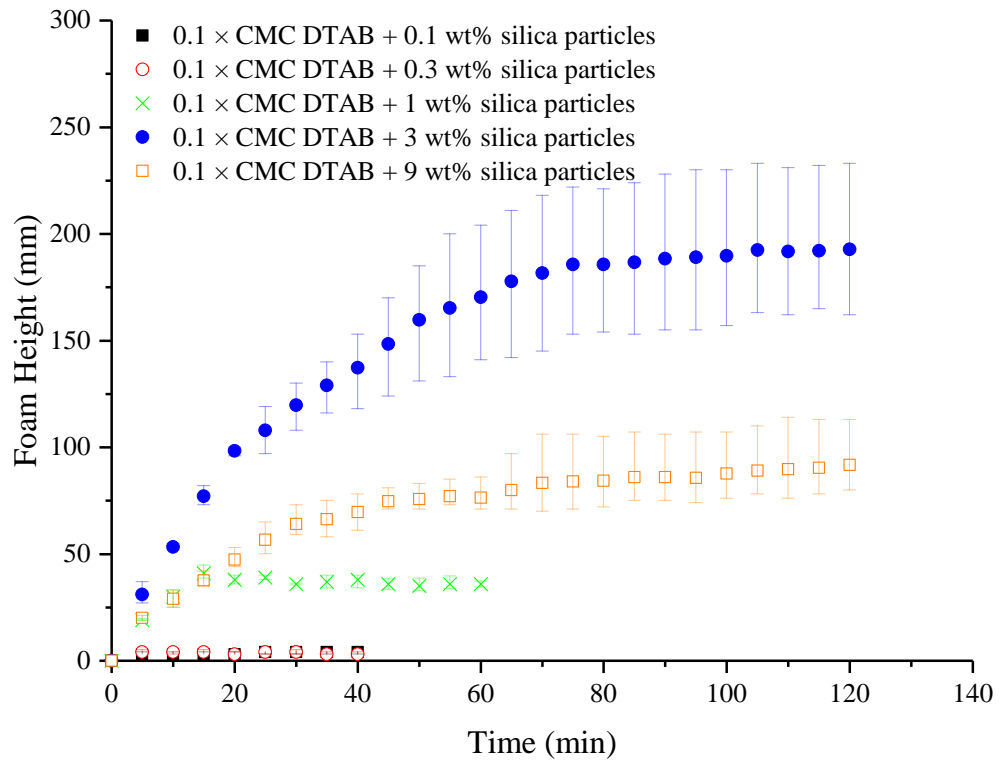


Figure G-1. The evolutions of foam height of mixtures of DTAB solution ($0.1 \times \text{CMC}$) and colloidal silica dispersions at different particle concentrations with the environmental relative humidity of $70.4 \pm 0.5\%$. The error bars represent the full range of independent observations.

The detailed results of evolution of foam height of mixture of DTAB solution ($0.1 \times \text{CMC}$) and colloidal silica dispersions (0.1 wt%) in each independent measurement at environmental relative humidity of $70.4 \pm 0.5\%$ are shown in Table G-10.

Table G-10. The detailed results of evolution of foam height of mixture of DTAB solution ($0.1 \times \text{CMC}$) and colloidal silica dispersions (0.1 wt%) in each independent measurement at environmental relative humidity of $70.4 \pm 0.5\%$

Time (min)	Trial 1 Foam Height (mm)			Trial 2 Foam Height (mm)			Trial 3 Foam Height (mm)			Average Foam Height (mm)	
	H ₁	H ₂	ΔH	H ₁	H ₂	ΔH	H ₁	H ₂	ΔH	ΔH	Error
	0	205	205	0	205	205	0	210	210	0	0
5	214	218	4	209	212	3	210	213	3	3	1
10	215	218	3	209	213	4	210	213	3	3	1
15	215	218	3	210	213	3	210	214	4	3	1
20	215	218	3	210	213	3	210	214	4	3	1
25	215	218	3	210	214	4	210	214	4	4	1
30	214	218	4	210	214	4	210	213	3	4	1
35	215	218	3	210	214	4	210	214	4	4	1
40	214	218	4	210	214	4	210	213	3	4	1

The detailed results of evolution of foam height of mixture of DTAB solution ($0.1 \times \text{CMC}$) and colloidal silica dispersions (0.3 wt%) in each independent measurement at environmental relative humidity of $70.4 \pm 0.5\%$ are shown in Table G-11.

Table G-11. The detailed results of evolution of foam height of mixture of DTAB solution ($0.1 \times \text{CMC}$) and colloidal silica dispersions (0.3 wt%) in each independent measurement at environmental relative humidity of $70.4 \pm 0.5\%$

Time (min)	Trial 1 Foam Height (mm)			Trial 2 Foam Height (mm)			Trial 3 Foam Height (mm)			Average Foam Height (mm)	
	H ₁	H ₂	ΔH	H ₁	H ₂	ΔH	H ₁	H ₂	ΔH	ΔH	Error
	0	211	211	0	219	219	0	218	218	0	0
5	220	225	5	219	223	4	217	221	4	4	1
10	220	224	4	219	223	4	217	220	3	4	1
15	220	224	4	219	224	5	217	221	4	4	1
20	220	223	3	219	222	3	217	221	4	3	1
25	220	224	4	219	223	4	217	220	3	4	1
30	220	223	3	219	224	5	217	221	4	4	2
35	220	223	3	219	223	4	217	220	3	3	1
40	220	224	4	219	222	3	217	220	3	3	1

The detailed results of evolution of foam height of mixture of DTAB solution ($0.1 \times \text{CMC}$) and colloidal silica dispersions (1 wt%) in each independent measurement at environmental relative humidity of $70.4 \pm 0.5\%$ are shown in Table G-12.

Table G-12. The detailed results of evolution of foam height of mixture of DTAB solution ($0.1 \times \text{CMC}$) and colloidal silica dispersions (1 wt%) in each independent measurement at environmental relative humidity of $70.4 \pm 0.5\%$

Time (min)	Trial 1 Foam Height (mm)			Trial 2 Foam Height (mm)			Trial 3 Foam Height (mm)			Average Foam Height (mm)	
	H ₁	H ₂	ΔH	H ₁	H ₂	ΔH	H ₁	H ₂	ΔH	ΔH	Error
	0	200	200	0	202	202	0	198	198	0	0
5	203	222	19	207	227	20	200	219	19	19	1
10	204	236	32	207	232	25	205	238	33	30	8
15	205	245	40	208	247	39	205	250	45	41	6
20	203	241	38	210	250	40	205	241	36	38	4
25	205	244	39	210	248	38	205	245	40	39	2
30	204	240	36	208	244	36	205	240	35	36	1
35	204	241	37	207	247	40	205	239	34	37	6
40	204	244	40	208	248	40	205	239	34	38	6
45	204	242	38	208	244	36	205	238	33	36	5
50	204	243	39	208	242	34	205	238	33	35	6
55	204	244	40	208	243	35	205	239	34	36	6
60	204	240	36	208	245	37	205	239	34	36	3

The detailed results of evolution of foam height of mixture of DTAB solution ($0.1 \times \text{CMC}$) and colloidal silica dispersions (9 wt%) in each independent measurement at environmental relative humidity of $70.4 \pm 0.5\%$ are shown in Table G-13.

Table G-13. The detailed results of evolution of foam height of mixture of DTAB solution ($0.1 \times \text{CMC}$) and colloidal silica dispersions (9 wt%) in each independent measurement at environmental relative humidity of $70.4 \pm 0.5\%$

Time (min)	Trial 1 Foam Height (mm)			Trial 2 Foam Height (mm)			Trial 3 Foam Height (mm)			Average Foam Height (mm)	
	H ₁	H ₂	ΔH	H ₁	H ₂	ΔH	H ₁	H ₂	ΔH	ΔH	Error
0	202	202	0	202	202	0	200	200	0	0	0
5	207	228	21	205	224	19	201	221	20	20	2
10	208	241	33	207	232	25	203	232	29	29	8
15	209	251	42	208	244	36	207	242	35	38	7
20	209	262	53	210	255	45	207	251	44	47	9
25	210	275	65	210	265	55	208	258	50	57	15
30	211	284	73	210	270	60	210	269	59	64	14
35	211	286	75	212	270	58	208	274	66	66	17
40	212	290	78	212	273	61	210	280	70	70	17
45	212	293	81	212	283	71	211	283	72	75	10
50	212	295	83	213	286	73	212	283	71	76	12
55	213	298	85	213	286	73	210	283	73	77	12
60	212	298	86	215	287	72	212	283	71	76	15
65	212	309	97	215	286	71	210	282	72	80	26
70	213	319	106	213	287	74	212	282	70	83	36
75	213	319	106	213	288	75	210	281	71	84	35
80	214	319	105	214	290	76	210	282	72	84	33
85	213	320	107	214	289	75	209	285	76	86	32
90	215	321	106	215	290	75	210	287	77	86	31
95	213	320	107	216	290	74	212	288	76	86	33
100	213	320	107	215	291	76	210	290	80	88	31
105	212	322	110	215	293	78	212	291	79	89	32
110	214	328	114	215	291	76	211	290	79	90	38
115	215	328	113	215	295	80	212	290	78	90	35
120	214	327	113	214	296	82	212	292	80	92	33

The detailed results of surface rheological properties in each independent measurement of DTAB solution ($0.1 \times \text{CMC}$) at oscillation amplitude of 0.25 and oscillation frequency of 0.5 Hz are shown in Table G-14.

Table G-14. The detailed results of surface rheological properties in each independent measurement of DTAB solution ($0.1 \times \text{CMC}$) at oscillation amplitude of 0.25 and oscillation frequency of 0.5 Hz

Trial	Surface elasticity (mN/m)	Surface dilatational viscosity (mN·s/m)	Gibbs elasticity (mN/m)
1	4.11	0.16	4.76
2	3.68	0.14	4.24
3	4.08	0.24	5.16
4	3.63	0.19	4.44
5	3.55	0.14	4.10
6	3.26	0.15	3.91
7	3.78	0.08	4.09
8	3.44	0.18	4.21
9	3.63	0.15	4.25
10	3.56	0.14	4.12
11	4.09	0.16	4.73
12	4.21	0.16	4.87
13	4.09	0.19	4.89
14	3.66	0.20	4.54
15	3.43	0.15	4.05
16	3.66	0.08	3.96
17	3.53	0.11	3.92
18	3.28	0.14	3.88
19	3.46	0.15	4.07
20	3.45	0.13	3.97
21	3.19	0.09	3.55
22	3.40	0.13	3.93
23	3.40	0.15	4.01
24	3.53	0.18	4.34
25	3.41	0.19	4.29

The detailed results of surface rheological properties in each independent measurement of mixture of DTAB solution ($0.1 \times \text{CMC}$) and colloidal silica dispersions (3 wt%) at oscillation amplitude of 0.25 and oscillation frequency of 0.5 Hz are shown in Table G-15.

Table G-15. The detailed results of surface rheological properties in each independent measurement of mixture of DTAB solution ($0.1 \times \text{CMC}$) and colloidal silica dispersions (3 wt%) at oscillation amplitude of 0.25 and oscillation frequency of 0.5 Hz

Trial	Surface elasticity (mN/m)	Surface dilatational viscosity (mN·s/m)	Gibbs elasticity (mN/m)
1	13.56	0.12	13.95
2	11.96	0.03	12.07
3	11.82	0.06	12.01
4	13.82	0.09	14.11
5	12.33	0.08	12.58
6	13.20	0.01	13.24
7	14.89	0.06	15.08
8	14.17	0.05	14.33
9	15.56	0.06	15.75
10	16.04	0.05	16.20
11	18.48	0.19	19.14
12	16.81	0.07	17.04
13	15.72	0.06	15.90
14	15.29	0.09	15.58
15	15.02	0.08	15.29
16	15.95	0.04	16.08
17	15.70	0.03	15.78
18	14.98	0.04	15.12
19	15.04	0.08	15.32
20	15.89	0.06	16.09
21	16.01	0.01	16.04
22	18.07	0.17	18.64
23	15.03	0.01	15.07
24	15.60	0.00	15.60

The detailed results of surface rheological properties in each independent measurement of DTAB solution ($0.25 \times \text{CMC}$) at oscillation amplitude of 0.25 and oscillation frequency of 0.5 Hz are shown in Table G-16.

Table G-16. The detailed results of surface rheological properties in each independent measurement of DTAB solution ($0.25 \times \text{CMC}$) at oscillation amplitude of 0.25 and oscillation frequency of 0.5 Hz

Trial	Surface elasticity (mN/m)	Surface dilatational viscosity (mN·s/m)	Gibbs elasticity (mN/m)
1	2.82	0.45	7.07
2	1.84	0.12	2.42
3	1.60	0.07	1.92
4	1.79	0.15	2.60
5	1.76	0.19	2.92
6	1.61	0.09	2.03
7	1.78	0.09	2.18
8	1.74	0.14	2.49
9	1.64	0.09	2.03
10	1.56	0.15	2.43
11	1.71	0.13	2.37
12	1.70	0.17	2.71
13	1.54	0.09	1.97
14	1.64	0.15	2.51
15	2.32	0.10	2.73
16	1.73	0.17	2.75
17	1.57	0.08	1.92
18	1.48	0.15	2.43
19	1.55	0.13	2.27
20	1.61	0.17	2.69
21	1.71	0.08	2.05
22	1.55	0.08	1.89
23	1.56	0.17	2.70
24	1.74	0.17	2.70
25	1.56	0.11	2.10

The detailed results of surface rheological properties in each independent measurement of mixture of DTAB solution ($0.25 \times \text{CMC}$) and colloidal silica dispersions (3 wt%) at oscillation amplitude of 0.25 and oscillation frequency of 0.5 Hz are shown in Table G-17.

Table G-17. The detailed results of surface rheological properties in each independent measurement of mixture of DTAB solution ($0.25 \times \text{CMC}$) and colloidal silica dispersions (3 wt%) at oscillation amplitude of 0.25 and oscillation frequency of 0.5 Hz

Trial	Surface elasticity (mN/m)	Surface dilatational viscosity (mN·s/m)	Gibbs elasticity (mN/m)
1	4.91	0.11	5.31
2	3.93	0.20	4.77
3	4.21	0.22	5.16
4	3.59	0.21	4.56
5	3.50	0.18	4.31
6	3.53	0.21	4.51
7	3.82	0.19	4.64
8	3.85	0.15	4.48
9	3.78	0.21	4.70
10	3.84	0.23	4.87
11	3.22	0.21	4.25
12	3.35	0.17	4.12
13	3.64	0.22	4.66
14	3.51	0.23	4.58
15	3.65	0.23	4.71
16	3.59	0.28	5.05
17	3.32	0.17	4.04
18	3.84	0.17	4.52
19	3.44	0.25	4.67
20	3.38	0.13	3.91
21	3.34	0.22	4.42
22	3.83	0.18	4.59
23	3.65	0.17	4.39
24	3.86	0.13	4.37
25	3.62	0.23	4.69

The detailed results of surface rheological properties in each independent measurement of DTAB solution ($0.5 \times \text{CMC}$) at oscillation amplitude of 0.25 and oscillation frequency of 0.5 Hz are shown in Table G-18.

Table G-18. The detailed results of surface rheological properties in each independent measurement of DTAB solution ($0.5 \times \text{CMC}$) at oscillation amplitude of 0.25 and oscillation frequency of 0.5 Hz

Trial	Surface elasticity (mN/m)	Surface dilatational viscosity (mN·s/m)	Gibbs elasticity (mN/m)
1	3.29	0.11	3.71
2	2.24	0.09	2.60
3	2.26	0.11	2.73
4	2.35	0.11	2.79
5	2.16	0.09	2.53
6	2.07	0.09	2.46
7	2.32	0.05	2.51
8	2.58	0.06	2.80
9	2.06	0.09	2.43
10	2.08	0.08	2.40
11	1.75	0.07	2.02
12	1.60	0.08	1.93
13	1.99	0.07	2.27
14	1.94	0.09	2.34
15	1.56	0.10	2.04
16	1.79	0.11	2.29
17	1.78	0.09	2.18
18	1.59	0.10	2.09
19	1.86	0.08	2.22
20	2.17	0.12	2.69
21	2.52	0.11	2.95
22	1.71	0.09	2.09
23	1.99	0.07	2.29
24	2.37	0.11	2.82

The detailed results of surface rheological properties in each independent measurement of mixture of DTAB solution ($0.5 \times \text{CMC}$) and colloidal silica dispersions (3 wt%) at oscillation amplitude of 0.25 and oscillation frequency of 0.5 Hz are shown in Table G-19.

Table G-19. The detailed results of surface rheological properties in each independent measurement of mixture of DTAB solution ($0.5 \times \text{CMC}$) and colloidal silica dispersions (3 wt%) at oscillation amplitude of 0.25 and oscillation frequency of 0.5 Hz

Trial	Surface elasticity (mN/m)	Surface dilatational viscosity (mN·s/m)	Gibbs elasticity (mN/m)
1	4.98	0.38	6.93
2	4.99	0.39	6.99
3	4.51	0.41	6.85
4	4.12	0.39	6.40
5	4.25	0.40	6.58
6	3.59	0.45	6.87
7	3.78	0.38	6.06
8	3.76	0.34	5.66
9	3.62	0.38	6.00
10	4.05	0.40	6.47
11	3.90	0.33	5.73
12	3.72	0.37	5.98
13	3.73	0.37	5.99
14	3.91	0.37	6.03
15	3.77	0.33	5.60
16	3.52	0.34	5.55
17	3.92	0.38	6.15
18	3.79	0.36	5.86
19	3.66	0.37	5.89
20	3.57	0.35	5.70
21	4.37	0.41	6.69
22	3.99	0.37	6.11
23	3.64	0.38	6.01
24	4.42	0.39	6.55
25	3.60	0.36	5.79

The detailed results of surface rheological properties in each independent measurement of mixture of DTAB solution ($1.05 \times \text{CMC}$) and colloidal silica dispersions (3 wt%) at oscillation amplitude of 0.25 and oscillation frequency of 0.5 Hz are shown in Table G-20.

Table G-20. The detailed results of surface rheological properties in each independent measurement of mixture of DTAB solution ($1.05 \times \text{CMC}$) and colloidal silica dispersions (3 wt%) at oscillation amplitude of 0.25 and oscillation frequency of 0.5 Hz

Trial	Surface elasticity (mN/m)	Surface dilatational viscosity (mN·s/m)	Gibbs elasticity (mN/m)
1	7.10	0.12	7.53
2	5.75	0.10	6.12
3	4.74	0.19	5.50
4	4.31	0.18	5.03
5	4.55	0.17	5.23
6	3.75	0.16	4.39
7	3.39	0.18	4.18
8	3.64	0.14	4.22
9	3.73	0.22	4.74
10	3.88	0.16	4.55
11	3.88	0.19	4.70
12	8.39	0.27	9.43
13	3.56	0.22	4.60
14	3.77	0.19	4.61
15	5.01	0.12	5.45
16	4.08	0.19	4.88
17	3.76	0.21	4.69
18	3.81	0.21	4.77
19	3.38	0.20	4.32
20	3.63	0.16	4.31
21	3.74	0.19	4.56
22	3.73	0.21	4.67
23	3.29	0.24	4.48
24	3.50	0.19	4.32
25	4.01	0.21	4.96

The detailed results of surface rheological properties in each independent measurement of DTAB solution ($2.5 \times \text{CMC}$) at oscillation amplitude of 0.25 and oscillation frequency of 0.5 Hz are shown in Table G-21.

Table G-21. The detailed results of surface rheological properties in each independent measurement of DTAB solution ($2.5 \times \text{CMC}$) at oscillation amplitude of 0.25 and oscillation frequency of 0.5 Hz

Trial	Surface elasticity (mN/m)	Surface dilatational viscosity (mN·s/m)	Gibbs elasticity (mN/m)
1	0.77	0.14	2.43
2	1.23	0.02	1.30
3	1.73	0.19	2.96
4	1.89	0.05	2.08
5	1.26	0.03	1.38
6	1.20	0.04	1.37
7	1.30	0.06	1.54
8	1.29	0.05	1.47
9	1.26	0.03	1.35
10	1.23	0.05	1.42
11	1.33	0.06	1.56
12	0.93	0.09	1.42
13	1.25	0.04	1.42
14	1.29	0.08	1.65
15	1.44	0.05	1.64
16	1.54	0.04	1.67
17	1.37	0.12	2.07
18	1.43	0.04	1.60
19	1.34	0.03	1.46
20	1.48	0.05	1.67
21	1.36	0.02	1.42
22	1.31	0.09	1.75
23	1.45	0.08	1.82
24	1.44	0.05	1.65
25	1.31	0.03	1.42

The detailed results of surface rheological properties in each independent measurement of mixture of DTAB solution ($2.5 \times \text{CMC}$) and colloidal silica dispersions (3 wt%) at oscillation amplitude of 0.25 and oscillation frequency of 0.5 Hz are shown in Table G-22.

Table G-22. The detailed results of surface rheological properties in each independent measurement of mixture of DTAB solution ($2.5 \times \text{CMC}$) and colloidal silica dispersions (3 wt%) at oscillation amplitude of 0.25 and oscillation frequency of 0.5 Hz

Trial	Surface elasticity (mN/m)	Surface dilatational viscosity (mN·s/m)	Gibbs elasticity (mN/m)
1	1.69	0.07	1.96
2	1.68	0.07	1.97
3	1.44	0.05	1.65
4	1.29	0.02	1.35
5	1.26	0.03	1.38
6	1.20	0.04	1.37
7	1.30	0.06	1.54
8	1.29	0.05	1.47
9	1.26	0.03	1.35
10	1.23	0.05	1.42
11	1.33	0.06	1.56
12	0.93	0.09	1.42
13	1.25	0.04	1.42
14	1.29	0.08	1.65
15	1.44	0.05	1.64
16	1.54	0.04	1.67
17	1.37	0.12	2.07
18	1.43	0.04	1.60
19	1.34	0.03	1.46
20	1.48	0.05	1.67
21	1.36	0.02	1.42
22	1.31	0.09	1.75
23	1.45	0.08	1.82
24	1.44	0.05	1.65
25	1.31	0.03	1.42

The detailed results of surface rheological properties in each independent measurement of mixture of DTAB solution ($0.1 \times \text{CMC}$) and colloidal silica dispersions (0.1 wt%) at oscillation amplitude of 0.25 and oscillation frequency of 0.5 Hz are shown in Table G-23.

Table G-23. The detailed results of surface rheological properties in each independent measurement of mixture of DTAB solution ($0.1 \times \text{CMC}$) and colloidal silica dispersions (0.1 wt%) at oscillation amplitude of 0.25 and oscillation frequency of 0.5 Hz

Trial	Surface elasticity (mN/m)	Surface dilatational viscosity (mN·s/m)	Gibbs elasticity (mN/m)
1	1.92	0.09	2.30
2	1.71	0.14	2.45
3	1.65	0.14	2.42
4	1.81	0.11	2.29
5	1.79	0.08	2.14
6	1.73	0.11	2.22
7	1.67	0.14	2.42
8	1.71	0.13	2.35
9	1.69	0.14	2.41
10	1.76	0.12	2.36
11	1.67	0.13	2.33
12	1.60	0.09	2.03
13	1.79	0.13	2.45
14	1.66	0.09	2.09
15	1.65	0.13	2.32
16	1.55	0.13	2.23
17	1.50	0.13	2.19
18	1.55	0.09	1.95
19	1.70	0.10	2.16
20	1.48	0.13	2.22
21	1.47	0.08	1.84
22	1.53	0.13	2.20
23	1.39	0.09	1.82
24	1.59	0.12	2.23
25	1.54	0.11	2.11

The detailed results of surface rheological properties in each independent measurement of mixture of DTAB solution ($0.1 \times \text{CMC}$) and colloidal silica dispersions (0.3 wt%) at oscillation amplitude of 0.25 and oscillation frequency of 0.5 Hz are shown in Table G-24.

Table G-24. The detailed results of surface rheological properties in each independent measurement of mixture of DTAB solution ($0.1 \times \text{CMC}$) and colloidal silica dispersions (0.3 wt%) at oscillation amplitude of 0.25 and oscillation frequency of 0.5 Hz

Trial	Surface elasticity (mN/m)	Surface dilatational viscosity (mN·s/m)	Gibbs elasticity (mN/m)
1	2.21	0.35	5.48
2	3.16	0.05	3.35
3	3.84	0.10	4.21
4	3.82	0.22	4.81
5	3.86	0.04	3.99
6	3.72	0.17	4.44
7	3.89	0.13	4.38
8	4.17	0.13	4.69
9	3.94	0.18	4.70
10	3.53	0.13	4.03
11	3.77	0.15	4.38
12	3.43	0.07	3.67
13	3.58	0.08	3.89
14	3.60	0.09	3.91
15	3.82	0.15	4.43
16	3.28	0.10	3.67
17	3.53	0.19	4.37
18	3.56	0.15	4.16
19	3.27	0.18	4.08
20	3.21	0.09	3.53
21	3.34	0.06	3.55
22	2.98	0.24	4.22
23	3.03	0.11	3.45

The detailed results of surface rheological properties in each independent measurement of mixture of DTAB solution ($0.1 \times \text{CMC}$) and colloidal silica dispersions (1 wt%) at oscillation amplitude of 0.25 and oscillation frequency of 0.5 Hz are shown in Table G-25.

Table G-25. The detailed results of surface rheological properties in each independent measurement of mixture of DTAB solution ($0.1 \times \text{CMC}$) and colloidal silica dispersions (1 wt%) at oscillation amplitude of 0.25 and oscillation frequency of 0.5 Hz

Trial	Surface elasticity (mN/m)	Surface dilatational viscosity (mN·s/m)	Gibbs elasticity (mN/m)
1	9.86	0.85	14.54
2	4.02	0.37	6.10
3	4.39	0.14	4.94
4	4.48	0.12	4.93
5	5.07	0.67	10.19
6	4.41	0.32	6.01
7	6.43	0.37	8.14
8	7.33	0.77	12.14
9	6.28	0.75	11.53
10	4.39	0.41	6.78

The detailed results of surface rheological properties in each independent measurement of mixture of DTAB solution ($0.1 \times \text{CMC}$) and colloidal silica dispersions (9 wt%) at oscillation amplitude of 0.25 and oscillation frequency of 0.5 Hz are shown in Table G-26.

Table G-26. The detailed results of surface rheological properties in each independent measurement of mixture of DTAB solution ($0.1 \times \text{CMC}$) and colloidal silica dispersions (9 wt%) at oscillation amplitude of 0.25 and oscillation frequency of 0.5 Hz

Trial	Surface elasticity (mN/m)	Surface dilatational viscosity (mN·s/m)	Gibbs elasticity (mN/m)
1	9.14	0.04	9.27
2	9.58	0.06	9.77
3	8.81	0.05	8.97
4	8.71	0.03	8.82
5	8.41	0.13	8.85
6	8.06	0.02	8.14
7	8.31	0.04	8.44
8	7.81	0.04	7.92
9	7.93	0.07	8.16
10	8.72	0.09	9.02
11	7.52	0.06	7.71
12	8.46	0.00	8.47
13	8.63	0.04	8.76
14	7.97	0.03	8.06
15	8.12	0.09	8.42
16	7.75	0.07	7.97
17	7.54	0.04	7.68
18	7.75	0.07	7.99
19	7.79	0.09	8.08
20	7.35	0.06	7.53
21	7.69	0.06	7.88
22	7.51	0.07	7.75
23	7.94	0.02	8.00
24	7.63	0.04	7.76
25	7.82	0.08	8.09

The estimation of equilibrium surface tension of DTAB solution ($0.1 \times \text{CMC}$) is shown in Figure G-2.

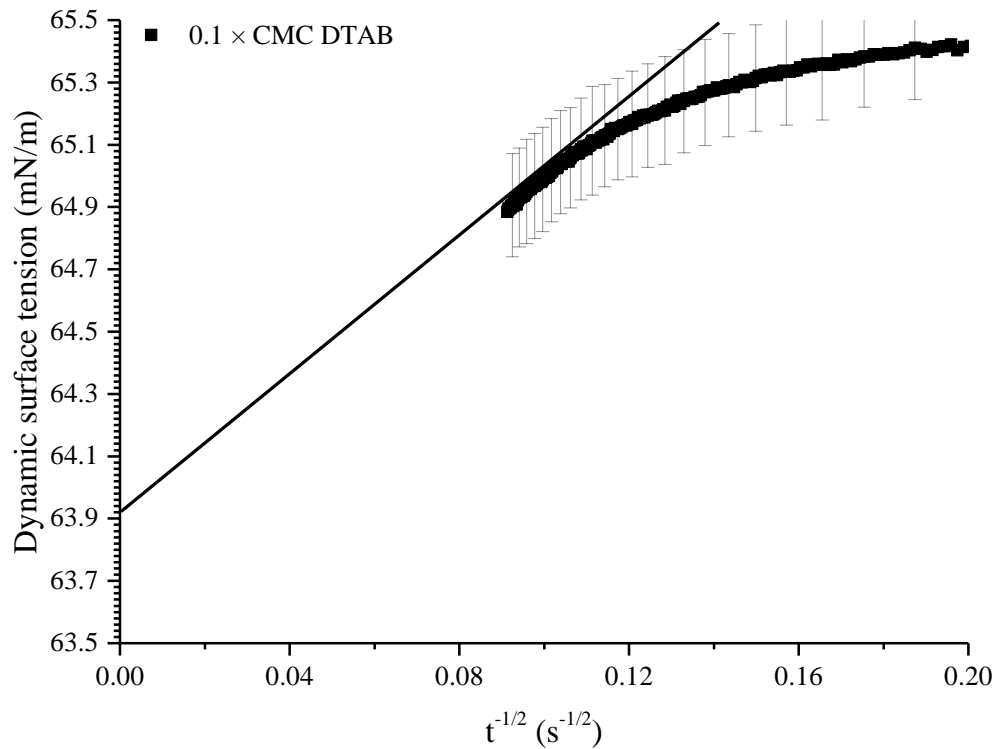


Figure G-2. Partial enlarged view of dynamic surface tension results of DTAB solution ($0.1 \times \text{CMC}$) against $t^{-1/2}$. The straight line represents a tangent and a linear extrapolation of dynamic surface tension to infinite time. The intercept at ordinate represents the estimated equilibrium surface tension. The error bars represent the standard deviation of the observations. All the errors of obtained data are calculated and only present 1 error bar in every 10 error bars for clarity.

The estimation of equilibrium surface tension of mixture of DTAB solution ($0.1 \times \text{CMC}$) and colloidal silica dispersions (3 wt%) is shown in Figure G-3.

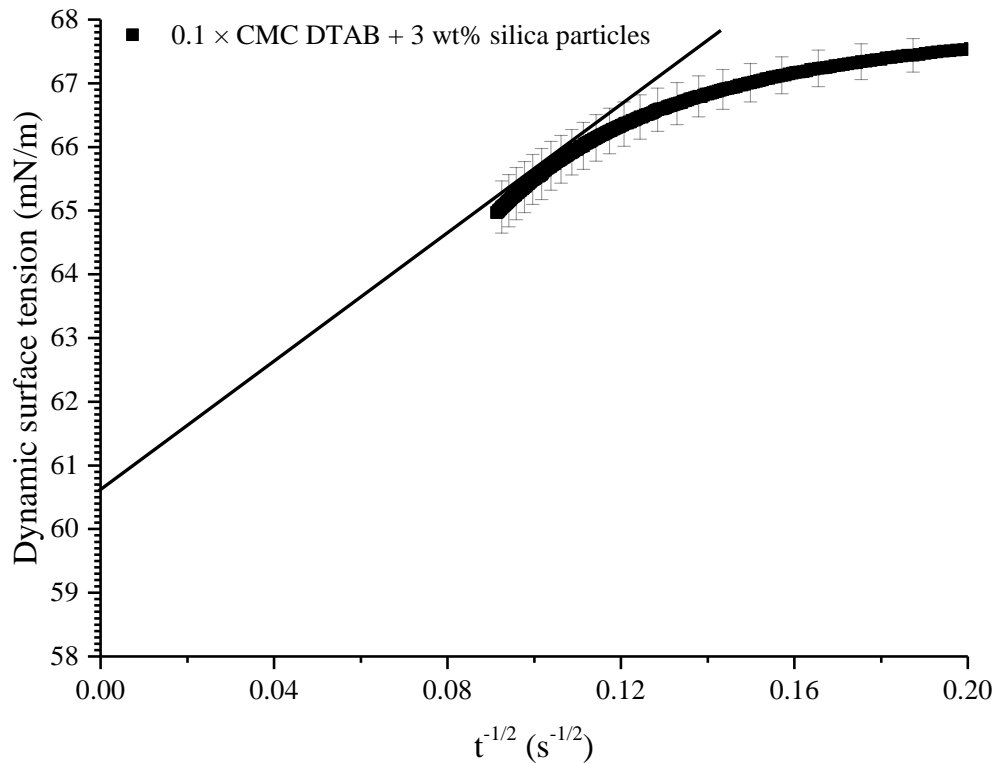


Figure G-3. Partial enlarged view of dynamic surface tension results of mixture of DTAB solution ($0.1 \times \text{CMC}$) and colloidal silica dispersions (3 wt%) against $t^{-1/2}$. The straight line represents a tangent and a linear extrapolation of dynamic surface tension to infinite time. The intercept at ordinate represents the estimated equilibrium surface tension. The error bars represent the standard deviation of the observations. All the errors of obtained data are calculated and only present 1 error bar in every 10 error bars for clarity.

The estimation of equilibrium surface tension of DTAB solution ($0.25 \times \text{CMC}$) is shown in Figure G-4.

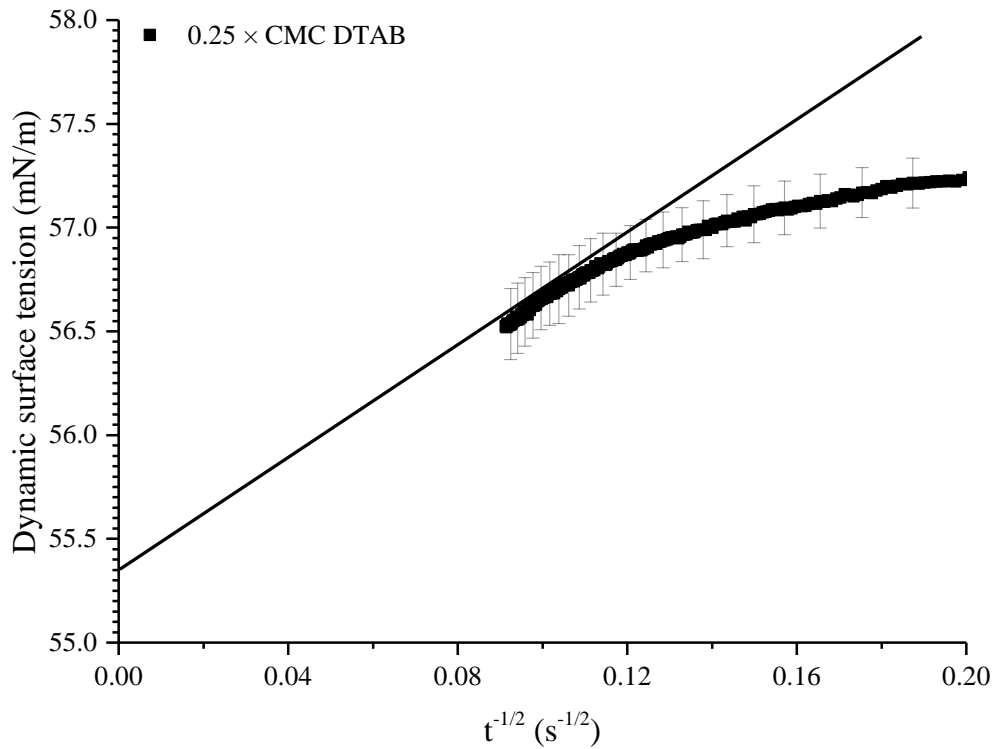


Figure G-4. Partial enlarged view of dynamic surface tension results of DTAB solution ($0.25 \times \text{CMC}$) against $t^{-1/2}$. The straight line represents a tangent and a linear extrapolation of dynamic surface tension to infinite time. The intercept at ordinate represents the estimated equilibrium surface tension. The error bars represent the standard deviation of the observations. All the errors of obtained data are calculated and only present 1 error bar in every 10 error bars for clarity.

The estimation of equilibrium surface tension of mixture of DTAB solution ($0.25 \times \text{CMC}$) and colloidal silica dispersions (3 wt%) is shown in Figure G-5.

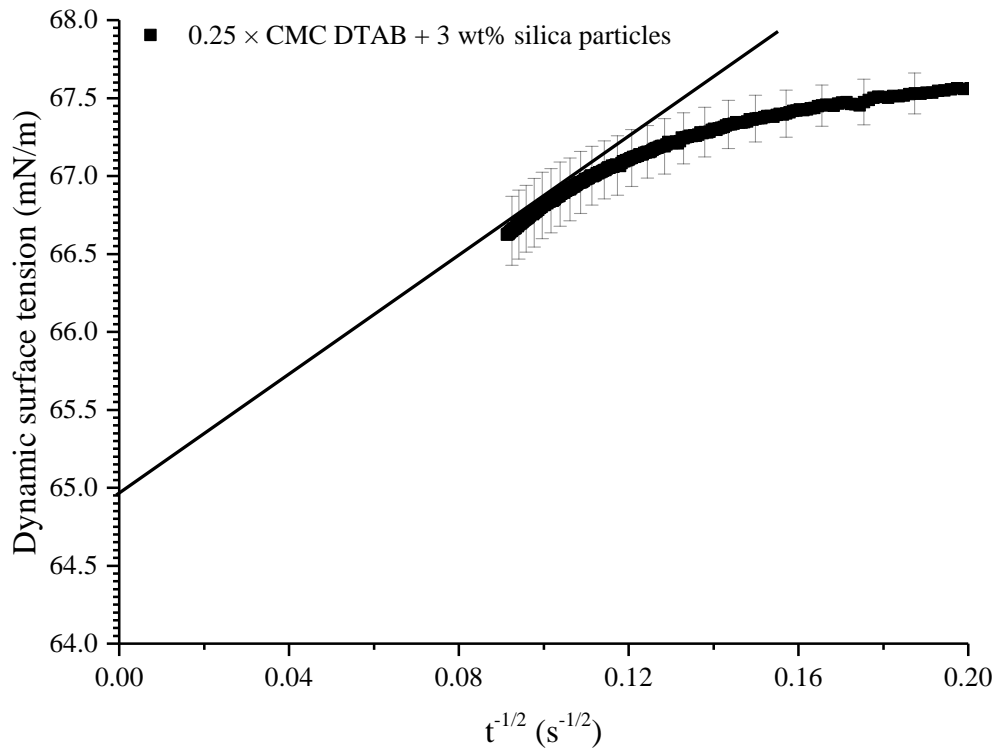


Figure G-5. Partial enlarged view of dynamic surface tension results of mixture of DTAB solution ($0.25 \times \text{CMC}$) and colloidal silica dispersions (3 wt%) against $t^{-1/2}$. The straight line represents a tangent and a linear extrapolation of dynamic surface tension to infinite time. The intercept at ordinate represents the estimated equilibrium surface tension. The error bars represent the standard deviation of the observations. All the errors of obtained data are calculated and only present 1 error bar in every 10 error bars for clarity.

The estimation of equilibrium surface tension of DTAB solution ($0.5 \times \text{CMC}$) is shown in Figure G-6.

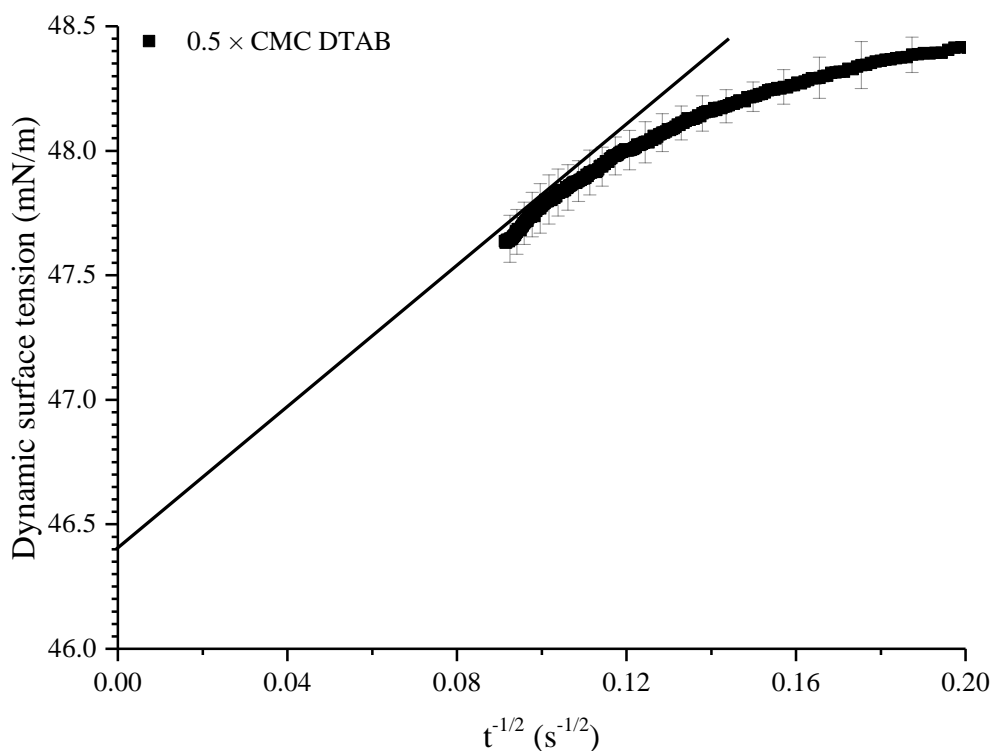


Figure G-6. Partial enlarged view of dynamic surface tension results of DTAB solution ($0.5 \times \text{CMC}$) against $t^{-1/2}$. The straight line represents a tangent and a linear extrapolation of dynamic surface tension to infinite time. The intercept at ordinate represents the estimated equilibrium surface tension. The error bars represent the standard deviation of the observations. All the errors of obtained data are calculated and only present 1 error bar in every 10 error bars for clarity.

The estimation of equilibrium surface tension of mixture of DTAB solution ($0.5 \times \text{CMC}$) and colloidal silica dispersions (3 wt%) is shown in Figure G-7.

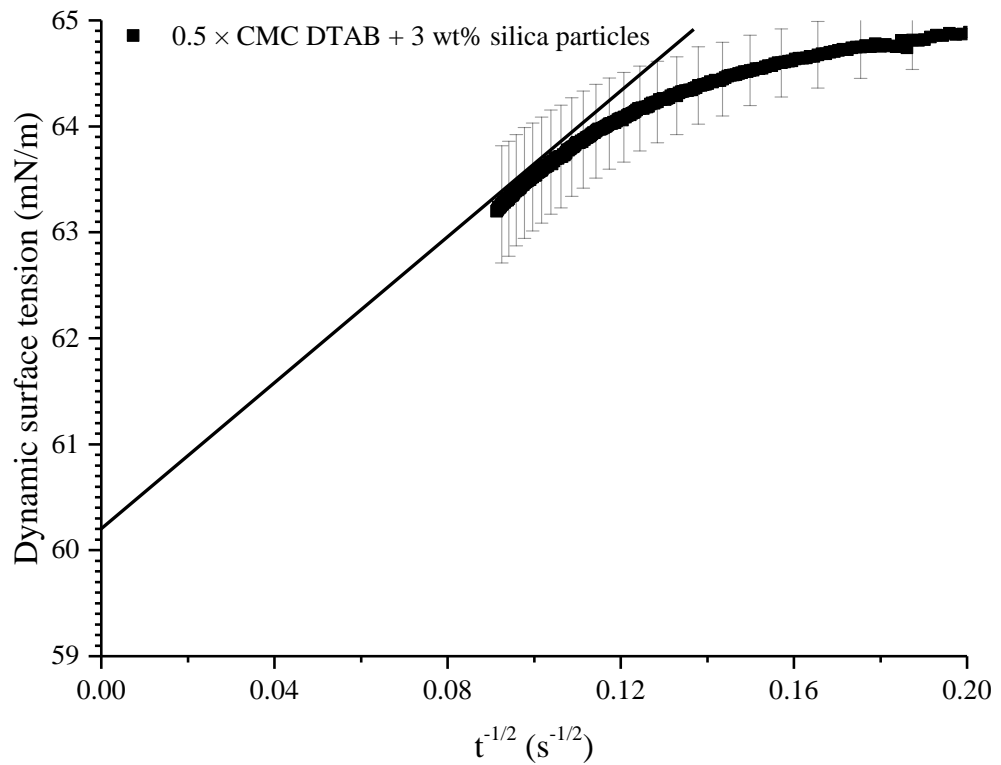


Figure G-7. Partial enlarged view of dynamic surface tension results of mixture of DTAB solution ($0.5 \times \text{CMC}$) and colloidal silica dispersions (3 wt%) against $t^{-1/2}$. The straight line represents a tangent and a linear extrapolation of dynamic surface tension to infinite time. The intercept at ordinate represents the estimated equilibrium surface tension. The error bars represent the standard deviation of the observations. All the errors of obtained data are calculated and only present 1 error bar in every 10 error bars for clarity.

The estimation of equilibrium surface tension of mixture of DTAB solution ($1.05 \times \text{CMC}$) and colloidal silica dispersions (3 wt%) is shown in Figure G-8.

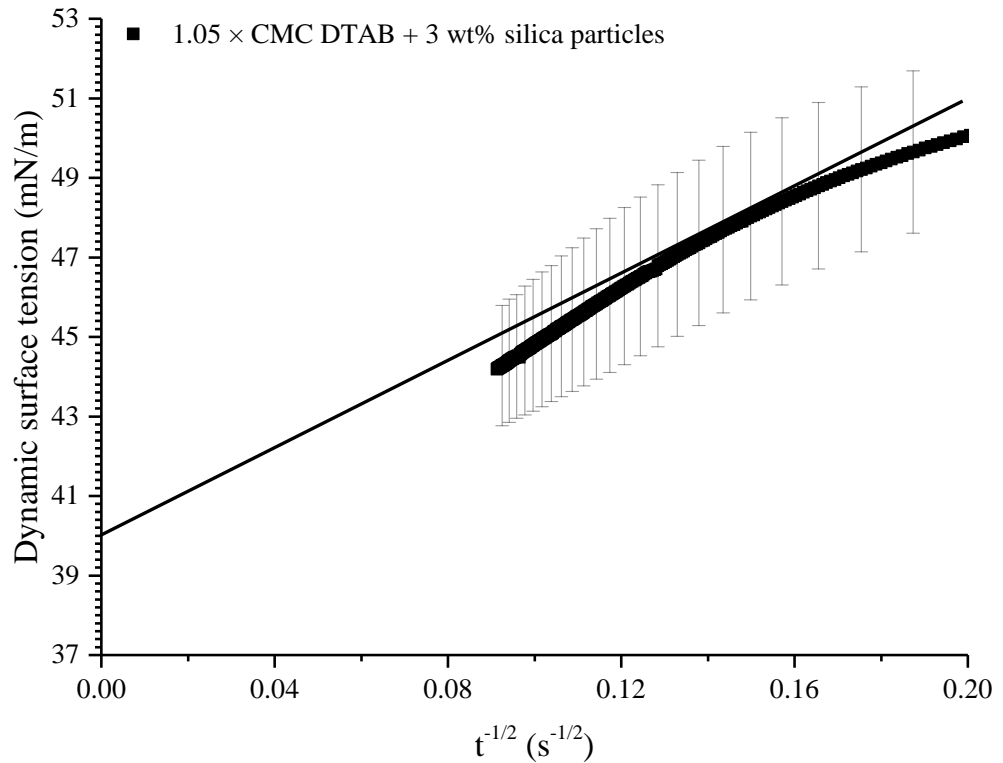


Figure G-8. Partial enlarged view of dynamic surface tension results of mixture of DTAB solution ($1.05 \times \text{CMC}$) and colloidal silica dispersions (3 wt%) against $t^{-1/2}$. The straight line represents a tangent and a linear extrapolation of dynamic surface tension to infinite time. The intercept at ordinate represents the estimated equilibrium surface tension. The error bars represent the standard deviation of the observations. All the errors of obtained data are calculated and only present 1 error bar in every 10 error bars for clarity.

The estimation of equilibrium surface tension of DTAB solution ($2.5 \times \text{CMC}$) is shown in Figure G-9.

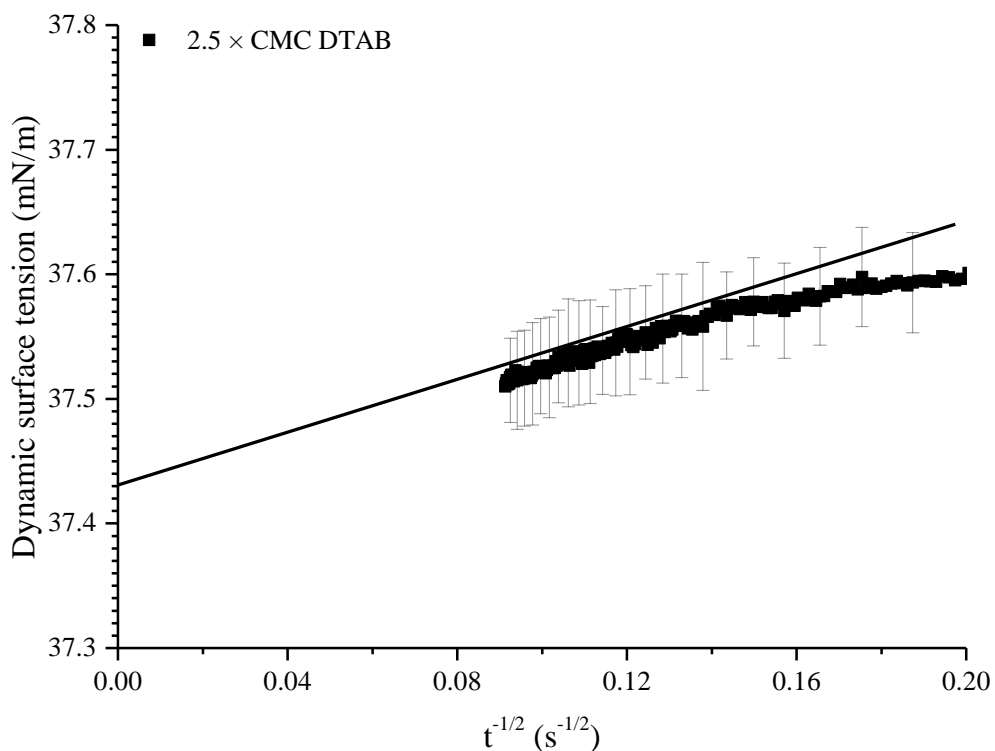


Figure G-9. Partial enlarged view of dynamic surface tension results of DTAB solution ($2.5 \times \text{CMC}$) against $t^{-1/2}$. The straight line represents a tangent and a linear extrapolation of dynamic surface tension to infinite time. The intercept at ordinate represents the estimated equilibrium surface tension. The error bars represent the standard deviation of the observations. All the errors of obtained data are calculated and only present 1 error bar in every 10 error bars for clarity.

The estimation of equilibrium surface tension of mixture of DTAB solution ($2.5 \times \text{CMC}$) and colloidal silica dispersions (3 wt%) is shown in Figure G-10.

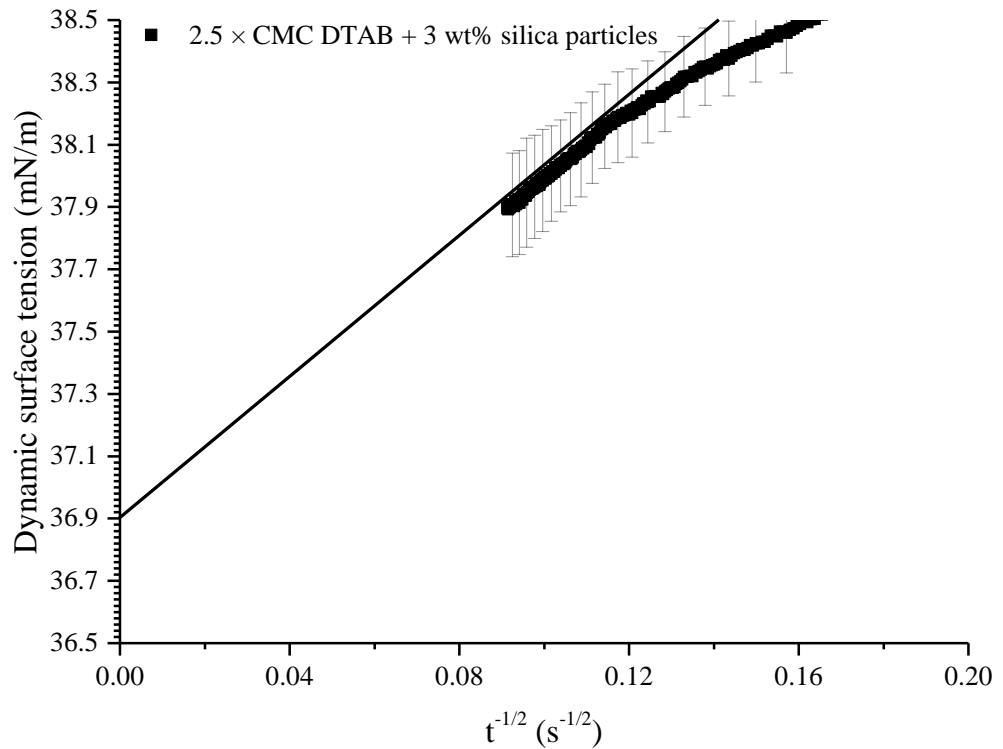


Figure G-10. Partial enlarged view of dynamic surface tension results of mixture of DTAB solution ($2.5 \times \text{CMC}$) and colloidal silica dispersions (3 wt%) against $t^{-1/2}$. The straight line represents a tangent and a linear extrapolation of dynamic surface tension to infinite time. The intercept at ordinate represents the estimated equilibrium surface tension. The error bars represent the standard deviation of the observations. All the errors of obtained data are calculated and only present 1 error bar in every 10 error bars for clarity.

The estimation of equilibrium surface tension of mixture of DTAB solution ($0.1 \times \text{CMC}$) and colloidal silica dispersions (0.1 wt%) is shown in Figure G-11.

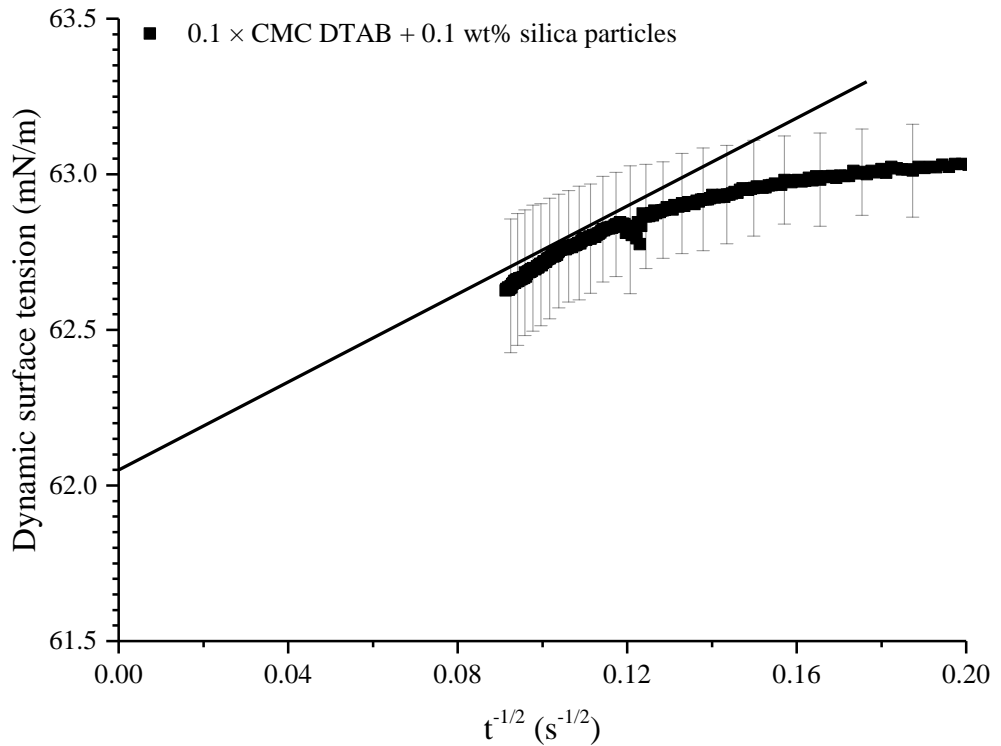


Figure G-11. Partial enlarged view of dynamic surface tension results of mixture of DTAB solution ($0.1 \times \text{CMC}$) and colloidal silica dispersions (0.1 wt%) against $t^{-1/2}$. The straight line represents a tangent and a linear extrapolation of dynamic surface tension to infinite time. The intercept at ordinate represents the estimated equilibrium surface tension. The error bars represent the standard deviation of the observations. All the errors of obtained data are calculated and only present 1 error bar in every 10 error bars for clarity.

The estimation of equilibrium surface tension of mixture of DTAB solution ($0.1 \times \text{CMC}$) and colloidal silica dispersions (0.3 wt%) is shown in Figure G-12.

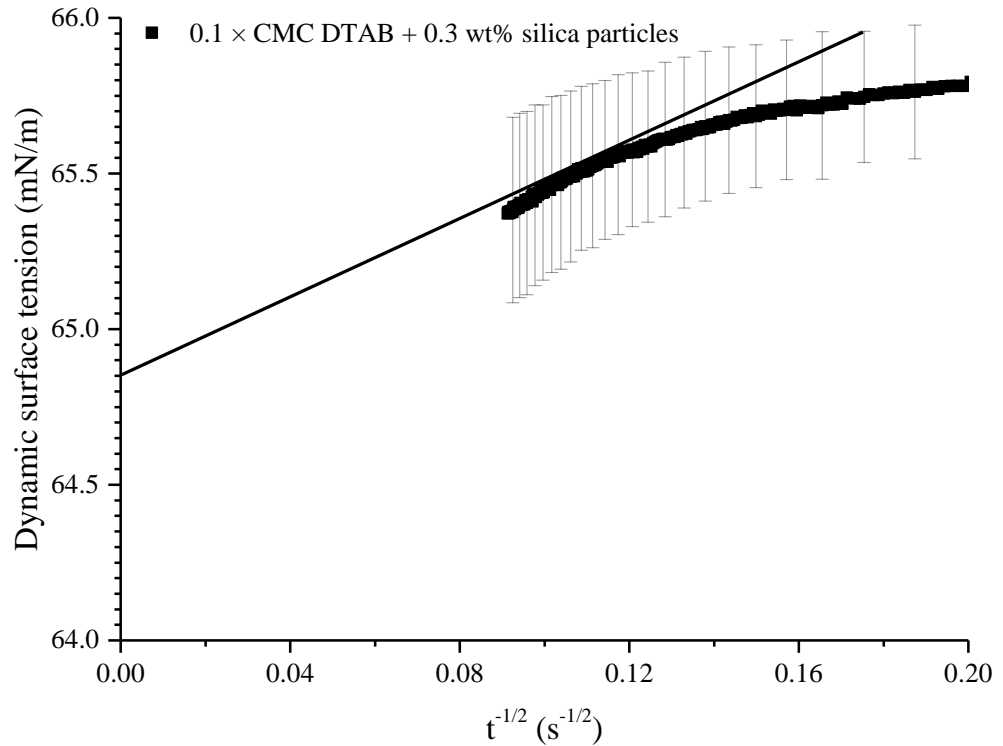


Figure G-12. Partial enlarged view of dynamic surface tension results of mixture of DTAB solution ($0.1 \times \text{CMC}$) and colloidal silica dispersions (0.3 wt%) against $t^{-1/2}$. The straight line represents a tangent and a linear extrapolation of dynamic surface tension to infinite time. The intercept at ordinate represents the estimated equilibrium surface tension. The error bars represent the standard deviation of the observations. All the errors of obtained data are calculated and only present 1 error bar in every 10 error bars for clarity.

The estimation of equilibrium surface tension of mixture of DTAB solution ($0.1 \times \text{CMC}$) and colloidal silica dispersions (1 wt%) is shown in Figure G-13.

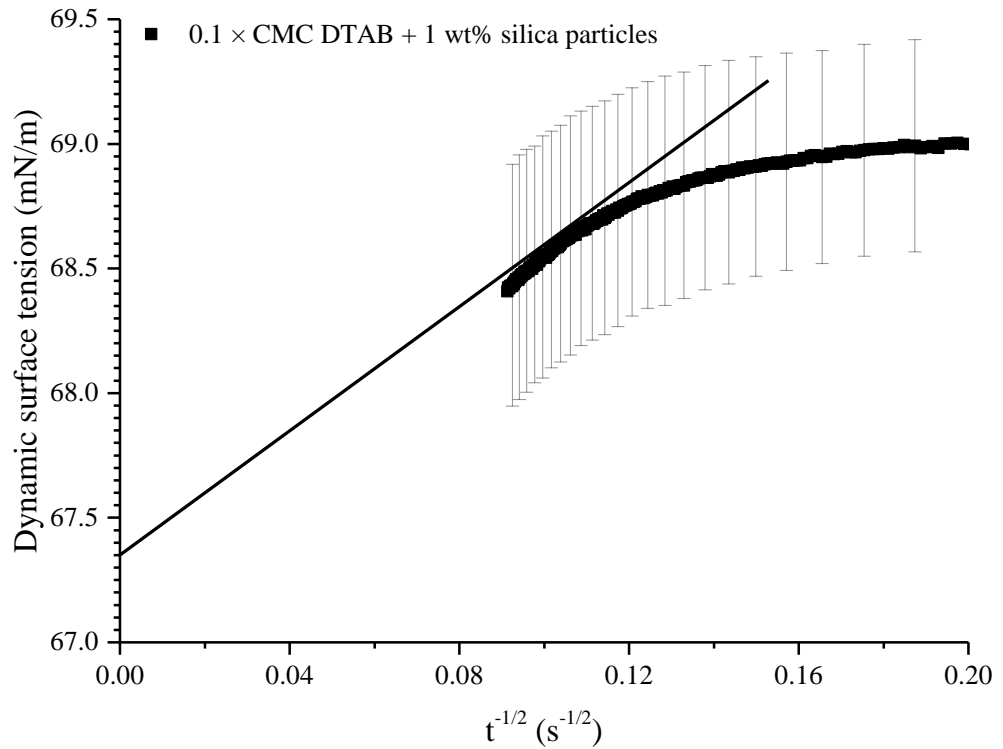


Figure G-13. Partial enlarged view of dynamic surface tension results of mixture of DTAB solution ($0.1 \times \text{CMC}$) and colloidal silica dispersions (1 wt%) against $t^{-1/2}$. The straight line represents a tangent and a linear extrapolation of dynamic surface tension to infinite time. The intercept at ordinate represents the estimated equilibrium surface tension. The error bars represent the standard deviation of the observations. All the errors of obtained data are calculated and only present 1 error bar in every 10 error bars for clarity.

The estimation of equilibrium surface tension of mixture of DTAB solution ($0.1 \times \text{CMC}$) and colloidal silica dispersions (9 wt%) is shown in Figure G-14.

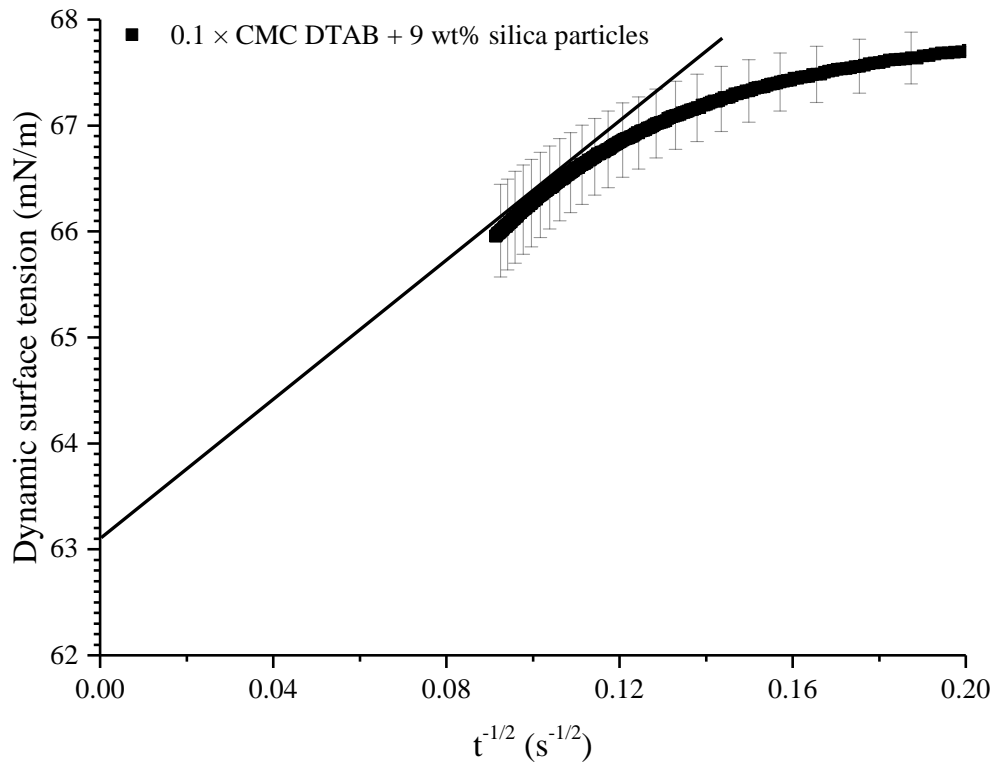


Figure G-14. Partial enlarged view of dynamic surface tension results of mixture of DTAB solution ($0.1 \times \text{CMC}$) and colloidal silica dispersions (9 wt%) against $t^{-1/2}$. The straight line represents a tangent and a linear extrapolation of dynamic surface tension to infinite time. The intercept at ordinate represents the estimated equilibrium surface tension. The error bars represent the standard deviation of the observations. All the errors of obtained data are calculated and only present 1 error bar in every 10 error bars for clarity.